UNIVERSITY OF PRISTINA-KOSOVSKA MITROVICA
REPUBLIC OF SERBIA

THE UNIVERSITY THOUGHT

PUBLICATION IN NATURAL SCIENCES

VOL. 6, N° 1, 2016.

PUBLISHED BY UNIVERSITY OF PRISTINA - KOSOVSKA MITROVICA

REPUBLIC OF SERBIA

ISSN 1450-7226

UNIVERSITY OF PRISTINA-KOSOVSKA MITROVICA, SERBIA
UNIVERSITY THOUGHT
PUBLICATION IN NATURAL SCIENCES

Aims and Scope

The University Thought - Publication in Natural Sciences (UNIV. THOUGHT, Nat. Sci.) is a scientific journal founded in 1994. by the University of Priština, and was published semi annually until 1998.

Today, the University Thought - Publication in Natural Sciences is an international, peer reviewed, Open Access journal, published semi annually in the online and print version by the University of Priština, temporarily settled in Kosovska Mitrovica, Serbia. The Journal publishes articles on all aspects of research in Biology, Chemistry, Geography, Information technologies, Mathematics and Physics in the form of original papers, short communications and reviews (invited) by authors from the country and abroad.

The University Thought - Publication in Natural Sciences serves as an interdisciplinary forum covering a wide range of topics for a truly international audience. Journal is endeavor of the University of Priština to acquaint the scientific world with its achievements and wish to affirm the intellectual potential and natural resources of own region. Our aim is to put forward attitude of principle that science is universal and we invite all scientists to cooperate wherever their scope of research may be. We are convinced that shall contribute to do victory of science over barriers of all kinds erected throughout the Balkans.

Editorial Office

Ive Lola Ribara 29; 38220, Kosovska Mitrovica, Serbia, e-mail: editor.utnsjournal@pr.ac.rs, office.utnsjournal@pr.ac.rs, office.utnsjournal@gmail.com; fax: +381 28 425 397

Available Online

This journal is available online. Please visit http://www.utnsjournal.pr.ac.rs to search and download published articles.

UNIVERSITY OF PRISTINA-KOSOVSKA MITROVICA, SERBIA
UNIVERSITY THOUGHT
PUBLICATION IN NATURAL SCIENCES

Vol. 6, N^{o} 1, 2016.

CONTENTS

BIOLOGY

CHEMISTRY

GEOGRAPHY

INFORMATION TECHNOLOGIES

MATHEMATICS

PHYSICS

UNIVERSITY THOUGHT
Publication in Natural Sciences, Vol. 6, N^{o} 1, 2016, pp. 1-4.
doi:10.5937/univtho6-10971
Original Scientific Paper

MORPHOLOGICAL CHARACTERISTICS OF THE HERMANN'S TORTOISE (*TESTUDO HERMANNI* GMELIN, 1789) IN THE SOUTH-EASTERN PART OF KOSOVO AND METOHIJA

Nenad Labus[1*], Aleksandra Savić[1], Nebojša Živić[1], Tatjana Babović-Jakšić[1]

[1]Faculty of Natural Sciences and Mathematics, University of Priština, Kosovska Mitrovica, Serbia.

ABSTRACT

In this paper we present the results of the analysis of morphological characteristics of the Hermann's tortoise from three localities in south-eastern part of Kosovo and Metohija. 75 adult Hermann's tortoises (33 males and 42 females) have been analyzed. Morphometric analisys has been done on 7 traits. We considered the plastron black pigmentation patterns and frequencies for each pigmentation states were calculated. Females were larger than males for all morphometric traits. Based on the most important dimensions of carapace and plastron length and width, the Hermann's tortoises from the south-eastern part of Kosovo and Metohija are the most similar to the individuals of the population from the southern part of the Balkan Peninsula (the southern part of Serbia and the northern part of Greece). In relation to the populations from central and eastern Serbia, individuals from our studed area have higher values.

Key words: morphometry, Hermann's tortoise, Kosovo and Metohija.

1. INTRODUCTION

Hermann's tortoise (*Testudo hermanni* Gmelin, 1789) is distributed over the northern Mediterranean region. It is distributed over most of the Balkan Peninsula while in the western Mediterranean (continental Spain, France and Italy, Balearic Islands, Corsica, Sardinia and Sicily) has an isolated distribution. Although it is most prevalent in areas with a Mediterranean climate, it can be found in inland regions of the Balkan Peninsula under the influence of continental climate (Bour, 1997), (Cheylan, 2001), (Fritz et al., 2006), (Ljubisavljević et al., 2014).

The Hermann's tortoise is widely distributed in Serbia, where it inhabits hilly areas and lower mountains (below 1200 m) south of the Sava and Danube rivers (Ljubisavljević et al., 2014), (Tomović et al., 2014).

It is generally accepted that two subspecies have been recognized within species *Testudo hermanni* (Fritz et al., 2006), (Bertolero et al., 2011), nominotypic *Testudo hermanni hermanni* and *Testudo hermanni boettgeri*. *T. h. hermanni* occupies the patchy western Mediterranean range, from Spain to Italy, while *T. h. boettgeri* inhabits the coastal areas of the Balkan Peninsula, from Croatia to Greece, including many islands in the Adriadic and Ionian seas, the European part of Turkey, and further inland in the Bosnia and Herzegovina, Serbia, Montenegro, Macedonia, Romania and Bulgaria.

Up to now, some of the Serbian populations of Hermann's tortoise have been included in morphological studies (Ljubisavljević et al., 2012), sexual dimorphism studies (Djordjević et al., 2011), (Djordjević et al., 2013), ecological studies (Golubović et al., 2013) and distributional studies (Ljubisavljević et al., 2014).

The main aim of this paper is to provide basic data about morphological characteristics of the Hermann's tortoise from south-eastern part of Kosovo and Metohija. Our aim was also to test the potential presence of gender differences.

2. MATERIALS AND METHODS

Morphological characteristics were analyzed using three localities from south-eastern part of Kosovo and Metohija: village Grnčar (42° 19' 38" N, 21° 24' E, 507 m a.s.l.), village Melci (42° 31' N, 21° 27' E, 800 m a.s.l.) and village Straža (42° 31' N, 21° 26' E, 716 m a.s.l.). We analysed 75 adult Hermann's tortoises (33 males and 42 females). Sex was determined by plastral concavity and by the presence of larger tails in

males. Specimens smaller than 10 cm carapace length were considered to be juveniles (Stubbs et al., 1984). All specimens were measured in the field, photographed and afterwards released at the place of capture.

Morphometric analysis has been done on 7 traits: SCL – midline straight carapace length, from the front of the nuchal scute, to the rear of the carapace; MCW – mid-body carapace width, straight width of the carapace, at the level of the 6th marginals; MaxCW – maximal carapace width, width of the carapace at the widest point, usually at the level of the 8th marginals; CH – carapace height; MPL – midline plastron length; MaxPL – maximal plastron length, length of the plastron from the tips of gulars to the tips of anals; MaxPW – maximal plastron width. All linear measurements were taken with a mechanical calliper (precision 0,01 mm) while, midline straight carapace length was taken by a flexible measuring tape (precision 1 mm), by the same person (A. S.).

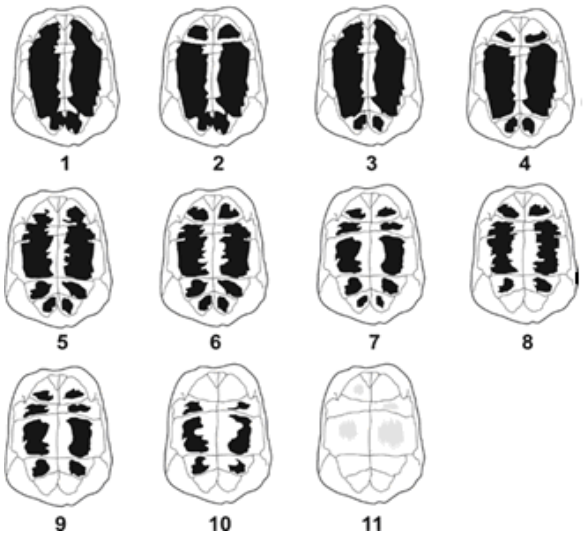

Fig. 1. Range of plastral pigmentation (modified scheme of Guyot & Devaux, 1997 according to Ljubisavljević et al., 2012): 1) continuous black pigmentation; 2) black spots on humeral scutes are isolated; 3) black spots on anal scutes are isolated; 4) black spots on anal and humeral scutes are isolated; 5) black spots on anal and femoral scutes are isolated; 6) black spots on anal, humeral and femoral scutes are isolated; 7) black spots are isolated on each scute and reduced in size; 8) black spots are lacking on anal scutes, while on humeral and femoral scutes are isolated; 9) black spots are lacking on anal scutes, while on other scutes are isolated and reduced in size; 10) black spots are lacking on anal and humeral scutes, while on other scutes are isolated and reduced in size; 11) black pigmentation is lacking.

We considered the extended plastron black pigmentation (Fig. 1) and frequencies for each pigmentation states were calculated. This was done according to modified scheme of (Guyot & Devaux, 1997), used in morphological study of the Hermann's tortoise by (Ljubisavljević et al., 2012). Since, preliminary analysis of (Ljubisavljević et al., 2012), revealed no significant sex related variations in the frequencies of black pigmentation, we performed qualitative analysis of these trait on the whole sample.

Programme package STATISTICA (version 7.0) has been used for statistical data analysis. For morphometric characters basic parameters of descriptive statistics have been separately calculated by genders: mean ($\bar{X}$), standard error (SE), range and standard deviation (SD). Analysis of variance (ANOVA) has been used to establish the significance of differences in respect of morphometric characters between the genders.

3. RESULTS AND DISCUSSION

3.1. Morphometric characters

Descriptive statistics of body size measurements of adult males and females of Hermann's tortoises from south-eastern part of Kosovo and Metohija are presented in Table 1.

The carapace length (SCL) of males ranged from 154.8 mm to 214.2 mm ($\bar{X}$ = 180.57 mm ± 2.04), respectively, from 164.2 to 232.6 mm ($\bar{X}$ = 200.83 mm ± 2.17) of females (Table 1). The mean value of the maximum carapace width (Max CW) of males amounted to 155.17 mm (± 1.90), while that of females was 163.46 mm (± 1.84). The maximum carapace width of 189.6 mm was recorded in a female individual, while the narrowest carapace of 122.6 mm, measured in one male individual. Maximum measured plastron length (Max PL) in males was 182.3 mm, and in females, 219.6 mm, while the minimum values were measured 137.5 mm in males and 141.3 mm in females. Average values of maximum plastron width (Max PW) amounted to 131.73 mm (± 1.40) in males, and 141.13 mm (± 1.49) in females. Carapace height (CH) amounted to an average 91.46 ± 1.27 mm in males and 102.78 ± 1.65 mm, in females.

These obtained values were in accordance with literature data (Willemsen & Hailey, 1999), (Willemsen & Hailey, 2003), (Bertolero et al., 2011), (Djordjević et al., 2011), (Ljubisavljević et al., 2012).

Based on the most important dimensions of carapace and plastron length and width, the Hermann's tortoises from the south-eastern part of Kosovo and Metohija are the most similar to the individuals of the population from the southern part of the Balkan Peninsula (the southern part of Serbia and the northern part of Greece). In relation to the populations from central and eastern Serbia, individuals from our studed area have higher values that is also in accordance with literature data (Djordjević et al., 2011), (Ljubisavljević et al., 2012).

Table 1. Descriptive statistics of morphometric characters of male and female Hermann's tortoise from south-eastern part of Kosovo and Metohija. Abbreviations of characters are given in "Materials and Methods".

Character	Male (n = 33)				Female (n = 42)			
	$\bar{X}$ ± SE	min	max	SD	$\bar{X}$ ± SE	min	max	SD
SCL	180.57±2.04	154.8	214.2	11.75	200.83±2.17	164.2	232.6	14.09
MCW	141.22±1.38	117.3	157.3	7.94	150.86±1.57	128.2	176.2	10.22
MaxCW	155.17±1.90	122.6	174.4	10.93	163.46±1.84	137.5	189.6	11.93
CH	91.46±1.27	75.6	113.3	7.33	102.78±1.65	83.7	133.3	10.75
MPL	140.77±1.78	123.4	165.5	10.25	167.82±2.39	126.3	197.2	15.50
MaxPL	160.27±1.87	137.5	182.3	10.76	183.75±2.31	141.3	219.6	15.01
MaxPW	131.73±1.40	109.3	147.1	8.07	141.13±1.49	120.2	163.2	9.70

Table 2. ANOVA with sex as the factor. Abbreviations of characters are given in "Materials and Methods". Bold – statistically significant *P* values ($P < 0.05$).

Character	F	*P*
SCL	44.065	0.00000
MCW	19.881	0.00003
MaxCW	9.595	0.00277
CH	26.763	0.00000
MPL	74.652	0.00000
MaxPL	57.368	0.00000
MaxPW	20.048	0.00003

The analysis of variance (ANOVA) showed that sexes significantly differed in all 7 characters (Table 2). Females were larger than males for all traits. These results are consistent with published dates for sexual dimorphism of the *Testudo* genus (Willemsen & Hailey, 1999), (Willemsen & Hailey, 2003), (Djordjević et al., 2011), (Ljubisavljević et al., 2012). The observed direction of sexual size dimorphism, with females larger than males is most common in chelonians and is usually explained by fecundity selection (Ceballos et al., 2013).

3.2. Qualitative traits

Analysis of plastron black pigmentation level has shown that in individuals of the Hermann's tortoise from the southeastern part of Kosovo and Metohija seven out of 11 states are present. The most common are the conditions that determine the fragmented and reduced black pigmentation (states 7 and 10). They were present in 37.7% and 29.5% of individuals. This type of plastron pigmentation is characteristic for the Hermann's tortoises from the southern part of Serbia (Ljubisavljević et al., 2012). On the other hand, conditions that show high level of black pigmentation (states 2 and 4), are present in only 11.4% of individuals. Pigmentation states 1, 3, 8 and 9 were not identified in the analyzed sample.

4. CONCLUSION

In this paper we present the results of the analysis of morphological characteristics of the Hermann's tortoise from south-eastern part of Kosovo and Metohija. Results of descriptive statistics showed that the Hermann's tortoises from the south-eastern part of

Kosovo and Metohija are the most similar to the individuals of the populations from the southern part of the Balkan Peninsula (the southern part of Serbia and the northern part of Greece). Variance analysis found the statistically significant difference in body size between the genders. Females had higher values for all characters. Fragmented and reduced plastron black pigmentation prevailed in 2/3 of individuals in the population.

Our results of analysis of external morphology of the Hermann's tortoise from south-eastern part of Kosovo and Metohija, are in accordance with previous studies of this species from Serbia.

REFERENCES

Berry, J.F., & Shine, R. 1980. Sexual size dimorphism and sexual selection in turtles (order testudines). Oecologia,44(2), pp. 185-191. doi:10.1007/BF00572678.

Bertolero, A., Cheylan, M., Hailey, A., Livoreil, B., & Willemsen, R.E. 2011. Testudo hermanni (Gmelin 1789): Hermann's tortoise. In A.G.J. Rhodin, P.C.H. Pritchard, P.P. van Dijk, R.A. Saumure, K.A. Buhlmann, J.B. Iverson, & R.A. Mittermeier Eds., Conservation biology of freshwater turtles and tortoises: A compilation project of the IUCN/SSC tortoise and freshwater turtle specialist group. Chelonian Research Monographs. 5, 059.1–059.20.

Bour, R. 1997. Testudo hermanni. In J.P. Gasc, A. Cabela, J. Crnobrnja-Isailović, D. Dolmen, K. Grossenbacher, P. Haffner, . . . A. Zuiderwijk Eds., Atlas of Amphibians and Reptiles in Europe.Paris: Societas Europaea Herpetologica and Museum National d'Histoire Naturelle, IEGB/SPN., pp. 178-179.

Cheylan, M. 2001. Testudo hermanni Gmelin, 1789: Griechische Landschildkröte. In U. Fritz Ed., Handbuch der Reptilien und Amphibien Europas.Wiebelsheim: Aula-Verlag. d. 3/IIIA, Schildkröten I.

Djordjević, S., Đurakić, M., Golubović, A., Ajtić, R., Tomović, Lj., & Bonnet, X. 2011. Sexual body size and body shape dimorphism of Testudo hermanni in centarl and eastern Serbia. Amphibia-Reptilia, 32, pp. 445-458.

Djordjević, S., Tomović, Lj., Golubović, A., Simović, A., Sterijovski, M., Đurakić, M., & Bonnet, X. 2013. Geographic (in-) variability of gender-specific traits in Hermann's tortoise. Herpetological Journal, 23, pp. 67-74.

Fritz, U., Auer, M., Bertolero, A., Cheylan, M., Fattizzo, T., Hundsdorfer, A.K., . . . Wink, M. 2006. A rangewide phylogeography of Hermann's tortoise, Testudo hermanni (Reptilia: Testudines: Testudinidae): Implications for taxonomy. Zoologica Scripta, 35(5), pp. 531-543. doi:10.1111/j.1463-6409.2006.00242.x

Golubović, A., Bonnet, X., Djordjević, S., Djurakić, M., & Tomović, Lj. 2013. Variations in righting behaviour across Hermann's tortoise populations. Journal of Zoology, 291(1), pp. 69-75.

Guyot, G., & Devaux, B. 1997. Variation in shell morphology and color of Hermann's tortoise, Testudo hermanni, in southern Europe. Chelonian Conservation and Biology, 2, pp. 390-395.

Ljubisavljević, K., Džukić, G., Vukov, D.T., & Kalezić, L.M. 2014. Distribution patternsof Hermann's Tortoise Testudo hermanni Gmelin, 1789, in the region of former Yugoslavia (Testudines: Testudinidae). Herpetozoa, 26(3-4), pp. 125-138.

Ljubisavljević, K., Vukov, T., Džukić, G., & Kalezić, M. 2012. Morphological variability of the Hermann's tortoise (Testudo hermanni) in the Central Balkans. Acta Herpetologica, 7(2), pp. 253-262.

Stubbs, D., Hailey, A., Pulford, E., & Tyler, W. 1984. Population ecology of European tortoise: Review of field techniques. Amphibia-Reptilia, 5, pp. 57-68.

Tomović, Lj., Ajtić, R., Ljubisavljević, K., Urošević, A., Jović, D., Krizmanić, I., . . . Džukić, G. 2014. Reptiles in Serbia: Distribution and diversity patterns. Bulletin of the Natural History Museum, 7, pp. 129-158.

Willemsen, R.E., & Hailey, A. 1999. Variation of adult body size of the tortoise Testudo hermanni in Greece: Proximate and ultimate causes. Journal of Zoology, 248, pp. 379-396.

Willemsen, R.E., & Hailey, A. 2003. Sexual dimorphism of body size and shell shape in European tortoises. Journal of Zoology, 260, pp. 353-365.

* E-mail: nenad.labus@pr.ac.rs

UNIVERSITY THOUGHT
Publication in Natural Sciences, Vol. 6, N^{o} 1, 2016, pp. 5-20.
doi:10.5937/univtho6-10562
Original Scientific Paper

ZOOGEOGRAPHICAL REGIONALIZATION OF THE SERBIA ACCORDING TO THE AFFINITY OF LOCAL FAUNAS OF THE SKIPPERS AND BUTTERFLIES (LEPIDOPTERA: HESPERIOIDEA & PAPILIONOIDEA)

Predrag Jakšić[1*]

[1]Faculty of Sciences and Mathematics, University of Niš, Niš, Serbia.

ABSTRACT

Integrated list of skippers and butterflies of Serbia is shown. We also conducted faunal analyses of established species. Based on previous research, some regions have been identified as center of certain faunal groups. Degree of similarity of selected areas is established by Jaccard index method. By Cluster analyses has identified links between isolated areas. Specific faunal elements of certain areas have been separated – they are diferencial species. Summerazing the obtain results, zoogeographical map of the skippers and butterflies of Serbia is done.

Key words: butterflies, faunal elements, zogeography, Serbia

1. INTRODUCTION

According to modern concept, diversity center of Lepidoptera in Palaearctic area is Western China. This area was settled by ancestor line from Gondvana (Varga, 2002). That is where migration and diversification began. Thanks to that greatest number of European skippers and butterflies belong to Palaearctic species group. East Asia species using the northern route (closed forest habitat) are indicated as Arboreal. East Asia species using the southern route (open habitats) are indicated as Oreal. Balkan Peninsula has been inhabited by both groups. That process has been repeated on several occasions from several directions. The success of migration depended on local environmental factors. Jagged territory enabled survival of species of different affinities. Thanks to that, particular territory has specific assemblage of species. That is, we talk about "faunal elements".

The main zoogeographical task is to establish faunal and areal elements of certain groups. Based on that, further on, zoogeographical data chart can be done.

The skippers and butterfliy faunal element research and definition has a long tradition. The first significant contribution was given by (Pagenstecher, 1909), than (Hormuzaki, 1929, 1930), (Rebel, 1932-33) as the leading expert of that time was first to conduct faunal analyses of skippers and butterflies of Balkan Peninsula. After Rebel several authors (see references: Annotated Bibliography) have contributed faunal elements definition. In this paper we addopted the system given by (Kudrna et al., 2015).

Vegetation and phytogeographic chart was first done by (Adamović, 1907), followed by Fukarek and (Jovanović, 1983), (Gajić, 1984) and (Stevanović et al., 1995).

The first zoogeographic chart of Serbia was done by (Kobelt, 1904) based on Mollusca. He singled out three provinces: Carpathian-Transilvanian, North Balkan as well as Albanian-Macedonian. Some times later (Pavlović, 1912), based on snail studies of Serbia in that time, singled out five provinces. The first zoogeographic chart of entire contemporary Serbian territory, was done by (Hadži, 1931) based on cryptobiotic species study. Finaly, (Matvejev, 1968) did zoogeographic chart of Serbia based on birds distribution.

Having that in mind we can come up with an assumption (as antithesis) that Serbia has skippers and butterflies with heterogenus composition and historically conditioned disposition and in a compliance with current ecological condition. Accordingly, Serbian territory in a sense of zoogeography, is not homogenus but with clearly distinguished areas.

2. MATERIALS AND METHODS

In order to answer these questions eleven provinces on the territory of Serbia has been chosen.

Faunistic data were taken from the existing literature (Tab. 1).

(Jaccard's, 1902) index was used to present the degree of dissimilarity between zoogeographic regions: R= 100 C/A+B - C

where:

A = number of species in the richest fauna;

B = number of species in the poorest fauna;

C = number of species common to both faunas.

For agglomerate clustering, UPGMA method were used (Sokal and Rohlf, 1995). Estimations were done using the program FLORA (Karadžić and Marinković, 2009).

3. RESULTS

Based on previous studies of butterfly fauna of Serbia (Tab. 1) list of established species has been done. Distribution of species is shown broken into 11 areas, that are set aside on basis of previous findings. Faunistic affiliation of each species is added, according to (Kudrna et al., 2015).

Table 1. List of provinces and previous papers on distribution of butterflies in Serbia.

No.	Provinces	Data for Butterflies (References)
1	Pannonicum	Andjus, 2008; Jakšić i Nahirnić, 2011; Jakšić et al., 2008; Lorković und Siladjev, 1982; Popović et al., 2014.
2	Dacicum	Andjus, 2008; Zečević, 2002.
3	Carpathicum	Gradojević,1930-31; Jakšić, 2006.; Zečević, 2002; Živojinović,1950.
4	Moesicum	Jakšić, 2011; Popović i Đurić, 2014; Swaay et al., 2007; Tuleschkow,1932.
5	W-Rhodope	Jakšić, 2003; Nahirnić, 2011; Swaay et al., 2007.
6	Serbicum	Gradojević,1930-31; Jakšić, 2015.
7	Dinaricum (Illyricum)	Dodok, 2003; Đurić & Franeta, 2011; Jakšić, 2011; Jakšić i Nahirnić, 2014.; Nahirnić et al. 2015.
8	Bertiscum	Jakšić, 2003-
9	Scardicum	Jakšić, 1998.
10.	10a. Sub-Aegean 10b. Sub-Adriaticum	Jakšić, 1986; Jakšić & Ristić, 1999; Kogovšek et al., 2012; Popović et al., 2014; Swaay et al., 2007.
11.	Ponišavlje	Popović i Đurić, 2014; Todorova, und Petkoff, P., 1915

Table. 2. List of butterfly species recorded in Serbia. Faunal elements according to (Kudrna et al., 2015).

		FAUNAL ELEMENTS (Kudrna, Pennerstorfer & Lux, 2015)	**1. PANNONICUM**	**2. DACICUM**	**3. CARPATHICUM**	**4. MOESICUM**	**5. W-RHODOPE**	**6. SERBICUM**	**7. DINARICUM (Illyricum)**	**8. BERTISCUM**	**9. SCARDICUM**	**10+11. FRAGMENTATED AREAS**
	LEPIDOPTERA											
	HESPERIOIDEA											
	HESPERIIDAE											
1	*Erynnis tages* (Linnaeus, 1758)	ES	1	1	1	1	1	1	1	1	1	1
2	*Carcharodus alceae* (Esper, 1780)	Med	1	1	1	1	1	1	1	1	1	1
3	*Carcharodus lavatherae* (Esper, 1783)	EM	1	1	0	1	0	1	1	0	0	1
4	*Carcharodus flocciferus* (Zeller, 1847)	EO	1	0	1	1	0	1	1	0	1	0
5	*Spialia phlomidis* (Herrich-Schäffer, 1845)	EO	0	0	0	0	0	0	1	0	0	1
6	*Spialia orbifer* (Hübner, 1823)	EO	1	1	0	1	1	1	1	1	1	0
7	*Syrichtus proto* (Ochsenheimer, 1808)	EO	0	0	0	0	0	0	0	0	1	0
8	*Syrichtus cribrellum* (Eversmann, 1841)	ES	0	0	0	0	0	0	0	0	0	1
9	*Pyrgus carthami* (Hübner, 1813)	EO	1	0	1	1	1	1	1	0	0	0
10	*Pyrgus sidae* (Esper, 1782)	EO	0	0	0	1	1	1	0	0	1	0
11	*Pyrgus andromedae* (Wallengren, 1853)	BM	0	0	0	0	0	0	0	0	1	0
12	*Pyrgus malvae* (Linnaeus, 1758)	ES	1	1	1	1	1	1	1	1	1	1

13	*Pyrgus serratulae* (Rambur, 1840)	ES	1	0	0	1	0	1	1	1	0	0
14	*Pyrgus cinarae* (Rambur, 1840)	EO	0	0	0	0	0	0	0	0	0	1
15	*Pyrgus armoricanus* (Oberthur, 1910)	EO	1	1	1	1	0	1	1	1	1	0
16	*Pyrgus alveus* (Hübner, 1803)	ES	1	0	1	1	0	1	1	1	1	0
17	*Pyrgus trenbevicensis* (Warren, 1926)	ES	0	0	1	0	0	0	1	0	0	0
18	*Heteropterus morpheus* (Pallas, 1771)	ES	0	0	1	0	0	1	1	0	0	0
19	*Carterocephalus palaemon* (Pallas, 1771)	Hol	0	0	0	1	0	1	1	1	0	1
20	*Thymelicus lineola* (Ochsenheimer, 1806)	Hol	0	0	1	1	1	1	1	1	1	1
21	*Thymelicus sylvestris* (Poda, 1761)	EO	1	0	1	1	1	1	1	1	0	0
22	*Thymelicus acteon* (Rottemburg, 1775)	EO	0	0	1	1	1	1	0	0	0	0
23	*Hesperia comma* (Linnaeus, 1758)	Hol	1	0	1	1	0	1	1	1	1	0
24	*Ochlodes sylvanus* (Esper, 1777*)*	ES	1	1	1	1	1	1	1	1	1	1
	PAPILIONOIDEA											
	PAPILIONIDAE											
25	*Zerynthia polyxena* (Schiffermüller, 1775)	EO	1	0	0	1	1	1	1	0	1	0
26	*Zerynthia cerisy* (Godart, 1822)	EO	0	1	1	1	1	0	0	0	0	1
27	*Parnassius mnemosyne* (Linnaeus, 1758)	EO	1	0	1	1	1	1	1	1	1	1
28	*Parnassius apollo* (Linnaeus, 1758)	ES	0	0	1	1	0	0	1	1	1	0
29	*Iphiclides podalirius* (Linnaeus, 1758)	ES	1	1	1	1	1	1	1	1	1	1
30	*Papilio machaon* (Linnaeus, 1758)	ES	1	1	1	1	1	1	1	1	1	1
	PIERIDAE											
31	*Leptidea sinapis* (Linnaeus, 1758) complex	ES	1	1	1	1	1	1	1	1	1	1
32	*Leptidea reali* (Reissinger, 1989) – *juvernica* Williams, 1946 complex	ES	0	0	1	1	1	1	1	1	1	1
33	*Leptidea duponcheli* (Staudinger, 1871)	EO	0	0	0	0	1	1	0	1	0	1
34	*Leptidea morsei* (Fenton, 1882)	ES	1	0	0	0	0	0	0	0	0	0
35	*Anthocharis cardamines* (Linnaeus, 1758)	ES	1	1	1	1	1	1	1	1	1	1
36	*Anthocharis gruneri* (Herrich-Schäffer, 1851)	EO	0	0	0	0	0	0	0	0	0	1
37	*Euchloe ausonia* (Hübner, 1806) complex	Med	1	1	0	0	0	0	0	0	0	1
38	*Aporia crataegi* (Linnaeus, 1758)	ES	1	1	1	1	1	1	1	0	1	1
39	*Pieris brassicae* (Linnaeus, 1758)	ES	1	1	1	1	1	1	1	1	1	1
40	*Pieris mannii* (Mayer, 1851)	EO	0	1	1	1	0	0	1	1	1	0
41	*Pieris rapae* (Linnaeus, 1758)	Hol	1	1	1	1	1	1	1	1	1	1
42	*Pieris ergane* (Geyer, 1828)	EO	0	0	0	1	0	1	1	1	1	0
43	*Pieris napi* (Linnaeus, 1758)	ES	1	1	1	1	1	1	1	1	1	1
44	*Pieris balcana* (Lorković, 1968)	ES	0	0	0	0	0	1	1	1	1	0
45	*Pontia edusa* (Fabricius, 1777)	ES	1	0	1	1	0	1	1	1	1	0
46	*Colias erate* (Esper, 1803)	ES	1	1	1	0	1	0	0	0	0	1
47	*Colias crocea* (Fourcroy, 1785)	EO	1	1	1	1	1	1	1	1	1	1
48	*Colias myrmidone* (Esper, 1781)	EO	1	1	1	0	0	0	0	0	0	0
49	*Colias balcanica* (Rebel, 1903)	Mon	0	0	0	0	0	0	1	0	0	0
50	*Colias hyale* (Linnaeus, 1758)	ES	1	1	1	1	1	1	1	1	1	1
51	*Colias alfacariensis* (Ribbe, 1905)	EO	1	1	1	1	1	1	1	1	1	1
52	*Gonepteryx rhamni* (Linnaeus, 1758)	ES	1	1	1	1	1	1	1	1	1	1
	RIODINIDAE											
53	*Hamearis lucina* (Linnaeus, 1758)	EM	1	1	1	1	1	1	1	1	1	1
	LYCAENIDAE											
54	*Lycaena phlaeas* (Linnaeus, 1761)	Hol	1	1	1	1	1	1	1	1	1	1
55	*Lycaena helle* (Schiffermüller, 1775)	ES	0	0	0	1	o	0	0	0	0	0
56	*Lycaena dispar* (Haworth, 1802)	ES	1	1	1	1	1	1	1	1	1	1
57	*Lycaena virgaureae* (Linnaeus, 1758)	ES	0	0	1	1	1	0	1	1	1	1
58	*Lycaena tityrus* (Poda, 1761)	ES	1	1	1	1	1	1	1	1	1	1
59	*Lycaena alciphron* (Rottemburg, 1775)	EO	0	1	1	1	1	1	1	1	1	0
60	*Lycaena hippothoe* (Linnaeus, 1760)	ES	0	0	0	0	0	0	1	0	0	0
61	*Lycaena candens* (Herrich-Schäffer, 1844)	Mon	0	0	1	1	0	0	1	1	1	0
62	*Lycaena thersamon* (Esper, 1784)	EO	0	0	1	1	1	1	1	1	1	1
63	*Thecla betulae* (Linnaeus, 1758)	ES	0	1	0	1	1	1	1	0	1	0
64	*Favonius quercus* (Linnaeus, 1758)	EO	1	1	1	1	1	1	1	1	1	0
65	*Callophrys rubi* (Linnaeus, 1758)	ES	1	1	1	1	1	1	1	1	1	1
66	*Satyrium w-album* (Knoch, 1782)	ES	1	1	0	1	0	1	1	1	1	0

67	*Satyrium pruni* (Linnaeus, 1758)	ES	1	1	0	1	0	1	1	0	1	0
68	*Satyrium spini* (Fabricius, 1787)	EO	1	1	1	1	1	1	1	1	1	0
69	*Satyrium ilicis* (Esper, 1779)	EO	0	1	0	1	1	1	1	1	1	0
70	*Satyrium acaciae* (Fabricius, 1787)	EO	1	1	1	1	1	1	1	1	0	1
71	*Lampides boeticus* (Linnaeus, 1767)	Tro	0	0	0	1	0	1	1	1	0	0
72	*Leptotes pirithous* (Linnaeus, 1767)	Tro	0	1	0	1	1	1	1	0	1	0
73	*Cupido minimus* (Fuessly, 1775)	ES	1	0	1	1	1	0	1	1	1	1
74	*Cupido osiris* (Meigen, 1829)	EO	0	0	1	1	0	1	1	0	1	1
75	*Cupido argiades* (Pallas, 1771)	Hol	1	0	1	1	1	1	1	0	0	1
76	*Cupido decolorata* (Staudinger, 1886)	EM	0	0	1	1	0	1	1	0	1	1
77	*Cupido alcetas* (Hoffmannsegg, 1803)	ES	1	1	1	1	0	1	1	0	1	1
78	*Celastrina argiolus* (Linnaeus, 1758)	ES	1	1	1	1	1	1	1	1	1	1
79	*Pseudophilotes vicrama* (Moore, 1865)	EO	0	0	0	1	1	1	1	0	1	1
80	*Pseudophilotes bavius* (Eversmann, 1832)	EM	0	0	0	0	0	0	0	1	1	0
81	*Scolitantides orion* (Pallas, 1771)	ES	0	1	1	1	1	0	1	1	1	1
82	*Glaucopsyche alexis* (Poda, 1761)	ES	1	1	0	1	0	1	1	1	1	1
83	*Iolana iolas* (Ochsenheimer, 1816)	EO	0	0	0	0	1	1	1	0	1	0
84	*Phengaris arion* (Linnaeus, 1758)	ES	0	1	1	1	0	1	1	1	1	1
85	*Phengaris teleius* (Bergsträsser, 1779)	ES	1	0	0	0	0	0	0	0	0	0
86	*Phengaris alcon* (Schiffermüller, 1775)	ES	0	0	0	1	1	1	1	1	1	0
87	*Kretania pylaon* (Fischer, 1832) complex	ES	1	0	1	1	0	1	1	0	0	0
88	*Plebeius argus* (Linnaeus, 1758)	ES	1	1	1	1	1	1	1	1	1	1
89	*Plebeius idas* (Linnaeus, 1760)	Hol	1	1	1	1	1	1	1	1	1	1
90	*Plebeius argyrognomon* (Bergsträsser, 1779)	ES	1	0	0	1	0	1	1	1	1	1
91	*Agriades optilete* (Knoch, 1781)	BM	0	0	0	0	0	0	0	0	1	0
92	*Eumedonia eumedon* (Esper, 1780)	ES	0	0	0	1	0	1	1	0	1	0
93	*Aricia agestis* (Schiffermüller, 1775)	ES	1	1	1	1	1	1	1	1	1	1
94	*Aricia artaxerxes* (Fabricius, 1793)	BM	0	1	0	1	1	1	1	1	1	0
95	*Aricia anteros* (Freyer, 1838)	Mon	0	0	1	1	0	0	1	1	1	1
96	*Cyaniris semiargus* (Rottemburg, 1775)	ES	1	1	1	1	1	1	1	1	1	1
97	*Polyommatus escheri* (Hübner, 1823)	EM	0	0	0	0	0	0	1	0	1	0
98	*Polyommatus dorylas* (Schiffermüller, 1775)	EO	0	0	1	1	1	0	1	1	1	0
99	*Polyommatus icarius* (Esper, 1789) *(syn. amandus)*	ES	1	0	0	1	1	1	1	0	1	1
100	*Polyommatus thersites* (Cantener, 1834)	ES	0	0	1	1	1	1	0	1	1	0
101	*Polyommatus icarus* (Rottemburg, 1775)	ES	1	1	1	1	1	1	1	1	1	1
102	*Polyommatus eros* (Ochsenheimer, 1808)	ES	0	0	1	1	0	0	1	0	1	0
103	*Polyommatus daphnis* (Schiffermüller, 1775)	EO	0	1	1	1	1	1	1	1	1	1
104	*Polyommatus bellargus* (Rottemburg, 1775)	EO	1	1	1	1	1	1	1	1	1	0
105	*Polyommatus coridon* (Poda, 1761)	EO	1	1	1	1	0	1	1	1	1	1
106	*Polyommatus admetus* (Esper, 1783)	EO	0	0	0	1	1	1	0	0	1	0
107	*Polyommatus ripartii* (Freyer, 1830)	EO	0	0	0	1	0	1	0	1	0	0
108	*Polyommatus damon* (Schiffermüller, 1775)	ES	0	0	0	0	0	0	0	1	1	1
	NYMPHALIDAE											
109	*Libythea celtis* (Laicharting, 1782)	EO	1	1	0	0	0	0	1	1	1	1
110	*Argynnis paphia* (Linnaeus, 1758)	ES	1	1	1	1	1	1	1	1	1	1
111	*Argynnis pandora* (Schiffermüller, 1775)	EO	1	1	1	1	0	1	1	1	1	0
112	*Argynnis aglaja* (Linnaeus, 1758)	ES	1	1	1	1	1	1	1	1	1	0
113	*Argynnis adippe* ([Schiffermüller], 1775)	ES	0	1	1	1	1	1	1	1	1	0
114	*Argynnis niobe* (Linnaeus, 1758)	ES	0	1	1	1	1	1	1	1	1	0
115	*Issoria lathonia* (Linnaeus, 1758)	ES	1	1	1	1	1	1	1	1	1	1
116	*Brenthis ino* (Rottemburg, 1775)	ES	0	0	0	1	0	0	0	0	0	0
117	*Brenthis daphne* (Bergsträsser, 1780)	ES	1	1	1	1	1	1	1	1	1	1
118	*Brenthis hecate* (Schiffermüller, 1775)	ES	0	1	1	1	1	1	1	0	1	0
119	*Boloria eunomia* (Esper, 1799)	Hol	0	0	1	1	1	0	0	0	0	0
120	*Boloria euphrosyne* (Linnaeus, 1758)	ES	0	0	1	1	1	1	1	1	1	1
121	*Boloria titania* (Esper, 1793)	Hol	0	0	0	0	0	0	1	1	1	0
122	*Boloria selene* (Schiffermüller, 1775)	Hol	0	0	1	1	0	0	1	0	0	0
123	*Boloria dia* (Linnaeus, 1767)	ES	1	1	1	1	1	1	1	1	1	1
124	*Boloria pales* (Schiffermüller, 1775)	Mon	0	0	0	0	0	0	0	1	1	0
125	*Boloria graeca* (Staudinger, 1870)	Mon	0	0	0	0	0	0	0	1	1	0
126	*Vanessa atalanta* (Linnaeus, 1758)	Hol	1	1	1	1	1	1	1	1	1	1

127	*Vanessa cardui* (Linnaeus, 1758)	Cos	1	1	1	1	1	1	1	1	1	1
128	*Aglais io* (Linnaeus, 1758)	ES	1	1	1	1	1	1	1	1	1	1
129	*Aglais urticae* (Linnaeus, 1758)	ES	1	1	1	1	1	1	1	1	1	1
130	*Polygonia c-album* (Linnaeus, 1758)	ES	1	1	1	1	1	1	1	1	1	1
131	*Polygonia egea* (Cramer, 1775)	EO	0	1	0	1	0	0	0	0	0	1
132	*Araschnia levana* (Linnaeus, 1758)	ES	1	0	1	1	1	1	1	0	1	1
133	*Nymphalis antiopa* (Linnaeus, 1758)	Hol	1	1	1	1	1	1	1	1	1	1
134	*Nymphalis polychloros* (Linnaeus, l758)	EO	1	1	1	1	1	1	1	1	1	1
135	*Nymphalis xanthomelas* (Esper, [1781])	ES	0	1	0	1	0	1	1	0	0	0
136	*Nymphalis l-album* (Esper, 1780)	ES	0	1	0	1	0	1	1	0	0	0
137	*Euphydryas maturna* (Linnaeus, 1758)	ES	0	1	0	0	0	0	1	1	0	1
138	*Euphydryas aurinia* (Rottemburg, 1775)	ES	0	0	0	0	0	0	1	0	0	0
139	*Melitaea cinxia* (Linnaeus, 1758)	ES	1	1	1	1	1	1	1	0	1	1
140	*Melitaea phoebe* (Goeze, 1779) complex	ES	1	1	1	1	0	1	1	1	1	1
141	*Melitaea arduinna* (Esper, 1784)	EO	0	0	1	1	1	0	0	0	0	0
142	*Melitaea trivia* (Schiffermüller, 1775)	EO	0	1	1	1	1	1	1	1	1	0
143	*Melitaea didyma* (Esper, 1779)	ES	1	0	1	1	1	1	1	1	1	1
144	*Melitaea diamina* (Lang, 1789)	ES	0	1	0	1	0	1	1	1	0	0
145	*Melitaea aurelia* (Nickerl, 1850)	EO	1	1	1	1	1	1	1	0	0	0
146	*Melitaea athalia* (Rottemburg, 1775)	ES	1	1	1	1	1	1	1	1	1	1
147	*Melitaea ornata* (Christoph, 1893)	ES	0	0	0	1	0	0	0	0	0	0
148	*Limenitis populi* (Linnaeus, 1758)	ES	1	1	1	1	1	0	1	1	1	1
149	*Limenitis camilla* (Linnaeus, 1764)	ES	1	0	1	1	1	1	1	1	0	0
150	*Limenitis reducta* (Staudinger, 1901)	EO	1	0	1	1	1	1	1	1	1	0
151	*Neptis sappho* (Pallas, 1771)	ES	1	1	1	1	1	1	1	1	0	1
152	*Neptis rivularis* (Scopoli, 1763)	ES	0	0	1	1	0	1	1	1	1	0
153	*Apatura metis* (Freyer, 1829)	ES	1	0	0	0	0	0	0	0	0	0
154	*Apatura ilia* (Schiffermüller, 1775)	ES	1	1	1	1	1	1	1	1	1	1
155	*Apatura iris* (Linnaeus, 1758)	ES	1	1	1	1	1	1	1	1	1	1
156	*Kirinia roxelana* (Cramer, 1777)	EO	0	0	1	1	1	1	0	0	0	0
157	*Kirinia climene* (Esper, 1784)	EO	0	0	1	1	1	0	0	0	0	0
158	*Pararge aegeria* (Linnaeus, 1758)	EO	1	1	1	1	1	1	1	1	1	1
159	*Lasiommata megera* (Linnaeus, 1767)	EO	1	1	1	1	1	1	1	1	1	1
160	*Lasiommata petropolitana* (Fabricius, 1787)	ES	0	0	0	1	0	0	1	1	1	0
161	*Lasiommata maera* (Linnaeus, 1758)	ES	1	1	1	1	1	1	1	1	1	1
162	*Lopinga achine* (Scopoli, 1763)	ES	0	0	1	0	0	0	0	0	0	0
163	*Coenonympha rhodopensis* (Elwes, 1900)	Med	0	0	0	1	1	0	1	1	1	0
164	*Coenonympha arcania* (Linnaeus, 1760)	EM	1	1	1	1	1	1	1	1	1	1
165	*Coenonympha glycerion* (Borkhausen, 1788)	ES	1	0	0	1	1	1	1	0	0	0
166	*Coenonympha orientalis* (Rebel, 1910)	Mon	0	0	0	0	0	0	1	1	0	0
167	*Coenonympha leander* (Esper, 1784)	EO	0	1	1	1	1	1	1	0	1	1
168	*Coenonympha pamphilus* (Linnaeus, 1758)	EO	1	1	1	1	1	1	1	1	1	1
169	*Pyronia tithonus* (Linnaeus, 1771)	EM	0	1	1	1	1	1	1	1	1	0
170	*Aphantopus hyperantus* (Linnaeus, 1758)	ES	1	1	1	1	1	1	1	1	1	1
171	*Maniola jurtina* (Linnaeus, 1758)	ES	1	1	1	1	1	1	1	1	1	1
172	*Hyponephele lycaon* (Kühn, 1774)	ES	1	0	1	1	0	1	1	1	1	0
173	*Hyponephele lupina* (Costa, 1836)	ES	0	0	0	0	0	1	0	0	1	0
174	*Erebia ligea* (Linnaeus, 1758)	ES	0	1	1	1	0	0	1	1	1	0
175	*Erebia euryale* (Esper, 1805)	Mon	0	0	0	1	0	0	1	1	1	0
176	*Erebia manto* (Schiffermüller, 1775)	Mon	0	0	0	0	0	0	0	1	0	0
177	*Erebia epiphron* (Knoch, 1783)	Mon	0	0	0	0	0	0	0	1	1	0
178	*Erebia orientalis* (Elwes, 1909)	Mon	0	0	0	1	0	0	0	0	0	0
179	*Erebia aethiops* (Esper, 1777)	EO	0	0	1	1	0	0	1	1	0	0
180	*Erebia medusa* (Fabricius, 1787)	ES	0	1	1	1	1	1	1	1	1	1
181	*Erebia albergana* (Prunner, 1798)	Mon	0	0	0	1	0	0	0	0	0	0
182	*Erebia gorge* (Esper, 1805)	Mon	0	0	0	0	0	0	0	0	1	0
183	*Erebia rhodopensis* (Nicholl, 1900)	Mon	0	0	0	0	0	0	0	1	1	0
184	*Erebia ottomana* (Herrich-Schäffer, 1847)	Mon	0	0	0	1	0	0	1	1	1	0
185	*Erebia cassioides* (Reiner & Hochenwarth, 1792)	Mon	0	0	0	0	0	0	0	1	1	0
186	*Erebia pronoe* (Esper, 1780)	Mon	0	0	0	0	0	0	0	1	1	0
187	*Erebia melas* (Herbst, 1796)	Mon	0	0	0	0	0	0	0	1	1	0

188	*Erebia oeme* (Hübner, 1804)	Mon	0	0	0	1	0	0	0	1	1	0
189	*Erebia pandrose* (Borkhausen, 1788)	BM	0	0	0	0	0	0	0	1	1	0
190	*Melanargia galathea* (Linnaeus, 1758)	EO	1	1	1	1	1	1	1	1	1	1
191	*Melanargia larissa* (Esper, 1784)	EO	0	0	1	0	0	0	1	0	1	1
192	*Satyrus ferula* (Fabricius, 1793)	EO	0	0	0	1	0	0	1	1	0	0
193	*Minois dryas* (Scopoli, 1763)	ES	1	0	1	1	1	1	1	1	0	0
194	*Hipparchia fagi* (Scopoli, 1763)	EM	0	1	0	1	0	1	1	0	1	0
195	*Hipparchia syriaca* (Staudinger, 1871)	EO	0	0	0	0	0	1	1	0	0	0
196	*Hipparchia semele* (Linnaeus, 1758)	EM	1	1	1	1	0	0	0	0	0	1
197	*Hipparchia volgensis* (Mazochin-Porshnjakov, 1952)	EM	1	0	1	1	1	1	1	1	1	0
198	*Hipparchia statilinus* (Hufnagel, 1766)	EM	1	0	0	1	0	1	1	1	1	1
199	*Arethusana arethusa* (Schiffermüller, 1775)	EO	0	1	1	1	1	1	1	1	0	1
200	*Brintesia circe* (Fabricius, 1775)	EO	1	1	1	1	1	1	1	1	0	1
201	*Chazara briseis* (Linnaeus, 1764)	ES	1	0	1	1	0	1	1	1	1	0

Following procedure summarizes results of faunal origin analyses, which is shown in Tab. 3 and Fig. 1.

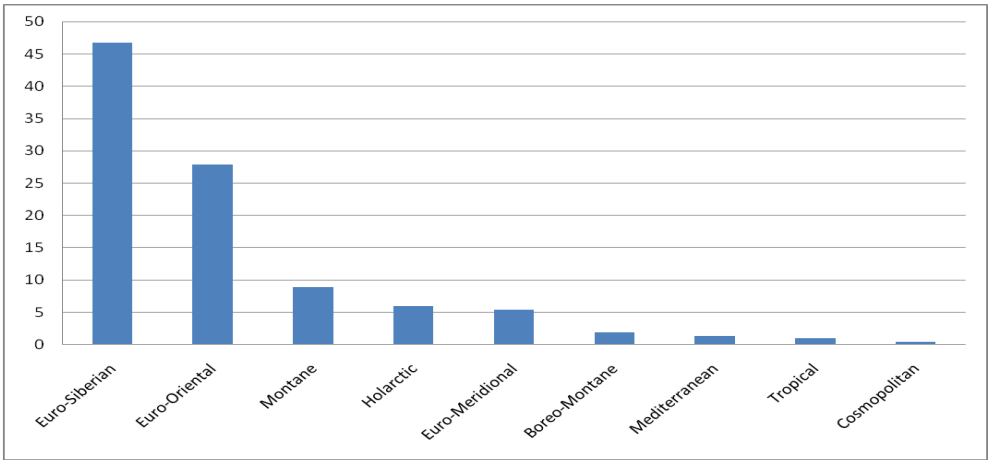

Fig. 1. Faunistic composition of Serbian butterflies.

Table. 3. Faunistic composition of Serbian butterflies: **ES** – Euro-Siberian, **EO** – Euro-Oriental, **Mon** – Montane, **Hol** – Holarctic, **EM** – Euro-Meridional, **BM** – Boreo-Montane, **Med** – Mediterranean, **Tro** – Tropical, **Cos** – Cosmopolitan.

	The assemblages of species ("faunal elements") of Serbian butterflies								
	ES	**EO**	**Mon**	**Hol**	**EM**	**BM**	**Med**	**Tro**	**Cos**
No.	94	56	18	12	11	4	3	2	1
%	46.76	27.86	8.95	5.97	5.47	1.9	1.4	1	0.5

Results show that 94 (46%) out of 201 established butterfly species belong to Euro-Siberian faunal elements. Besides them Euro-Oriental elements stand out with 56 (27%) species. The other seven groups of faunal elements together make up only1/4 species in butterfly fauna of Serbia.

Further procedure analyses degree of closiness/difference between 11 appointed regions, comparing number of common species (Tab. 4). The results show that list number of common species in Pannonicum and Dacicum area compared to other areas. This is understandable because it is about fauna of plains, with modified steppa character versus hill-mountain fauna areas with primary forest vegetation. Large mountain ranges of Serbia have the largest number of common species, resulting in greatest number of habitats. Additionaly the value has been enlarged by dominant Euro-Siberian species as most represented one in that area.

Table. 4. An overview of a total number of butterfly species in the studied areas (A) and the number of species common to both faunas (C).

	A. TOTAL NO. OF SPECIES	C								
		2. DACICUM	3. CARPATHICUM	4. MOESICUM	5. W-RHODOPE	6. SERBICUM	7. DINARICUM (Illyricum)	8. BERTISCUM	9. SCARDICUM	10 + 11. FRAGM. AREAS
1. PANNONICUM	**102**	70	85	94	74	88	98	79	78	68
2. DACICUM	**99**		81	92	78	87	89	77	83	73
3. CARPATHICUM	**124**			119	92	102	112	96	101	77
4. MOESICUM	**159**				108	127	139	114	119	81
5. W-RHODOPE	**111**					95	98	85	92	68
6. SERBICUM	**135**						126	102	107	76
7. DINARICUM (Illyricum)	**156**							113	124	85
8. BERTISCUM	**134**								113	76
9. SCARDICUM	**144**									78
10+11. FRAGMENT. AREAS	**97**									-

Table. 5. The degree of similarity coefficient (%) of the butterfly fauna in the analyzed areas obtained by Jaccard's coefficient.

	2. DACICUM	3. CARPATHICUM	4. MOESICUM	5. W-RHODOPE	6. SERBICUM	7. DINARICUM (Illyricum)	8. BERTISCUM	9. SCARDICUM	10.+11. FRAGM. AREAS
1. PANNONICUM	53	60	56	53	59	61	50	46	52
2. DACICUM		57	55	59	59	53	49	52	59
3. CARPATHICUM			72	64	65	67	59	60	53
4. MOESICUM				67	76	79	64	65	46
5. W-RHODOPE					63	58	53	56	48
6. SERBICUM						76	61	62	49
7. DINARICUM (Illyricum)							64	70	50
8. BERTISCUM								68	49
9. SCARDICUM									48

Biology

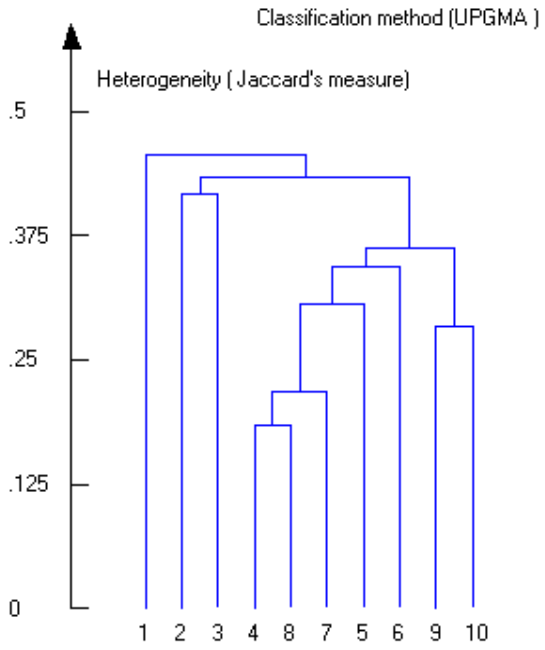

Fig. 2. Cluster tree of areas in Serbia according to composition of butterfly fauna.

Jaccard's coefficient analyses show the same value. The biggest difference exist between submediterranian and continental areas, as well as Pannonicum and Dacicum areas on one hand and inland on the other (Tab. 5).

In that sense Cluster analyses show clear confines within analyzed areas – four clusters. On the other hand, Cluster analyzes indicate mutual proximity of some regions within given Cluster (Fig. 2; Tab. 6). For example, it is completely normal for Pannonia region and Dacia area to be in the same Cluster, the same goes for Šar-Planina Mt. (Scardicum) area and Prokletije Mt. (Bertiscum).

As it is shown in Tab. 4 and Tab. 5 the exsistence of large number of common species in compared areas disables their zoogeographical separation. Actually, this fact indicates that analyzed area belongs to same zoogeographical unit of higher order. However, for zoogeographical separation into low order units, differential species can serve the purpose. These are the specific elements of fauna, usually presented in one area (Tab. 7).

Table. 6. Belonging to the clusters of selected regions in Serbia.

Cluster 1	Cluster 2	Cluster 3	Cluster 4
1. Fragment. areas: 10a. Sub-Aegean 10b. Sub-Adriaticum 11. Ponišavlje	2. Pannonicum 3. Dacicum	4. Moesicum 5. Carpathicum 6. W-Rhodope 7. Serbicum 8. Dinaricum (Illyricum)	9. Bertiscum 10. Scardicum

Table. 7. Differential species (specific faunal elements) of certain regions.

		FAUNAL ELEMENTS (Kudrna, Pennerstorfer & Lux, 2015)	**1. PANNONICUM**	**2. DACICUM**	**3. CARPATHICUM**	**4. MOESICUM**	**5. W-RHODOPE**	**6. SERBICUM**	**7. DINARICUM (Illyricum)**	**8. BERTISCUM**	**9. SCARDICUM**	**10 + 11. FRAGMENTATED AREAS**
	LEPIDOPTERA											
	HESPERIOIDEA											
	HESPERIIDAE											
7	*Syrichtus proto* (Ochsenheimer, 1808)	EO									1	
8	*Syrichtus cribrellum* (Eversmann, 1841)	ES										1
11	*Pyrgus andromedae* (Wallengren, 1853)	BM									1	
14	*Pyrgus cinarae* (Rambur, 1840)	EO										1

	PAPILIONOIDEA											
	PIERIDAE											
33	*Leptidea duponcheli* (Staudinger, 1871)	EO					1	1		1		1
34	*Leptidea morsei* (Fenton, 1882)	ES	1									
36	*Anthocharis gruneri* Herrich-Schäffer, 1851	EO										1
37	*Euchloe ausonia* (Hübner, 1806) complex	Med	1	1								1
48	*Colias myrmidone* (Esper, 1781)	EO	1	1	1							
49	*Colias balcanica* Rebel, 1903	Mon							1			
	LYCAENIDAE											
55	*Lycaena helle* (Schiffermüller, 1775)	ES				1						
80	*Pseudophilotes bavius* (Eversmann, 1832)	EM								1	1	
85	*Phengaris teleius* (Bergsträsser, 1779)	ES	1									
91	*Agriades optilete* (Knoch, 1781)	BM									1	
97	*Polyommatus escheri* (Hübner, 1823)	EM							1		1	
102	*Polyommatus eros* (Ochsenheimer, 1808)	ES			1	1			1		1	
108	*Polyommatus damon* (Schiffermüller, 1775)	ES								1	1	1
	NYMPHALIDAE											
116	*Brenthis ino* (Rottemburg, 1775)	ES				1						
119	*Boloria eunomia* (Esper, 1799)	Hol			1	1	1					
121	*Boloria titania* (Esper, 1793)	Hol							1	1	1	
122	*Boloria selene* (Schiffermüller, 1775)	Hol			1	1			1			
124	*Boloria pales* (Schiffermüller, 1775)	Mon								1	1	
125	*Boloria graeca* (Staudinger, 1870)	Mon								1	1	
131	*Polygonia egea* (Cramer, 1775)	EO		1		1						1
138	*Euphydryas aurinia* (Rottemburg, 1775)	ES							1			
141	*Melitaea arduinna* (Esper, 1784)	EO			1	1	1					
153	*Apatura metis* (Freyer, 1829)	ES	1									
157	*Kirinia climene* (Esper, 1784)	EO			1	1	1					
162	*Lopinga achine* (Scopoli, 1763)	ES			1							
166	*Coenonympha orientalis* (Rebel, 1910)	Mon							1	1		
173	*Hyponephele lupina* (Costa, 1836)	ES						1			1	
176	*Erebia manto* (Schiffermüller, 1775)	Mon								1		
177	*Erebia epiphron* (Knoch, 1783)	Mon								1	1	
178	*Erebia orientalis* (Elwes, 1909)	Mon				1						
181	*Erebia albergana* (Prunner, 1798)	Mon				1						
182	*Erebia gorge* (Esper, 1805)	Mon									1	
183	*Erebia rhodopensis* (Nicholl, 1900)	Mon								1	1	
184	*Erebia ottomana* (Herrich-Schäffer, 1847)	Mon				1			1	1	1	
185	*Erebia cassioides* (Reiner & Hochenwarth, 1792)	Mon								1	1	
186	*Erebia pronoe* (Esper, 1780)	Mon								1	1	
187	*Erebia melas* (Herbst, 1796)	Mon								1	1	
188	*Erebia oeme* (Hübner, 1804)	Mon				1				1	1	
189	*Erebia pandrose* (Borkhausen, 1788)	BM								1	1	
191	*Melanargia larissa* (Esper, 1784)	EO			1				1		1	1
195	*Hipparchia syriaca* (Staudinger, 1871)	EO						1	1			
196	*Hipparchia semele* (Linnaeus, 1758)	EM	1	1	1	1						1

There are 46(23%) of these specific faunal elements. Their mapping can regionalize Serbia zoogeographicaly (Fig. 3).

The question of demarcation level mark remains open. Clasification principles and demarcation level defined in details by (Fosberg & Pearsall, 1993). According to the modified Sclater-Wallace scheme of zoogeographical subdivision of land we have levels of Region-Subregion-Province.

Here separated entities could be identified as Province or Subprovince. In literature, the terms “Region”, “District”, “Area” etc. are also encountered for the same level of demarcation.

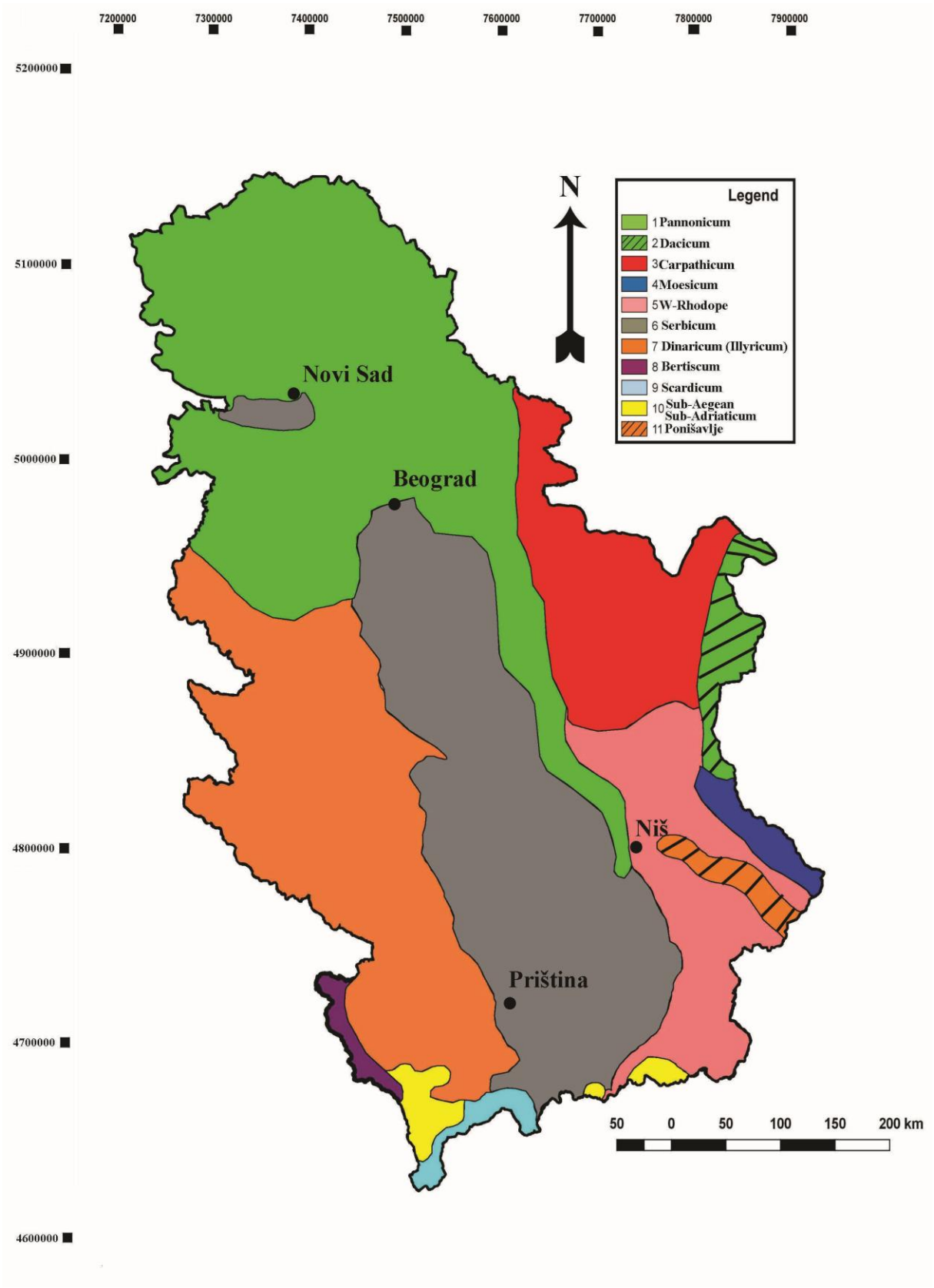

Fig. 3. Zoogeographical regionalization of the Serbia according to the affinity of local faunas of the butterflies (Lepidoptera: Hesperioidea & Papilionoidea). See text below for further details. (Drawn by PhD AleksandarValjarević using GIS software's QGIS 2.14.2 and Global Mapper V 17.1. Data for map using by professor PredragJakšić, and after that georectified and digitized in Transverse Mercator projection and WGS 84 datum.)

Biology

Main characteristics of selected provinces:

1. The Pannonicum Province

Geographically it extends to Pannonia and Peripannonia area comprising Vojvodina (except Fruška Gora Mt. and Vršac Mountains), Mačva and Morava Valley.

Fauna is poorer due to strong anthropogenic pressure.

Clima: Cfwb x″, where C = mild temperate-mesothermal climate; f = significant precipitation during all seasons; w = dry winters (in which the driest winter month average precipitation is less than one tenth the wettest summer month average precipitation); b = warmest month averaging below 22°C (but with at least 4 months averaging above 10°C); x″ = the second precipitation maximum occurs in autumn.

Natural Potential Vegetation: *Genisto-Quercetum roboris s. lat.; Festucion rupicolae Aceri tatarici-Quercetum.*

Dominant biome type:

Biomes of submediterranean broad-leaved woodlands and schrubs and Biomes of steppes and woodland steppes.

Typical species of butterflies: *Leptidea morsei* (Fenton, 1882), *Euchloe ausonia* (Hübner, 1806), *Colias erate* (Esper, 1803), *Colias myrmidone* (Esper, 1781), *Phengaris teleius* (Bergsträsser, 1779), *Apatura metis* (Freyer, 1829), *Hipparchia semele* (Linnaeus, 1758).

2. The Dacicum Province

It includes parts of Vlaska lowland in Serbia, in other words area of former Dacian Sea in Timok region, Ključ, and Vidin region.

Fauna is exceptionally poorer due to strong anthropogenic pressure.

Clima: Cfwax″, where C = mild temperate-mesothermal climate; f = significant precipitation during all seasons; w = dry winters (in which the driest winter month average precipitation is less than one tenth the wettest summer month average precipitation); a = warmest month averaging above 22°C; x″ = the second precipitation maximum occurs in autumn.

Natural Potential Vegetation: *Quercetum pedunculiflorae moesiacum.*

Dominant biome type:

Biomes of submediterranean broad-leaved woodlands and schrubs; Biomes of steppes and woodland steppes and Biomes of south-European mostly broad-leaved woodlands.

Typical species of butterflies: *Euchloe ausonia* (Hübner, 1806), *Colias erate* (Esper, 1803), *Colias myrmidone* (Esper, 1781), *Polygonia egea* (Cramer, 1775), *Melanargia larissa* (Esper, 1784), *Hipparchia semele* (Linnaeus, 1758).

3. The Carpathicum Province

Geographically it includes Vršac Mountains, Djerdap, Miroc, Homolje, Kucaj towards Rtanj Mt.

Clima: dominant Cfwbx″, where C = mild temperate-mesothermal climate; f = significant precipitation during all seasons; w = dry winters (in which the driest winter month average precipitation is less than one tenth the wettest summer month average precipitation); b = warmest month averaging below 22°C (but with at least 4 months averaging above 10°C); x″ = the second precipitation maximum occurs in autumn; as well as Dfwb x″.

Natural Potential Vegetation: *Fagetum montanum s. lat.*

Dominant biome type:

Biomes of south-European mostly broad-leaved woodlands.

Typical species of butterflies: *Colias myrmidone* (Esper, 1781), *Polyommatus eros* (Ochsenheimer, 1808), *Boloria eunomia* (Esper, 1799), *Boloria selene* (Schiffermüller, 1775), *Melitaea arduinna* (Esper, 1784), *Kirinia climene* (Esper, 1784), *Lopinga achine* (Scopoli, 1763), *Hipparchia semele* (Linnaeus, 1758).

4. The Moesicum Province

Geographically it includes Stara Planina Mt.

Clima: Dfwbx″, where D = continental-microthermal climate (a mean temperature above 10°C in the warmest months and a coldest month average below −3°C); f = significant precipitation during all seasons; w = dry winters (in which the driest winter month average precipitation is less than one tenth the wettest summer month average precipitation); b=warmest month averaging below 22°C (but with at least 4 months averaging above 10°C); x″ = the second precipitation maximum occurs in autumn.

Natural Potential Vegetation: *Abieti-Fagetum s. lat., Piceetum excelsae montanum s. lat., Piceetum excelsae subalpinum s. lat., Pinetum mugi s.lat.*

Dominant biome type:

Biomes of European mostly coniferous forests of boreal type, some with elements of broad-leaved forests.

Typical species of butterflies: *Lycaena helle* (Schiffermüller, 1775), *Polyommatus eros* (Ochsenheimer, 1808), *Brenthis ino* (Rottemburg, 1775), *Boloria eunomia* (Esper, 1799), *Boloria selene* (Schiffermüller, 1775), *Polygonia egea* (Cramer, 1775), *Melitaea arduinna* (Esper, 1784), *Kirinia climene* (Esper, 1784), *Erebia orientalis* Elwes, 1909, *Erebia albergana* (Prunner, 1798), *Erebia ottomana* (Herrich-Schäffer, 1847), *Erebia oeme* (Hübner, 1804), *Hipparchia semele* (Linnaeus, 1758).

5. The W- Rhodope Province

It includes Rhodope Mountains in Serbia, towards Rtanj Mt. in the North.

Clima: Dfwbx″, where D = continental-microthermal climate (a mean temperature above 10°C in the warmest months and a coldest month average below −3°C); f = significant precipitation during all seasons; w = dry winters (in which the driest winter month average precipitation is less than one tenth the wettest summer month average precipitation); b = warmest month averaging below 22°C (but with at least 4 months averaging above 10°C); x″ = the second precipitation maximum occurs in autumn.

Natural Potential Vegetation: *Quercetum frainetto-cerris s. lat., Fagetum montanum s. lat.*

Dominant biome type:

Biomes of south-European mostly broad-leaved woodlands.

Typical species of butterflies: *Leptidea duponcheli* (Staudinger, 1871), *Boloria eunomia* (Esper, 1799), *Melitaea arduinna* (Esper, 1784), *Kirinia climene* (Esper, 1784). Also, *Colias balcanica* Rebel, 1903 can be expected in this area because it is distributed on the opposite side of border in Bulgaria

6. The Serbicum Province

It includes Šumadija and extends towards Skopska Crna Gora Mt. in the South; in the West it is bordered by River Ibar and extends towards Kopaonik Mt. and Rudnik Mt. Butterfly fauna of Fruska Gora Mt. also belongs to this area.

Clima: Cfwbx″, where C = mild temperate-mesothermal climate; f = significant precipitation during all seasons; w = dry winters (in which the driest winter month average precipitation is less than one tenth the wettest summer month average precipitation); b = warmest month averaging below 22°C (but with at least 4 months averaging above 10°C); x″ = the second precipitation maximum occurs in autumn.

Natural Potential Vegetation: *Quercetum frainetto-cerris s.lat.*

Dominant biome type:

Biomes of submediterranean broad-leaved woodlands and schrubs; Biomes of south-European mostly broad-leaved woodlands and Biomes of steppes and woodland steppes.

Typical species of butterflies: *Leptidea duponcheli* (Staudinger, 1871), *Hyponephele lupina* (Costa, 1836), *Hipparchia syriaca* (Staudinger, 1871).

7. The Dinaricum (Illyricum) Province

It covers an area from Cer Mt. in the North to Metohija Valley. In the East it extends to Kopaonik Mt. and towards border with Montenegro and Bosnia and Herzegovina in the West.

Clima: Dfwbx″, where D = continental-microthermal climate (a mean temperature above 10°C in the warmest months and a coldest month average below −3°C); f = significant precipitation during all seasons; w = dry winters (in which the driest winter month average precipitation is less than one tenth the wettest summer month average precipitation); b = warmest month averaging below 22°C (but with at least 4 months averaging above 10°C); x″ = the second precipitation maximum occurs in autumn.

Natural Potential Vegetation: *Quercetum frainetto-cerris s. lat., Fagetum montanum s. lat. Piceetum excelsae montanum s. lat.*

Dominant biome type:

Biomes of submediterranean broad-leaved woodlands and schrubs; Biomes of south-European mostly broad-leaved woodlands and Biomes of European mostly coniferous forests of boreal type.

Typical species of butterflies: *Colias balcanica* Rebel, 1903, *Polyommatus escheri* (Hübner, 1823), *Polyommatus eros* (Ochsenheimer, 1808), *Boloria titania* (Esper, 1793), *Boloria selene* (Schiffermüller, 1775), *Euphydryas aurinia* (Rottemburg, 1775), *Coenonympha orientalis* Rebel, 1910, *Erebia ottomana* (Herrich-Schäffer, 1847), *Melanargia larissa* (Esper, 1784), *Hipparchia syriaca* (Staudinger, 1871).

8. The Bertiscum Province

It includes Paštrik, Prokletije Mt. of Metohia, Bogićevica, Hajla, Žljeb and Mokra Gora Mt.

Clima: ET = polar and alpine climate with average temperatures below 10°C for all 12 months of the year.

Natural Potential Vegetation: *Quercetum petraeae s. lat., Piceetum excelsae montanum s. lat., Pinetum heldreichii s. lat., Oxytropidion dinaricae, Seslerion comosae.*

Dominant biome type:

Biomes of European mostly coniferous forests of boreal type.

Typical species of butterflies: *Leptidea duponcheli* (Staudinger, 1871), *Pseudophilotes bavius* (Eversmann, 1832), *Polyommatus damon* (Schiffermüller, 1775), *Boloria titania* (Esper, 1793), *Boloria pales* (Schiffermüller, 1775), *Boloria graeca* (Staudinger, 1870), *Coenonympha orientalis* Rebel, 1910, *Erebia manto* (Schiffermüller, 1775), *Erebia epiphron* (Knoch, 1783), *Erebia rhodopensis* Nicholl, 1900, *Erebia ottomana* (Herrich-Schäffer, 1847), *Erebia cassioides* (Reiner & Hochenwarth, 1792), *Erebia pronoe* (Esper, 1780), *Erebia melas* (Herbst, 1796), *Erebia oeme* (Hübner, 1804), *Erebia pandrose* (Borkhausen, 1788).

9. The Scardicum Province

Geographically it covers Šar-Planina Mt., Ošljak Mt., Kodža-Balkan Mt., Rudoka Mt., Vraca Mt., Korab Mt. and Koritnik Mt.

Clima: ET = polar and alpine climate with average temperatures below 10^{o}C for all 12 months of the year.

Natural Potential Vegetation: *Abieti-Fagetum s. lat., Piceetum excelsae montanum s. lat., Pinetum peucis s. lat., Edraiantho-Seslerion, Seslerion comosae.*

Dominant biome type:

Biomes of stony grounds, pastures and woody on stony and Biomes of European mostly coniferous forests of boreal type.

Typical species of butterflies: *Syrichtus proto* (Ochsenheimer, 1808), *Pyrgus andromedae* (Wallengren, 1853), *Pseudophilotes bavius* (Eversmann, 1832), *Agriades optilete* (Knoch, 1781), *Polyommatus escheri* (Hübner, 1823), *Polyommatus eros* (Ochsenheimer, 1808), *Polyommatus damon* (Schiffermüller, 1775), *Boloria titania* (Esper, [1793]), *Boloria pales* (Schiffermüller, 1775), *Boloria graeca* (Staudinger, 1870), *Hyponephele lupina* (Costa, 1836), *Erebia epiphron* (Knoch, 1783), *Erebia gorge* (Esper, 1805), *Erebia rhodopensis* Nicholl, 1900, *Erebia ottomana* (Herrich-Schäffer, 1847), *Erebia cassioides* (Reiner & Hochenwarth, 1792), *Erebia pronoe* (Esper, 1780), *Erebia melas* (Herbst, 1796), *Erebia oeme* (Hübner, 1804), *Erebia pandrose* (Borkhausen, 1788), *Melanargia larissa* (Esper, 1784).

10a. The Sub-Aegean Province (fragments)

It includes Serbian parts of Crna Reka River basin and Serbian part of River Pčinja.

Clima: Cfwbx″, where C = mild temperate-mesothermal climate; f = significant precipitation during all seasons; w = dry winters (in which the driest winter month average precipitation is less than one tenth the wettest summer month average precipitation); b = warmest month averaging below 22^{o}C (but with at least 4 months averaging above 10^{o}C); x″ = the second precipitation maximum occurs in autumn.

Natural Potential Vegetation: *Querco-Carpinetum orientalis s. lat.*

Dominant biome type:

Biomes of submediterranean broad-leaved woodlands and shrubs.

Typical species of butterflies: *Pyrgus cinarae* (Rambur, 1840), *Anthocharis gruneri* Herrich-Schäffer, 1851, *Euchloe ausonia* (Hübner, 1806), *Leptidea duponcheli* (Staudinger, 1871), *Polygonia egea* (Cramer, 1775).

10b.The Sub-Adriaticum Province (fragments)

It includes the valley of Beli Drim River and associated tributaries: Prizrenska Bistrica River, Topluga River, and Erenik (Ribnik) River.

Clima: Cfwbx″, where C = mild temperate-mesothermal climate; f = significant precipitation during all seasons; w = dry winters (in which the driest winter month average precipitation is less than one tenth the wettest summer month average precipitation); b = warmest month averaging below 22^{o}C (but with at least 4 months averaging above 10^{o}C); x″ = the second precipitation maximum occurs in autumn.

Natural Potential Vegetation: *Quercetum trojanae s. lat.*

Dominant biome type:

Biomes of submediterranean broad-leaved woodlands and shrubs.

Typical species of butterflies: *Zerynthia cerisy* (Godart, 1822), *Euchloe ausonia* (Hübner, 1806), *Leptidea duponcheli* (Staudinger, 1871), *Polyommatus damon* (Schiffermüller, 1775), *Polygonia egea* (Cramer, 1775).

11. The Ponišavlje Province

It covers valleys of Nišava River, Visočica River, Jerma River and associated tributaries including southern slopes of Stara Planina Mt. and Vidlič Mt.

Clima: Cfwbx″, where C = mild temperate-mesothermal climate; f = significant precipitation during all seasons; w = dry winters (in which the driest winter month average precipitation is less than one tenth the wettest summer month average precipitation); b = warmest month averaging below 22^{o}C (but with at least 4 months averaging above 10^{o}C); x″ = the second precipitation maximum occurs in autumn.

Natural Potential Vegetation: *Syringo-Carpinetum orientalis, Quercetum Frainetto–cerris s. lat.*

Dominant biome type:

Biomes of submediterranean broad-leaved woodlands and shrubs.

Typical species of butterflies: *Syrichtus cribrellum* (Eversmann, 1841), *Leptidea duponcheli* (Staudinger, 1871), *Polyommatus damon* (Schiffermüller, 1775).

4. Discussion and conclusions

Although in general it belongs to Central European faunal type, butterfly fauna of Serbia could still be zoogeographicaly separated. This separation is enabled by specific geological and tectonic history, diversifying ecological condition in territory, by richness and presence of specific faunal elements. Phytogeographical separation of Serbia (Gajić, 1984) identifies four main provinces: Pannonia, Moesia, Illiricum and Skardicum-Pind. (Hadži, 1931) geographical chart have three entities separated: Pannonia, Moesia and Illiricum. In this paper, presented chart basically coincides with Gajić and Hadži with one difference, that 11 zoogeographical entities have been recognized.

Acknowledgements

I am grateful to Dr Ana Savić, University of Niš, Faculty of Sciences; Dr Dragana Ranđelović, University of Belgrade, Faculty of Mining and Geology (Department for Mineralogy, Crystallography, Petrology and Geochemistry) and to Dr Aleksandar Valjarević, University of Priština (Kosovska Mitrovica), Faculty of Sciences, for their valuable assistance and useful advices.

References With Annotated Bibliography

Adamović, L. 1909. Die Vegetationsverhältnisse der Balkanländer. In A. Engler& O. Drude Eds., Die Vegetation der Erde.Leipzig. Band XI.

Andjus, Lj. 2008. Butterflies (Lepidoptera, Hesperioidea and Papilionoidea) from the collection of the Natural History Museum in Belgrade. Natural History Museum in Belgrade, Belgrade, 40, pp. 1-94.

Carnelutti, J. 1981. Horološka, ekološka in zoogeografska analiza makrolepidopterov slovenskega ozemlja.Ljubljana.

Dennis, R.L.H., Williams, W., & Shreeve, T.G. 1998. Faunal structures among European butterflies: Evolutionary implications of bias for geography, endemism and taxonomic affiliation. Ecography, 21(2), pp. 181-203. doi:10.1111/j.1600-0587.1998.tb00672.x

Dodok, I. 2003. Dnevni leptiri (Lepidoptera: Hesperioidea I Papilionoidea) klisure reke Đetinje u zapadnoj Srbiji / The Butterflies fauna (Lepidoptera: Hesperioidea & Papilionoidea) in the Gorge of the Djetinja River in West Serbia.Zaštita prirode, 54(1-2), pp. 89-105.

Đurić, M., & Franeta, F. 2011. First study of the butterflies (Lepidoptera: Papilionoidea) of Mt. Mučanj. Acta entomologica serbica, 16(1/2), pp. 81-90.

Fosberg, F.R., & Pearsall, H.S. 1993. Clasification of non-marine ecosystems. Atoll Research Bulletin, 389, pp. 1-38.

Fukarek, P., Jovanović, B., & eds., 1983. Karta prirodne potencijalne vegetacije SFR Jugoslavije 1: 1. 000. 000.Skopje: Naučno veće vegetacijske karte Jugoslavije, Šumarski fakultet.

Gajić, M. 1984. Florni elementi Srbije. In M. Janković& et al. Eds., Vegetacija SR Srbije I..Beograd: SANU., pp. 317-397.

Gross, F.J. 1961. Zur Evolution euro-asiatischer Lepidopteren. In Verhandlungen der Deutschen Zoologischen Gesellschaft.Saarbrücken., pp. 461-477.

Gradojević, M. 1930. Leptirovi Srbije - Diurna / Les papillons de Serbie I. Diurna. Glasnik Jugoslovenskog entomoloskog društva, Beograd, 5-6(1-2), pp. 133-158.

Hadži, J. 1931. Zoogeografska karta Kraljevine Jugoslavije.Beograd: Zbirka karata Geografskog Društva.

Hormuzaki, C. 1929. Grundlinien für die Biogeographie und Biogenese der Europäischen Makrolepidopteren.Buletinul Facultati de stinte din Cernauti, 3, pp. 111-159.

Hormuzaki, C. 1930. Die Entwicklung der europäischen Lepidopterenfauna seit der Tertiärzeit im Lichte der Paläoggeographie, Pflanzengeographie und Paläontologie. Buletinul Facultati de stinte din Cernauti, 4, pp. 50-135.

Ilešić, S. 1961. Geografska regionalizacija Jugoslavije / Sur les problèmes de la délimitation et classification des régions géographiques d'après

l'example de la Yougoslavie. Geografski vestnik, Ljubljana, 33, pp. 3-25.
Jaccard, P. 1902. Lois de distribution florale dans la zone alpine. Bull. Soc. Vaudoise Sci. Nat., 38, pp. 69-130.
Jakšić, P. 1979. Dnevni leptiri SAP Kosovo.Priština., pp. 1-150.
Jakšić, P. 1986. Specifični elementi faune Lepidoptera nekih kosovskih klisura. Priroda Kosova. Priština, 6, pp. 93-107.
Jakšić, P. 1998. Altitudinal distribution and biogeographical division of the butterflies of Balkan Peninsula (Lepidoptera Hesperioidea & Papilionoidea). University Thought, 5(2), pp. 77-88.
Jakšić, P. 1998. Dnevni leptiri (Lepidoptera: Hesperioidea & Papilionoidea) Šar-planine / The Butterflies of the Šar-planina Mt. (Lepidoptera: Hesperioidea & Papilionoidea). Zaštita prirode, Beograd, 50, pp. 229-252.
Jakšić, P., & Ristić, G. 1999. New and rare species of Lepidoptera in Yugoslavia. Acta entomologica serbica, 4(1/2), pp. 63-74.
Jakšić, P. 2003. Dnevni leptiri (Lepidoptera: Hesperioidea and Papilionoidea) Suve planine. Zaštita prirode, Beograd,54(1-2), pp. 71-87.
Jakšić, P. 2003. Fauna leptira (Lepidoptera: Zygaenidae, Hesperioidea i Papilionoidea). In L. Amidžić, M.M. Janković, & P. Jakšić Eds., Metohijske Prokletije - prirodna i kulturna baština / Prokletije of Metohija: The natural and cultural heritage.Beograd: Zavod za zaštitu prirode Srbije., pp. 234-261.
Jakšić, P. 2006. Pregled utvrđenih vrsta dnevnih leptira borskog područja (Lepidoptera: Hesperioidea I Papilionoidea). SANU, Zbornik radova o fauni Srbije, 7, pp. 35-86.
Jakšić, P., Verovnik, R., & Dodok, I. 2008. Overview of Prime Butterfly Areas in Serbia/Pregled Odabranih područja za dnevne leptire u Srbiji. In P. Jakšić Ed., Prime Butterfly Areas in Serbia: A tool for nature conservation in Serbia / Odabrana područja za dnevne leptire - put za ostvarenje zaštite prirode u Srbiji.Beograd: Habiprot Ed., pp. 43-203.
Jakšić, P. 2011. Butterfly species (Lepidoptera: Hesperioidea & Papilionoidea) new to the Serbian fauna. Biologica Nyssana, 2(1), pp. 45-50.
Jakšić, P., & Nahirnić, A. 2011. Dnevni leptiri Zasavice. Službeni glasnik i Specijalni rezervat prirode "Zasavica", Beograd, , pp. 1-100.
Jakšić, P., & Nahirnić, A. 2014. Vodič kroz faunu dnevnih leptira Kopaonika.Kopaonik: JP Nacionalni Park "Kopaonik"., pp. 1-183.
Jakšić, P. 2015. Aspects of butterfly zoogeography of some Pannonian island mountains. Matica Srpska J. Nat. Sci. Novi Sad., 128, pp. 7-19.
Jakšić, P. 2015. On the new and rare Lepidoptera in Serbian fauna. Matica Srpska J. Nat. Sci. Novi Sad., 129, pp. 73-83.
Karadžić, B., Marinković, S., 2009. Kvantitativna ekologija. – Institut za biološka istraživanja “Siniša Stanković”, Beograd.
Kobelt, W. 1904. Iconographie der Land-und Süsswasser-Mollusken mit vorzüglicher berücksichtigung der Europaischen noch nicht abgebildeten Arten.Wiesbaden.
Kogovšek, N., Deželak, U., Gredar, T., Popović, M., Ramšak, B., & Tratnik, N. 2012. Poročilo o delu skupine za dnevne metulje. In Zbornik Ekosistemi Balkana Srbija.Ljubljana: Društvo študentov biologije., pp. 21-28.
Kostrowicki, A.S. 1969. Geography of the Palaearctic Papilionoidea (Lepidoptera).Krakow: Panstwowe wydawnictwo naukowe.
Kudrna, O., Pennerstorfer, J., & Lux, K. 2015. Distribution Atlas of European Butterflies and Skippers.Schwanfeld: Wissenschaftlicher Verlag Peks e. K.
de Lattin, G. 1967. Grundriss der Zoogeographie.Stuttgart: Gustav Fischer Verlag.
Lorković, Z., & Siladjev, S. 1982. Der Erstfund der Raupe von Apatura metis (Freyer) in Europa und deren Biotop (Lep., Nymphalidae). Atalanta, 13(2), pp. 126-135.
Matvejev, S. 1968. Kopnena fauna Srbije sa faunističkom kartom. – Enciklopedija Jugoslavije, Srbija 7: pp. 659-667. Leksikografski zavod FNRJ, Zagreb.
Matvejev, S. 1980. Faunistička karta Srbije. In Enciklopedija Jugoslavije.Zagreb: Jugoslavenski leksikografski zavod., p. 661. 7.
Matvejev, S.D., & Puncer, I.J. 1989. Karta bioma - predeli Jugoslavije i njihova zaštita.Beograd: Prirodnjački muzej u Beogradu.
Mihailović, D.T., Lalić, B., Drešković, N., Mimić, G., Djurdjević, V., & Jančić, M. 2014. Climate change effects on crop yields in Serbia and related shifts of Köppen climate zones under the SRES-A1B and SRES-A2. Int. J. Climatol, November. doi:10.1002/joc.4209
Nahirnić, A. 2011. Supplement to butterfly fauna (Hesperioidea and Papilionoidea) of Grza River Gorge (Eastern Serbia). Biologica Nyssana, Niš, 2(2), pp. 107-117.
Nahirnić, A., Jakšić, P., & Viborg, A.L. 2015. Colias caucasica balcanica (Pieridae) rediscovered in Montenegro, with additional new records for Serbia. Phegea, 43(1), pp. 6-10.
Pagenstecher, A. 1909. Die geographische Verbreitung der Schmetterlinge.Jena: Gustav Fischer Verlag.
Pavlović, S.P. 1912. Mekušci iz Srbije I. Suvozemni puževi.Beograd: Državna štamparija Kraljevine Srbije.
Popović, M., Radaković, M., Đurđević, A., Franeta, F., & Verovnik, R. 2014. Distribution and threats of Phengaris teleius (Lepidoptera: Lycaenidae) in Northern Serbia. Acta Zoologica Academiae Scientiarum Hungaricae, 60(2), pp. 173-183.
Popović, M., Radevski, Đ., Miljević, M., & Đurić, M. 2014. First record of Pyrgus cinarae (Lepidoptera: Hesperiidae) in Serbia. Acta entomologica

serbica, 19(1/2), pp. 45-51. Serb. Summary, Figs. 1-3, map 1.
Popović, M., & Đurić, M. 2014. Dnevni leptiri Stare planine (Lepidoptera: Papilionoidea) / Butterflies of Stara Planina (Lepidoptera: Papilionoidea).Beograd: Javno preduzeće "Srbijašume"; Beograd: HabiProt, Str.., pp. 1-207.
Rebel, H. 1932. Zur Frage der europäischen Faunenelemente. Annalen des Naturhistorischen Museum in Wien, 46, pp. 49-55.
Sokal, R.R., & Rohlf, F.J. 1995. Biometry, 3rd ed.New York: W.H. Freeman Co.
Stevanović, V., Jovanović, S., & Lakušić, D. 1995. Diverzitet vegetacije Jugoslavije. In V. Stevanović& V. Vasić Eds.,Biodiverzitet Jugoslavije sa pregledom vrsta od međunarodnog značaja.Beograd: Biološki fakultet i Ecolibri.
van Swaay, C., Jakšić, P., & Đurić, M. 2007. Notes on some summer butterflies (Lepidoptera: Hesperioidea and Papilionoidea) of Eastern Serbia. Acta entomologica serbica, Beograd, 12(1), pp. 1-10.
Szabo, E. 2002. Biogeographical Analysis of the Butterfly Fauna of the Eastern and Southern Carpathians.Debrecen: University of Debrecen, Faculty of Science.
Szent-Ivanny, J. 1937. Sketch of the zoogeographical division of the Carpathians Basin regarding the distribution of the Macrolepidoptera. Annales Musei Nationalis Hungarici, Pars Zoologica, 31, pp. 129-136.
Todorova, W., & Petkoff, P. 1915. Beitrag zur Macrolepidopteren-Fauna der Umgebung von Tzaribrod und Trn.Sofia: Arbeiten der Bulgarischen Naturforschenden Gesellschaft., pp. 128-147.
Tuleschkow, K. 1932. Erster Beitrag zur Schmetterlingsfauna des Westbalkans (Westliche Stara-Planina).София: ТрудоветЬ на БЬлгарското Природоизпитателно Дружество., pp. 307-312. 15 16.
Varga, Z. 1977. Das Prinzip der areal analytischen Methode in der Zoogeographie und die Faunelemente-Einteilung der europäischen Tagschmetterlinge (Lepidoptera: Diurna). Acta biologica debrecina, Debrecin, 14, pp. 223-285.
Varga, Z. 2002. Zoologische Forschungen in den Hochgebirgen von Zentralasien: Erlebnisse und Ergebnisse.Humboldt Nachrichten, 21, pp. 3-53.
Warnecke, G. 1959. Verzeichnis der boreoalpinen Lepidopteren. Zitschrift der Wiener Entomologischen Geselschaft,44(2), pp. 17-26.
Wiltshire, E.P. 1945. Studies in the geography of Lepidoptera. III: The zoogeographical classification of West Palearctic species. The Entomologist, 78(987), pp. 113-116.
Zaragüeta-Bagils, R., Bourdon, E., Ung, V., Vignes-Lebbe, R., & Malécot, V. 2009. On the International Code of Area Nomenclature (ICAN). Journal of Biogeography, 36(8), pp. 1617-1619.
Zečević, M. 2002. Fauna leptira Timočke krajine (Istočna Srbija).Bor: Bakar; Zaječar: Narodni muzej.
Živojinović, S. 1950. Fauna insekata šumske domene Majdanpeka / Le Faune des Insectes du Domaine forestier de Majdanpek.Beograd: Srpska akademija nauka. Posebna izdanja, knjiga CLX, Institut za ekologiju i biogeografiju, knjiga 2.

* E-mail: jaksicpredrag@gmail.com

UNIVERSITY THOUGHT
Publication in Natural Sciences, Vol. 6, N^{o} 1, 2016, pp. 21-26.
doi:10.5937/univtho6-10437
Original Scientific Paper

A SENSITIVE KINETIC SPECTROPHOTOMETRIC DETERMINATION OF TRACES OF TUNGSTEN IN SOLUTION BASED ON ITS INHIBITORY EFFECT ON THE DECOLORIZATION REACTION OF POTASSIUM PERMANGANATE

Branka Petković[1*], Ružica Micić[1], Ranko Simonović[1]

[1]Faculty of Natural Sciences and Mathematics, University of Piština, Kosovska Mitrovica, Serbia.

ABSTRACT

The present work describes a rapid and sensitive method for the determination of ultramicro amounts of tungsten (VI) based on its inhibitory effect on the oxidation of 4-hidroxycoumarine by potassium permanganate in the presence of hydrochloric acid. The sensitivity of the method is 20 ng/cm^3. The probable relative error is -4.8-13 % for the W(VI) concentration range 250 to 20 ng/cm^3, respectively. Kinetic equations for the investigated process which determine the order of the reactions regarding to each reaction parameter under certain experimental conditions were proposed, and they allowed quantification of the unknown concentrations W(VI) in solution. The detection and quantification limit of the method are 4.5 and 15.1 ng/cm^3. The effects of certain foreign ions upon the reaction rate were determined for the assessing the selectivity of the method.

Key words: Kinetic method, spectrophotometric determination, inhibition, tungsten(VI), 4-hidroxycoumarine.

1. INTRODUCTION

Tungsten is a metal which occurs naturally in the lithosphere, usually in small concentrations and it is also found in oceans and sometimes in other groundwaters in trace amounts (Koutsospyros et al., 2006). This metal is biologically active and it can be found in a number of tungsten-containing enzymes (W-enzymes) (L'vov et al., 2002).

Tungsten usually can be found in the most stable oxidation state VI, but it also occurs in the oxidation states III, IV and V. It has the highest melting/boiling points among elements, a tensile strength at high temperature, resistance to corrosion and a high density and hardness. Because of these unique properties, tungsten has various applications in industry. It is used as a filament in incandescent lamps, as steels in magnetos, springs, contact points, spark plugs, and valves and for other products. (Koutsospyros et al., 2006).

In the past, tungsten was considered as less toxic element due to its insolubility and insufficient knowledge about environmental or toxicological effects (Koutsospyros et al., 2006), (Tajima, 2003). Recently, it has been reported that dissolution of metallic tungsten particles may cause adverse environmental effects such as soil acidification as well as direct and indirect toxic effects in plants, and other living organisms (Strigul a, 2010). Based on these studies, the environmental regulations of tungsten as a "nontoxic" and "environmentally inert" definitely need re-evaluation (Strigul a, 2010), (Strigul b et al., 2010).

It is very difficult to determine tungsten besides the other transition metals, especially in trace levels using chemical methods. It has been determined by different techniques (mostly by spectrophotometric methods (Rohilla et al., 2013), (Masti et al., 2002), ICP-MS (JIS G 1220, 1994), (JIS G 1258, 2000), (Strekopytov et al., 1997) and electrochemical methods (Alvarado-Gámez et al., 2015), (Tanaka et al., 2001), (Zarei et al., 2010).

The kinetic spectrophotometric methods are known as sensitive methods for element quantification (Muller et al., 1980). By studding red-ox reactions of permanganate with organic compounds (Petković et al., 2007), (Micić et al., 2006), it is noticed that tungsten has performed inhibitory effect on the oxidation of 4-hidroxycoumarine by $KMnO_4$ in the presence of hydrochloride acid (pH 1.2-2). The reaction was recorded spectrophotometrically, based on measuring the decrease in the absorbance of the solution. The aim of this work was to investigate the possibility of sensitive and selective tungsten determination by measuring the rate of change in

absorbance of reaction system (4-hidroxycoumarine by $KMnO_4$ in the presence of hydrochloride acid and W(VI)) with time at 525 nm.

2. EXPERIMENTAL

2.1. Apparatus

The investigated reaction rate was folowed by spectrophotometric method at Perkin-Elemer Lambda 15 spectrophotometer, with thermostated cylindrical cells, length 10 cm. All pH values were measured by the radiometer PHM 29Bb pH-meter and a combined glass-calomel electrode, GK2311C. Before the beginning of the reaction, all solutions were termostated in water-bath. The optimal wavelength of 525 nm, as a higher absorbance maximum of $KMnO_4$, was applied for kinetic measurements.

2.2. Reagents

The $KMnO_4$ solution (0.02 mol/dm^3) was prepared from an ampoule produced by „Merck“. The 4-hidroxycoumarine $1\cdot10^{-3}$ mol/dm^3 solution was made by direct weighing of the solid substance. The HCl solution (0.2 mol/dm^3) was prepared from 37% concentrated HCl solution. The basic W(VI) solution 1000 ng/cm^3 was prepared by dissolving 1.7942 g $Na_2WO_4\cdot2H_2O$ (analytical grade) in deionized water with conductivity less than 0.5 μS. The exact concentration was determined volumetrically. Analytical grade reagents, deionized water and polyethylene vessels were used throughout.

2.3. Procedure

Inhibited reaction was followed spectrophotometrically by monitoring the change in absorbance at 525 nm. The initial concentrations of each of the reactants were varied in turn systematically (Muller et al., 1980), (Alekseev, 1973), while the initial concentrations of the other reactants were being kept constant. The same procedure as in previous works (Petković et al., 2007), (Micić et al., 2006) was used in experiments. The selected volumes of the reactants were put into a 20 cm^3 standard flask, in order: 4-hidroxycoumarine, HCl, inhibitor and water to make up the exact predetermined volume. The flask was kept in the thermostat for 10 min, and then the solution was filled up with $KMnO_4$ to the mark and vigorously shaken. The cell of the photometer was rinsed well and filled with the solution. The absorbance was measured every 15 s, for 3–6 min the time has been measured at the moment of $KMnO_4$ addition. The initial concentrations of the reagent solutions after dilution to 20 cm^3 were: $1\cdot10^{-5} - 4\cdot10^{-5}$ mol/dm^3 4-hidroxycoumarine, $1.5\cdot10^{-5} - 4.5\cdot10^{-5}$ mol/dm^3 $KMnO_4$, $1.0\cdot10^{-2} - 5.62\cdot10^{-2}$ mol/dm^3 H_3O^+ ions; 10–250 ng/cm^3 W(VI).

3. RESULTS AND DISCUSSION

The determination of ultramicro amounts of tungsten(VI) is based on its inhibitory effect on the oxidation of 4-hidroxycoumarine by $KMnO_4$ in the presence of hydrochloric acid in strong acidic solution - pH less then 2. It is interesting that above the value of pH=2, W(VI) influences catalytically on the same reaction. Catalitic effect of W(VI) on mention reaction can used for determination of W(VI) in acetate buffer, but selectivity of the method is much lower than in proposed method with inhibitotory effect. On the basis of the results obtained by investigation of the indicatory reaction kinetics for the determination of W(VI) nanogram amounts, the kinetic method was elaborated for W(VI) trace determination within the range from 20 to 250 ng/cm^3 W(VI).

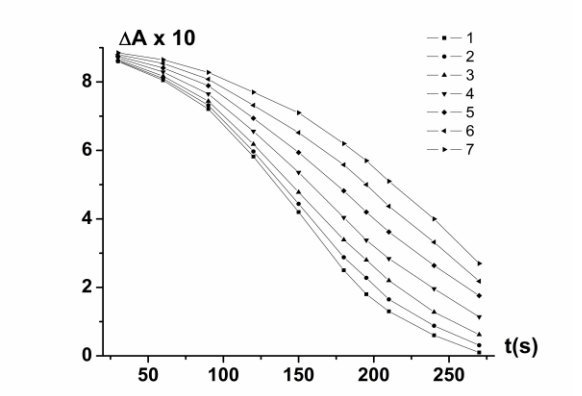

Fig.1. Change of absorbance (ΔA) for different concentrations W(IV) (ng/cm^3), T = 298 K, l = 10 cm; **1**-0.0; **2**-20**;** **3**-50; **4**-100; **5**-150**;** **6**-200; **7**-250; $C_{KMnO4}=3.6\cdot10^{-5}$; $C_{4\text{-}OHcoum}=2.75\cdot10^{-5}$ mol/dm^3

Based on the shape of the curves obtained by mesuring absorbance for different concentartions of W(VI) depending of time (*Fig. 1*), the differencial time method for processing the kinetic data was selected (Muller et al., 1980). The maximum difference between non-catalytic and catalytic reactions occured at 195 s and this time is selected as optimal and fixed in further experiments.

3.1. Effect of pH

The effect of pH on non-inhibited and inhibited reaction rates is shown in *Fig. 2*. It appears that there is a complex relationship between pH and the reaction rate, i.e. a reaction order is variable with respect to hydrogen-ion concentration for the range of studied concentrations. For further work, pH =1.74 was selected for quantitative applications.

It is important to notice that W(VI) could be separated from Mo(VI) (which also shows inhibiting effect on permanganate reaction with coumarine), by monitoring the change in absorbance at 525 nm on pH lower than 1.2.

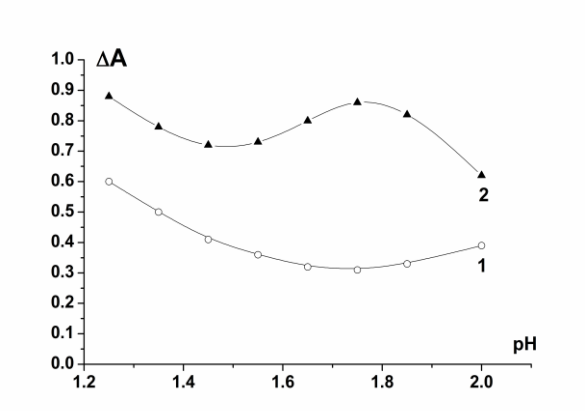

Fig. 2. Dependence of the reaction rate on pH. Initial conditions: $3.6 \cdot 10^{-5}$ mol/dm^3 $KMnO_4$; $2.75 \cdot 10^{-5}$ mol/dm^3 4-hidroxycoumarine; 200 ng/cm^3 W(VI)*; temperature* 25±0.1 °C*; 1-inhibited reaction; 2-non-inhibited reaction.*

3.2. Effect of 4-hydroxyl coumarine concentration

The dependence of ΔAon the 4-hidroxycoumarine concentration is shown in *Fig. 3*. The maximum difference between the rates of inhibited and non-inhibited reactions has been observed for 4-hidroxycoumarine concentration of $2.75 \cdot 10^{-5}$ mol/dm^3. The inhibited reaction is the first-order in the full range of examined concentrations, while the basic non-inhibited reaction is the first-order for the concentrations of 4-hidroxycoumarine less than $2.75 \cdot 10^{-5}$ mol/dm^3.

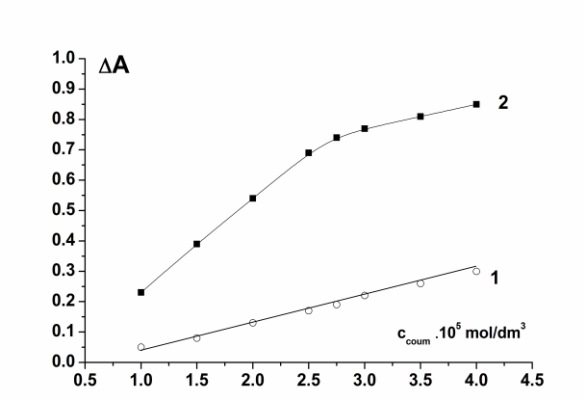

Fig. 3. Dependence of the reaction rate on 4-hidroxycoumarine concentration. Initial conditions*:* $3.6 \cdot 10^{-5}$ mol/dm^3 $KMnO_4$; pH = 1.74; 200 ng/cm^3 W(VI); temperature 25 ±0.1 °C; *1-inhibited reaction; 2-non-inhibited reaction*

3.3. Effect of potassium permanganate concentration

The dependence of the reaction rates on the concentration of $KMnO_4$ is shown in *Fig.4.*

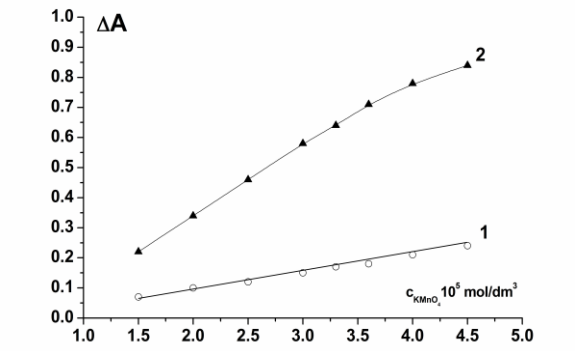

Fig. 4. Dependence of the reaction rate on $KMnO_4$ concentration. Initial conditions*:* $2.75 \cdot 10^{-5}$mol/dm^3 4-hidroxycoumarine; pH = 1.74; 200 ng/cm^3 W(VI); temperature 25±0.1 °C*;* 1-inhibited reaction; 2-non-inhibited reaction.

It is obviously from *Fig. 3* that the inhibited reaction is the first-order in the all range of presented concentrations, while the basic non-inhibited reaction is the first-order for the concentrations less than $3.6 \cdot 10^{-5}$ mol/dm^3.

3.4. Effect of tungsten (VI) concentration

Under optimal conditions $3.6 \cdot 10^{-5}$ mol/dm^3 $KMnO_4$; $2.75 \cdot 10^{-5}$ mol/dm^3 4-hidroxycoumarine pH = 1.74), the tungsten (VI) concentration has been varied from 10 to 250 ng/cm^3. *Fig. 5* shows the calibration line which can be used for determination of W(VI) in the interval of concentration mentioned above at temperatures 20±0.1 °C (1) and 25±0.1 °C (2).

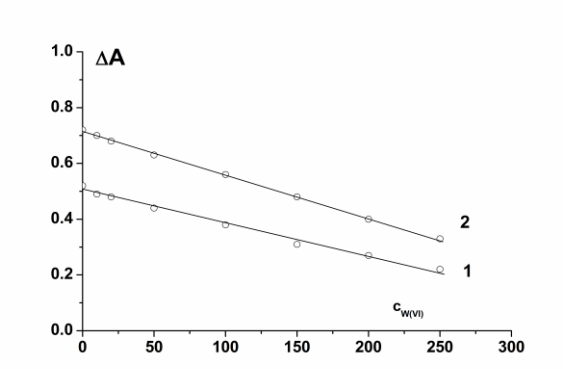

Fig. 5. Dependence of the reaction rate on W(VI) concentration. Initial conditions: $3.6 \cdot 10^{-5}$ mol/dm^3 $KMnO_4$; $2.75 \cdot 10^{-5}$ mol/dm^3 4-hidroxycoumarine; pH = 1.74; 1-temperature 20 ±0.1 °C; 2-temperature 25±0.1 °C.

Based on calibration line (2), at 25°C, the unknown concentration of W(VI) can be determined by following equation:

$$c_{W(VI)} = \frac{0.72 - \Delta A}{0.00152} (=) \text{ng/cm}^3 \qquad (1)$$

where ΔA is the change of absorbance for indicator substance ($KMnO_4$) after 195 s from the beginning of the reaction.

The limits of detection (LOD) and quantitation (LOQ) were found to be 4.5 and 15.1 ng/cm^3 and they are evaluated using the following equations:

$$\text{LOD} = 3.3\ S / b \qquad (2)$$

$$\text{LOQ} = 10\ S / b \qquad (3)$$

where S is the residual standard deviation of the calibration line and b is the slope of the calibration line.

The relationship between the reaction rates and the concentrations of the reacting components can be explained by the following kinetic equations (at constant pH):

For the inhibited reaction ($C_{coum} \leq 4 \cdot 10^{-5}$ mol/dm^3; $C_{MnO4^-} \leq 4.5 \cdot 10^{-5}$ mol/dm^3 and $20 \leq C_{W(VI)} \leq 250$ g/cm^3):

$$-\left(\frac{dc}{dt}\right) = k \cdot c_{coum} \cdot c_{MnO_4^-} \cdot c_{W(VI)}^{-1} \qquad (4)$$

where k is the constant which is proportional to the constant rate of inhibited reaction.

For the non-inhibited reaction ($C_{coum} \leq 2.75 \cdot 10^{-5}$ mol/dm^3; $C_{MnO4^-} \leq 3.6 \cdot 10^{-5}$ mol/dm^3):

$$-\left(\frac{dc}{dt}\right) = k_0 \cdot c_{coum} \cdot c_{MnO_4^-} \qquad (5)$$

where k_0 is the constant which is proportional to the constant rate of non-inhibited reaction.

Accuracy and precision are presented in *Table 1*. The probable relative error ranges from 13 to - 4.8 % for W(VI) concentration from 20 to 250 ng/cm^3

Table 1. Accuracy and precision of tungsten W(VI) determination

Taken (μ) *(ng/cm^3)*	*Found* ($\bar{x}$) *(ng/cm^3)*	*n*	$\frac{100 \cdot t \cdot S}{\bar{x}\sqrt{n}}$ *(%)*	$\frac{\bar{x} - \mu}{\mu} \cdot 100$ (%)
20	23	5	9.61	13.0
50	54	5	4.64	8.0
100	104	5	3.12	4.0
250	238	5	2.80	-4.8

$\bar{x}$ – mean value ; μ – true value; S– standard deviation;

t – Student's test for 95% confidence;

$\frac{100 \cdot t \cdot S}{\bar{x}\sqrt{n}}$ – precision; $\frac{\bar{x} - \mu}{\mu} \cdot 100$ – accuracy.

3.5. Interference study

To access the selectivity of the method, influences of some foreign ions on the inhibited reaction rates were studied, at the constant W(VI) concentration of 200 ng/cm^3.The method has relative good selectivity . The results are presented in *Table 2.*

Table 2. Influence of interfering ions for determination of W(VI) by proposed method ***** W(VI) concentration of 200 ng/cm^3.

Tolerance limit Foreign ion/W(VI)*	Ion added	Comment
10^4	Cl^-, Na^+, K^+, NH_4^+, Mg^{2+}, Sr^{2+}, Ca^{2+}, Ba^{2+}	does not interfere
400	Hg^{2+}, Cd^{2+}, Sn^{2+},Pb^{2+}, Ni^{2+}	does not interfere
200	Al^{3+}, Co^{2+}, Cu^{2+}, Fe^{3+}, Cr^{3+},Pd^{2+}, Pt^{4+}	does not interfere
100	Zn^{2+}, Zr^{4+}, Ti^{3+}, AsO_4^{3-}, Sb^{3+}, Bi^{3+},	practically does not interfere
50	PO_4^{3-}, SCN^-, $C_2O_4^{2-}$ and citrate	have a slightly inhibiting effect
40	Ag^+	have a slightly catalytic effect
10	VO^{2+}	inhibit the reaction
5	MoO_4^{2-}	inhibit the reaction
1	Mn^{2+}, Au^{3+}	catalyze the reaction

4. CONCLUSION

This work describes kinetic method for the determination of trace amounts of tungsten (VI), which is based on the inhibitory effect on the oxidation of 4-hidroxycoumarine by $KMnO_4$ at pH=1.74. The optimal conditions for this kinetic spectrophotometric method are found and equation which allowed determination of unknown concentration of tungsten by measuring the absorbance after 195 s from the beginning of the reaction, at 525 nm, is evaluated. The interference study suggests a relative good selectivity, indicating possibility of successful determination in complex matrix of a real sample. Statistic calculations based on obtained results for five times repeated determinations under the same conditions show good accuracy and precision.

REFERENCES

Alekseev, V.N. 1973. Kurs kachestvenogo polumikro analiza. Moscow: Khimya.

Alvarado-Gámez, A.L., Alonso-Lomillo, M.A., Domínguez-Renedo, O., & Arcos-Martínez, M.J. 2015. A chronoamperometric screen printed carbon biosensor based on alkaline phosphatase inhibition for W(IV) determination in water, using 2-phospho-L-ascorbic acid trisodium salt as a substrate. Sensors (Basel), 15(2), pp. 2232-43. pmid:25621602.

-JIS G 1220. 1994. Iron and steel: Methods for determination of tungsten content.Tokyo: Japanese Industrial Standards Committee.

-JIS G 1258. 2000. Iron and steel: Methods for inductively coupled plasma atomic emission spectrometry (Amendment 1).Tokyo: Japanese Industrial Standards Committee.

Koutsospyros, A., Braida, W., Christodoulatos, C., Dermatas, D., & Strigul, N. 2006. A review of tungsten: From environmental obscurity to scrutiny. J. Hazard. Mater, 136, pp. 1-19.

L'vov, N.P., Nosikov, A.N., & Antipov, A.N. 2002. Tungsten-containing enzymes. Biochemistry Mosc., 67(2), pp. 196-200. pmid:11952415. doi:10.1023/A:1014461913945

Masti, S.P., Seetharamappa, J., & Melwanki, M.B. 2002. Extractive Spectrophotometric Determination of Tungsten(VI) in Alloy Steels Using Ethopropazine Hydrochloride. Analytical Sciences, 18(8), pp. 913-915. doi:10.2116/analsci.18.913

Mićić, R.J., Simonović, R.M., & Petković, B.B. 2006. Kinetic Spectrophotometric Determination of Traces of Manganese(II) by Its Catalytic Effect on Oxidation of 4-Hidroxycoumarine with Potassium Permanganate in River Water Samples. Analytical Letters, 39, pp. 425-433.

Muller, H., Oto, M., & Werner, G. 1980. Katalytishe metoden in der spurenanalyse.Leipzig: Akademische Verlagsgesellschaft Geest und Portig K. G..

Petković, B.B., Simonović, R.M., & Micić, R.J. 2007. Determination of Ultramicroquantities of Au(III) by Its Catalytic Effect on 4-Hydroxyl Coumarone

Oxidation with Potassium Permanganate. J. Anal. Chem., 62, pp. 697-700.
Rohilla, J., Baweja, R.K., & Kumar, S. 2013. Spectrophotometric determination of tungsten (VI) after extraction of its 6-chloro-3-hydroxy-2-phenyl-4-oxo-4H-1-benzopyran complex into chloroform. Arch. Appl. Sci. Res., 5, pp. 81-89.
Strekopytov, S.V., & Dubinin, A.V. 1997. Determination of Zr, Hf, Mo, W and Th in standard reference samples of ocean sediments by inductively coupled plasma mass spectrometry. J. Anal. Chem., 52, pp. 1171-1174.
Strigul, N. 2010. Does speciation matter for tungsten ecotoxicology. Ecotoxicol. Environ. Saf, 73, pp. 1099-1113.
Strigul, N., Koutsospyros, A., & Christodoulatos, C. 2010. Tungsten speciation and toxicity: Acute toxicity of mono- and poly-tungstates to fish. Ecotoxicol. Environ. Saf., 73, pp. 164-171.
Tajima, Y. 2003. 'The effects of tugstophosphate and tungtosiloicate on various stress promoters transformation', Escherichia Coli. J. Inorg. Biochem, 94, pp. 155-160.
Tanaka, T., Sakairi, Y., & Ishiyama, T. 2001. Determination of Tungsten in Iron and Steel by Adsorptiv Stripping Voltammetry. Anal. Sci., 17, pp. 949-952.
Zarei, K., Atabati, M., & Shoari, R. 2010. Catalytic adsorptive stripping voltammetry determination of ultratrace amount of thungsten using factorial design for optimization. J Anal. Chem., 65, pp. 518-524.

* E-mail: branka.petkovic@pr.ac.rs

UNIVERSITY THOUGHT
Publication in Natural Sciences, Vol. 6, N^o 1, 2016, pp. 27-31.
doi:10.5937/univtho6-10474
Original Scientific Paper

KINETICS STUDY OF THE DISPROPORTIONATION OF THE IODOUS ACID IN AQUEOUS SULFURIC ACID SOLUTION

Smiljana Marković[1*], Biljana Petrović[2]

[1]Faculty of Technological Sciences, University of Priština, Kosovska Mitrovica, Serbia.
[2]Faculty of Science, University of Kragujevac, Kragujevac, Serbia.

ABSTRACT

In this paper we reported the kinetics of the disproportionation reaction of iodous acid (HOIO) in aqueous sulfuric acid solutions (0.18 mol/dm^3) studied by spectrophotometrical measurements of the absorbance at suitable wavelength. The changes of the absorbance were caused because the absorbing I_2 molecule species were generated during the reaction. The disproportionation rate constants are calculated at the temperature range between 285 and 303 K with average values: k^{285} = (0.90 ± 0.08) dm^{3}mol^{-1}s^{-1}, k^{291} = (1.10 ± 0.10) dm^{3}mol^{-1}s^{-1}, k^{298} = (1.30 ± 0.07) dm^{3}mol^{-1}s^{-1}and k^{303} = (1.50 ± 0.10) dm^{3}mol^{-1}s^{-1}, respectively. The corresponding activation energy was determined, for the chosen temperature interval, by a graphical method. In addition, obtained value of activation energy is E_a = 38 ± 5 kJ/mol. The negative value of Gibbs energy change and other thermodinamical parameters show that is the disproportionation reaction thermodynamically feasible.

Key words: iodous acid, disproportionation reaction, rate constants, activation energy.

1. INTRODUCTION

The homogeneous disproportionation reaction of HOIO in aqueous solutions of H_2SO_4, can be considered as bimolecular chemical reaction:

$$2\ HOIO \longrightarrow IO^-_3 + 2\ H^+ + HOI$$

Namely, the iodous acid simultaneously oxidized to iodate and reduced to hypoiodous acid. According to the published results, this process is proved to be very complex. (Noszticzius et al., 1983), (Lengyel et al., 1996), (Hegedűs et al., 2001). Also, rate constant for the disproportionation reaction was determined in strong acidic water solutions and it was found that the process is slow and autocatalytic (Lengyel et al., 1996).

High acidity of solution, from sulfuric acid addition, is one of the major factor that cause the complexity of the mechanism of studied process.

Because of the high sulfuric acid concentration used in the preparation of HOIO, the experimental conditions for studying the disproportionation are very limited. Reaction mechanism models of this complex system include large number of elementary steps, or those, which can be presented as elementary steps with undetermined reaction rate constants. This is likely cause of lack of compliance between calculated value from the mathematical model data and experimental results. As the consequence, it is rather difficult to obtain reproducible experimental measurement. The limitations in mechanism discussion are referred to the obtained results.

The values of some kinetic parameters, such as reaction rate constant, activation energy and Arrhenius constant were relatively precisely and accurately calculated on the base of limited experimental data. More precisely in the literature are given some data for the rate constant at 298 K. However, data differs from author to author. For example, Noszticzius (Noszticzius et all., 1983) obtained value of the rate constant of 5.4 dm^{3}mol^{-1}s^{-1} in H_2SO_4 concentration range between 0.05 and 0.15 moldm^{-3} at 298 K, while Lengyel (Lengyel et all., 1996) obtained value for the rate constant of 25 dm^{3}mol^{-1}s^{-1} in the similar experimental conditions at 298 K.

Taking into account that the rate constants are significantly different, we investigated and reported the results for disproportionation reaction and its temperature and acidity dependence under different experimental conditions (Markovic et al., 2002, 2015), (Markovic & Rakicevic, 2006), (Markovic & Cekerevac, 2009), (Markovic & Petrovic, 2010).

In this paper, since our reaction system operates at relatively high acid concentration, we reinvestigated

the reaction close to our experimental conditions. The Hindmarsh version of the Gear's integrator (Markovic et al., 2002) is used for the numerical simulation.

Otherwise, experimental relevant data for the kinetics of iodous acid disproportionation, based on the values obtained in our experiments and data obtained in our numerical calculations, are compared with results obtained in some other investigations found in literature.

2. EXPERIMENTAL

The experiments are performed in a similar way as described in our previous papers (Markovic et al., 2002), (Markovic & Petrovic, 2010) where the process is studied at isothermal conditions.

Experimental solution is prepared with double distilled water with conductivity meter tested purity. The stock solutions are prepared using pro analysis chemicals produced by "Merck".

To obtain HOIO, it is necessary to prepare the solution that contains intermediary species I^{3+}. The mixture of iodine (I) iodine (III) species reaction solution is prepared by dissolving I_2 and KJO_3 (in relation 1:5) in concentrated sulfuric acid (96%) (Noszticzius et al., 1983). Species I^{3+} are stable exclusively in the presence of iodate added in excess. The role of excess of iodate is to prevent formation of I^+. In this case complex reaction proceeds, which can be described by stoichiometry of the chemical reaction:

$$I_2 + 3\,IO^-_3 + 8\,H^+ \longrightarrow 5\,IO^+ + 4\,H_2O$$

Obtained IO^+ ion, formulated as liquid iodosile sulfate $(IO)_2SO_4$, quickly decomposes in water solution of H_2SO_4 and than I^{3+} is presented in the form of iodous acid HOIO:

$$IO^+ + H_2O \longrightarrow H_2IO^+ \longrightarrow H^+ + HIO_2$$

The spectrophotometer measurements of the absorbance changes at 469 nm (absorbance maximum), corresponding to absorption by the I_2 molecule species, is indirectly monitored by the UV-v is spectroscopic method in 10-mm quartz cuvettes. The temperatures of the reaction mixtures were maintained constant with an accuracy of ± 0.2°C by circulating water from a thermostatic bath.

The fresh solutions for experiments are prepared by dilution of stock solution of reactants before every new series of measurements to obtain reproducible results. The prepared solutions are kept in dark vessels and experiments are performed in semidarkness conditions and absence of direct overhead lights.

3. RESULTS AND DISCUSSION

The disproportionation reaction of iodous acid (HOIO) was studied at different experimental conditions by different experimental method. According to the previously published results, (Noszticzius et al., 1983), (Lengyel et al., 1996) the values of the obtained rate constants for disproportionation reaction are very different. Results evaluated from our spectrophotometric measurements in temperature range from 285-303 K enable the calculation of the rate constants for the reaction of disproportionation of HOIO. All values are given in Table 1.

The light absorbance is caused exclusively by I_2 molecule absorption (Awtrey & Connik, 1951).

The increase of the concentration of originated I_2 during the reaction was followed at 469 nm (absorbance maximum). The other part on the spectrum was unchanged during the reaction. The molar absorption coefficient value for I_2 is determined from the calibration diagram and it is equal to $\varepsilon = 746$ m^2mol^{-1}.

Determination of the concentration other relevant species, such as H^+, H_2IO^+, and IO_3^- in the pH range between 1 and 2, formed during the disproportionation reaction, was discussed in detail in the paper (Markovic et al., 2015).

The reactions were followed under the different initial concentration of reactant (for the iodous acid from 1.00×10^{-4} to 1.40×10^{-4} $moldm^{-3}$ and iodate from 1.00×10^{-4} to 4.80×10^{-4} $moldm^{-3}$) at different values temperature (285, 291, 298 and 303 K) with constant solution acidity (0.18 $moldm^{-3}$ H_2SO_4).

The numerical simulation of obtained experimental data was performed in a manner similar to one described in previous paper (Markovic et al., 2002). The method consists of converting the chemical reactions by equations (denoted by (R1) to (R4) for direct reactions and (R-1) to (R-4) for a reverse reactions) given mechanism in the model. Accepting a model of the mechanism and using the experimentally measured value for the rate constants, could be carried out successful simulation.

Table 1. Rate constants for the disproportionation reaction of HOIO calculated in the temperature range from 285 to 303 K by measuring the increasing I_2 molecule specie absorption at 469 nm.

T (K)	[HOIO] ($moldm^{-3}$)x10^4	[IO_3^-] ($moldm^3$)x10^4	[H_2SO_4] (mol/dm^3)	k ($dm^3mol^{-1}s^{-1}$)	k_{av} ($dm^3mol^{-1}s^{-1}$)
285	1.00	3.23	0.18	0.98	
	1.10	3.23		0.96	
	1.20	3.23		0.87	
	1.00	4.80		0.83	0.90 ± 0.08
	1.30	4.80		0.92	
	1.40	4.80		0.82	
291	1.20	4.80	0.18	1.20	
	1.00	3.23		1.13	
	1.00	4.80		1.10	
	1.30	4.80		1.02	1.10 ± 0.10
	1.30	3.23		1.06	
	1.40	4.80		1.03	
298	1.00	3.23	0.18	1.25	
	1.20	4.80		1.33	
	1.10	3.23		1.30	
	1.30	4.80		1.32	1.30 ± 0.07
	1.40	4.80		1.37	
	1.10	1.00		1.26	
303	1.00	3.23	0.18	1.33	
	1.10	3.23		1.53	
	1.00	4.80		1.40	1.50 ± 0.10
	1.30	3.23		1.50	
	1.20	4.80		1.56	
	1.40	4.80		1.60	

Due to the numerical simulation of the experimental absorbance, values are converted into concentration using the Lambert-Beer's Law (equation $\mathcal{A} = \xi \cdot l \cdot c$).

The kinetic of the disproportionation process was sensitive to both $k_{(Eq.1)}$ and $k_{(Eq.2)}$, so the rate low could be represent by equations (1) and (2):

$$d\,[HOIO]/dt = k_{(Eq.1)}[HOIO]^2 \qquad (1)$$

$$d\,[HOIO]/dt = k_{(Eq.2)}[HOIO][HOI] \qquad (2)$$

The rate constant determination for reaction between HOIO and HOI does not significantly affect to the other reactions and could be neglected, probably because of the very narrow limit of feasible experimental conditions.

Following experimental data, the mechanism of disproportionation reaction of iodous acid is discussed. The assumed mechanism of the reaction of iodous acid includes sequence of reactions, comprising the step of the intermediary species HOI generation, which is presented as follows.

In the first step HOIO disproportionate to iodate and intermediate HOI:

$$2\,HOIO \longrightarrow IO^-_3 + H^+ + HOI \qquad (R1)$$

The intermediate species HOI relatively rapidly reacts with HOIO generating another intermediary iodide ion I^-:

$$HOI + HOIO \longrightarrow IO^-_3 + 2\,H^+ + I^- \qquad (R2)$$

The last intermediate I^- reacts very fast with HOIO forming HOI and also with HOI forming I_2:

$$HOIO + I^- + H^+ \leftrightarrow 2\,HOI \qquad (R3)$$

$$HOI + I^- + H^+ \leftrightarrow I_2 + H_2O \qquad (R4)$$

The reverse reactions of (R3) and (R4) have not a significant role in the kinetics under consideration. Therefore, the overall stoichiometry of the disproportionation reaction is:

$$5\,HOIO = I_2 + 3\,IO^-_3 + H_2O + 3\,H^+ \qquad (R5)$$

However, the process of disproportionation is very complex and only iodine could be tracked continually by spectrophotometer. The reactions (R3) and (R4) are very fast. Consequently, the kinetic are sensitive only to reactions (R1) and (R2).

Although the reverse reactions of iodine hydrolysis are present in disproportionation and they do not have a significant role in the kinetics.

In our experiments, the complete reaction of I_2 forming is much faster than obtained in the former

experiments with Hg^{2+}, were disproportionation of HOIO was studied in similar experimental conditions (Markovic et al., 2002), (Markovic & Rakicevic, 2006), (Markovic & Cekerevac, 2009), (Markovic & Petrovic, 2010). From these reasons experiments must be performed very precise and carefully.

Also, the reactions were followed for 10 to 15 minutes, while disproportionation reactions in the presence of excess of Hg^{2+} ions were studied several hours. It is obvious that disproportionation reaction and the intermediary reactions of iodine formations in absence of Hg^{2+} ions are notably faster and might be autocatalytic, what is in agreement with previous observations (Noszticzius et al., 1983), (Lengyel et al., 1996). The comparison of both experimental and calculated values with literature data supports our opinion.

The rate constants increase with temperature, but they are somehow different from those cited in literature. The effect of sulfuric acid and temperature is probably one of the main reasons for the different values of the rate constants of disproportionation reaction. Although some of them have the same order of magnitude. In paper (Markovic et al., 2002) we found that their values are approximately one-half of those obtained by Noszticzius. Comparing our values with values reported in the literature by Lengyel (Lengyel et al., 1996) can be concluded that we obtained 15 times lower rate constant and approximately 1.5 times lower than the values obtained when the Hg^{2+} -ion was in excess (Markovic et al., 2002).

The value of the activation energy was determined graphically for the temperature interval from 285 to 303 K, using the Arrhenius relation presented by eq.(3):

$$k = A\, exp(-E_a/RT) \qquad (3)$$

A is a constant, E_a is the activation energy and T is the thermodynamic temperature. Average activation energy of 38 ± 5 $kJmol^{-1}$ is determined graphically as the slope of straight line from the lnk = f(1/T) dependencies. In the Fig 1 is present the linear form of the Arrhenius equation.

The intercept of the Arrhenius plot with the ordinate gives a pre-exponential factor which is $A = 2 \times 10^9$ $dm^3mol^{-1}s^{-1}$.

Activation energy value is relatively low comparing with previously found (Markovic et al., 2002) and it confirm the presence of the catalytic impacts in the disproportionation process (Markovic & Cekerevac, 2009), (Főrsterling & Varga, 1993), (Hegedűs et al., 2001). There were found that the presence of sulfuric acid increases the rate of the observed reaction; it was assumed that its impact is significant in an overall catalytic mechanism of the process, (Markovic & Petrovic, 2010).

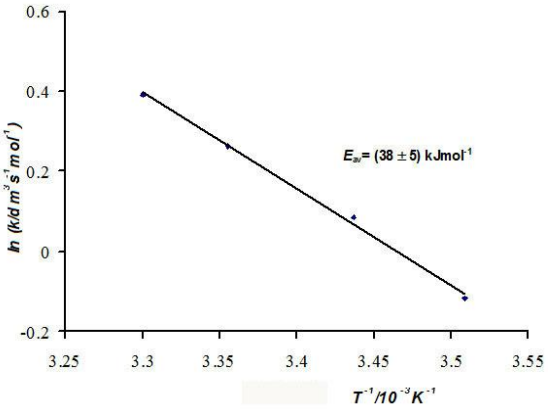

Fig. 1 The Arrhenius equation dependence of lnk *vs.* 1/T.

On the base of the date obtained in the corresponding temperature interval other thermodynamic parameters are also calculated: ΔH = (-17 ± 1) $kJmol^{-1}$, ΔS = (199 ± 3) JK^{-1} mol^{-1}, ΔG = (-42 ± 3) $kJmol^{-1}$.

The negative values of Gibbs energy of reaction (1), the overall reactions (R5) for disproportionation of HOIO shows thermodynamically possibility for given values of the initial concentration of reactants and the temperature in studied system.

The ionic strength of the studied solutions usually does not affect on the rate of the process until the disproportionation of the neutral molecule HOIO occurred. Although its impact is likely in the area in which they appear intermediate ionic species. Therefore, in this case is not taken into consideration.

4. CONCLUSION

On the base of series of spectrophotometer measurements of the absorbance change of I_2 molecule species at 469 nm, generated during the chemical reaction, the rate for the disproportionation of HOIO in the temperature range between 285 and 303 K have been calculated. The observed rate constants varied between k^{285} = (0.90 ± 0.08) $dm^3mol^{-1}s^{-1}$ and k^{303} = (1.5 ± 0.1) $dm^3mol^{-1}s^{-1}$, respectively, depending of the temperature. In the given temperature interval the disproportionation rate of HOIO increases about 1.6 times.

Value of activation energy of 38 ± 5 kJmol^{-1} was determined graphically for the chosen temperature interval. Subsequently, the Arrhenius constant was calculated (2 x 10^{9} dm^{3}mol^{-1}s^{-1}) as well.

The kinetics of disproportionation of HOIO and its thermodynamic parameters, the negative values of Gibbs energy in the investigated temperature range, show that the process is thermodynamically possible.

REFERENCES

Awtrey, A. D., & Connik, R. E. J., 1951. The Absorption Spectra of I_2, I_3^-, I^-, IO_3^-, $S_4O_6^=$ and $S_2O_3^=$. Heat of the Reaction $I_3^- = I_2 + I^-$, Journal of the American Chemical Society, 73 (4) pp.1842-1843.

Főrsterling, H. D., & Varga, M., 1993. Bromous acid/cerium (4+): reaction and $HBrO_2$ disproportionation measured in sulfuric acid solution at different acidites, The Journal of Physical Chemistry, 97 (30), pp. 7932-7938-524.

Hegedűs, L., Wittman, M., Noszticzius, Z., Yan, S., Sirimungkala, A., Főrsterling, H. D., & Field, R. J. 2001. HPLC analysis of complete BZ systems, Evolution of the chemical composition in cerium and ferroin catalysed batch oscillators: experiments and model calculations, Faraday Discussions, (120) 21-38, pp. 85-104.

Lengyel, I., Li, J., Kustin, K., & Epstein, I. R., 1996. Rate constants for reactions between iodine and chlorine-containing species: a detailed mechanism of chlorine dioxside/chlorite-iodite reaction, Journal of the American Chemical Society, 118 (15), pp. 3708-3719.

Marković, S., Rakicević, N., & Mišljenović, Đ., 2002. The temperature dependence of the disproportionation reaction of iodous acid in aqueous sulfuric acid solutions, Journal of the Serbian Chemical Society, 67(5) pp. 347-351, DOI: 10298/JSCO205347M.

Marković, S., & Rakićević, N., 2006. Determination of the rate of iodous acid disproportionation in aqueous sulfuric acid solution, Reaction Kinetics and Catalysis Leters, 89 (1) pp. 3-8, DOI: 10.107/S114-0.06-0.080-9.

Marković, S., & Cekerevac, M., 2009. The rate of the disproportionation of iodous acidity at diferent acidity values in aqueous sulfuric acid solution, Reaction Kinetics and Catalysis Leters, 97 pp. 13-18, DOI: 10.107/S114-0.09-0.03-7.

Marković, S., & Petrović, B., 2010. Kinetics of the disproportionation reaction HIO_2 in aqueous acid solutions, International Journal of Chemical Kinetics Inter, 42 pp. 687-691, DOI: 10.102 /kin20516.

Marković, S., Karkalić, R., & Petrović, B., 2015. Disproportionation reaction of iodous acid, HOIO. Determination of the concentrations of the relevant ionic species H^+, H_2OI^+, and IO^{3-}, Research on Chemical Intermediates, 41 (3) pp. 1293-1330, DOI: 10.107/s164-0.1273-2.

Noszticzius, Z., Noszticzius, E., & Schelly, Z. A., 1983. Use of ion selective electrodes for monitoring oscillating reactions, 2. Potential response of bromide-iodide selective electrodes in slow corrosive processes, Disproportionation of bromous and iodous acids. A Lotka-Voltera model for the halate oscillators, The Journal of Physical Chemistry, 87 (3), pp. 510-524.

* E-mail: markovicsmiljana@gmail.com

UNIVERSITY THOUGHT
Publication in Natural Sciences, Vol. 6, N^{o} 1, 2016, pp. 32-38.
doi:10.5937/univtho6-10634
Original Scientific Paper

THE SYNTHESIS AND NMR SPECTRAL ASSIGNMENTS OF 3-NITRO-4-((6-NITROBENZOTHIAZOL-2-YL)AMINO)-2*H*-CHROMEN-2-ONE

Biljana Dekić[1], Niko Radulović[2], Milenko Ristić[1], Vidoslav Dekić[1*]

[1]Faculty of Science and Mathematics, University of Priština, Kosovska Mitrovica, Serbia.
[2]Faculty of Science and Mathematics, University of Niš, Niš, Serbia.

ABSTRACT

Complete assignment of the ^{1}H and ^{13}C NMR chemical shifts of new coumarin derivate was described in this paper. A new coumarin derivate was synthesized in good yield by reaction of 4-chloro-3-nitrocoumarin and 6-nitrobenzothiazol-2-amine in ethyl acetate in the presence of triethylamine. The complete spectral assignment was achieved using of 1D (^{1}H and ^{13}C NMR) and 2D (^{1}H-^{1}H-COSY, NOESY, HSQC and HMBC) NMR experiments.

Key words: coumarins, synthesis, spectral analysis, ^{1}H NMR, ^{13}C NMR, 2D NMR

1. INTRODUCTION

Coumarins are important group of naturally occurring compounds, usually occur as secondary metabolites present in seeds, root, and leaves of many plant species (Murray et. al., 1982), (O'Kennedy et. al., 1997). They have important effects in plant biochemistry and physiology, acting as antioxidants, enzyme inhibitors and precursors of toxic substances and involved in the actions of plant growth hormones and growth regulators, the control of respiration, photosynthesis, as well as defense against infection (Kostova, 2005). Many of coumarin derivatives, obtained from natural sources and synthesized, have been shown to possess a remarkably broad spectrum of biological activity including antibacterial (El-Agrody et. al., 2001), (Pratibha et. al., 1999), antifungal (Patonay et. al., 1984), (Shaker et. al., 1996), (El-Farargy et. al., 1991), anticoagulant (Manolov et. al., 1995), anti-inflammatory (Emmanuel-Giota et. al., 2001), antitumor (Raev et. al., 1990), (Nofal et. al., 2000) and anti-HIV activity (Xie et. al., 1999). In industry coumarins are utilized as flavoring agents in toothpastes, foods, detergents, tobaccos, alcoholic and beverages (O'Kennedy et. al., 1997). They are also used as optical brightening agents and laser dyes due to their emission properties (Zahradnik, 1992).

Considering to wide range of medicinal and physiological properties and extensive use, coumarin derivative has been intensively studied and therefore of utmost importance that the synthesis and structure determination of these compounds should be achieved by a simple and effective method.

In continuation of our previous work (Dekić et. al., 2010), (Dekić et. al., 2013), we report herein synthesis of new coumarin derivate and complete assignments of their ^{1}H and ^{13}C NMR spectral data based on a combination of 1D and 2D (^{1}H-^{1}H-COSY, NOESY, HSQC and HMBC) NMR experiments.

2. EXPERIMENTAL

2.1. General remarks

Melting points were determined on a Kofler hot-plate apparatus and are uncorrected. HRMS(EI) spectra were recorded on a JEOL Mstation JMS 700 instrument (JEOL, Germany). The IR measurements (ATR - attenuated total reflectance) were carried out with a Thermo Nicolet model 6700 FTIR instrument. For TLC, silica gel plates (Kiesel 60 F_{254}, Merck) were used. Visualization was affected by spraying the plates with 1:1 (v/v) aqueous sulfuric acid and then heating. All the reagents and solvents were obtained from commercial sources (Aldrich, USA; Merck, Germany; Fluka, Germany) and used as received, except that the solvents were purified by distillation.

All NMR spectra were recorded at 25°C in DMSO-d_6 with TMS as an internal standard. Chemical shifts are reported in ppm (δ) and referenced to TMS (δH = 0 ppm) in ^{1}H NMR spectra or to residual DMSO-d_6/$^{13}CD_3SOCD_3$ (δH = 2.50 ppm, δC = 39.52 ppm) in heteronuclear 2D spectra. Scalar couplings are reported in Hertz. 20 mg of sample was dissolved in 1

ml of DMSO-d_6, and 0.7 ml of the solution transferred into a 5 mm Wilmad, 528-TR-7 NMR tube.

The ^{1}H and ^{13}C NMR spectra of synthesized compound were recorded on a Bruker Avance III 400 MHz NMR spectrometer (^{1}H at 400 MHz, ^{13}C at 100 MHz), equipped with a 5-mm dual ^{13}C/^{1}H probe head. The ^{1}H spectra were recorded with 16 scans, 1 s relaxation delay, 4 s acquisition time, 0.125 Hz digital FID resolution, 51 280 FID size, with 6410 Hz spectral width, and an overall data point resolution of 0.0003 ppm. The ^{13}C spectra were recorded with Waltz 161H broadband decoupling, 1024 scans, 0.5 s relaxation delay, 1 s acquisition time, 0.5 Hz digital FID resolution, 65 536 FID size, 31 850 Hz spectral width, and an overall data point resolution of 0.005 ppm.

Standard pulse sequences were used for 2D spectra. COSY and NOESY spectra were recorded at spectral widths of 5 kHz in both *F*2 and *F*1 domains; 1 K × 512 data points were acquired with 32 scans per increment and the relaxation delays of 2.0 s. The mixing time in NOESY experiments was 1 s. Data processing was performed on a 1K × 1K data matrix. Inverse-detected 2D heteronuclear correlated spectra were measured over 512 complex points in *F*2 and 256 increments in *F*1, collecting 128 (HSQC) or 256 (HMBC) scans per increment with a relaxation delay of 1.0 s. The spectral widths were 5 and 27 kHz in *F*2 and *F*1 dimensions, respectively. The HSQC experiments were optimized for C–H couplings of 145 Hz; the HMBC experiments were optimized for long-range C–H couplings of 10 Hz. Fourier transforms were performed on a 512 × 512 data matrix. π/2 Shifted sine-squared window functions were used along *F*1 and *F*2 axes for all 2D spectra.

2.2. Synthesis

2.2.1. Synthesis of 4-chloro-3-nitrocoumarin (3)

4-Chloro-3-nitrocoumarin (3), was synthesized in the two reaction steps according to a previously published procedure (Kaljaj et. al., 1987). In the first reaction step, 4-hydroxycoumarin (1) was nitrated in glacial AcOH by 72% aqueous HNO_3 to give 4-hydroxy-3-nitrocoumarin (2) (scheme 1). Starting compound for the synthesis of the new coumarin derivative 4-chloro-3-nitrocoumarin (3) was prepared from 4-hydroxy-3-nitrocoumarin in the reaction with phosphorus oxychloride and *N*,*N*-dimethylformamide in the second reaction step. Melting point, IR and ^{1}H NMR spectral data were identical to those described.

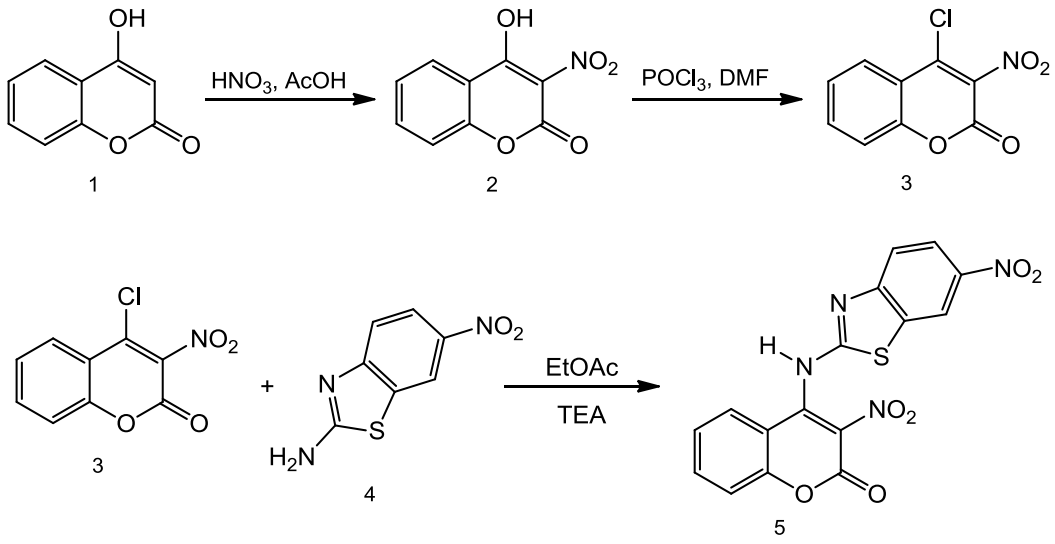

Scheme 1. Synthesis of 3-nitro-4-((6-nitrobenzothiazol-2-yl)amino)-2*H*-chromen-2-one.

2.2.2. Synthesis of 3-nitro-4-((6-nitrobenzothiazol -2-yl) amino)-2H-chromen-2-one (5)

In the ethyl acetate solution of 4-chloro-3-nitrocoumarin (3) (2 g, 8.8 mmol) and 6-nitrobenzothiazol-2-amine (4) (1.72 g, 8.8 mmol) was added triethylamine (2 ml, 14.4 mmol) and refluxed for 2 h. After cooling, the precipitated solid was filtered off and washed with ethyl acetate and water. Purity of the synthesized compounds was checked by TLC. The target product, 3-nitro-4-((6-

nitrobenzothiazol-2-yl)amino)-2*H*-chromen-2-one (5), was obtained as yellow powder, m.p. 178-180 °C, in good yield - 86%.

HRMS(EI): M^+ ($C_{16}H_8N_4O_6S$) 381.0157, requires 381.0165 (Δ= - 0.8 mmu).

IR (neat): 3284 (N-H), 3067 (Ar-H), 2945 and 2885 (C-H), 1733 (C=O), 1642 (C=C), 1526 and 1324 (NO_2), 1123, 1055, 966, 857, 751 cm^{-1}.

3. RESULTS AND DISCUSSION

The new coumarin derivative, 3-nitro-4-((6-nitrobenzothiazol-2-yl)amino)-2*H*-chromen-2-one (5) were obtained in the reaction of 4-chloro-3-nitrocoumarin (3) and 6-nitrobenzothiazol-2-amine (4) in ethyl acetate, as a yellow powder in good yield of 86%.

The structure of compound 5 was confirmed using IR and NMR spectroscopy, and HRMS.

The IR spectra of synthesized compound contained characteristic bands of N-H at 3284 cm^{-1} and Ar-H bond at 3067 cm^{-1}. The strong vibration corresponding to carbonyl group appeared at 1733 cm^{-1}. The IR absorptions due to the presence of the NO_2 group appeared at 1526 and 1324 cm^{-1}.

High-resolution electron impact mass spectrometry (HR-EIMS) of compound **5** indicated a molecular formula of $C_{16}H_8N_4O_6S$ ($[M]^+$ at m/z 381.0157, Δ= - 0.8 mmu).

The ^1H NMR spectrum of synthesized compound exhibited six aromatic methine signals, three doublet of doublets at 7.18, 7.91 and 8.18 ppm, one doublet at 8.77 ppm, one doublet of triplets at 7.23 ppm and multiplet at 7.50 to 7.52 ppm corresponding to two protons, based on the data obtained by signal integration (Fig. 1). The ^1H NMR spectrum also showed a broad singlet at 8.97 ppm. Due to their chemical shift this signal was assigned to proton of the secondary amino group.

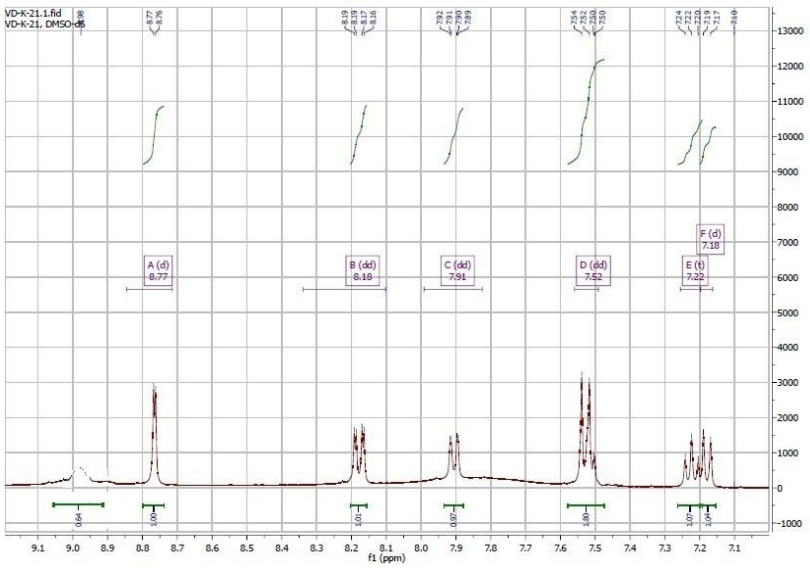

Fig. 1. The ^1H NMR spectrum of 3-nitro-4-((6-nitrobenzothiazol-2-yl)amino)-2*H*-chromen-2-on.

The cross peaks observed in the NOESY spectrum (Fig. 2) differentiated two groups of signals, one belonging to protons bonded to coumarin moiety and second corresponding to protons bonded to benzotiazole substituent. The first group of protons comprised four signals, two doublets of doublets at 7.18 and 7.91 ppm, one triplet of doublet at 7.23 ppm and one signal from multiplet at 7.50 to 7.52 ppm, while the second group consist doublet at 8.77 ppm, doublet of doublets at 7.52 ppm, and the second signal from multiplet at 7.50 to 7.52 ppm (Fig. 3).

From the structure of compound can be concluding that the group of four protons belongs to the coumarin moiety.

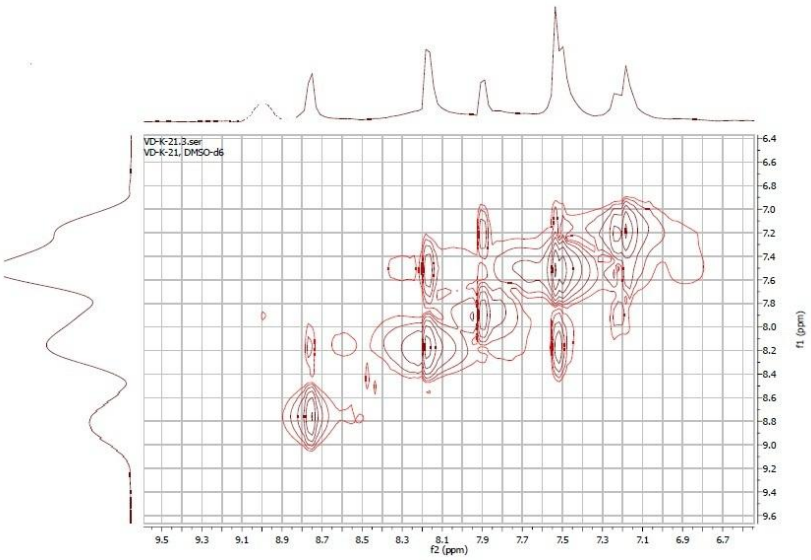

Fig. 2. The NOESY spectrum of 3-nitro-4-((6-nitrobenzothiazol-2-yl)amino)-2*H*-chromen-2-one.

Assignments of these signals are provided due to NOESY correlation of signal at 7.91 ppm with the signal of the proton of the secondary amino group (8.97 ppm). This correlation assigns spatially closer H-5. The assignment of H-5 is in accordance with the multiplicity of this signal due to one vicinal coupling with H-6 (J = 8.0 Hz) and one long-range coupling with H-7 (J = 1.6 Hz).

The rest of the protons from this group were easily assigned by their mutual NOESY correlations (Table 1).

The chemical shift of carbon atoms to which these protons were bonded to was subsequently determined from the HSQC spectrum (Fig. 4, Table 1).

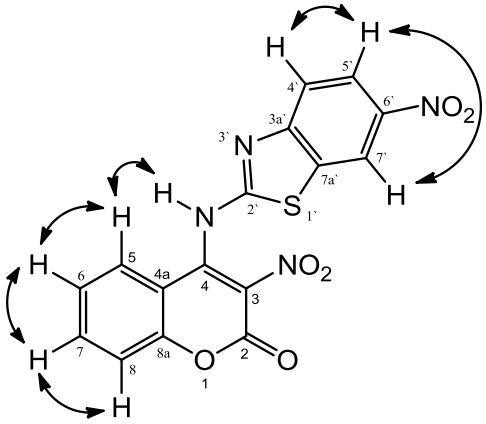

Fig. 3. The NOESY correlations of 3-nitro-4-((6-nitrobenzothiazol-2-yl)amino)-2*H*-chromen-2-one.

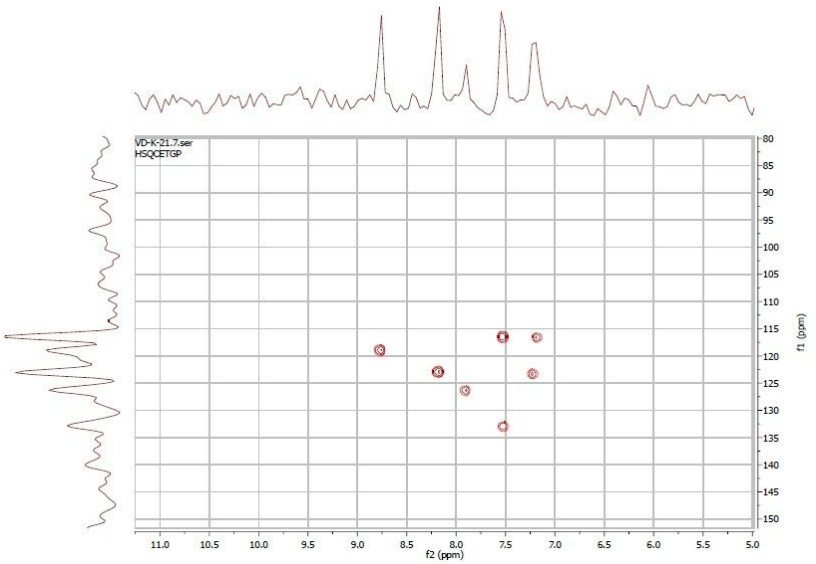

Fig. 4. The HSQC spectrum of 3-nitro-4-((6-nitrobenzothiazol-2-yl)amino)-2H-chromen-2-one.

The assignment of these carbons was additionally supported through HMBC correlations between H-5 and C-7, H-6 and C-8, H-7 and C-5 and H-8 and C-6 (Fig. 5). Quaternary carbon atoms from coumarin moiety were assigned due to HMBC spectral data (Fig. 6). This spectrum showed simultaneous correlations of H-5 and H-7 with the signal at 152.9 ppm assigned to C-8a. Mentioned carbon atom correlated with H-8, due to characteristic interaction trough two bonds, similar to the previously studied compounds (Dekić et. al., 2010), (Dekić et. al., 2013). In a similar manner H-6 and H-8 posses simultaneous correlations signal at 122.3 ppm assigned to C-4a. The last three-bond correlation of H-5 with a C-signal at 167.5 ppm was assigned C-4.

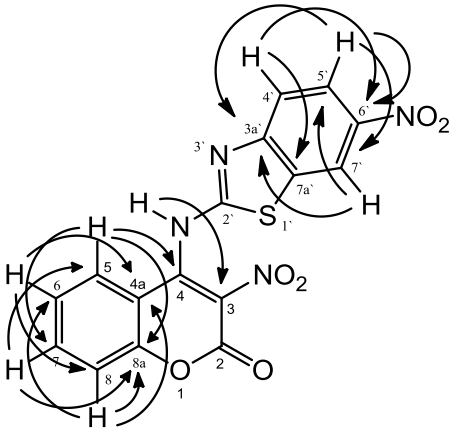

Fig. 5. The HMBC correlations of 3-nitro-4-((6-nitrobenzothiazol-2-yl)amino)-2*H*-chromen-2-one.

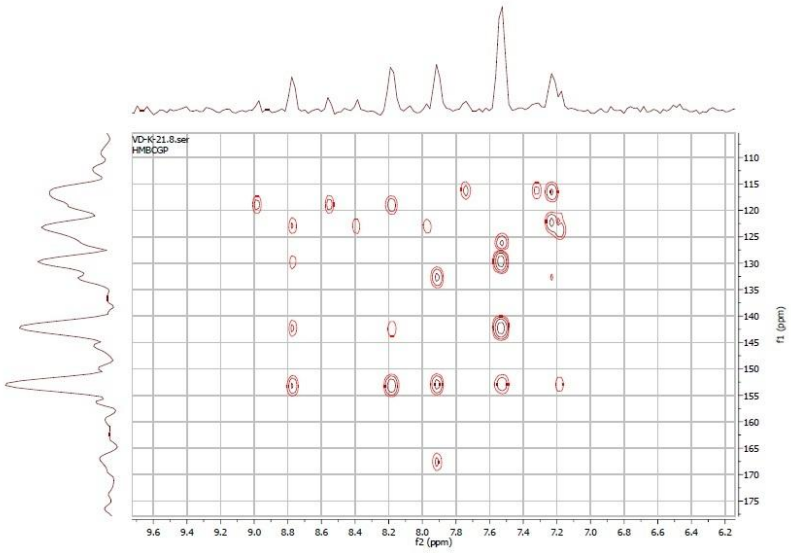

Fig. 6. The HMBC spectrum of 3-nitro-4-((6-nitrobenzothiazol-2-yl)amino)-2*H*-chromen-2-one.

The assignment of the aromatic methine signals of the second group was performed starting from their multiplicity and coupling constants. Simultaneous correlations of doublet of doublets at 8.18 ppm in NOESY spectrum with the both remaining signals from this group assigned this resonance to H-5`. The rest of the aromatic protons were easily assigned due to appropriate coupling constants of H-5` with them (*J* = 8.8, 2.4 Hz). Doublet at 8.77 ppm, according to small coupling constant corresponding to long-distance coupling (*J* = 2.4 Hz), were thereby assigned to H-7'. Finally, the last aromatic proton signal which observed in the multiplet at 7.50 to 7.52 ppm, were attributed to H-4'. The chemical shift of the carbons to which these protons were bonded to was subsequently determined from the HSQC spectrum (Table 1).

The assignment of quaternary carbon atoms was performed starting from the correlations in HMBC spectrum. H-4' and H-5' showed through space interactions with carbon at 142.3 ppm assigned to C-6', wherein H-5' coupled through two bonds. The HMBC spectrum also showed the correlation of H-4' with the carbon at 118.9 ppm which was readily assigned to C-7a'. In the similar manner H-5'and H-7' showed the simultaneous correlations with the signal at 153.2 ppm assigned to quaternary C-3a'.

The proton resonance for the secondary amino group showed a three-bond correlation with the signal at 118.9 ppm, previously attributed to C-7`. Having in mind that the positions through tree bonds in the substituent side of molecule occupy the heteroatoms it's clear that the mentioned carbon belongs to coumarin moiety and attributed to C-3.

Table 1. NMR data of compound 5 in DMSO-d_6.

Position	δ_H, m (*J*, Hz)	δ_C	NOESY[a]	HMBC[b]
2		157.9		
3		118.9		
4		167.5		
4a		122.3		
5	7.91 dd (8.0, 1.6)	126.1	6	7, 8a, 4
6	7.23 td (8.0, 1.2)	123.4	5,7	4a, 8
7	7.50 -7.52 m	132.6	6,8	5, 8a
8	7.18 dd (8.4, 1.2)	116.5	7	4a, 6, 8a
8a		152.9		
N-H	8.97 brs		5	3
2`		172.0		
3a`		153.2		
4`	7.50 -7.52 m	116.3	5`	6`, 7a`
5`	8.18 dd (8.8, 2.4)	123.0	4`	3a`, 6`, 7`
6`		142.3		
7`	8.77 d (2.4)	118.9		3a`, 5`, 6`, 7a`
7a`		129.7		

[a]NOESY interactions of the hydrogen from the column "Position" with the corresponding hydrogen from the column "NOESY".
[b]HMBC interactions of the hydrogen from the column "Position" with the corresponding carbons from the column "HMBC".

The last two carbon signals at 157.9 ppm and 172.0 ppm in the ^{13}C NMR spectrum (Fig. 7), were attributed to C-2 i C-2', respectively, based on their chemical shifts, since no H interactions were observed in any of the 2D spectra and by comparison with the analogous signals in the previously studied compounds (Dekić et. al., 2010), (Dekić et. al., 2013).

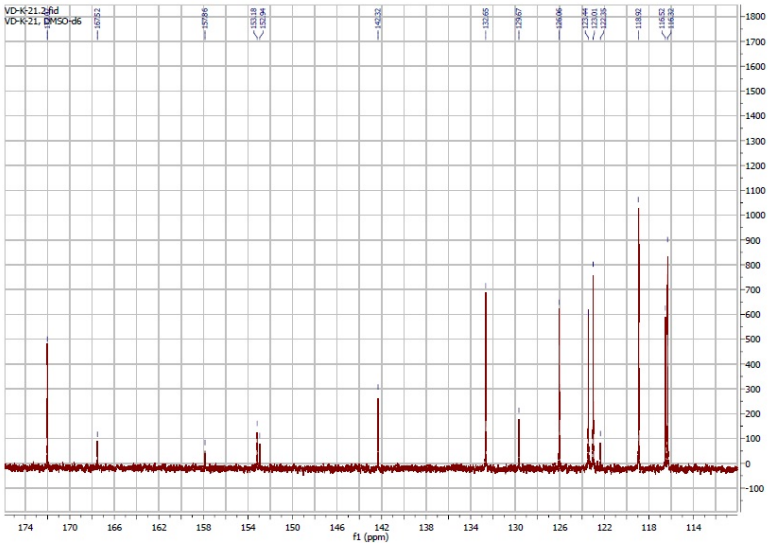

Fig. 7. The ^{13}C NMR spectrum of 3-nitro-4-((6-nitrobenzothiazol-2-yl)amino)-2*H*-chromen-2-one.

ACKNOWLEDGEMENTS

This work was supported by the Ministry of Education, Science and Technological Development of Serbia [Project No. 172061, and 45022].

REFERENCES

Dekić, V., Dekić, B., & Radulović, N. 2013. ^{1}H and ^{13}C NMR spectral assignments of an amino acid-coumarin hybrid.Facta Universitatis Series: Physics,

Chemistry and Technology, 11(3), pp. 101-107. doi:10.2298/fupct1301101d

Dekić, V., Radulović, N., Vukićević, R., Dekić, B., Skropeta, D., & Palić, R. 2010. Complete assignment of the ^{1}H and ^{13}C NMR spectra of antimicrobial 4-arylamino- 3-nitrocoumarin derivatives. Magnetic resonance in chemistry ,48(11), pp. 896-902. pmid:20821411. doi:10.1002/mrc.2681

El-Agrody, A.M., El-Latif, A.M.S., El-Hady, N.A., Fakery, A.H., & Bedair, A.H. 2001. Heteroaromatization with 4-Hydroxycoumarin part II: Synthesis of some new pyrano[2, 3-d]pyrimidines, [1, 2, 4] triazolo[1, 5-c] pyrimidines and pyrimido [1, 6-b]-[1, 2, 4] triazine derivatives. Molecules, 6, pp. 519-527.

El-Farargy, A.F. 1991. Synthesis and some reactions of 8-terc-butyl-6-hydroxy-4-methylcoumarin. Egyptian Journal of Pharmaceutical Sciences, 32, p. 625.

Emmanuel-Giota, A.A., Fylaktakidou, K.C., Hadjipavlou-Litina, D.J., Litinas, K.E., & Nicolaides, D.N. 2001. Synthesis and biological evalution of several 3-(coumarin-4-yl) tetrahydroisoxazole and 3-(coumarin-4-yl) dihydropyrazole derivatives. Journal of Heterocyclic Chemistry, 38, pp. 717-722.

Kaljaj, V., Trkovnik, M., & Stefanović-Kaljaj, L. 1987. Synthesis of new heterocyclocoumarins starting with 3-cyano-4-chlorocoumarin. Journal of the Serbian Chemical Society, 52(4), pp. 183-185.

Kostova, I. 2005. Synthetic and natural coumarins as cytotoxic agents. Curr Med Chem Anticancer Agents, 5(1), pp. 29-46. pmid:15720259

Manolov, I., & Danchev, N.D. 1995. Synthesis, toxicological and pharmacological assessment of some 4-hydroxycoumarin. European Journal of Medicinal Chemistry, 30, pp. 531-536.

Murray, R.D.H., Mendez, J., & Brown, S.A. 1982. The natural coumarins: Occurance, chemistry and biochemistry.New York: Wiley & Sons.

Nofal, Z.M., El-Zahar, M., & El-Karim, A.S. 2000. Novel coumarin derivatives with expected biological activity.Molecules, 5, pp. 99-113.

O'kennedy, R., & Thornes, R.D. 1997. Coumarins: Biology, applications and mode of action.Chichester: Wiley & Sons.

Patonay, T., Litkei, G.Y., Bognar, R., Erdei, J., & Misztic, C. 1984. Synthesis, antibacterial and antifungal activity of 4-hydroxy-coumarin derivatives, analogues of Novobiocin. Pharmazie, 39, pp. 86-91.

Pratibha, S., & Shreeya, P. 1999. Synthesis, characterization and antimicrobial studies of some novel 3-arylazo-7-hydroxy-4-methyl-coumarin. Indian Journal of Chemistry, 38, pp. 1139-1142.

Raev, L., Voinov, E., Ivanov, I., & Popov, D. 1990. Antitumor activity of some coumarin derivatives. Pharmazie, 45, pp. 696-698.

Shaker, R.M. 1996. Synthesis and reactions of some new 4H-pyrano [3, 2-c] benzopyran-5-one derivatives and their potential biological activities. Pharmazie, 51, pp. 148-151.

Zahradnik, M. 1992. The production and application of fluorescent brightening agents.Chichester: Wiley & Sons.

* E-mail: vidoslav.dekic@pr.ac.rs

UNIVERSITY THOUGHT
Publication in Natural Sciences, Vol. 6, N^{o} 1, 2016, pp. 39-43.
doi:10.5937/univtho6-10411
Original Scientific Paper

MATRIX PIXEL AND KERNEL DENSITY ANALYSIS FROM THE TOPOGRAPHIC MAPS

Dragica Živković[1*]

[1]Faculty of Geography, University of Belgrade, Belgrade, Serbia.

ABSTRACT

Complex networks with building density play a significant role in many fields of science, especially in urban sciences. That includes road networks, hydrological networks, computer networks and building changes into geo-space through some period. Using these networks we can solve the problems like the shortest path, the total capacity of networks, density population or traffic density in an urban or suburban area. In this paper for quantifying the complexity of road networks and a novel method for determining building density by using a matrix pixel analysis and Kernel distribution with a concrete example of the city of Belgrade. Both of them represent geo-spatial data. In this case we have analyzed road networks, building density, with the help of specially created software for analyzing pixels on the maps from 1971, including the properties of geo-spatial data we have analyzed from old topographic maps in ratio 1:25.000.

Key words: matrix, pixel, analysis, networks, geo-spatial, Belgrade.

1. INTRODUCTION

Main The resilience and total capacity of many road networks and changes of geo-spatial data makes it possible to study their long period of evolution in space and time (Helbing, 2003). In addition human road networks present the progress of civilization and a degree of self-organized structures that respond to changes in internal and external pressure by gradual geometric changes. The other important view is the changes of building structures and their properties in the city (Gudmundsson & Mohajeri, 2013). The urban road network and building density have been displayed as the city growth through different methods of assessment.

Topographic map represent a frozen time point of geo-spatial data. The raster data from topographic maps are not good enough to fully explain potential geo spatial phenomena.

In this paper we used the new matrix pixel analysis method including the distribution of building density (according to the Kernel density estimator) for displaying geo spatial data of the city of Belgrade from the 1971 topographic map (Chen et. al., 2004). The pixel analysis serves for exploring the geospatial map data. Regarding that period, we observed urban changes in the city as well as the shape and properties of the road network in Belgrade (Knežević, 2010). By combining different methods, we explore the micro and macro features of the city road network. In that purpose we used Geographic Information System (GIS), which examines the road network and the city road network patterns. The other calculations of the road network changes of the city of Belgrade, where about the number of nods, the length and the shape of the road network. The source for creating a digital road map in 1971were topographic maps (used for military purposes) in the proportion of 1:25,000 and by the aero-photo images from 1963, 1965 and 1970. The data were digitized by software QGIS 2.6 Brighton (Open Source Software). The obtained digitized map was then used for the presentation of the city road network as well as for the presentation of the building density of the city of Belgrade. In this way, we get quantity and quality features of the urban city zones in 1971.

The city of Belgrade is the largest city and the capital of the Republic of Serbia. It is located at the mouth of Sava and Danube rivers. The city is divided into 17 municipalities; they are classified into 10 urban and 7 suburban whose centers are smaller towns. Most of the municipalities are situated on the southern side of the Danube and Sava rivers, in the Šumadija region. Only three municipalities are located on the north of the Srem region and Banat region.

2. METHODS

It gives, if In this paper we used the topographic maps from 1971, made by Yugoslav National Army and they were in HGS (Hermanns Kogel Datum) Gauss-Crueger zone 7 projection. The source for data of the 1971 population census was Statistical Office of the Republic of Serbia. After the scanning of the maps, we get the raster format. We marked all the map roads with the specially designed software (JS software for color properties) and by the matrix pixel analysis, and later we digitized them and converted into a vector format. All these maps were geo-referenced and digitized in QGIS 2.6. Brighton (Open Source Software), after the maps were imported into a GIS environment as a tif extension. Then the maps were reprojected in UTM (Universal Transverse Mercator, WGS84 datum) projection with help of open source QGIS 2.6. Brighton software. To align the different maps (geo-referencing) we used the main streets as the reference points on the images. The road network were drown in vector format on the geo-referenced maps in an QGIS 2.6. Brighton environment. Following this the *Geometry Tools, Extract Nodes, Road Graph Plug in Settings* and *Plug in Vertices Counter* was used to build the entire network datasets for every map. In this analysis, intersections of streets are regarded as nodes, and the streets are regarded as links between nodes. On Belgrade topographic maps, we have marked two kinds of the usually used road signs. Then we get entire Belgrade road network, which has been digitized. The road network is divided according to the azimuth, length, area and shape. After digitization, we divided all the road signs in categories. In the matrix pixel model we digitize the points inside the sub-pixel, separating the borders of two different pixels (see Fig. 1). After inserting the points we digitize the raster format pictures to get the vector format pictures. On that way we get points of the matrix analysis by pixels. The vectorized points, derived from the matrix pixel analysis, determine the positions of all the buildings on the map. Then all the points have been inserted and converted into the QGIS 2.6. Brighton (Open Source Software). Example of the vector format points inside the sub-pixel form on the raster format picture is given on the Fig.3b. Next, we made the layer that contains the points which represent the building density. Following this, the layers were converted into GIS shape – file format. We used *Heatmap plug in* and *Kernel shape* (quartic-bewight density function with radius of 100m between points). The obtained layer is in GeoTiff extension. To create a building density map we used *Create Heatmap* tool. In the layer *Style* we classify six belts of building density with dataset. In tool *Raster, Extraction* we choose *Contour lines* with interval between contour lines 1 (maximal value).

3. RESULTS

Munsell color system and the matrix pixel analysis**.** The Munsell color system was introduced by A.H Munsell. This system is especially used in map designing and includes three dimensions of color: hue, value and chroma. These equal steeps of hue, value and chroma were determined through a color difference experiment completed by thousands of people. In the Munsell color system, 100 equal visual increments of hue are arranged in a circle. Pairs of hues opposite each other on the circle are usually called the complementary hues (Munsell,1975). The Munsell colors are specified by value, the perceived lightness of a color relative to physically existing black and white endpoints. The Munsell value scale is divided into 11 equal visual steps of grayness from 0 (black) to 10 (white).

The reflectance of each steep has been measured carefully. The relationship among the three dimensions of color in the Munsell system can be visualized as forming a three dimensional color solid. Equation (1), defines the amount of reflectance per unit from the raster images and the equation (2) is the Chebyshev polynomial inverse equation for which we use the units from the Munsell color model *V*, (see Table 1.).

Table 1. Munsell color equation table with main data.

Reflectance Munsell Color equation in Chebyshev polynomial inverse form	
I	W_i
0	**-1.5323707**
1	**30.6459571**
2	**-97.1723668**
3	**292.9487603**
4	**-608.8463883**
5	**870.8293729**
6	**-840.7901111**
7	**521.7276980**
8	**-187.6371487**
9	**29.7284594**

$$R = 1.2219V - 0.2311V^2 + 0.23951V^3 - 0.021009V^4 + 0.0008404V^5 \quad (1)$$

$$V = \sum_{i=0}^{9} W_i = \left(\sqrt{R}\right)^i \quad (2)$$

The matrix pixel analysis is a sub-pixel analysis of a pixel field. Basically, it is the term soft pixel classification that is used for sub pixel classification (Hurvich, 1957). One of the initial steps in this analysis is locating the sub-pixel field within the sub-pixel components. In this case, we used the algorithm *pixel-swapping*. The spatial resolution of all the pixels is divided into the 16 (4x4) cells. For all the sub-pixels we calculate the distance from the major pixel (given in percentage) and denote it with A_i (see Eq. (3)).

$$A_i = \sum_{j=1}^{n} \lambda_{ij} Z(u_j) \quad (3)$$

where n is the number of bordering pixels, $Z(u_j)$ is the percentage and represent the distance within the pixel j , and λ_{ij} is the pixel weight which depends on the major pixel distance (see Eq. (4)),

$$\lambda_{ij} = \exp\left(\frac{-h_{ij}}{a}\right) \quad (4)$$

where h_{ij} is the distance of the sub-pixels (i, j) from the border of the pixel, a is the nonlinear parameter of the exponential model (Levkowitz, 1997).

3.1. Cartographic signs of buildings

On topographic maps for a better perception a cartographer always inputs topographic signs of objects (Muslims, 2006). A point, a line and area marks constitute the primitive building blocks of pictorial representation. The signs on the maps mark the basic graphic elements because they can be used to create all visual designs on the map. The points and symbols are individual signs, usually they are represented like dots, triangles and so on, used to denote a position, the location of a feature and finally present a location for spatial summary data. For example, they include a coordinate location, a tower position or the centroid of some distribution. The line symbols are individual linear signs used to represent a variety of geographical phenomena. Lines usually represent rivers, roads, political boundaries, ocean currents. For instance, contour lines used to represent elevation and sometimes the line of sea depth. Area symbols are markings existing throughout a map area to indicate that the region has some common attributes, for example water, administrative jurisdiction, an area of mixed, coniferous, deciduous forest. Volume symbols represent the vertical or intensity dimension of geo-spatial data through space. In landform mapping for example the terrain surface may be marked with volume symbols. In our case, the building signs have been usually displayed in urban city zones. If a sign is not in the map proportion and projection, it will not be involved in processing. The majority of signs that mark buildings and industrial elements on maps are displayed in the gray scale color system. Their final digitization will produce an entirely new vector map. The total number of all the topographic signs in the urban parts of Belgrade is 234154 (Čolović, 1984). The most frequently used cartographic signs on maps are signs for buildings, building blocks and factories (see Fig.2).

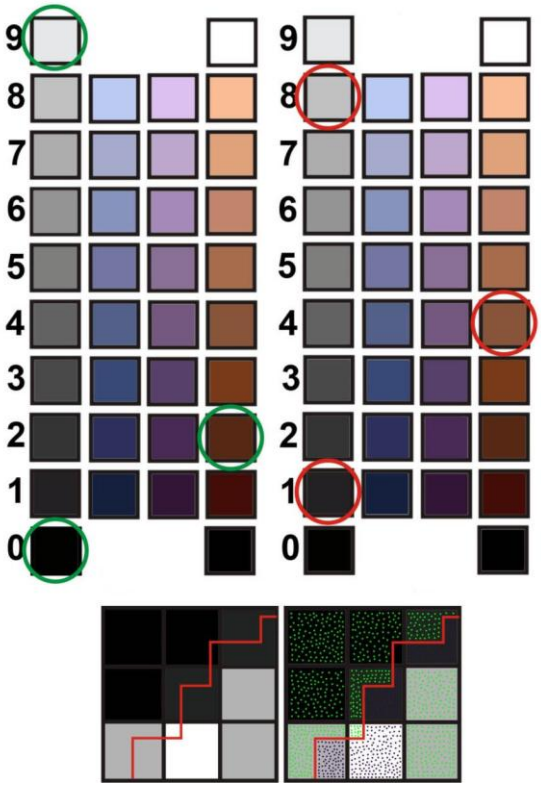

Fig. 1. The chart of the Munsell color model with the three main hues marked with green rings on the all topographic maps in the territory of Serbia. Fig.3b. The chart of the Munsell color model with the three main hues marked with red rings on the topographic maps of the urban area of the city of Belgrade. Fig.3c. Pixel field presented on the topographic map. Fig.3d. Matrix pixel analysis of the pixel field. The figure was generated using the specially created software in JS code for map color properties, AdobePhotoshop and Corel Photo-Pain..

The observed changes of the building density in the central zones can contribute to the conclusions of the fast growth of Belgrade. The data from the map are very important for many sciences dealing with past-based predictions. For instance, such research can be used in urban science for solving the traffic problems in spatially planning disciplines. By using precise techniques, such as the matrix pixel analysis, it is possible to magnify geo spatial data up to the five-meter precision level.

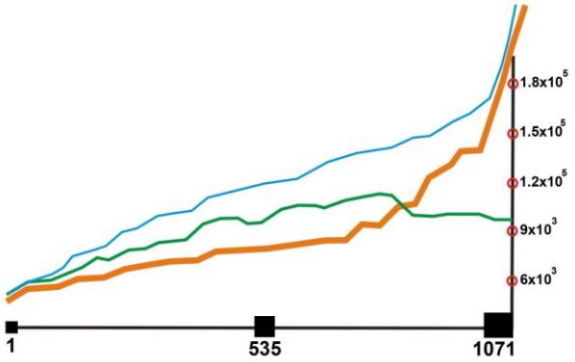

Fig. 2. Color analysis on the maps in the urban part of the city of Belgrade. The brown line is the total index of colors, blue is the color contrast, green is the ratio of color contrast. The X-axis is the number of tested maps, the Y-axis is the number of colors. The figure was generated with CorelDraw.

3.2. Results of software color analysis the Java Script software for map color properties.

Topographic maps in Serbia were made 50 years ago. They are the biggest achievement of the technical cartography era. Today, most of them are scanned and converted into a raster format (usually can be found in jpg, tiff, png extensions and etc). For an application of a matrix pixel analysis, we have created specialized software which evaluates the most frequently used colors on a maps. We have made the software for their analysis in the Java Script Code (JS software for map color properties).The JS software for map color properties explains basic color parameters including luminosity, contrasts and calculate the average color values in the RGB and hexadecimal system (DiBase et. al 1992). The formula for the assessment of the contrast parameter has been tested in a sample bigger than 10^6 of different colors which can be found on topographic maps in raster format. This software gives the color order when the two colors are compared, including the color index, a color map contrast among the map signs and the background and the ratio of color index. The color contrast is obtained by the Pogson Law at a micro level and it shows the color luminosity per pixel, while the Pogson ratio law on macro scales is used for the pixel shine of colors in images (Chen, 1999). The standard RGB color system is presented on the 8-bits color system, and define the 256^3 or 1677216 different colors. The image of the raster format inserted into the software is of the size 500 x 400 pixels or 17.64 x 14.11 cm. It is 29.35 pixels per centimeter. In minimal terms, it is 1x 1 pixels or 0.026 x 0.026 pixels or in maximal terms it is 118.11 pixels per centimeter. The most of the signs have been presented in grayscale hues (Saks,2008), (see Fig.1). This software was tested on the topographic maps of Belgrade and the total area included is equal 359960000m^2, which is at the same time the urban city area. The ringed colors on the Fig. 2a represent the most frequently used colors on the topographic maps of Serbia. Those colors are represented in RGB color system by (1, 1, 1; 84, 41, 24; 229, 229, 229) or (010101; 542918; E5E5E5) in the hexadecimal color system. The ringed colors on the Fig. 2b represent three usually used colors on the topographic map of urban part of Belgrade and that are the following colors (34, 34, 34; 138, 84, 60; 193, 193, 193) in the RGB color system or (222222; 8A543C; C1C1C1) in the hexadecimal color system. The formula for calculating the average color contrast is given in Eq. (5).

$$\frac{(299R_1 + 587G_1 + 114B_1)}{1000} \updownarrow \frac{(299R_2 + 587G_2 + 114B_2)}{1000} \quad (5)$$

R_1 and R_2 are the values of red in the RGB color system from the first and second map sample, respectively; G_1 and G_2 are the values of green in the RGB color system from the first and second map sample, B_1 and B_2 are the values of blue in the RGB color system from the first and second map sample. The formula of index colors (Eq. 6) typifies the relative luminance for all the signs in the RGB system for the values of red, green and blue.

$$\begin{aligned} &((R_{RGB} + 0.049)/1.035)^{2.5} \\ &((G_{RGB} + 0.049)/1.035)^{2.5} \\ &((B_{RGB} + 0.049)/1.035)^{2.5} \end{aligned} \quad (6)$$

$$C_1/C_2 = \frac{(299R_1 + 587G_1 + 114B_1)}{1000} / \frac{(299R_2 + 587G_2 + 114B_2)}{1000}. \quad (7)$$

Value C_1/C_2 is given in percentage (C_1/C_2 is multiplied with 100). The results of the complete color

analysis on urban Belgrade topographic maps are given in Fig.6. There was observed 47 different parts of the map in ratio 1:25,000 for the urban part of the Belgrade. The average color of these maps is # 542918 in the hexadecimal color system and in the RGB color system (84,41,24). The average color contrast of building objects and the background color on the maps are 580, the index of the average color for building signs is 33.131, of background color it is 228.61.The ratio of average color on the maps when the color of building signs is compared with the background color is 0.86:1.

4. Results and discussion

Complex networks have an important role in many fields of science. These include computer, social, neural, road networks. But, comparing a road network with building density, there can be found the conditions that effect the city growth. A road network usually differs in the angles of major road span, including the length, azimuth, nods, shape and finally the total area. The road network on topographic maps is displayed through different line width and color.

In investigating the road network features, we have analyzed the entire Belgrade road network with the open source software QGIS 2.6. The studied situation of the urban part of Belgrade was observed in 1971. By the 1971 population census the entire number of people in the urban parts of Belgrade was 1209369.The entire road network in city urban and suburban area in 1971 was 4144.536 km^2 (or 4144536000 m^2). The urban area was 359.96 km^2 (or 359960000 m^2). Also, there was 141176 nods. The nod positions indicate the major crossroads of the road network. The main road directions are divided into 14 major directions. For the major road directions we calculated the total azimuth spanning from 0^0 to 360^0. The total azimuth of the suburban and urban part is 167.23^0, while road network azimuth of the solely urban part is 203.34^0. The road network feature presented by the polygon can answer the major roads features. The Belgrade road network is represented by the regular polygon tetradecagon (inner angle is 154.28^0, outer angle is 25.71^0). It is convex, cyclic, equilateral and isogonal. The total road network length in 1971 was 3949.8 km or 3949800 m.

References

Chen, S. 1999. Beta Kernel estimators for density function. Computational Statistics & Data Analysis, 31(2), pp. 131-145.

Chen, S., Hanzo, L., & Wolfgang, A. 2004. Kernel-Based Nonlinear Beamforming Construction Using Orthogonal Forward Selection With the Fisher Ratio Class Separability Measure. IEEE Signal Processing Letters, 11(5), pp. 478-481. doi:10.1109/LSP.2004.826509.

Čolović, M. 1984. Topographic signs.Belgrade: Geographic-Military Institute of Serbia, Military book press., pp. 11-34.

Dibase, D., Maceachren, A., & Kryger, J. 1992. Design in Scientific Visualization. Cartography and Geographical Information Systems, 19(2), pp. 201-256.

Gudmundsson, A., & Mohajeri, N. 2013. Entropy and order in urban streets networks. Scientific reports, 3(3324), pp. 1-7. Retrieved from http://www.nature.com/srep/2013/131125/srep03324/full/srep03324.html

Helbing, D. 2003. A section-based queueing-theoretical traffic model for congestion and travel time analysis in networks. Journal of Physics A: Mathematical and General, 36(46), pp. 593-598. doi:10.1088/0305-4470/36/46/L03.

Hurvich, L.M., & Jameson, D. 1957. An opponent-process theory of color vision. Psychological Review, 64(6, Pt.1), pp. 384-404. pmid:13505974. doi:10.1037/h0041403.

Knežević, A. 2010. Social position, residential problems and characteristics of household and families of Roma population in Belgrade. Glasnik Srpskog Geografskog društva, 90(1), pp. 257-276.

Levkowitz, H. 1997. Color theory and modeling for computer graphics, visualization, and multimedia application.Norwell, Massachusetts: Kluwer Academic Publishers., pp. 27-36.

Munsell, A. 1975. A color notation, 12nd ed.Baltimore: Munsell Color Co.., pp. 131-156.

Muslims, A., Foody, A., & Atkinson, M. 2006. Localized soft classification for super-resolution mapping of the shoreline,. International Journal of Remote Sensing, 27(2), pp. 2271-2285.

Saks, R. 2008. Job creation and housing construction: Constraints on Metropolitan area employment growth. Journal of Urban Economics, 64(1), pp. 178-195.

* E-mail: dragicanbgd@gmail.com

UNIVERSITY THOUGHT
Publication in Natural Sciences, Vol. 6, N° 1, 2016, 44-48.
doi:10.5937/univtho6-10739
Original Scientific Paper

GIS MODELLING OF SOLAR POTENTIAL IN TOPLICA REGION

Aleksandar Valjarević[1*]

[1]Faculty of Natural Sciences and Mathematics, University of Priština, Kosovska Mitrovica, Serbia.

ABSTRACT

In this paper we investigated possible potential solar area on Toplica region based on GIS (Geographical Information system) and using a special kriging method with the help of open sources GIS software Quantum GIS. This kriging method is very special to vectorized and calculated the small area. The statistical approach calculated between datasets of three meteorological stations (Niš, Prokuplje, Kuršumlija). Data using of insolation from that meteorological stations from the period of (1953-2013) is useful for a solution to calculating solar potential. The also used parameter is hypsometry of relief of the whole area of Toplica region. Area of Toplica region is 2.231 km² with a population of 90600 citizens. Divided into fourth municipalities (Prokuplje, Žitoradja, Black, Kuršumlija). The GIS modeling indicates that ideal areas for solar development are located the potential places in Toplica region. Only 13.6 km² of the head model scores that were in the 90-100% range. However, given the statewide high insolation values with minimal variance, solar projects may be better suited for small-scale residential or commercial projects.

Key words: Solar, potential, Toplica region, GIS, isolines, maps.

1. INTRODUCTION

The average intensity of solar radiation on the territory of the Republic of Serbia is 1.1 kWh/m^2/per day in the north and 1.7 kWh/m^2/per day in the south – in January and from 5.9 kWh/m^2/ per day to 6.6 kWh/m^2/per day – in July. On an annual basis, the average energy value of global radiation for the Republic of Serbia amounts to 1200 kWh/m^2/per year in northwestern Serbia, 1550 kWh/m^2/per year in southeastern Serbia, while in the central Serbia it amounts to 1400 kWh/m^2/per year (Pavlović & Čabrić, 1986). Today is the age of changes point about climate in the Earth. Greenhouse gases concentrations have risen over the last 200 years from greater fossil fuel and coal use (Radosavljević et al., 2010). That values today has incredible numbers. For that global warming has caused prediction for using new sources of energies in renewable oblique. One of them is solar energy (Lambić, 2010). The whole area of Toplica District is situated in the south-east part of Serbia (Pavlović, 2010). That would be a good reason for solar energy potential. Serbia has the average about 272 sunny days and probably more than 2300 sunny hours (Lambić et al., 2010). In Toplica District, the situation is very good, because more than 249 sunny days and more than 2115 sunny days. The slope of terrain in Toplica slightly positioned by Toplica valley in direction east-west (Malczewski, 2006). That is a lot of hills and mountains located in the south-west position. Multicriteria analysis in a vector data model (vector data, line, and polygon representation) is derived from a raster data model (Kuzevicova & Hurcikova, 2008). GIS data model selection and elimination can lead to different solutions (Ramachandra & Shruthi, 2007). Other geographical variables such as settlements schedule, settlements density, access to roads and location of slope grid area also play the main role (Yue & Wang, 2006). GIS is a very helpful tool for a variety of environmental, planning, waste management, water resources all applications have been undertaken using special GIS tool of multicriteria modeling techniques.2.

2. DATA AND METHODS

The Toplica region is situated in the south of Serbia, located in the south-east part between the mountains of Jastrebac in the north, Kopaonik in the west, Vidojevica ,Sokolovica, Radan and Prolom in the south (Rudić, 1978). More than 76% of this land area have a lot of sunny days. The climate of Toplica region is moderately continental, with cold winters and

hot summers, with a wide range of extreme temperatures and an unequal distribution of rainy months which causes different values of semi- aridity classes (Prokuplje, strategic document). The average annual temperature is 12.1°C, and the annual amount of precipitation is 690 mm for the 1953-1999 periods. The data from the three meteorological stations have been used for the calculation of the number of sunny days in the 1953-1999 periods. These stations are operated by the Republic Hydrometeorological Service of Serbia (http://www.hidmet.gov.rs/). Data sets for each of the meteorological stations were downloaded and used for the calculations of the sunny days and intermediate value of the sunny days and intermediate value of isoline. The correlation coefficients for the data from these meteorological stations were above 0.6.

3. METHODS

The variables used in this work have been obtained from the analogue database, and we have digitized them all. We observed the following variables: potential solar classes, relief slopes, population density, settlements distribution, grid location, slope direction models and the locations of the road networks in the Toplica region. The precision of the classes was determined by the superabundance and quality of data for solar potential, the complexity of the slopes terrain and the geographic variability of the situated location. The insolation values were derived from the Republic Hydrometeorological Service on maximum and minimum scales for the period presented (George & Maxwell, 1999). The Grid cells were put out at 100 m resolution and were validated with the ground measurement of shade tools with the help of GIS tools (Voivontas et al., 1998), (Joerin et al., 2001). Using open sources QGIS 2.6, the seven solar potential categories estimates were rescaled from 0 to 1 by dividing the maximum value in the grid. Each data set was resampled to 100 m using a special filter into GIS. Average isoline vector files were obtained from a digital shape when we derived data from DEM (Digital Elevation Model). The data from DEM were downloaded from the official website (http://earthexplorer.usgs.gov/) in a very high resolution. The grid was rescaled from 0 (least, welcome) to the value of 1 (ideal, close). Since all the data consisted of polygons, it was necessary to convert them into a grid like points in a 100 m resolution. Then, the data were standardized by 0 to 1 values. Ideal conditions exist where population density is the lowest. The distance of the roads is 560 m in the biggest places with solar potential. In order to exploit things easily, the locations which were closer to the existing roads were considered more suitable. The grid and slope directions were categorized according to their suitability for development. The three classes of the slope are given and also one class of grid valued in a 100 m resolution. The grid area which was not favorable for solar potential included the sparse, as well as the taller vegetation, lakes, valleys, streams an, etc. The non-ideal land cover grid contained pine and the deforested areas that would be difficult to develop. Other GIS data were derived from the distribution of settlements with precision coordinates which was given in WGS 84 system. The relief map of the Toplica region shows us that the it is Toplica river flows through the central part of the valley. In the north, Jastrebac Mountain is situated, but not good for potential solar area places, because the slopes have a greater value than 20 degrees. In the south-west area, close to the Kosovo border, the mountains of Radan, Prolom, Sokolica are the best places for solar potential. Other good potential places for solar energy in the Toplica region are in the south of the area, in the mountains Vidojevica and Rgajske. Based on the complete processing of GIS data in seven categories (relief, density, road networks, grid resolution, slope directions, settlements distributions and isoline mean distribution), inter mountains and hills basins (shrubs, plays, and grassland) have the greatest potential for solar development.

3.1. Special GIS tools

The view shed analysis is a very important tool in the GIS selection and data processing. For all GIS data, we used two software with open sources GIS Quantum and Global Mapper 17. The combination of both gave fantastic results. After downloading DEM from the official USGS website in the next step we transformed and resized the file. The DEM file of resolution 100 m was inputted into the GIS software Global Mapper and with the help of other software Quantum GIS, we marked the area of the Toplica region. With a special GIS tool (Viewshed tool), in Global Mapper 17. We selected the view shed analysis tool as the current tool. This tool allows us to perform a viewshed analysis using the loaded DEM elevation grid data with a specified user transmitter location,

height and radius (Global Mapper Forum). We selected all areas within the places with solar potential. All areas within the radius selected are colored with a specified color. The option View Angle Selections gives us the complete radial area. When we performed the view shed analysis over the entire area, we found the potential solar place areas starting at 0 to 360 degrees. With the other special tool Fresnel Zone Specification, we found all points into the grid with slope <10°degree. Another special tool into the GIS software is the kriging method analysis. With the help of Quantum GIS 2.6 we give priority to this method which was employed through the QGIS extension Spatial Analyst. Although there are a few methods, an ordinary kriging method is given priority because it includes autocorrelation and the statistical relationship among the measured points. Thus, with this method the weights are based not only on the distance between the measured points and the predicted location, but also on the overall spatial arrangement of the measured points (Forum of QGIS; Hutchinson, 1994), and it minimizes the variance of the error estimation. Based on its input point features, it creates a surface raster with a spherical semivariogram model for each data of isolines.

3.2. Meteorological data

We used data from three meteorological stations (Nis,Kursumlija,Prokuplje, Table 1.) and calculated average isolines for the 1953-1999 periods (See Fig.1).

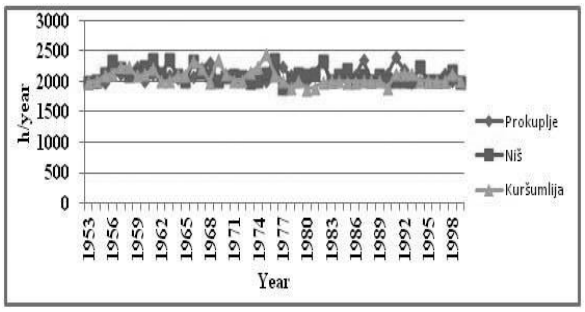

Fig. 1. Trends of average year insolation in the period (1953-1999).

The three meteorological stations have a relatively uninformed altitude which varies between 204 m and 383 m, while the last station Prokuplje has not always worked properly, and Nis meteorological station is very close to the Toplica region. These stations are operated by the Republic Hydrometeorological Service of Serbia (http://www.hidmet.gov.rs/). With all data sets of sunny days we created the average isolines data from those meteorological stations, and after that, we had them put into GIS (see Fig. 2). When we exported all data in the hours of sunny days.

Table 1. List of meteorological stations and their geographical coordinates and altitudes.

Meteorological Station	Longitude	Latitude	Altitude (m)
Niš	21°54′	43°20′	204
Kuršumlija	21°16′	43°08′	383
Prokuplje	21°36′	43°14′	266

4. RESULTS

In order to understand the land cover characteristics, we determined all classes when we inserted the data (Johnston et al., 1994), (Meyer et al., 2009). According to the multi-criteria of the GIS solar model, larger solar potentials should be located in the south-west and the south part of the Toplica region. In the south of the town Kursumlija, there exists a cluster of high scores. The model scores near the mountain of Vidojevica, 25 km south from the town of Prokuplje are also high (Fig. 2). These areas are located in the sparsely populated urban area. Other isolated patches of good GIS model scores are located in the towns and that are not good area because of the high of slopes directions. Although GIS model scores vary significantly, the potential solar data indicate that there is only a slight difference between model classes since most of the Toplica region receives sufficient insolation (see Fig.2). The site in Kuršumija municipality is close to a good network connection line, so the potential to deliver solar power to the region is unlimited. The other parts of the Toplica region have medium or small results of GIS score. More than 12% of the area is not within the range and don't have a result. The results it's from 0.1 to 65%, on the 55% of the area, 65.1 to 80% is on the 11% of the area, 80.1 to 90% is on the 17.1% of the area, and only 4.9 % of the area has the highest score for the solar potential. The solar farms should be built if the model score is more than 70%. That is a score sufficient enough to use the solar potential.Road networks and densely populated settlements are not gods for explorations.

4. DISCUSSION

Place of a great solar potential. Some solar panels already exist in the Topolica region. Some of them are located near the Kosovo border (Merdare, for example). In the mountain of Jastrebac GIS, multi-criteria scores are >30%. The lowest scores are on the hills in the north-west of the mountain Jastrebac, with the medium altitude 200-350 m. On the south-west part of the region, all places receive high total direct insolation. Around 4.9% of the area belongs to the classes of the solar GIS model from 90.1-100%. This part of the area (109 km^2), in Serbia, is not small. The solar potential GIS model may be useful as a filter to find areas that are comparatively more suitable. This multi-criteria GIS analysis is a good pathway for the future discovering of places with a solar potential, because of the filtering potential the potential places and divided into classes ("see Fig. 2.").

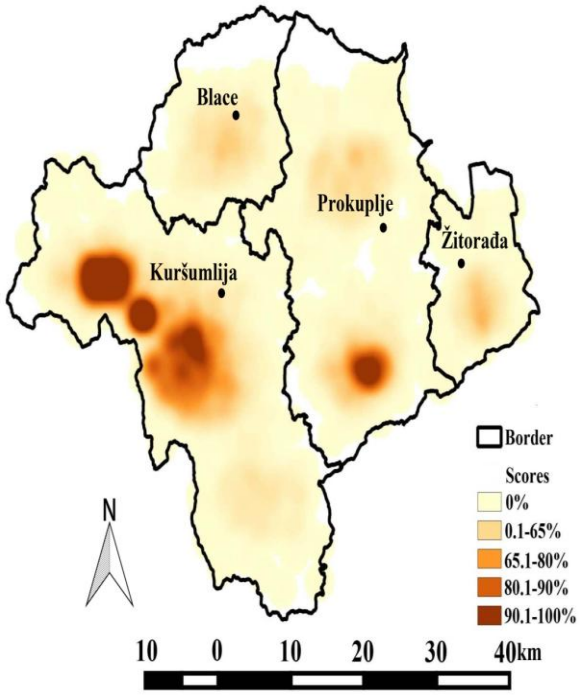

Fig. 2. Map of average solar potential in the Toplica region. Drawn by Aleksandar Valjarević.

5. CONCLUSION

The total area of the Toplica region is 2231km^2 divided into five classes. The first one has no scores, and they cover 12% of territory or 268 km^2. Other classes 0.1 to 65% cover 55 % of the territory or 1227 km^2. The result of 65.1% to 80% of area 245 km^2 or 11%. The result 80.1 to 90% has the total area of 382 km^2 or 17.1%. And the best scores 90.1% to 100% have 4.9% of the area or 109 km^2. Although GIS model scores vary significantly, potential solar data indicate that there is only a slight difference between the model classes. Since the Toplica region receives a large amount of total direct insolation, it is more advantageous to evaluate the solar potential on a local scale for homes than for businesses. The Toplica region gives a great opportunity for building new solar panels and solar farms. South-east Serbia and the Toplica region have a good chance for new renewable sources in the future.

ACKNOWLEDGEMENT

This work was financially supported by the Serbian Ministry of Education and Science, project No.III44006.

REFERENCES

Documents for strategic development in Municipality Prokuplje in period 1953-2010, (Available 12 January, 2016), http://www..prokuplje.org.rs/cms/cir/strateskadokumenta

George, R., & Maxwell, E. 1999. High-resolution maps of solar collector performance using a climatological solar radiation model. In: Campbell-Howe R, Wilkins-Crowder B, Editors. Proceeding of the American Solar Energy Society, Annual Conference, Portland. ME, pp. 243-248.

Global mapper forum, (Available 12 Mach, 2016), http://www.globalmapperforum.com/forums/forum/php

Hutchinson, F., & Gessler, P. 1994. Splines-more than just a smooth interpolator. Geoderma, 62, pp. 45-67. doi:10.1016/0016-7061(94)90027-2.

Joerin, F., Theriault, M., Musy. A. Using GIS and outranking multicriteria analysis. International Journal of Geographical Information Science, 15, pp. 153-174, doi:10.1080/13658810051030487.

Johnston, K., Ver Hoef, M., Krivoruchko, K., & Lucas, N. 2001, Using ArcGIS geostatistical analyst. ESRI, Redlands. USA.

Kuzevicova, Z., & Hurcikova, V. 2008. Accessibility determination of solar radiation by using GIS tools. Acta Montanica Slovaca, 13, pp. 363-367.

Lambić, M., Tasić, N., Pavlović, T., & Stojićević, D. 2006. Solarna energetika - instalacije i objekti. Solar:Zrenjanin.

Malczewski, J. 2006. GIS-based multicriteria decision analysis: a survey of the literature. International Journal of Geographical Information Science, 20, pp. 703-726, doi:10.1080/13658810600661508.

Meyer, V., Scheuer, S., & Haase, D. 2009. A multicriteria approach for flood risk mapping exemplified at the Mulde river Germany. Natural

Hazards, 48, pp. 17-39, doi:10.1007/s11069-008-9244-4.
Qgis.org. 2016. Changelog for QGIS 2.4., (Available 12 March. 2016), https://www.qgis.org/en/site/forusers/visualchangelog240/index.html#feature-qlr-qgis-layer-files
Pavlović, T., & Cabrić B. 1986. Physics and techniques of solar energy. Građevinska knjiga, pp. 101-109.
Pavlović, T. 2002. Development of Solar Energetics in Serbia, SANU: Belgrade.
Radosavljević, M., Pavlović,T., & Lambić.,M. 2010. Solarica Serbica, Zrenjanin: Solar, Serbia.
Ramachandra, T., & Shruthi, B. 2007. Spatial mapping of renewable energy potential. Renewable and Sustainable Energy Reviews, 11, pp. 1460-1480. doi:10.1016/j.rser.2005.12002.
Rudic, V. 1978. Population of Toplica, SANU:Belgrade.
USGS, United States Geological Survey., (Available 12.03.2016), htpp://www.usgs.gGov
Voivontas, D., Assimacopoulos. D., Mourelatos ,A., Corominas J. 1998. Evaluation of renewable energy potential using a GIS decision supports system. Renewable Energy, 13, pp. 333-344, doi:10.1016/S0960-1481(98)00006-8.
Yue, D., & Wang, S. S. 2006. GIS-based evaluation of multifarious local renewable energy sources: case study of the Chigu area of southwestern Taiwan., Energy Policy, 34, pp. 730-42, doi:10.1016/j.enpol.2004.07.003

* E-mail: aleksandar.valjarevic@pr.ac.rs

UNIVERSITY THOUGHT
Publication in Natural Sciences, Vol. 6, N^{o} 1, 2016, pp. 49-54.
doi:10.5937/univtho6-10409
Original Scientific Paper

CLIMATIC REGIONS OF KOSOVO AND METOHIJA

Radomir Ivanović[1*], Aleksandar Valjarević[1], Danijela Vukoičić[1], Dragan Radovanović[1]

[1]Faculty of Science and Mathematics, University of Priština, Kosovska Mitrovica, Serbia.

ABSTRACT

The following the average and extreme values of climatic elements, specific climatic indices and field research, we can select three climatic types in Kosovo and Metohija - the altered Mediterranean, continental and mountainous type. The altered Mediterranean type is present in southern and western Metohija, to be specific, it affects the Prizren Field, the Suva Reka and Orahovac Valley as well as the right bank of the Beli Drim from Pećka Bistrica to the Serbia - Albania border. Gradually and practically unnoticeably, it transforms itself into a moderate continental type which dominates over the remaining valley and mountainous parts of Kosovo. It affects parts of northern Metohija, Drenica and the entire Kosovo valley along with smaller sidelong dells - Malo Kosovo and Kosovsko Pomoravlje. Because of their exquisite heights, the mountains that complete the Kosovo Metohija Valley have a specific climatic type, at their lower slopes it is sub - mountainous and at the higher ones it is typically mountainous. Within these climatic types, several climatic sub regions are present. Their frontiers are not precise or sharp. Rather, their climatic changes are gradual and moderate from one sub-region to the other.

Key words: Climatic regions, climatic sub-regions, Kosovo and Metohija.

1. INTRODUCTION

The climatic regional division of Kosovo and Metohija has been made following the previous experiences of exploration with a great engagement in the very field. The quantity and the quality indicators of the regions and sub-regions have been determined according to the analysis of basic climatic elements (air temperature, precipitation, winds etc.) over many years. Apart from the average annual values, a special attention has been paid to annual flows, the position of extreme values, a number of typical days (summer, tropical, winter, icy), the lasting of a particular phenomenon (snow presence) as well as the other quantity indicators of a particular climatic region. Also, in order to show the climatic differences in Kosovo and Metohija in the best possible way, specific climate indicators have been in use- the rain factor (RF), the drought index (I), the thermo-drome quotient (q), (Vujević, 1956), as the assessment of dryness on an annual basis has been determined by Seljanin`s hydro thermic quotient (HTQ) adjusted to the conditions in Serbia (Otorepec, 1973). The data of standard meteorological stations that have been used are distributed in the territory of Kosovo and Metohija, one of which is the main one, eight of which are eight second class stations and 40 precipitation stations. The current distribution of stations is not good, but anyway it offers the possibilities of observing Kosovo and Metohija climate. Some stations have experienced the interruption of their work, so this is why the standard interpolation method has been used.

2. GEOGRAPHICAL POSITION OF KOSOVO AND METOHIJA

Starting with the basic principle of climatic regions, both regional and typological, also considering the known definition of climatic regions – a climatic region is a particular place with specifically unique climate that is more or less different from the neighboring territories (Rakićević, 1980), we have come to the clear differentiation of similar yet different regions and sub-regions. The specific position of Kosovo and Metohija, its topographic diversity and other factors, have caused that even at a shorter mutual distance considerably different climatic types and sub-types have been formed. The very fact that over the Kosovo and Metohija territory there passes a frontier of the Mediterranean and continental pluvio metric regime (Vujević, 1955), is indicative of the climatic differences that are dominant in the area.

2.1. Region with altered Mediterranean climatic features

In this climatic type, three similar yet different climatic sub-regions have been selected- the West Metohija sub-region, the Central Metohija sub-region and the Prizren sub-region.

I_a-West Metohija Climatic Sub-region. In geographic terms, this sub-region covers the territory of Dečani Podgora, Đakovica Has and the middle flow of the River Erenik and the Dečanska Bistrica. The sub-region has been selected because of the great amount of precipitation, the greatest one in the valley landscape of Kosovo (Junik 1424mm) and the specific pluviometric regime which is nearest the South Adriatic-Montenegrin type (the maximum value in November, December and January, with the minimum value in June, July and August). It is also recognizable for a huge amount of air humidity as the relative humidity on an annual basis is 76.7% as the annual value of the hydro thermic quotient is 1.39%. The three summer months are dry with the HTQ from 0.7 to 0.9. The rain factor value is the greatest in the valley landscape of Kosovo and Metohija, higher than 90. Winters are not particularly cold; the presence of frosty days is 79.5 as of the icy ones is 14.1. The average annual temperature is from 10 to 11°C, the vegetation period (tav. >5°C) is 259 days long while the temperature sum is 3759°C.

I_b-Central Metohija (Orahovac) climatic sub-region. It covers the territory from the confluence of the rivers Klina and Pećka Bistrica to the north to the middle flow of the River Topluga to the south. It embraces the basin of the Beli Drim middle flow with its larger part on the left bank. To the east, it spreads itself to the slopes of the Drenica Mountains, the Crnovljeva and Nerodimska Mountains, while to the west it borders the West Metohija sub-region. It differs from the previous one in terms of a considerably smaller amount of precipitation and to a certain extent higher temperatures. The average annual air temperature is higher than 11°C. The winters are not particularly cold while the summers are very warm, even hot, which is supported by the number of hot days (104) and very hot days (38). The entire length of vegetation period is 271 days with the temperature sum of approximately 4000°C. This sub-region receives a considerably smaller amount of precipitation than the previously described sub-region - Orahovac 767mm, Suva Reka 688 mm. The maximum amount of precipitation is in November and the secondary maximum is in May. The smallest amount of precipitation is in August, with the secondary one in March. According to the values of the rain factor, these regions are classified as arid (RF<60) in accordance with the annual values the HTQ is insufficiently moist. A small number of snowy days (V. Krusa 14.8), a short presence of the snow cover (Orahovac 28.6) as well as a small number of stormy days, fewer than ten, is indicative of the moderate sub-regional climate which has been utilized through the cultivation of the famous Metohija vineyards that boast excellent grape quality.

Ic-*Prizren Climatic Sub-region*. It covers the area of the Prizren field and the lower flow of the River Beli Drim. The average annual temperature verges 12°C. The average January temperature is positive (0.16°C) while the average July temperature is higher than 22°C. Therefore, the summers are hot and dry as the winters are mild and rainy. In this sub-region, there is the greatest number of summer days (96.8) and tropical days (33.3) as well as tropical nights (2.6) with the smallest number of frosty days in Kosovo (69.4). The vegetation period is 273 days long with the temperature sum of 4187°C. In this sub-region, there are more than 2000 hours of sunshine. Prizren and the Beli Drim Valley approximately receive 750 mm of precipitation as its fringes receive slightly more. The maximum value of precipitation is in November and there is a less visible maximum in May. The minimum value of precipitation is in August and the secondary minimum is in February. The high temperatures and smaller amounts of precipitation have caused the smaller values of the HTQ. Its annual value is just 1.12, which makes these regions insufficiently moist. In July and August, the HTQ value is just 0.6 to 0.8, so that these months are seen as extremely dry.

2.2. Region of continental climatic features

North and east from the region of altered Mediterranean climate, there are territories of moderately continental climate. These regions comprise three thirds of the entire Kosovo territory, i.e. for the remaining Kosovo parts, they involve 1000 m above sea level of the absolute height.

II-a North Metohija (Peć-Istok) Sub-region. It spreads itself between the West Metohija and Orahovac sub-regions to the south, and to the mountain wall of the North East Prokletije to the north. Therefore, it comprises the middle flow of the River Pećka Bistrica and Klina, the upper flow of the

River Beli Drim and Metohija Podgor. The average annual temperatures verge 11°C Peć (11.1°C), and it is only the field of Klina that has a slightly lower temperature -10.7°C. The average January temperature is between -0.02°C in Istok and -0.07°C in Klina, while the average July temperatures very between 20 and 21°C. In thermic sense, Metohija Podgor is slightly warmer than the bottom of the Metohija Plateau. Podgor`s shelter from northern winds and the local geographic position of Klina affect this assessment a great deal. On an annual basis, there falls 750 mm of precipitation, slightly more falls in Peć (871mm) and even less falls in Istok, 659 mm. The maximum precipitation is in November, December and January, with the specifically differentiated secondary maximum in May. The minimum precipitation is during the two summer months, July and August. According to the monthly HTQ values, these months are seen as dry or very dry. The Drought index is 31.5 in Istok and 41.5 in Peć. Snow is a regular winter phenomenon but the snow cover hardly ever preserves, only 16.4 days in Istok, i.e. 22.5 days in Klina. The Field of Klina features an increased number of foggy days (48.4 days) especially during autumn.

*II-b North Kosovo (Ibar) Sub-region***.** It covers the territory of northern Kosovo, i.e. parts of Ibarski Kolašin, the suburbs of Kosovska Mitrovica and the valley of the Ibar middle flow to the place of Lešak. To the south, it spreads itself to Vučitrn and it also involves northern Drenica, the high plateau of Ljušta. The average annual temperature is 10.2°C, the minimum one is in January -0.8°C, as the maximum temperature is in July 20°C. In thermic sense, this sub-region represents the transition from warmer Metohija and colder Kosovo. The vegetation period is 247 days long with the temperature sum of 3543°C. These parts of Kosovo receive extremely small amounts of precipitation (Kosovska Mitrovica 614mm, Lešak 625 mm). In pluviometric sense, there is a strong continental effect. The maximum precipitation value is in May or June with the differentiated secondary maximum in November. The minimum precipitation value is in November and in March with the secondary minimum in August. The fact that the annual HTQ is only 1.03 is indicative of the dryness of this sub-region. From May to September these parts are viewed as insufficiently moist, being viewed as extremely dry during the hottest months. The general feature of this sub-region is exquisite dryness in the warmer part of the year, moderate climates with no extremes, dry winters with little snow and rare snow cover.

II–c Malo Kosovo Climatic Sub-region. Malo Kosovo is a small sideway valley at the eastern slope of the Kosovo valley. Surrounded by mountains, it has somewhat different features when compared with the remaining part of Kosovo. The surrounding mountains play a crucial role in terms of regional climate especially the mountain of Kopaonik. The average annual temperature is lower than 10°C. The average winter temperature is negative and even summers are colder than what seems to be the case in other climatic sub-regions. The vegetation period is 241 days long with the entire temperature sum of 3450°C. On an annual basis, Malo Kosovo approximately receives 700 mm of downfall. The November and May maximums are approximately of the same values with the minimum values in August, March and February. There are not many snowy days (about 30) but the snow cover and low winter temperatures last long (43.5 days in Podujevo and 54.7 days in Kisela Banja). This part of Kosovo and Metohija also features a great level of windiness.

II-d Kosovo-Drenica Climatic Sub-region. In terms of the area it occupies**,** this the largest climatic sub-region in Kosovo and Metohija. It involves the central part of the Kosovo Valley, from Vučitrn in the north and Lipljan in the south. It also occupies the territory in Drenica, from Srbica to Glogovac and it also comprises the eastern parts of the Metohija Valley. The low mountains between the Drenica Valley Kosovo Polje also belong to it. The average annual temperature is lower than 10°C but the average winter temperature is positive (0.3°C). The summers are fresh because the average July temperature is just 19.8°C. The main feature of winter is also shown by a great number of frosty days, some 100 of these, and icy days with more than 20. The vegetation period is 245 days long with the temperature sum of 3512°C. Central Kosovo and Eastern Metohija are the driest regions in Kosovo and Metohija. They only receive 600 mm of precipitation. The precipitation regime is the closest to the continental type. The maximum precipitation is in May or June as the secondary maximum is in November, being hardly visible. The precipitation maximum is near the end of winter –in February or in March, with the secondary one being practically non-existent as the dry period stretches through the entire summer. The main feature of this region is a high level of dryness. Long dry periods are common with the

longest one lasting for 58 days. The average annual HTQ value is only 1.06 (insufficiently moist) as in July and in August the HTQ values gets as low as 0.08, which makes them dry. The region is also featured by considerable windiness, especially in the Lipljan area.

II–e South Kosovo Climatic Sub-region. It stretches itself in the southern part of the Kosovo Valley, from the divergence of the rivers Sitnica and Nerodmika in the north to the Kačanik Gorge in the south. The average annual temperature is 9.8°C but the average winter temperature is positive. The warmest month is July with 19.8°C. The vegetation period is 244 days long with the temperature sum of 3505°C. The South Kosovo climatic sub-region is featured by an increased amount of precipitation - Uroševac with almost 700 mm, Štimlje near 800 mm and Kačanik with 860 mm. In the pluviometric regime, the spring maximum in May is differentiated and the summer minimum is in August. Dry periods are common with the longest one lasting for 56 days. The average annual HTQ value is 1.26 which makes it an insufficiently dry area. The sub-region is also featured by great windiness. There is only 104‰ of silence in Uroševac.

II-f Gnjilane Climatic Sub-Region. This is also a sideway valley at the eastern edges of the Kosovo Valley. It is separated from it by low divergence so that Kosovo Valley climatic influences are dominant. To the north, it is sheltered by the Novo Brdo Mountain Area, as to the south, it sheltered by Skopska Crna Gora. This has affected the great continental feature of this sub-region. The average annual temperature is higher than 10°C. The coldest month is January with -0.9°C and the warmest moth is July with 20.7°C. This is, to a certain extent, a sub-region warmer than those nearby, so that the vegetation period is 250 days long with the temperature sum of 3680°C. The Gnjilane Valley and the Kriva Reka Basin are one of the driest areas in Serbia. The annual amount of precipitation is smaller than 600 mm. The greatest amount of precipitation is in May and the smallest one is in March. Long droughts are one of the features of this climatic region. The longest dry period in Kosovska Kamenica lasted for 52 days, and, in Dunav in Skopska Crna Gora, it lasted for 61 days. On average, snow appears over a 20 or 30–day period, and the snow cover lasts for 30 days in the lower parts, or more than 40 days at the edges. There is the greatest frequency of silence in Kosovo and Metohija.

2.3. Region of mountain climatic features

III-a Mountain Climatic Region. Besides the climatic regions of valleys and fields, climatic regions with mountainous and sub-mountainous climate can be selected in Kosovo and Metohija. Apart from Dragaš, there are no meteorological stations in these, so their basic climatic indicator have been obtained indirectly through gradients. All the edges of mountains and valleys between 1000 and 1500 metres of height have sub-mountainous climate. Above the sub- mountainous climatic belt, there is a zone of original mountainous climate. It is limited to the smaller areas of Šar Planina, Ošljak and the Prokletije Mountain. *III-a Prokletije Sub-region.* It occupies the territory from the Junika mountains in the south, across Đeravica, Koprivnik, the mountain of Mokra, Hajla, Žljeb, Rusolija to Mokra Gora, in the north-east. The average negative monthly temperature only occurs at heights above 2200m as the average negative monthly temperatures are from November to April, i.e. six months. The amount of precipitation decreases from the south-north direction. The largest amount of precipitation is received in the south-west parts of the Prokletije Mountains, at approximately 2300 m, in the spring region of the River Pećka Bistrica 2200mm, while the north-east parts of the Prokletije Mountains receive considerably less 1200mm (Ivanovic, 1991). The greatest amount of precipitation occurs in November and in December as the smallest one occurs in August. The relative disruption of precipitation decreases from the south (more than 7) to the north (Čečevo 5.26).

III-b Šar Planina Sub-region. It involves the northern slopes of Šar Planina Mountain from the Kačanicka Gorge in the east to Koritnik in the west. Apart from Šar Planina, Ošljak, Jezerska and Žar Mountain belong to this region. Two dells are embedded between these mountains, Sirinić and Sredska with more moderate climate than the nearby regions so these can be differentiated as vineyards. The average annual temperature in Dragaš (1060m) is 8.3°C as the negative monthly temperatures are four to five months over the year. Šar Planina Mountain receives more than 800 mm of precipitation with the astern parts receiving slightly more than the western parts (Jažince 1011mm, Dragaš 813mm). The central parts of Šar Planina Mountain (Zaplužje) have 49, the

eastern parts 42 and the western ones 34 snowy days. The snow cover lasts for 62.4 days in Dragaš, up to 95 days in Zaplužje. Wind is common. The participation of silence is just 197%. The south wind also known as Jugo or Solunac has characteristics of the foehn wind.

III-c Kopaonik Sub-region. The southern and western slopes of Kopaonik belong to Kosovo and Metohija. Apart from Kopaonik, the mountain of Rogozna also belongs to this sub-region. The average annual temperature is 3.7°C (The meteorological observatory of Kopaonik is at the northern slopes at 1760 m above sea level). The coldest month is January with -5.2°C as the warmest month is August with 12.8°C. The average negative monthly temperatures occur over 4 to five months. Kopaonik receives a very small amount of precipitation. The precipitation station of Borčane (1100 m above sea level) only receives 728 mm of precipitation. The biggest number of precipitation is in May as the smallest one is in February and March. There are about 43 snowy days and the snow cover lasts for 76 days on average. There is noticeable windiness-the participation of silence is 174%.

III-d East Kosovo Sub-region. It is located in the easternmost part of the province, between Malo Kosovo in the north and the Krivorečki Basin and the Gnjilane Valley in the south. It is composed of low mountains, 1200m high, among which Koznica, Prugovac and Žegavac domineer. The average annual temperature is from 8 to 10°C and negative temperatures occur over two to three months. The annual amount of precipitation is approximately 800 mm. There are approximately 30 snowy days and the snow cover lasts for about 50 days.

4. RESULTS AND DISCUSSION

Kosovo and Metohija have specific climate. The influences of the Mediterranean and the Eurasian continent intermingle in this territory. Thereby, it is at the transitional stage from real Mediterranean climate to real continental climate. Mediterranean influences are the strongest in southern Metohija and we move to the north and east of the province, they become weaker, so that at the easternmost frontiers, there is a visible continental feature of the climate. This has, of course, influenced the possibility of climate differentiation in Kosovo and Metohija, with the exact number of climatic regions. The high mountains surrounding the territory have influenced the selection of mountainous climatic regions with a number of sub-regions In Kosovo and Metohija and that with geo-spatial analysis in GIS software derived specially map (Valjarević et al., 2015), (Fig. 1) one may select:

- The altered Mediterranean region with three sub-regions,
- The moderately continental climatic region with three sub-regions.
- The mountainous climatic region with three sub-regions.

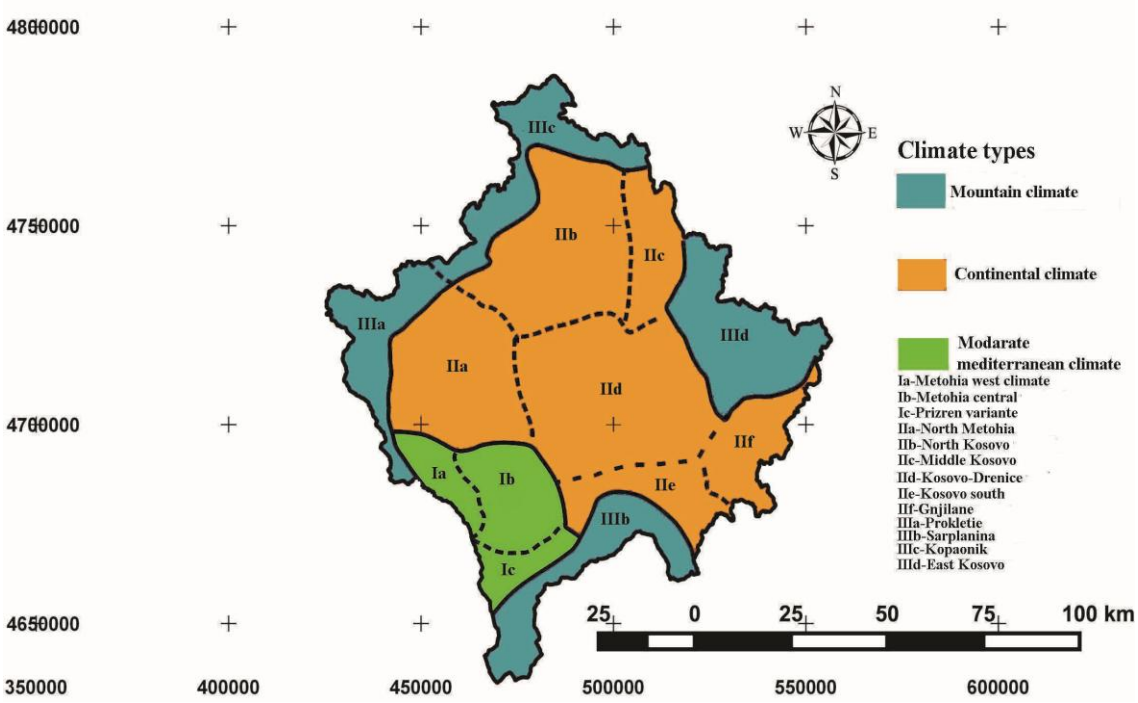

Fig. 1. Climatic Regions in Kosovo and Metohija.

ACKNOWLEDGEMENT

This work was financially supported by the Serbian Ministry of Education and Science, project No.III4008.

REFERENCES

Ivanović, R. 1991. Količina i režim padavina na Prokletijama. . In: 13. Kongres geografa Jugoslavije. Priština.

Ivanović, R. 1996. Stepen kontinentalnosti klime Kosova i Metohije. In Zbornik radova „Fizičko geografski procesi na Kosovu i Metohiji“ I. PMF Priština.

Labus, D. 1981. Klimatski rejoni Kosova i Metohije. In Geografska istraživanja 3.Priština: Geografsko društvo Kosova i Metohije.

Otorepec, S. 1973. Prilog agroklimatskom rejoniranju uslova vlaženja u Jugoslaviji po HTK Seljaninova. Arhiv za poljoprivredne nauke, Beograd, 26(96).

Radovanović, M. 1996. Klimatska regionalizacija Metohije. GI "Jovan Cvijić" SANU, Beograd, 48. Posebna izdanja.

Rakićević, T. 1980. Klimatsko rejoniranje Srbije. Zbornik radova PMF Beograd, 27.

Valjarević, A., Srećković-Batoćanin, D., Živković, D., & Perić, M. 2015. GIS analysis of dissipation time of landscape in the Devil's city (Serbia). Acta Montanistica Slovaca, 20(2), pp. 148-155.

Vujević, P. 1955. Razlika u visini letnjih i jesenjih padavina kao merilo njihovog maritimiteta odnosno, kontinentaliteta. Zbornik radova GI "Jovan Cvijić" SANU, . knj. 10.

Vujević, P. 1956. Klimatološka statistika.Beograd: Naučna knjiga.

* E-mail: radomir.ivanovic@pr.ac.rs

UNIVERSITY THOUGHT
Publication in Natural Sciences, Vol. 6, N^{o} 1, 2016, pp. 55-59.
doi:10.5937/univtho6-9797
Original Scientific Paper

LEVEL CROSSING RATE OF MACRODIVERSITY WITH THREE MICRODIVERSITY SC RECEIVERS OVER GAMMA SHADOWED NAKAGAMI-*M* CHANNEL

Goran Petković[1], Stefan Panić[2*], Branimir Jakšić[1]

[1]Faculty of Technical Sciences, University of Priština, Kosovska Mitrovica, Serbia.

[2]Faculty of Natural Sciences and Mathematics, University of Priština, Kosovska Mitrovica, Serbia.

ABSTRACT

Macrodiversity system with macrodiversity selection combining (SC) receiver and three microdiversity SC receivers operating over Gamma shadowed Nakagami-m multipath fading environment is considered in this work. Level crossing arte of signals at outputs microdiversity SC receivers are calculated and by using these formulas, closed form expression for average level crossing rate of macrodiversity SC receiver output signal is evaluated. Average fade duration of proposed macrodiversity system can be calculated as ratio of outage probability and level crossing rate. By using obtained results the influence of Nakagami-m multipath fading severity parameter, Gamma shadowing severity parameter and shadowing correlation parameter on average level crossing rate is analyzed and discussed.

Key words: gamma shadowed, level crossing rate, Nakagami-*m*, macrodiversity, microdiversity, selection combiner.

1. INTRODUCTION

Macrodiversity techniques can be used to reduce simultaneously long term fading and short term fading effects on system performance of wireless communication systems. Macrodiversity reception has application in cellular mobile radio systems. Macrodiversity system is consisting of macrodiversity SC receiver and two or more microdiversity receivers. Macrodiversity receiver combines signals with multiple antennas at base station resulting in reduction of short term fading effects and macrodiversity receiver combines signals with two or more base stations resulting in reduction of long term fading effects on system performance (Stuber, 2003), (Goldsmith, 2005).

Level crossing rate is important the second order performance measure of wireless communication system which can be calculated as average value of random process the first derivative. Average fade duration is defined as average time that resultant signal bellow specified level and can be calculated as ratio of outage probability and level crossing rate (Lee, 1993). Outage probability is the first order performance measure of wireless system and is defined as probability that resultant signal falls bellow of specified threshold. Nakagami-*m* distribution can be used to describe signal envelope variation in fading channels. This distribution has one parameter *m*. When parameter m goes to one, Nakagami-*m* distribution reduces to Rayleigh distribution and when *m* goes to infinity Nakagami-*m* multipath fading channel becomes no fading channel. Long term fading channel can be described by using Gamma distribution (Proakis, 2001), (Panic et al., 2013).

There are more works in open technical literature consisting performance of wireless macrodiversity communication systems operating over composite fading channels in the presence long term fading and short term fading. In (Stefanovic et al., 2011) macrodiversity system with macrodiversity SC receiver and two microdiversity MRC receivers operating over Gamma shadowed Nakagami-*m* multipath fading channel and the second order performance of proposed wireless communication system such as the average level crossing rate and the average fade duration are calculated. Average fade duration and average level crossing rate of wireless communication system in the presence Gamma long term fading and Rician short term fading are evaluated and the influence of Rician factor on level crossing rate is analyzed in (Sekulovic & Stefanovic, 2012) and

(Panic et al., 2014). In (Stefanovic et al., 2014) macrodiversity system with two microdiversity SC receivers in the presence Gamma large scale fading and *k*-μ small scale fading is considered and the second order performance measures are evaluated.

In this paper, wireless microdiversity communication system with macrodiversity SC receiver and three microdiversity SC receivers operating over Gamma shadowed Nakagami-*m* multipath fading channel. Average level crossing rates signals at outputs of microdiversity SC receivers are calculated and by using these formulas, closed form expression of macrodiversity SC receiver output signal is calculated. By using this expression average fade duration of proposed macrodiversity system can be evaluated. To the best author's knowledge, average level crossing rate of macrodiversity reception with macrodiversity SC receiver and three microdiversity SC receivers in the presence Gamma shadowing and Nakagami-*m* multipath fading.

2. LEVEL CROSSING RATE SIGNALS AT OUTPUTS OF MICRODIVERSITY SC RECEIVERS

Wireless macrodiversity communication system considered in this paper is shown at Fig. 1. Macrodiversity reception system consists of macrodiversity selection combinig receiver and three microdiversity SC receivers. Macrodiversity SC receiver selects microdiversity SC receiver with the highest signal envelope average power to provide service to user. Microdiversity SC receivers have two inputs.

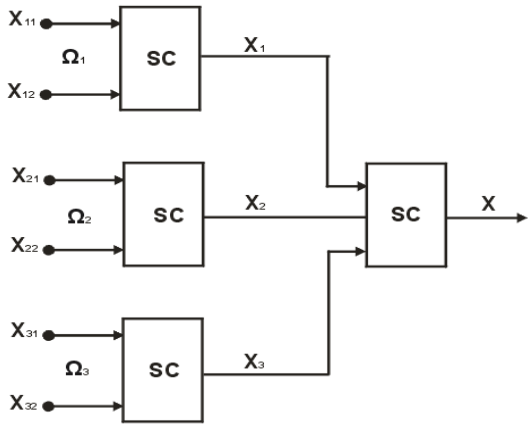

Fig. 1 Macrodiversity system.

Signal envelope at inputs and outputs of microdiversity receivers and at inputs and output of macrodiversity SC receiver are denoted at Figure 1. Signal envelopes average power at inputs of microdiversity SC receivers are denoted with Ω_1, Ω_2 and Ω_3. Random variables x_{ij}, i=1,2, j=1,2 follow Nakagami-*m* distribution (Djordjevic et al., 2015):

$$p_{x_{ij}}\left(x_{ij}\right)=\frac{2}{\Gamma\left(m\right)}\left(\frac{m}{\Omega_i}\right)^m x_{ij}^{2m-1}e^{-\frac{m}{\Omega_i}x_{ij}^2},\quad x_{ij}\geq 0 \qquad (1)$$

where m is Nakagami-*m* multipath fading severity parameter. Cumulative distribution function of x_{ij} is:

$$F_{x_{ij}}\left(x_{ij}\right)=\frac{1}{\Gamma\left(m\right)}\gamma\left(m,\frac{m}{\Omega_i}x_{ij}^2\right),\quad x_{ij}\geq 0 \qquad (2)$$

Joint probability density function of x_i and $\dot{x}_i$ is:

$$\begin{aligned}p_{x_i\dot{x}_i}\left(x_i\dot{x}_i\right)&=p_{x_{i1}\dot{x}_{i1}}\left(x_i,\dot{x}_i\right)F_{x_{i2}}\left(x_i\right)+\\&+p_{x_{i2}\dot{x}_{i2}}\left(x_i,\dot{x}_i\right)F_{x_{i1}}\left(x_i\right)=\\&=2p_{x_{i1}\dot{x}_{i1}}\left(x_i,\dot{x}_i\right)F_{x_{i2}}\left(x_i\right)=\\&=\frac{2}{\Gamma\left(m\right)}\left(\frac{m}{\Omega_i}\right)^m x_i^{2m-1}e^{-\frac{m}{\Omega_i}x_i^2}\times\\&\times\frac{1}{\sqrt{2\pi\beta_1}}e^{-\frac{\dot{x}_i^2}{2\beta_1}},\quad i=1,2,3\end{aligned} \qquad (3)$$

where $\beta_1=\pi^2 f_m^2\frac{\Omega_i}{m}$, f_m is maximal Doppler frequency.

Average level crossing rate of microdiversity SC receivers output signals is (Djosic et al., 2015):

$$\begin{aligned}N_{x_i}&=\int_0^\infty d\dot{x}_i\cdot\dot{x}_i\cdot p_{x_i\dot{x}_i}\left(x_i\dot{x}_i\right)=2N_{x_{i2}}F_{x_{i2}}\left(x_i\right)=\\&=\frac{4\pi f_m}{\Gamma\left(m\right)}\left(\frac{m}{\Omega_i}\right)^{m-\frac{1}{2}}x_i^{2m-1}e^{-\frac{m}{\Omega_i}x_i^2}\times\frac{1}{\Gamma\left(m\right)}\gamma\left(m,\frac{m}{\Omega_i}x_i^2\right)\end{aligned} \qquad (4)$$

where $\gamma(n,x)$ is the incomplete Gamma function (Gradshteyn, & Ryzhik, 2000), (Prudnikov et al., 2015).

Random variable Ω_1, Ω_2 and Ω_3 follow correlated Gamma distribution:

$$\begin{aligned}p_{\Omega_1\Omega_2\Omega_3}\left(\Omega_1\Omega_2\Omega_3\right)&=\frac{1}{\Gamma\left(c\right)\left(1-\rho^2\right)^2\rho^{c-1}\Omega_0^{c+2}}\times\\&\times e^{-\frac{\Omega_1+\left(1+\rho^2\right)\Omega_2+\Omega_3}{2\Omega_0\left(1-\rho^2\right)}}\sum_{i_1=0}^{\infty}\left(\frac{\rho}{\Omega_0\left(1-\rho^2\right)}\right)^{2i_1+c-1}\times\end{aligned}$$

$$\times\frac{1}{i_1!\Gamma(i_1+c)}\sum_{i_2=0}^{\infty}\left(\frac{\rho}{\Omega_0\left(1-\rho^2\right)}\right)^{2i_2+c-1}\times$$
$$\times\frac{1}{i_2!\Gamma(i_2+c)}\Omega_1^{i_1+c-1}\Omega_2^{i_1+i_2+c-1}\Omega_3^{i_2+c-1} \quad (5)$$

where c is Gamma long term fading severity parameter, ρ is Gamma long term fading correlation coefficient and Ω_0 is signal envelope average power. Previously expression is derived for case when correlation matrix is exponential.

3. LEVEL CROSSING RATE OF MACRODIVERSITY SC RECEIVER OUTPUT SIGNAL

Average level crossing rate of output of macrodiversity SC receiver is:

$$N_x=\int_0^{\infty}d\Omega_1\int_0^{\Omega_1}d\Omega_2\int_0^{\Omega_1}d\Omega_3 N_{x_1/\Omega_1}p_{\Omega_1\Omega_2\Omega_3}(\Omega_1\Omega_2\Omega_3)+$$
$$+\int_0^{\infty}d\Omega_2\int_0^{\Omega_2}d\Omega_1\int_0^{\Omega_2}d\Omega_3 N_{x_2/\Omega_2}p_{\Omega_1\Omega_2\Omega_3}(\Omega_1\Omega_2\Omega_3)+$$
$$+\int_0^{\infty}d\Omega_3\int_0^{\Omega_3}d\Omega_1\int_0^{\Omega_3}d\Omega_2 N_{x_3/\Omega_3}p_{\Omega_1\Omega_2\Omega_3}(\Omega_1\Omega_2\Omega_3)=$$
$$=I_1+I_2+I_3 \quad (6)$$

The integral I_1 is:

$$I_1=\int_0^{\infty}d\Omega_1\int_0^{\Omega_1}d\Omega_2\int_0^{\Omega_1}d\Omega_3 N_{x_1/\Omega_1}p_{\Omega_1\Omega_2\Omega_3}(\Omega_1\Omega_2\Omega_3)=$$
$$=\frac{4\pi f_m}{\Gamma(m)}m^{2m-3/2}x^{4m-1}\sum_{j_1=0}^{\infty}\frac{1}{(m+1)_{(j_1)}}m^{j_1}x^{2j_1}\times$$
$$\times\sum_{i_1=0}^{\infty}\left(\frac{\rho}{\Omega_0\left(1-\rho^2\right)}\right)^{2i_1+c-1}\frac{1}{i_1!\Gamma(i_1+c)}\times$$
$$\times\sum_{i_2=0}^{\infty}\left(\frac{\rho}{\Omega_0\left(1-\rho^2\right)}\right)^{2i_2+c-1}\frac{1}{i_2!\Gamma(i_2+c)}\times$$
$$\times\frac{1}{i_1+i_2+c}\sum_{j_2=0}^{\infty}\frac{1}{(i_1+i_2+c+1)_{(j_2)}}\left(\frac{1+\rho^2}{\Omega_0\left(1-\rho^2\right)}\right)^{j_2}\times$$
$$\times\frac{1}{i_2+c}\sum_{j_3=0}^{\infty}\frac{1}{(i_2+c+1)_{(j_3)}}\left(\frac{1}{\Omega_0\left(1-\rho^2\right)}\right)^{j_3}\times$$
$$\times\left(\frac{2mx^2\Omega_0\left(1-\rho^2\right)}{3+\rho^2}\right)^{-m+i_1+i_2-\frac{j_1}{2}+\frac{j_2}{2}+\frac{j_3}{2}+\frac{3c}{2}+\frac{1}{4}}\times$$
$$\times K_{-2m+2i_1+2i_2-j_1+j_2+j_3+3c+\frac{1}{2}}\left(2\sqrt{\frac{2mx^2\left(3+\rho^2\right)}{\Omega_0\left(1-\rho^2\right)}}\right) \quad (7)$$

where $(a)_n$ denoting the Pochhammer symbol (Gradshteyn, & Ryzhik, 2000) and where $K_n(x)$ is the modified Bessel function of the second kind, order n and argument x.

The integral I_2 is:

$$I_2=\int_0^{\infty}d\Omega_2\int_0^{\Omega_2}d\Omega_1\int_0^{\Omega_2}d\Omega_3 N_{x_2/\Omega_2}p_{\Omega_1\Omega_2\Omega_3}(\Omega_1\Omega_2\Omega_3)=$$
$$=\frac{4\pi f_m}{\Gamma(m)}m^{2m-3/2}x^{4m-1}\sum_{j_1=0}^{\infty}\frac{1}{(m+1)_{(j_1)}}m^{j_1}x^{2j_1}\times$$
$$\times\sum_{i_1=0}^{\infty}\left(\frac{\rho}{\Omega_0\left(1-\rho^2\right)}\right)^{2i_1+c-1}\frac{1}{i_1!\Gamma(i_1+c)}\times$$
$$\times\sum_{i_2=0}^{\infty}\left(\frac{\rho}{\Omega_0\left(1-\rho^2\right)}\right)^{2i_2+c-1}\frac{1}{i_2!\Gamma(i_2+c)}\times$$
$$\times\frac{1}{i_1+c}\sum_{j_2=0}^{\infty}\frac{1}{(i_1+c+1)_{(j_2)}}\left(\frac{1}{\Omega_0\left(1-\rho^2\right)}\right)^{j_2}\times$$
$$\times\frac{1}{i_2+c}\sum_{j_3=0}^{\infty}\frac{1}{(i_2+c+1)_{(j_3)}}\left(\frac{1}{\Omega_0\left(1-\rho^2\right)}\right)^{j_3}\times$$
$$\times\left(\frac{2mx^2\Omega_0\left(1-\rho^2\right)}{3+\rho^2}\right)^{-m+i_1+i_2-\frac{j_1}{2}+\frac{j_2}{2}+\frac{j_3}{2}+\frac{3c}{2}+\frac{1}{4}}\times$$
$$\times K_{-2m+2i_1+2i_2-j_1+j_2+j_3+3c+\frac{1}{2}}\left(2\sqrt{\frac{2mx^2\left(3+\rho^2\right)}{\Omega_0\left(1-\rho^2\right)}}\right) \quad (8)$$

4. NUMERICAL RESULTS

Average level crossing rate of macrodiversity reception with macrodiversity SC receiver and three microdiversity SC receivers versus resulting signal for several values of Gamma parameter c and correlation coefficient ρ is presented on Fig. 2. Level crossing rate increases for lower values of resulting signal and level crossing rate decreases for higher values resulting signal. The influence of resulting signal on level crossing rate is higher for lower values of resulting

signal. As Gamma parameter *c* increases average level crossing rate decreases resulting in system performance improvement. The influence of Gamma parameter *c* on average level crossing rate is higher for higher values of resulting envelope. When Gamma parameter *c* increases, maximum of curve goes to higher values of resulting signal and maximum has higher values.

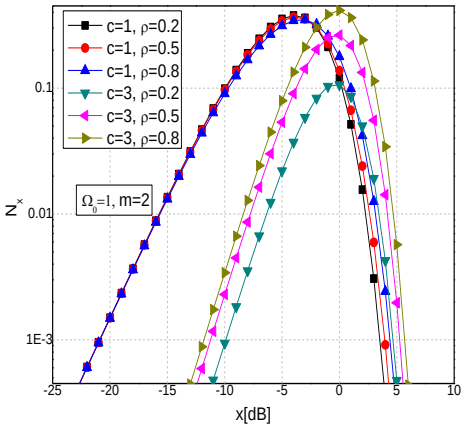

Fig. 2 Level crossing rate of macrodiversity SC receiver output signal envelope.

As correlation coefficient increases, average level crossing rate increases in system performance degradation. When correlation coefficient goes to one, the least signal occurs at both microdiversity receivers simultaneously. The influence of correlation on average level crossing rate is higher for higher values of Gamma parameter *c*.

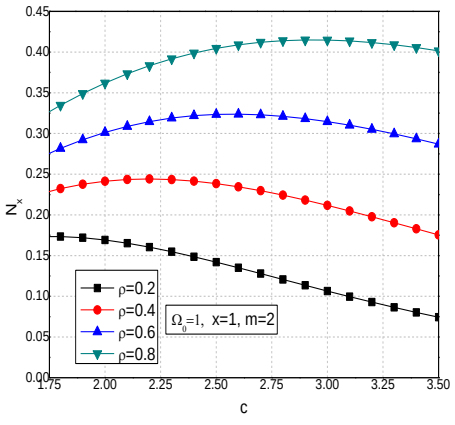

Fig. 3 Level crossing rate of macrodiversity SC receiver output signal envelope versus Gamma shadowing severity parameter *c*.

Normalized average level crossing rate versus Gamma long term fading severity parameter *c* for several values of correlation coefficient and for average power Ω_0=1, resulting signal *x*=1 and Nakagami parameter *m*=2 is shown on Fig. 3. When parameter increases, curves have maximum. For higher values of parameter *c*, average level crossing rate decreases as parameter c increases. Average level crossing rate increases as correlation coefficient increases. The influence coefficient ρ on average level crossing rate is higher for higher values of parameter *c*.

5. Conclusion

Macrodiversity system with microdiversity selection combining receiver (SC) and three microdiversity selection combining receivers operating over correlated Gamma shadowed Nakagami-m multipath fading environment is considered. Macrodiversity SC reception mitigates Gamma long term fading effects and microdiversity SC reception reduces Nakagami-*m* short term fading effects on system performance. Long term fading is correlated due to three base stations are shadowed by the same obstacle. Short term fading is independent because antenna spacing at microdiversity is achieved that correlation coefficient of multipath fading goes to zero (Krstic et al., 2014). In this paper closed form expressions for average level crossing rate of macrodiversity SC receivers output signals are calculated and these expressions are used for calculation average level crossing rate of macrodiversity SC receiver output signal. By using this formula can be calculated average fade duration of proposed macrodiversity system as ratio of outage probability and average level crossing rate. By using derived expression for average level crossing rate can be evaluated average fade duration and average level crossing rate of macrodiversity techniques with three microdiversity SC receivers in composite Gamma long term fading and short Nakagami-m fading channel. The system performance is better for lower values of level crossing rate. When Nakagami-*m* multipath fading severity parameter increases, average level crossing rate decreases resulting in system performance improvement. Also, system performance is better for higher values of Gamma long term fading severity parameter. When correlation coefficient goes

to one macrodiversity system becomes microdiversity system.

REFERENCES

Djordjević, N., Jakšić, B., Matović, A., Matović, M., & Smilić M. 2015. Moments of Microdiversity EGC receivers and Macrodiversity SC Receiver Output Signal over Gamma Shadowed Nakagami-m Multipath Fading Channel, Journal of Electrical Engineering, 66 (6), pp. 348-351, doi:12.2478/jee-2015/0058.

Djošić, D., Stefanović, D., & Stefanović C. 2015. Level crossing rate of Macro-diversity system with Two Micro-diversity SC Receivers over Correlated Gamma Shadowed α-μ Multipath Fading Channel, IETE Journal of Research, doi: 10.1080/03772063.2015.1075913.

Goldsmith, A. 2005. Wireless communications. Cambridge: Cambridge University press.

Gradshteyn, I. S., & Ryzhik, I. M. 2000. Table of Integrals, Series and Products. San Diego: Academic Press.

Krstić, D., Glabowski, M., Radenković, D., & Temelkovski, I. 2014. Level crossing rate of MRC receiver over η-μ multipath fading, Proceedings of 9th International Symposium on Communication System Networks& Digital Signal Processing CSNDSP, 23th-25th July 2014. Manchester.

Lee, W. C. Y. 1993. Mobile Communications Design Fundamentals, 2nd ed. New York: John Wiley & Sons Inc.

Panic, S., Bandjur, Dj., Jaksic, B., Dinic, I., Zdravkovic, S, & Jaksic, D. 2014. Level crossing rate of macrodiversity system operating over gamma shadowed Rician fading channel, Proceedings of X International Symposium Industrial Electronics INDEL, 6th-8th November 2014. Banja Luka.

Panic, S., Stefanovic, M., Anastasov, J., & Spalevic, P. 2013. Fading and Interference Mitigation in Wireless Communications. USA: CRC Press.

Proakis, J. 2001. Digital Communications, 4nd ed. New York: McGraw-Hill.

Prudnikov, A. P., Brychkov, Y. A., & Marichev, O. I. 1986. Integrals and Series Volume 3: More Special Functions, 1st ed. New York: Gordon and Breach Science Publishers.

Stefanovic, D., Panic, S., & Spalevic, P. 2011. Second-order statistics of SC macrodiversity system operating over Gamma shadowed Nakagami-m fading channels, International Journal of Electronics and Communications, 65 (5), pp. 413-418. doi: 10.1016/j.aeue.2010.05.001

Stuber, G. L. 2003. Mobile communication, 2nd ed. Dordrecht: Kluwer Academic Publisher.

Sekulovic, N., & Stefanović, M. 2012. Performance Analysis of System with Micro- and Macrodiversity Reception in Correlated Gamma Shadowed Rician Fading Channels, Wireless Personal Communications (publisher: Springer), 65 (1), pp. 143-156

Stefanovic, M., Jaksic, B., Stefanovic, C., Markovic, A., Smilic, M., & Dinic, I. 2014. Level Crossing Rate of Macrodiversity System with Three Microdiversity SC Receivers Operating over Gamma Shadowed Multipath Fading Channel, Proceedings of International Scientific Conference UNITECH, 21th-29th November 2014. Gabrovo.

* E-mail: stefan.panic@pr.ac.rs

UNIVERSITY THOUGHT
Publication in Natural Sciences, Vol. 6, N^{o} 1, 2016, pp. 60-66.
doi:10.5937/univtho6-10768
Original Scientific Paper

THE RULE BASED CLASSIFICATION MODELS FOR MHC BINDING PREDICTION AND IDENTIFICATION OF THE MOST RELEVANT PHYSICOCHEMICAL PROPERTIES FOR THE INDIVIDUAL ALLELE

Davorka Jandrlić[1*]

[1]Faculty of Mechanical Engineering, University of Belgrade, Belgrade, Serbia.

ABSTRACT

Binding of proteolyzed fragments of proteins to MHC molecules is essential and the most selective step that determines T-cell epitopes. Therefore, the prediction of MHC-peptide binding is principal for anticipating potential T cell epitopes and is of immense relevance in vaccine design. Despite numerous methods for predicting MHC binding ligands, there still exist limitations that affect the reliability of a prevailing number of methods. Certain important methods based on physicochemical properties have very low reported accuracy. The aim of this paper is to present a new approach of extracting the most important physicochemical properties that influence the classification of MHC-binding ligands. In this study, we have developed rule based classification models which take into account the physicochemical properties of amino acids and their frequencies. The models use k-means clustering technique for extracting the relevant physicochemical properties. The results of the study indicate that the physicochemical properties of amino acids contribute significantly to the peptide-binding and that the different alleles are characterized by a different set of the physicochemical properties.

Key words:K – mean clustering, The rule based classification, MHC - peptide binding.

1. INTRODUCTION

Binding of peptides, derived by the intracellular processing of protein antigen(s) (Ag(s)) to MHC proteins, is the most selective step in defining T-cell epitopes. Computational methods, based on reverse immunology, are essential steps in the identification of T-cell epitope candidates, and complement epitope screening by predicting the best binding peptides.

Computational epitope-prediction programs are trained on the known peptide-binding affinities to a particular MHC molecule (or a defined set of MHC molecules) and fall into two categories (Brusić et al., 2004), (Yang et al.,2009): sequence-based and structure-based. The focus of this study is on sequence-based methods. A detailed list of the majority of currently available predictors with their prediction precision is described in (Luo et al., 2014).

Most of the predictors are based on sparse or BLOSUM50 encoding of peptide sequences, and different methods of machine learning are used: ANN, HMM, Decision Tree and SVM. Of all the predictors presented above, only POPI (Tung et al., 2007) uses physicochemical (PC) properties as input features. However, this predictor gives a evaluation qualitative of prediction with very low reported accuracy (~ 60%) (Luo et al., 2015). This was the reason for the investigation of the influence of different PC properties on peptide-binding.

The models obtained here predict MHC-binding ligands with very high accuracy. However, the main purpose of the developed models was not the prediction of MHC binding ligands, but rather identification of those PC characteristics that have the greatest impact on the classification of peptides into binders and non-binders. Fromour previous research (Mitić et al., 2014), (Pavlović et al., 2014), (Jandrlić et al, 2016) there was evidence that there were some characteristics that influence the binders appearance, for example, hydrophobicity, hydrophilicity, appertaining to ordered protein structure, etc., and there is certainly a great need for reliable methods based on high-quality experimental data for classification and prediction of MHC binding ligands and epitopes as a complement to existing ones.

2. EXPERIMENTAL

2.1. Materials and methods

In order to avoid the problems of inconsistent data to obtain reliable models, such as differing measures of binding affinity, etc., we chose to use only the data from the Immune Epitope Database (IEDB) (http://www.iedb.org/), June 2015 version, which is regularly updated, as the most reliable source of MHC-binding ligands. All experimentally proven MHC-binding ligands for all available alleles were downloaded. The research has been limited to peptides of 9 amino acids (AAs) in length because nonamers are the most common MHC-I epitopes, and to peptides of 15 amino acids (AAs) in length for MHC-II class, because there are only enough experimental data to construct good models for that length of the peptide. The data for those ligands for which there were no qualitative and quantitative measures (binding affinity and verification of whether a ligand is positive or negative), ligands labeled as both positive and negative, and as being found in the same protein at the same position and peptides containing AA not in α = {A, R, N, D, C, Q, E, G, H, I, L, K, M, F, P, S, T, W, Y, V}, were discarded. For all the alleles listed in Table 1 we created separate models and provided the results. For each of the allele the numbers of positive and negative epitopes involved in developing and testing the model are shown.

Table 1. Overview of alleles for which prediction models were made, as well as the number of positive and negative ligands (peptides) per studied allele.

Allele	No. of ligands	Trainset (Positive/Negative)	Test set (Positive/Negative)
HLA-A*02:01	5915	2010/2130	416/789
HLA-A*03:01	4014	970/1839	416/789
HLA-A*11:01	3306	972/1341	417/576
HLA-A*02:03	2304	793/819	340/352
HLA-B*15:01	3160	1010/1201	433/516
HLA-B*07:02	2606	97/1127	299/483
HLA-A*01:01	2577	347/1456	149/625
HLA-A*02:06	1695	733/452	315/195
HLA-A*24:02	1568	609/488	261/210
HLA-A*02:02	1339	618/319	265/137
HLA-B*08:01	1570	388/710	167/305
HLA-A*26:01	2534	244/1528	106/656
HLA-A*A31:01	2970	644/1434	277/615
HLA-DRB1*04:01	1321	657/267	282/115
HLA-DRB1*01:01	4987	2977/513	1276/221

2.1.1. Model building

The most important step in designing a reliable classification model is the choice of methodology for representing the data and feature selection. The most convenient way to represent the input data is in the form of a vector. That is why each peptide has to be represented by a vector whose components are obtained by the application of some weighting function. The representation of peptides in the form of vectors of its PC properties is also not uncommon, but as mentioned above, these methods are not shown very well in term of accuracy. The possible problem could be that each allele is generalized and all are characterized by the same group of PC properties (by applying principal component analyses or factor analyses). In this study, the peptide is represented using its combination unigrams and bigrams frequencies and specific PC properties, as described below.

2.1.2. Calculating the frequency of AAs

Calculating the frequency of AAs at appropriate positions in a peptide is aimed at extracting the features of occurrence of AAs in peptide binders and non-binders, which would enable easier classification. Instead of the standard calculation of AA frequency by position in a peptide, we used a modified calculation of frequency which was successfully implemented in document classification. Δ-TFIDF technique was first introduced in (Martineau et al., 2009) for the document classification problems, where this technique was applied to terms within a text, providing better results in classification of documents, than those obtained by a simple calculation of the frequency of terms or binary encoding. The task of classifying documents can easily be turned into the task of classifying peptides into binding and non-binding ligands. In a similar way, we calculated the Δ-TFIDF for individual AAs and bigrams in a peptide.

In our case, the term t, element of this method, is an AA (unigram) or bigram from the set of all AAs that occur in a peptide. For instance, in a peptide p = LVIKALLEV, t could be from the set {L, V, I, K, A, L, L, E, V, LV, VI, IK, KA, AL, LL, LE, EV}. Table 2 shows the basic definition and equations used for calculation of AA frequencies, applying Δ-TFIDF technique.

Table 2. Frequency measures

Equation	Definition
$df(t,S)$	Represents the frequency of the term *t* in a set of peptides *S*.
$idf(t,S) = log_2 \frac{\|S\|}{df(t,S)}$	Represents the inverse frequency of the term *t* in the set of peptides *S*, where $\|S\|$ is the cardinality of set S.
$tf(t, Peptide)$	Represents the number of occurrences of the term *t* in the peptide *Peptide* itself.

Taking into account equations from the table 2, the Δ -TFIDF measure, is introduced as:

$$\Delta tfidf(t_i, Peptide, S^+, S^-) = tf(t_i, Peptide) * \log_2 \frac{|S^+|}{df(t_i, S^+)} * \frac{df(t_i, S^-)}{|S^-|} \quad (1)$$

where t_i is AA or bigram in peptide Peptide from set S, at position i. S^+ and S^- are the subsets of S, of positive ligands (binders) and negative ligands (non binders), respectively. $|S^+|$ and $|S^-|$ are the cardinalities of the positive and negative sets. This way of transforming the frequency of AAs in a peptide gives greater importance to AAs that are not equally represented in the positive and negative sets, and less importance to those AAs that are more or less equally represented (the same holds for bigrams). Using the Δ -TFIDF measure, each peptide is represented as a vector of weights of its AAs and bigrams. If peptides are 9 AAs in length, an assigned vector is 9 + 8 = 17 in length. An obvious problem arises with peptides that have AAs or bigrams that do not occur in both classes, i.e. where $df(t, S^{\pm}) = 0$. Another problem is the non-linearity of AA frequency. These issues are resolved with the introduction of smoothing factors (Joachims, 1997). Here we engaged the Δ-BM25 smoothing measure (Joachims, 2005), a corrected frequency calculation, so as to avoid division with 0 in those cases where an AA occurs in only one of the sets. The Δ-BM25-IDF measure was chosen because it was found to be the best solution in the classification of texts (Joachims, 2005). With the inclusion of the Δ-BM25 smoothing factor, frequency is calculated through the equation:

$$\Delta BM25\ idf(t_i) = log \frac{(|S^+| - \Delta idf(t_i, S^+) + 0.5) * \Delta idf(t_i, S^-) + 0.5}{(|S^-| - \Delta idf(t_i, S^-) + 0.5) * \Delta idf(t_i, S^+) + 0.5} \quad (2)$$

This technique is simple and easily applied and understood.

2.1.3. Encoding peptide using physicochemical properties

The PC properties of the AAs are the information that could point to the similarity between AAs or bigrams within the peptide. The 119 PC properties (23 kinds of electronic properties, 37 kinds of steric properties, 54 kinds of hydrophobic properties and 5 kinds of hydrogen bond) were taken from the paper (Tian et al., 2009). Instead of using all PC properties for peptide representation, the common practice of reducing the number of properties which uses principal component analysis (PCA) or factor analyses (FA) and then selects some of the principal components or factors. This way, all the alleles are generalized, irrespective of whether certain properties are characteristic for a single allele. The aim of this research was to investigate specific allele characteristics and to evaluate influence of each individual PC property on classification peptides into MHC binders or non-binders. The peptide is firstly encoded with single PC property, in this way peptide is represented with vector of length 17 (9 + 8) with the numerical value obtained by applying PC property on appropriate consecutive AAs and bigrams from that peptide. This procedure is carried out for every single PC.

2.1.4.Classification rule based model building and selection of the most important physicochemical properties

To evaluate the importance of single PC property, for each PC property *fk* (k = 1,..., 119) and every single allele, a new rule based classification model was constructed. The set of all peptides associated with single allele is divided into a training and test subsets (70:30%). The peptides in both sets were

encoded with Δ-BM25 technique applied on unigrams and bigrams (see 2.1.2) and the component values were multiplied by the appropriate PC property value (see 2.1.3). For example, for the first PC property the following vector was obtained:

$$\begin{aligned}[w_{f_1}] &= w \cdot f_1 \\ &= [w_{11} \cdot f_1(AA_1), \dots, w_{19} \cdot f_1(AA_9), \\ &\quad w_{21} \cdot \frac{f_1(AA_1) + f_1(AA_2)}{2}, \dots, w_{28} \\ &\quad \cdot \frac{f_1(AA_8) + f_1(AA_9)}{2}]\end{aligned} \tag{3}$$

Then the k-means clustering technique (Hartigan, 1975) was applied to the positive (binders) and negative (non-binders) subsets of the training set, individually, with k = 3, three centroids per set are found that define the clusters. As a measure of the distance of the vector from the centroids, Euclidean distance was used. The number of clusters was determined empirically. Increasing the number of clusters increases the precision of the methods, but decreases the recall. Silhouette method was used for validation of consistency of the data within clusters (Rousseeuw, 1986).

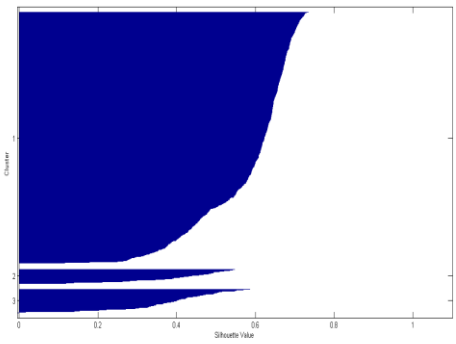

Fig. 1 Visualization of the clusters from thepositive training set for the HLA-A*1101 allele, where the peptides (binders) are encoded with the best PC property.

Fig. 1. represents clusters visualization of silhouette measure forallele HLA-A*1101. The silhouette value for each point *i* is a measure of how similar that point is to points in its own cluster, when compared to points in other clusters. The silhouette value ranges from -1 to +1. A high silhouette value indicates that *i* is well-matched to its own cluster, and poorly-matched to neighboring clusters. If most points have a high silhouette value, then the clustering solution is appropriate. The main purpose of clustering is to find the centroids, cluster representatives, that define all peptides from positive set and negative set. The centroids could serve as leading points for separating binders from non-binders.

The rule based binary classification models were made and identification of the best PC properties was done through the following steps:

1. Each peptideis encoded in the abovementioned manner; it is understood that if a peptide is closer to one of the positive class centroids, then it is a binder, but if it is closer to one of the negative class centroids, then it can be considered a non-binder.
2. For individual PC property the model is constructed (step 1.), the model was applied on the test set and the Kappa statistic, Accuracy, Precision and Recall are calculated (as described in the chapter 2.2);
3. The procedure (step 1. and 2.) is carried out for each of the PC properties.
4. Ten models with the highest accuracy are selected. The PC property involved in peptide encoding for the input into these models have been chosen as the best.
5. Finally, a consensus model is constructed from these ten best models. The consensus model takes into account results from *k* number of models (*k* is fewer or equal to 10) and if *k* number of these models are in agreement that peptide is binder then the observed peptide is considered a binder. Otherwise, the peptide is considered as non-binder. The choice of threshold for value *k* is treated as a maximization problem in terms of accuracy of the final model, on the training set. The minimal number of individual models is chosen to achieve the best accuracy.
6. The consensus model is tested on a set of peptides which were not presented during the training stage (Test Set, see Table 1).

The 119 models obtained in step 2. (for single allele) served for the selection of the 10 “best” PC properties (for unigrams and bigrams); and their construction was to compare the contributions of individual PC properties in the separation of binders from non-binders for a particular allele. The results of the consensus model constructed from the 10 best models are shown in Table 3, in the chapter Results. The list of 10 best PC properties (identified from these models) for each individual allele is presented in Supplement.

2.2. Performance evaluation

To evaluate the performance of our methods comprehensively, we report standard performance

measures, including accuracy, precision, recall and Kappa statistic as follows:

$$Accuracy = \frac{\mathrm{TP} + \mathrm{TN}}{TP + FP + TN + FN}$$

$$Precision = \frac{\mathrm{TP}}{TP+FP} \quad (4)$$

$$Recall = \frac{\mathrm{TP}}{TP + FN}$$

where *TP*, *TN*, *FP* and *FN* respectively denote the number of true positives (correctly predicted binders), true negatives (correctly predicted non-binders), false positives (falsely predicted binders) and false negatives (falsely predicted non-binders).

Calculation of Cohen's kappa is performed according to the following formula:

$$Kappa = \frac{\Pr\ (a)\ - \Pr\ (e)}{1 - \Pr\ (e)}$$

$$\Pr(a) = \frac{TP+TN}{TP+FP+FN+TN} \quad (5)$$

$$\Pr(e) = \frac{(TP + FP) * (TP + FN) + (TN + FP) * (TN + FN)}{(TP + FN + FP + TN)^2}$$

Pr(a) represents the actual observed agreement, and *Pr(e)*represents chance agreement (Roy et al., 2015). Cohen's kappa analysis returns values between −1 (no agreement) and 1 (complete agreement).

3. RESULTSAND DISCUSSION

The results and performance measures of developed models for each individual allele are presented in the table 3. The measures of the training set indicate how well binders and non-binders are separated by calculated centroids of positive and negative clusters respectively. The measures of accuracy for all models are over 94% indicating that the centroids represent the binders and non binders well, i.e. binders indeed cluster around the 3 positive cluster centroids selected in this way. Similarly, non-binders cluster around negative3 centroids. Chosen PC properties are very good for characterizing binders related to individual allele.

Furthermore, clustering peptide into two groups - binders and non binders - is not a feasible task, and cannot be done just by applying *k*-means clustering algorithm on the entire set of peptides. In this research, it was established that a selection of three appropriate centroids for positive ligands (binder), based on extracted PC properties, describes very well the entire bindersset for single alleles (the same conclusion holds for negative ligands, as well). The results on test sets indicate how well the developed rule-based classification model generalizes on the blind set. Accuracy for almost all models on test sets is close to or over 80%, which confirms that certain combinations of physicochemical properties of AAs in peptide separates binders from non-binders with high accuracy. All models are tested on another MHC class I and II dataset collected from the MHCBN repository (http://www.imtech.res.in/raghava/mhcbn/mhcbinder_download.html). There is no overlapping between these datasets and IEDB datasets. The results on this dataset for all models also show high accuracy (see Supplement where comparative results for all datasets are shown).

Table 3. Comparative performance evaluation in terms of precision/recall/accuracy for: developed rule based classification models on training and test sets, the best currently existing predictor NetMHCpan (for MHC I)/NetMHCIIpan (for MHC class II) and MHCPred predictor.

Allele	Training	Test	NetMHCPan2.8	MHCPred
HLA-A0201	0.93 / 0.95 / 0.94	0.87 / 0.82 / 0.85	0.97 / 0.83 / 0.91	0.73 / 0.76 / 0.74
HLA-A0301	0.88 / 0.98 / 0.95	0.76 / 0.71 / 0.82	0.90 / 0.86 / 0.92	0.43 / 0.86 / 0.56
HLA-A1101	0.93 / 0.97 / 0.95	0.86 / 0.72 / 0.83	0.97 / 0.86 / 0.93	0.42 / 0.99 / 0.43
HLA-A0203	0.95 / 0.98 / 0.97	0.81 / 0.75 / 0.79	0.96 / 0.88 / 0.92	0.54 / 0.88 / 0.57
HLA-B1501	0.95 / 0.98 / 0.97	0.90 / 0.79 / 0.86	0.99 / 0.80 / 0.90	N/A
HLA-B0702	0.95 / 0.99 / 0.98	0.84 / 0.65 / 0.82	0.92 / 0.92 / 0.94	N/A
HLA-A0101	0.93 / 0.99 / 0.97	0.78 / 0.51 / 0.88	0.72 / 0.97 / 0.92	0.55 / 0.71 / 0.83
HLA-A0206	0.98 / 0.99 / 0.98	0.79 / 0.84 / 0.76	0.94 / 0.89 / 0.90	0.63 / 0.83 / 0.59
HLA-A2402	0.98 / 0.98 / 0.98	0.72 / 0.71 / 0.70	0.88 / 0.85 / 0.85	N/A
HLA-A3101	0.89 / 0.97 / 0.95	0.72 / 0.61 / 0.81	0.86 / 0.82 / 0.90	0.41 / 0.41 / 0.63
HLA-A0202	0.99 / 0.99 / 0.99	0.81 / 0.91 / 0.79	0.96 / 0.85 / 0.88	0.77 / 0.78 / 0.70
HLA-B0801	0.98 / 0.99 / 0.98	0.84 / 0.74 / 0.86	0.97 / 0.87 / 0.95	N/A
HLA-A2601	0.87 / 0.99 / 0.98	0.73 / 0.51 / 0.91	0.78 / 0.90 / 0.95	N/A
Allele	**Training**	**Test**	**NetMHCIIPan20**	**MHCPred**
HLA-DRB10101	0.99 / 0.94 / 0.95	0.88 / 0.92 / 0.82	0.97 / 0.92 / 0.91	0.85 / 0.99 / 0.85
HLA-DRB10401	0.98 / 0.98 / 0.98	0.78 / 0.93 / 0.76	0.95 / 0.80 / 0.64	0.72 / 0.99 / 0.72

The consensus threshold value represents the number of models, based on individual PC property, that are enough to include in the consensus model to achieve the best accuracy. The values of threshold k smaller than ten indicate that for a good classification model it is not necessary to use all ten PC properties and that a smaller number of k properties have enough influence to separate binders from non-binders for that allele. An interesting finding is that for MHC II class alleles (HLA-DRB1*01:01 and HLA-DRB1*04:01) there are only three PC properties that have enough influence on decision when the peptide is a potential binder. The list of PC properties associated for all involved alleles is presented in the Supplement. On the basis of alleles that are associated with the same physicochemical properties we can make a conclusion about similarity of alleles themselves. It is expected that alleles classified into the same supertype (Sidney et al., 2001), share data about most important PC

properties. It also can be seen that some of PC information is shared between different supertypes. Fig. 2 presents six of the most important *PC* properties, in the sense of being common for the largest number of alleles, their relationship is depicted with arrows from allele to PC property. It could be seen that an allele HLA-A*68:02 is characterized with PC properties: PC21, PC90, PC58, PC1 (pK-C, Partition coefficient, Flexibility parameter for no rigid neighbors, alpha-NH chemical shifts) and share importan PC properties as allele HLA-A*11:01 and HLA-A*31:01 which is to be expected as they belong to the same supertype A3. However, for allele HLA-A*02:03 and allele HLA-B*08:01 the common PC properties are crucial for separating binders from non-binders even if these two alleles do not belong to the same supertype. This confirm the claim by Heckerman (Heckerman et al., 2007) that there are some characteristics that are common for binders independent off allele and supertypes specific characteristics. All this information could be used in consideration for making better MHC binding prediction models. We have analyzed this information and used it as input features in different machine learning models, which produce even better results (this part of research is submitted for publication elsewhere).

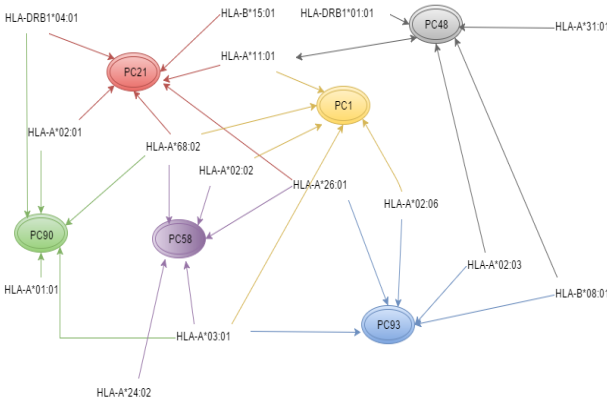

Fig. 2. The first six PC properties, according to number of alleles that are assigned to, that best separate binders from non binders: PC1 - alpha-NH chemical shifts; PC48 – Bulkiness; PC58 - Flexibility parameter for no rigid neighbors; PC90 - Partition coefficient; PC21- pK-C; PC93 Average gain ratio in surrounding hydrophobicity (all of them are taken from (Tian et al., 2009)and HLA – alleles related to them.

4. Conclusion

In this study, the new position-dependent method for classifying peptides into MHC binders and non-binders, is presented. Binary rule based classification models were made for 13 different alleles of MHC class I and 2 alleles for MHC class II. Vector components used as input features into models that represent peptides were obtained based on the physicochemical properties of the consecutive amino acids and bigrams contained in the peptides and application of the weighting technique for frequency calculation well established in the problems of the text categorization and opinion mining problems, but had never before been used for this type of problem. The models obtained have high accuracy. The goal of developed models was not to beat currently existing predictors, but to identify the most relevant PC properties for classification peptides into MHC binding ligands and non-binding ligands. However, in order to demonstrate the usefulness and reliability of the models developed, we compared them with two predictors: NetMHC(II)pan (Nielsen et al., 2007), (Nielsen et al, 2008) which is refered as the best curruntly existing predictors and MHCPred (Pingping et al, 2003). Summary results are shown in Table 3. and graphical presentation of comparative analyses is illustrated in Fig 3. The developed models had a significanty higher predictive performance than MHCPred predictor, but lower that NetMHCpan predictor.It should be noted that the test set for evaluation of these three predictors was blind test only for models developed here, but probably involved in training for NetMHC(II)pan models.

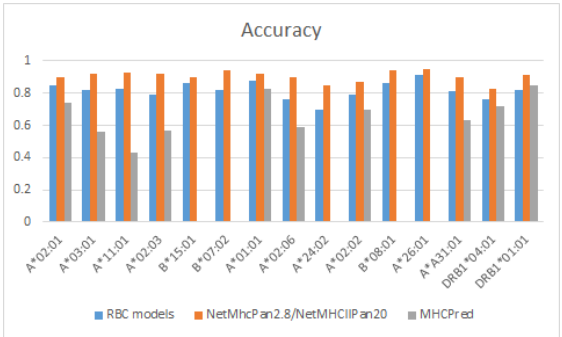

Fig. 3. The comparative analysis of the accuracy of the rule-based classification (RBC) models, NetMHC(II) Pan and MHC Pred predictor.

It is demonstrated that the certain PC properties have huge impact on the separation binders from non-binders and that their combination with a frequency measure can serve as input features in the new models for predicting MHC binding ligands. One would

expect that machine learning models with the these input parameters provide even better performance.

ACKNOWLEDGEMENT

The work presented has been financially supported by the Ministry of Education, Science and Technological Development, Republic of Serbia, Projects No. 174002.

REFERENCES

Brusic, V., Bajic, V.B., & Petrovsky, N. 2004. Computational methods for prediction of T-cell epitopes: A framework for modelling, testing, and applications. Methods, 34(4), pp. 436-43, pmid:15542369.

Hartigan, J.A. 1975. Clustering Algorithms.New York, NY: USA John Wiley & Sons..

Heckerman, D., Kadie, C., & Listgarten, J. 2007. Leveraging information across HLA alleles/supertypes improves epitope prediction. J Comput Biol, 14(6), pp. 736-746. doi:10.1089/cmb.2007.R013.

Jandrlić, R.D., Lazić, M.G., Mitić, S.N., & Pavlović, D.M. 2016. Software tools for simultaneous data visualization and T cell epitopes and disorder prediction in proteins. Journal of Biomedical Informatics, . doi:10.1016/j.jbi.2016.01.016.

Joachims, T. 1997. A probabilistic analysis of the rocchio algorithm with tfidf for text categorization. . In: InInternational Conference on Machine Learning, ICML.

Joachims, T. 2005. Text categorization with Support Vector Machines: Learning with many relevant features. Sprnger.Lecture Notes in Computer Science, 1398, pp. 137-142.

Luo, H., Ye, H., Ng, H.W., Shi, L., Tong, W., Mendrick, D.L., & Hong, H. 2015. Machine Learning Methods for Predicting HLA-Peptide Binding Activity. Bioinform Biol Insights, 9(3), pp. 21-29, doi:10.4137/BBI.S29466.

Mitić, S.N., Pavlović, D.M., & Jandrlić, R.D. 2014. Epitope distribution in ordered and disordered protein regions: Part A. T-cell epitope frequency, affinity and hydropathy. J Immunol Methods, 406, pp. 83-103, doi:10.1016/j.jim.2014.02.012.

Martineau Justin, , & Finin Tim, 2009. Delta TFIDF: An Improved Feature Space for Sentiment Analysis. . In: Proceedings of the Third AAAI Internatonal Conference on Weblogs and Social Media. San Jose, CA: AAAI Press. May.

Nielsen, M., Lundegaard, C., Blicher, T., Lamberth, K., Harndahl, M., Justesen, S., & et al., 2007. NetMHCpan, a method for quantitative predictions of peptide binding to any HLA-A and -B locus protein of known sequence.PLoS One, 2(8). doi:10.1371/journal.pone.0000796.

Nielsen, M., Lundegaard, C., Blicher, T., Peters, B., Sette, A., Justesen, S., & et al., 2008. Quantitative predictions of peptide binding to any HLA-DR molecule of known sequence: NetMHCIIpan. PLoS Comput Biol, 4(7), p. 1000107, doi:10.1371/journal.pcbi.1000107.

Pavlović, D.M., Jandrlić, R.D., & Mitić, S.N. 2014. Epitope distribution in ordered and disordered protein regions. Part B: Ordered regions and disordered binding sites are targets of T- and B-cell immunity. J Immunol Methods, 407, pp. 90-107, doi:10.1016/j.jim.2014.03.027.

Pingping Guan, I.A.D., Christianna Zygouri, , & Flower, D.R. 2003. MHCPred: A server for quantitative prediction of peptide-MHC binding., pp. 3621-3624.

Rousseeuw, P.J. 1986. Silhouettes: A graphical aid to the interpretation and validation of cluster analysis. Journal of Computational and Applied Mathematics, . doi:10.1016/0377-0427(87)90125-7.

Roy, K., Kar, S., & Das, R.N. 2015. A Primer on QSAR/QSPR Modeling. Retrieved from http://www.springer.com/978-3-319-17280-4

Sidney, J., Southwood, S., Mann, D.L., Fernandez-Vina, M.A., Neuman, M.J., & Sette, A. 2001. Majority of peptides binding HLA-A*0201 with high affinity crossreact with other A2-supertype molecules. Hum Immunol, 62, pp. 1200-1216.

Tian, F., Yang, L., Lv, F., Yang, Q., & Zhou, P. 2009. In silico quantitative prediction of peptides binding affinity to human MHC molecule: An intuitive quantitative structure-activity relationship approach. Amino Acids, 36(3), pp. 535-554, doi:10.1007/s00726-008-0116-8.

Tung, C.W., & Ho, S.Y. 2007. POPI: predicting immunogenicity of MHC class I binding peptides by mining informative physicochemical properties. Bioinformatics, 23(8), pp. 942-949, doi:10.1093/bioinformatics/btm061.

Yang, X., & Yu, X. 2009. An introduction to epitope prediction methods and software. Rev Med Virol, 19(2), pp. 77-96, doi:10.1002/rmv.602

.

* E-mail: djandrlic@mas.bg.ac.rs

UNIVERSITY THOUGHT
Publication in Natural Sciences, Vol. 6, N° 1, 2016, pp. 67-70.
doi:10.5937/univtho6-11214
Original Scientific Paper

A NOTE ON MAPPINGS AND ALMOST MENGER AND RELATED SPACES

Ljubiša Kočinac[1*]

[1]Faculty of Sciences and Mathematics, University of Niš, Niš, Serbia.

ABSTRACT

We consider behaviour of the almost Menger, almost Rothberger, almost Hurewicz, and almost γ-set properties under several kinds of mappings between topological spaces.

Key words: Almost Menger, almost Hurewicz, almost Rothberger, almost γ-set, ɵ-continuity, weak continuity.

1. INTRODUCTION

Throughout the paper (X,τ), or shortly X, will denote a topological space on which no separation axioms are assumed unless explicitly stated. For a subset A of (X,τ), Int(A) and Cl(A) will denote the interior and the closure of A, respectively. Our other notation and terminology are standard as in (Engelking, 1989).

The following classical covering properties were defined long time ago. A topological space X is said to be:

(1) A *Menger space* (or has the *Menger (covering) property*) (Menger,1924), (Hurewicz, 1925) if for each sequence $(\mathcal{U}_n)_{n\in\mathbf{N}}$ of open covers of X there exists a sequence $(\mathcal{V}_n)_{n\in\mathbf{N}}$ of finite sets such that for each $n\in\mathbf{N}$, $\mathcal{V}_n$ is a subset of $\mathcal{U}_n$ and $\bigcup_{n\in\mathbf{N}}\mathcal{V}_n$ is an open cover of X;

(2) A *Hurewicz space* (Hurewicz, 1925) if for each sequence $(\mathcal{U}_n)_{n\in\mathbf{N}}$ of open covers of X there is a sequence $(\mathcal{V}_n)_{n\in\mathbf{N}}$ such that for each n, $\mathcal{V}_n$ is a finite subset of $\mathcal{U}_n$ and each $x\in X$ belongs to $\bigcup\mathcal{V}_n$ for all but finitely many n;

(3) A *Rothberger space* (Rothberger, 1938) if for each sequence $(\mathcal{U}_n)_{n\in\mathbf{N}}$ of open covers of X there exists a sequence $(U_n)_{n\in\mathbf{N}}$ such that for each $n\in\mathbf{N}$, $U_n\in\mathcal{U}_n$ and $\{U_n: n\in\mathbf{N}\}$ is an open cover of X;

(4) A *γ-set* (Gerlits & Nagy, 1982) if for each sequence $(\mathcal{U}_n)_{n\in\mathbf{N}}$ of ω-covers of X there is a sequence $(U_n)_{n\in\mathbf{N}}$ such that for each $n\in\mathbf{N}$, $U_n\in\mathcal{U}_n$ and each $x\in X$ belongs to U_n for all but finitely many n.

[Recall that an open cover $\mathcal{U}$ of a space X is called an *ω-cover* if X does not belong to $\mathcal{U}$ and each finite subset of X is contained in a member of $\mathcal{U}$.]

For more information about these spaces we refer the reader, for example, to (Kočinac, 2006), (Kočinac, 2015). Note that the first two properties are between two important covering properties -- σ-compactness and Lindelöfness. In the last two decades these spaces and their relations with other mathematical disciplines (such as game theory, Ramsey theory and so on) have been systematically studied by a big number of mathematicians. Also, some weaker forms of these properties were investigated from different points of view, see (Babinkostova et. al., 2012), (Babinkostova et. al., 2013), (Daniels, 1988), (Di Maio & Kocinac, 2008), (Kocev, 2009), (Kočinac, 1999), (Kočinac, 2001), (Pansera, 2012), (Sabah et al., 2016), (Sakai, 2013).

In (Kočinac, 1999), Kočinac introduced almost Menger and almost Rothberger spaces as generalizations of almost Lindelöf spaces introduced in (Willard, & Dissanayake, 1984). In (Di Maio & Kocinac, 2008) the almost Menger property was considered in hyperspaces. Further investigation of almost Menger spaces was done in (Kocev, 2009), and (Babinkostova et. al., 2012), (Babinkostova et. al., 2013). In (Kocev, 2009), the almost γ-sets have been introduced.

Definition 1.1. (a) (Kočinac, 1999) A space (X,τ) is *almost Menger* if for each sequence $(\mathcal{U}_n)_{n\in\mathbf{N}}$ of open covers of X there is a sequence $(\mathcal{V}_n)_{n\in\mathbf{N}}$ of finite sets such that for each $n\in\mathbf{N}$, $\mathcal{V}_n$ is a finite subset of $\mathcal{U}_n$ and $\bigcup_{n\in\mathbf{N}}\bigcup\{\mathrm{Cl}(V): V\in\mathcal{V}_n\}=X$;

(b) (Kočinac, 1999) A space X is *almost Rothberger* if for each sequence $(\mathcal{U}_n)_{n\in\mathbf{N}}$ of open covers of X there is a sequence $(U_n)_{n\in\mathbf{N}}$ such that for each $n\in\mathbf{N}$, $U_n\in\mathcal{U}_n$ and $\bigcup_{n\in\mathbf{N}}\mathrm{Cl}(U_n)=X$;

(c) (Kocev, 2009) A space X is an *almost γ-set* if for each sequence $(\mathcal{U}_n)_{n \in \mathbf{N}}$ of ω-covers of X there exists a sequence $(U_n)_{n \in N}$ such that for each $n \in \mathbf{N}$, $U_n \in \mathcal{U}_n$ and each $x \in X$ belongs to $\mathrm{Cl}(U_n)$ for all but finitely many n.

In this paper we introduce the class of almost Hurewicz spaces and consider behaviour of the almost Menger, almost Hurewicz, almost Rothberger and almost γ-set properties under several kinds of mappings between topological spaces. Note that these properties are useful in studying of non-regular spaces.

2. RESULTS

We recall now the notion of (strong) θ-continuity which is an important slight generalization of continuity.

A mapping $f: X \to Y$ is *θ-continuous* (Fomin, 1941), (Fomin, 1943), see also (Pansera, 2012) (*strongly θ-continuous*) (Long & Herrington, 1981) if for each $x \in X$,and each open set V in Y containing $f(x)$ there is an open set U in X containing x such that $f(\mathrm{Cl}(U))$ is a subset of $\mathrm{Cl}(V)$ ($f(\mathrm{Cl}(U))$ is a subset of V).

Evidently, each strongly θ-continuous mapping is θ-continuous.

Theorem 2.1. *A θ-continuous image of an almost Menger space is also almost Menger.*

Proof. Let X be an almost Menger space and $Y = f(X)$ its image under a θ-continuous mapping $f: X \to Y$. Let $(\mathcal{V}_n)_{n \in N}$ be a sequence of open covers of Y. Fix $x \in X$. For each $n \in \mathbf{N}$ there is a set $V(x,n) \in \mathcal{V}_n$ containing $f(x)$. Since f is θ-continuous there is an open set $U(x,n)$ in X containing x such that $f(\mathrm{Cl}(U(x,n))$ is a subset of $\mathrm{Cl}(V(x,n))$. Therefore, for each n the set $\mathcal{U}_n := \{U(x,n): x \in X\}$ is an open cover of X. As X is almost Menger there is a sequence $(\mathcal{H}_n)_{n \in N}$ of finite sets such that for each n, $\mathcal{H}_n = \{U(x_i,n): i \leq k_n\}$ is a subset of $\mathcal{U}_n$ and $X = \bigcup_{n \in N} \bigcup \{\mathrm{Cl}(H): H \in \mathcal{H}_n\}$. To each $U(x_i,n) \in \mathcal{H}_n$ assign a set $W(x_i,n) \in \mathcal{V}_n$ such that $f(\mathrm{Cl}(U(x_i,n))$ is a subset of $\mathrm{Cl}(W(x_i,n))$ and set $\mathcal{W}_n = \{W(x_i,n): i \leq k_n\}$. We obtain the sequence $(\mathcal{W}_n)_{n \in N}$ of finite subsets of $\mathcal{V}_n$, $n \in \mathbf{N}$, such that

$$Y = f(X) = f(\bigcup_{n \in N} \bigcup \{\mathrm{Cl}(H): H \in \mathcal{H}_n\}),$$

which is by the previous a subset of

$$\bigcup_{n \in N} \bigcup \{\mathrm{Cl}(W): W \in \mathcal{W}_n\},$$

i.e. Y is almost Menger. □

Recall that a mapping $f: X \to Y$ is called *almost continuous* (Singal & Singal, 1968) if the preimage of any regular open set V in Y is open in X. Each almost continuous mapping is θ-continuous. So, the above theorem extends and generalizes the following result:

Corollary 2.2. (Kocev, 2009), Theorem 2.3 *The almost Menger property is preserved by almost continuous mappings.*

Similarly to the proof of Theorem 2.1 one proves the following theorem.

Theorem 2.3. *A θ-continuous image of an almost Rothberger space is also almost Rothberger.*

Corollary 2.4. *The almost Rothberger property is preserved by almost continuous mappings.*

Definition 2.5. A space X is said to be an *almost Hurewicz space* if for each sequence $(\mathcal{U}_n)_{n \in \mathbf{N}}$ of open covers of X there is a sequence $(\mathcal{V}_n)_{n \in N}$ such that for each n, $\mathcal{V}_n$ is a finite subset of $\mathcal{U}_n$ and for each $x \in X$, x belongs to $\mathrm{Cl}(\bigcup \mathcal{V}_n)$ for all but finitely many n.

Theorem 2.6. *A θ-continuous image of an almost γ-set is an almost Hurewicz space.*

Proof. Let $(\mathcal{V}_n)_{n \in \mathbf{N}}$ be a sequence of open covers of Y. Let $x \in X$. For each $n \in \mathbf{N}$ there is $V(x,n) \in \mathcal{V}_n$ containing $f(x)$. Since f is θ-continuous there is an open set $U(x,n)$ in X containing x such that $f(\mathrm{Cl}(U(x,n)))$ is a subset of $\mathrm{Cl}(V(x,n))$. For each n let $\mathcal{U}_n$ be the set of all finite unions of sets $U(x,n)$, $x \in X$. Evidently, each $\mathcal{U}_n$ is an ω-cover of X. As X is an almost γ-set there is a sequence $(U_n)_{n \in N}$ such that for each n, $U_n \in \mathcal{U}_n$ and each $x \in X$ does not belong to $\mathrm{Cl}(U_n)$ for at most finitely many n.

Let $U_n = U(x_1,n) \cup U(x_2,n) \cup \ldots \cup U(x_{i(n)},n)$. To each $U(x_j,n)$, $j \leq i(n)$, assign a set $V(x_j,n) \in \mathcal{V}_n$ with $f(\mathrm{Cl}\})(U(x_j,n)))$ a subset of $\mathrm{Cl}(V(x_j,n))$. Let $y = f(x) \in Y$. Then from $x \in \mathrm{Cl}(U_n)$ for all $n \geq n_0$ for some $n_0 \in \mathbf{N}$, we get $x \in \mathrm{Cl}(U(x_p,n))$ for some $1 \leq p \leq i(n)$ which implies $y \in f(\mathrm{Cl}(U(x_p,n)))$ which is a subset of $\mathrm{Cl}(V(x_p,n))$. If we put $\mathcal{W}_n = \{V(x_j,n): j = 1,2, \ldots, i(n)\}$, we obtain the sequence $(\mathcal{W}_n)_{n \in N}$ of finite subsets of $\mathcal{V}_n$, $n \in \mathbf{N}$, such that each $y \in Y$ belongs to all but finitely many sets $\bigcup\{\mathrm{Cl}(W): W \in \mathcal{W}_n\}$. This just means that Y is an almost Hurewicz space. □

Theorem 2.7. *A strongly θ-continuous image Y of an almost Menger space X is a Menger space.*

Proof. Let $(\mathcal{V}_n)_{n \in \mathbf{N}}$ be a sequence of open covers of Y. Let $x \in X$. For each $n \in \mathbf{N}$ there is a set $V_{x,n} \in \mathcal{V}_n$ containing $f(x)$. Since f is strongly θ-continuous there is an open set $U_{x,n}$ in X containing x such that $f(\mathrm{Cl}(U_{x,n}))$ is a subset $V_{x,n}$. Therefore, for each n, the set $\mathcal{U}_n := \{U_{x,n}: x \in X\}$ is an open cover of X. As X is almost Menger there is a sequence $(\mathcal{F}_n)_{n \in \mathbf{N}}$ of finite sets such that for each n, $\mathcal{F}_n$ is a subset of $\mathcal{U}_n$ and $X = \bigcup_{n \in \mathbf{N}} \bigcup \{\mathrm{Cl}(F): F \in \mathcal{F}_n\}$.To each $F \in \mathcal{F}_n$ assign a set $W_F \in \mathcal{V}_n$ with $f(\mathrm{Cl}(F))$ a subset of W_F and put $\mathcal{W}_n = \{W_F: F \in \mathcal{F}_n\}$. We obtain the sequence $(\mathcal{W}_n)_{n \in \mathbf{N}}$ of finite subsets of $\mathcal{V}_n$, $n \in \mathbf{N}$, which witnesses for $(\mathcal{V}_n)_{n \in \mathbf{N}}$ that Y is a Menger space, as it is easily checked. □

In a quite similar way we prove the following theorem.

Theorem 2.8. *A strongly θ-continuous image Y of an almost Hurewicz (almost Rothberger) space X is a Hurewicz (Rothberger) space.*

A mapping $f: X \to Y$ is called *contra-continuous* (Dontchev, 1996), if the preimage of each open set in Y is closed in X. f is said to be *precontinuous* (Mashhour et al.,1982) if $f^{\leftarrow}(V)$ is a subset of $\mathrm{Int}(\mathrm{Cl}(f^{\leftarrow}(V)))$ whenever V is open in Y.

Theorem 2.9. *A contra-continuous, precontinuous image Y of an almost Menger space X is a Menger space.*

Proof. Let $(\mathcal{V}_n)_{n \in \mathbf{N}}$ be a sequence of open covers of Y. Since f is contra-continuous for each $n \in \mathbf{N}$ and each $V \in \mathcal{V}_n$ the set $f^{\leftarrow}(V)$ is closed in X. On the other hand, because f is precontinuous $f^{\leftarrow}(V)$ is a subset of $\mathrm{Int}(\mathrm{Cl}(f^{\leftarrow}(V)))$, so that $f^{\leftarrow}(V)$ is a subset $\mathrm{Int}(f^{\leftarrow}(V))$, i.e. $f^{\leftarrow}(V) = \mathrm{Int}(f^{\leftarrow}(V))$. Therefore, for each n, the set $\mathcal{U}_n = \{f^{\leftarrow}(V): V \in \mathcal{V}\}$ is a cover of X by open sets. As X is an almost Menger space there is a sequence $(\mathcal{G}_n)_{n \in \mathbf{N}}$ such that for each n, $\mathcal{G}_n$ is a finite subset of $\mathcal{U}_n$ and $\bigcup_{n \in \mathbf{N}} \bigcup \{\mathrm{Cl}(G): G \in \mathcal{G}_n\} = X$. Then $\mathcal{W}_n = \{f(G): G \in \mathcal{G}_n\}$ is a finite subset of $\mathcal{V}_n$ for each $n \in \mathbf{N}$ and $\bigcup_{n \in \mathbf{N}} \bigcup \mathcal{W}_n$ is an open cover of Y. This means that Y is a Menger space. □

Recall that a mapping $f: X \to Y$ is called *weakly continuous* (Levine, 1960), (Levine, 1961), if for each $x \in X$ and each neighbourhood V of $f(x)$ there is a neighbourhood U of x such $f(U)$ is contained in $\mathrm{Cl}(V)$.

Theorem 2.10. *A weakly continuous image Y of a Menger space X is an almost Menger space.*

Proof. Let $(\mathcal{V}_n)_{n \in \mathbf{N}}$ be a sequence of open covers of Y. Let $x \in X$. Then for each $n \in \mathbf{N}$ there is a $V \in \mathcal{V}_n$ such that $f(x) \in V$. Since f is weakly continuous there is an open set $U_{x,n}$ in X such that $x \in U_{x,n}$ and $f(U_{x,n})$ is a subset of $\mathrm{Cl}(V)$. The set $\mathcal{U}_n := \{U_{x,n}: x \in X\}$ is an open cover of X. Apply the fact that X is a Menger space to the sequence $(\mathcal{U}_n)_{n \in \mathbf{N}}$ and find a sequence $(\mathcal{F}_n)_{n \in \mathbf{N}}$ of finite sets such that for each n, $\mathcal{F}_n$ is a subset of $\mathcal{U}_n$ and $\bigcup_{n \in \mathbf{N}} \mathcal{F}_n$ is an open cover of X. To each n and each $U \in \mathcal{F}_n$ assign a set $V_U \in \mathcal{V}_n$ such that $f(U)$ is a subset of $\mathrm{Cl}(V_U)$ and put $\mathcal{W}_n = \{V_U: U \in \mathcal{F}_n\}$. Then

$$Y = f(X) = f\left(\bigcup_{n \in \mathbf{N}} \bigcup \{U: U \in \mathcal{F}_n\}\right)$$

which is contained in

$$\bigcup_{n \in \mathbf{N}} \bigcup \{\mathrm{Cl}(V_U): U \in \mathcal{F}_n\},$$

i.e. Y is an almost Menger space. □

References

Babinkostova, L., Pansera, B. A., & Scheepers, M. 2012. Weak covering properties and infinite games. Topology Appl., 159, pp. 3644-3657.

Babinkostova, L., Pansera, B. A., & Scheepers, M. 2013. Weak covering properties and selection principles. Topology Appl., 160, pp. 2251-2271.

Daniels, P. 1988. Pixley-Roy spaces over subsets of the reals. Topology Appl., 29, pp. 93-106.

di Maio, G., & Kocinac, D. R. Lj. 2008. Some covering properties of hyperspaces. Topology Appl., 155, pp. 1959-1969.

Dontchev, J. 1996. Contra-continuous functions and strongly S-closed spaces. Inter. J. Math. Math. Sci., 19, pp. 303-310.

Engelking, R. 1989. General Topology, 2nd ed.Berlin: Heldermann. Sigma Ser. Pure Math Vol. 6.

Fomin, S. V. 1941. Extensions of topological Spaces. Dokl. Acad. Nauk SSSR, 32, pp. 114-116.

Fomin, S. V. 1943. Extensions of topological spaces. Ann. Math., 44, pp. 471-480.

Gerlits, J., & Zs. Nagy, 1982. Some properties of C(X) I. Topology Appl., 14, pp. 151-161.

Hurewicz, W. 1925. Uber eine Verallgemeinerung des Borelschen Theorems. Math. Z., 24, pp. 401-421.

Kocev, D. 2009. Almost Menger and related spaces. Mat. Vesnik, 61, pp. 173-180.

Kočinac, Lj. 1999. Star-Menger and related spaces II. Filomat, 13, pp. 129-140.

Kočinac, D. R. Lj. 2001. The Pixley-Roy topology and selection principles. Quest. Answers Gen. Topology, 19, pp. 219-225.

Kočinac, D. R. Lj. 2006. Some covering properties in topological and uniform spaces. Proc. Steklov Inst. Math., 252, pp. 122-137.

Kočinac, D. R. Lj. 2015. Star selection principles: A survey. Khayyam Journal of Mathematics, 1, pp. 82-106.

Levine, N. 1960. Strong continuity in topological spaces. Amer. Math. Monthly, 67, pp. 269-269.

Levine, N. 1961. A decpomposition of continuity in topolo gical spaces. Amer. Math. Monthly, 68, pp. 44-46.

Long, P. E., & Herrington, L. L. 1981. Strongly θ-continuous functions. J. Korean Math. Soc., 18, pp. 21-28.

Mashhour, A. S., El-Monsef, A. M. E., & El-Deep, S.N. 1982. On precontinuous and weak precontinuous mappings.Proc. Math. Phys. Soc. Egypt, 53, pp. 47-53.

Menger, K. 1924. Einige Überdeckungssätze der Punktmengenlehre, Sitzungsberichte. Math. Astronomie, Physik, Meteorologie und Mechanik, 133, pp. 421-444. Abt. 2a.

Pansera, B. A. 2012. Weaker forms of the Menger property. Quaest. Math., 35, pp. 161-169.

Porter, J. R., & Woods, R. G. 1988. Extensions and Absolutes of Hausdorff Spaces.Springer Verlag.

Rothberger, F. 1938. Eine Verschärfung der Eigenschalft C. Fund. Math., 30, pp. 50-55.

Sabah, A., ud Din Khan, M., & Kočinac, D. R. Lj. 2016. Covering properties defined by semi-open sets. submitted.

Sakai, M. 2013. The weak Hurewicz property of Pixley-Roy hyperspaces. Topology Appl., 160, pp. 2531-2537.

Singal, M. K., & Singal, A. R. 1968. Almost continuous mappings. Yokohama Math. J., 16, pp. 63-73.

Willard, S., & Dissanayake, U. N. B. 1984. The almost Lindelöf degree. Canadian Math. Bull., 27, pp. 452-455.

* E-mail: lkocinac@gmail.com

UNIVERSITY THOUGHT doi:10.5937/univtho6-10134
Publication in Natural Sciences, Vol. 6, N^{o} 1, 2016, pp. 71-74. Original Scientific Paper

IMPLEMENTATION OF GRADIENT METHODS FOR OPTIMIZATION OF UNDERAGE COSTS IN AVIATION INDUSTRY

Nataša Kontrec[1*], Milena Petrović[1]

[1]Faculty of Mathematics and Sciences, University of Priština, Kosovska Mitrovica, Serbia.

ABSTRACT

Underage costs are not easily quantifiable in spare parts management. These costs occur when a spare part is required and none are available in inventory. This paper provides another approach to underage cost optimization for subassemblies and assemblies in aviation industry. The quantity of spare parts is determined by using a method for airplane spare parts forecasting based on Rayleigh's model. Based on that, the underage cost per unit is determined by using the Newsvendor model. Then, by implementing a transformed accelerated double-step size gradient method, the underage costs for spare sub-assemblies and assemblies in airline industry are optimized.

Key words: cost optimization, gradient methods, spare parts.

1. INTRODUCTION

The main goal of this paper is to present an innovative implementation of gradient methods in optimization of underage costs for spare parts in aviation industry. The gradient methods represent methods for systematic research and solution finding in an iterative procedure for unconstrained optimization problems. The underage cost is defined as the cost per unit of product in case of negative inventory level at the end of the product's usability period. All airline companies share a common goal of minimizing these costs on one side and increasing the level of aircraft's availability on the other. Hence, this paper further elaborates on some of the methods of unconditional optimization.

2. THEORETICAL PART

Due to the fact that minimizing underage costs is critical, the problem will be presented as follows.
Minimizing given objective function is required:

$$(\min) \mathrm{f}\left(x\right), \quad x \in R^n, \tag{1}$$

where for some point x^* the expression (1) is satisfied. Defined point x^*can be described trough the next two definitions:
Def: Point x^* is the local minimum point if there exists a neighborhood U(x^*) such that

$$f(\mathrm{x}^*) \leq f(\mathrm{x}) \tag{2}$$

for each vector $x \in U\left(x^*\right)$.

Point x^* is the point of strict local minimum if there exists a neighborhood $U(x^*)$ such that

$$f(\mathrm{x}^*) < f(\mathrm{x}) \tag{3}$$

for each vector $x \neq x^*$ and $x \in U\left(x^*\right)$.
Def: Point $x^*$is the global minimum point if

$$f(\mathrm{x}^*) \leq f(\mathrm{x}), \quad \forall \mathrm{x} \in \mathrm{R}^n. \tag{4}$$

Then, the neighborhood $U(x^*)$ of that point exists for each vector $x \neq x^*$ and $x \in U\left(x^*\right)$such that:

$$f(\mathrm{x}^*) < f(\mathrm{x}), \quad \forall \mathrm{x} \in \mathrm{R}^n. \tag{5}$$

The practice proved it was easier to find local minimum points than finding the global minimum point. Thus, finding the global minimum point could be reduced to determination of several local minimums and then identifying the smallest. The smallest one will be declared as the global minimum. Finding the local minimum is even easier if the search is conducted at the descending vector direction. If the objective function is differentiable, than the gradient method should be used.

As stated above, the gradient methods are numerical iterative methods. In order to determine the minimal function value by using such a method, it is necessary to define the size of the iterative step and search direction since both are crucial elements of each gradient iterative scheme. There are several iterative methods, each defined in a specific way, relevant for this work. Some of them are presented in articles (Andrei, 2006), (Stanimirović et al., 2010),

(Petrović et al., 2014), (Petrović et al., 2015), (Stanimirović et. al. 2015). After their comparison, it has been concluded that the TADSS method (Stanimirović et. al., 2015) (***T**ransformed **A**ccelerated **D**ouble **S**tep **S**ize*) outperforms all other gradient iterative methods.

The essence of the TADSS method is in proper setting of numerical iterations, in order to obtain a satisfying approximate solution to the problem. The iteration process for this method is defined as:

$$x_{k+1} = x_k - \left[\alpha_k \left(\gamma_k^{-1} - 1\right) + 1\right] g_k, \qquad (6)$$

where α_k denotes the size of the iterative step – can be computed as in algorithm 1. Since the TADSS is an accelerated optimization method, the acceleration parameter that presents a multiplying factor of the size of the iterative step has to be defined. Determination of this factor is based on Taylor's expansion and appropriated approximation of Hessian and can be calculated as:

$$\gamma_{k+1} = 2\frac{f\left(x_k + 1\right) - f\left(x_k\right) + \left(\alpha_k \left(\gamma_k^{-1} - 1\right) + 1\right)\left\|g_k\right\|^2}{\left(\alpha_k \left(\gamma_k^{-1} - 1\right) + 1\right)^2 \left\|g_k\right\|^2} \qquad (7)$$

where g_k denotes a gradient vector of objective function at the *k*-th iterative point.The iterative step, according to this method, can be computed as in (7). The size of the iterative step α_k can be determined by using the following backtracking procedure:

Algorithm 8: Backtracking line search procedure for calculating iterative step $\alpha_\kappa$starting at $\alpha = 1$

Requirements: Objective function *f(x)*, the direction d_k of the search at the point x_k, real numbers $0<\sigma<0.5$ and $\eta\in(0,\sigma)$

1. Set $\alpha = 1$.
2. While $f\left(x_k + \alpha d_k\right) > f\left(x_k\right) + \sigma\alpha g_k d_k$, take $\alpha := \eta\alpha$.
3. Return $\alpha_\kappa = \alpha$.

Algorithm 9: Transformed accelerated double step size method (TADSS method)

Requirements: $0 < \rho < 1,\ 0 < \tau < 1, x_0, \gamma_0 = 1$.

1. Set*k = 0*, compute $f(x_0)$, g_0 and take $\gamma_0 = 1$.
2. If $\left\|g_k\right\| < \varepsilon$ then go to Step 8, else go to the next step.
3. Find the stepα_κ applying the Algorithm 1.
4. Compute the next interative pointx_{k+1} using (6).
5. Determine scalar γ_{k+1} using (7)
6. If $\gamma_{k+1}<0$ take $\gamma_{k+1}= 1$.
7. Set*k:= k + 1*, and go to the Step 2.
8. Return x_{k+1} and $f(x_{k+1})$.

3. EXPERIMENTAL

3.1. Method evaluation and presentation

An innovative model for spare parts assessment in aviation industry is presented in paper (Kontrec et al., 2015). This paper also includes a method for determining the required quantities of spare parts in inventory and, on those basis, determining the underage costs per unit of product. As these costs refer to individual parts, the goal of this paper is to optimize the underage costs for subassemblies or assemblies comprised of several such parts.

If the quantity of spare parts is determined, as conducted in paper (Kontrec et al., 2015), then the underage costs can be calculated by using the Newsvendor model (Hill, 2011). The Newsvendor model is widely known model used mostly when evaluation of a certain stochastic variable is required. This evaluation is a compromise between the loss that has occurred when the value of stochastic variable is underestimated and the loss that will occur if the value of that stochastic variable is overestimated, as follows:

$$q = \Phi^{-1}\left(\frac{c_u}{c_o + c_u}\right) \qquad (10)$$

Φ^{-1} denotes Inverse distribution function; c_o denotes cost per unit of product in case of positive level of inventory at the end of the product's usability period; c_u denotes the underage cost i.e. cost of unmet demand for spare part.

As on the basis of formula (10) only underage costs for individual parts can be determined, in cases where entire assembly or subassembly need to be replaced, minimizing underage costs can be conducted by using the TADSS method.

In that case, the objective function can be expressed as in (11):

$$(min)c_{uk} = \sum_{k=1}^{n} c_{oi}\left(\frac{\Phi\left(\frac{1-\exp\left(-\frac{w_{ik}{}^2\pi}{4T_{ut_i}{}^2}\right)}{\frac{\sqrt{2}w_{ik}\pi}{4T_{ut_i}}\exp\left(-\frac{w_{ik}{}^2\pi}{4T_{ut_i}{}^2}\right)}\right)}{1-\Phi\left(\frac{1-\exp\left(-\frac{w_{ik}{}^2\pi}{4T_{ut_i}{}^2}\right)}{\frac{\sqrt{2}w_{ik}\pi}{4T_{ut_i}}\exp\left(-\frac{w_{ik}{}^2\pi}{4T_{ut_i}{}^2}\right)}\right)}\right) \qquad (11)$$

$i = 1,\ldots,m$

Wherein:

c_{uk} - underage cost in certain flight hour w_k, $k = 1,\ldots,n$

c_{oi} -price per unit of the part of the assembly, where $i=1,...,m$, and $m$represents the number of parts comprised in the assembly.

T_{uti}-total unit time of i-th part comprised in the assembly.

Decision variables are:

$$w_k = \left(w_{1k}, w_{2k}, \ldots, w_{nk}\right), \tag{12}$$

Initial values of decision variables are values from environment of points that represent the life cycle duration of each part:

$$w_0 = \left(T_{ut_1} - \Delta T_{ut_1}, T_{ut_2} - \Delta T_{ut_2}, \ldots, T_{ut_n} - \Delta T_{ut_n}\right) \tag{13}$$

If we implement TADSS method to the defined objective function (10), we can conclude that the size of the iterative step is:

$$w_{k+1} = w_k - \left[\alpha_k\left(\gamma_k^{-1} - 1\right) + 1\right] g_k, \tag{14}$$

while the acceleration parameter can be expressed as follows:

$$\gamma_{k+1} = 2\frac{f\left(w_k + 1\right) - f\left(w_k\right) + \left(\alpha_k\left(\gamma_k^{-1} - 1\right) + 1\right)\left\|g_k\right\|^2}{\left(\alpha_k\left(\gamma_k^{-1} - 1\right) + 1\right)^2 \left\|g_k\right\|^2} \tag{15}$$

Based on all of the aforementioned, the objective function gradient can be calculated as stated in (16):

$$g_k = \sum_{k=1}^{n} 2c_{o_i} \frac{\exp\left(-\frac{16\mathrm{T}_{ut_i}^2 \exp\left(\frac{2\pi}{4T_{ut_i}^2} w_k^2\right)\left(1-\exp\left(\frac{-\pi}{4T_{ut_i}^2} w_k^2\right)\right)^2}{2\pi^2}\right)\left(\frac{2\frac{\pi}{T_{ut_i}} w_k^2 \exp\left(\frac{-\pi}{4T_{ut_i}^2} w_k^2\right)\left(1-\exp\left(\frac{-\pi}{4T_{ut_i}^2} w_k^2\right)\right)}{\sqrt{2}\pi} - \frac{\sqrt{2}w_k^2}{T_{ut_i}}\right)}{\sqrt{\pi}\left(1-\Phi\left(\frac{4\mathrm{T}_{ut_i}^2 \exp\left(\frac{-\pi}{4T_{ut_i}^2} w_k^2\right)\left(1-\exp\left(\frac{-\pi}{4T_{ut_i}^2} w_k^2\right)\right)}{\sqrt{2}\pi}\right)\right)} * \left(\frac{\Phi\left(\frac{4\mathrm{T}_{ut_i}^2 \exp\left(\frac{-\pi}{4T_{ut_i}^2} w_k^2\right)\left(1-\exp\left(\frac{-\pi}{4T_{ut_i}^2} w_k^2\right)\right)}{\sqrt{2}\pi}\right)}{\left(1-\Phi\left(\frac{4\mathrm{T}_{ut_i}^2 \exp\left(\frac{-\pi}{4T_{ut_i}^2} w_k^2\right)\left(1-\exp\left(\frac{-\pi}{4T_{ut_i}^2} w_k^2\right)\right)}{\sqrt{2}\pi}\right)\right)} + 1\right) \tag{16}$$

When the total unit time $\mathrm{T_{ut}}$ of assemblies/subassemblies' constitutive parts and prices of those parts are known, then on the basis of (16) their minimum underage costs in specific time intervals can be determined. These intervals or inspection points can be determined as conducted in papers (Wu, 2013), (Tian, 2013).

4. RESULTS AND DISCUSSION

Main contribution of this paper is to provide the possibility to minimize underage costs for spare assemblies and subassemblies in aviation industry. As previously stressed, these costs are hard to quantify. In most cases, only a rough assessment of these costs is conducted. These assessments are complex and hardly ever completely objective and impartial. Some consequences of the lack of spare parts, such as damage to a company's reputation due to unforeseen delays, are almost impossible to quantify as cost. Hence, the contribution of this paper is even more significant. Moreover, the gradient methods have not been utilized in cost optimization until now. This paper combines the Transformed Accelerated Double Step Size method, method for spare parts inventory forecasting based on Rayleigh's model and the Newsvendor model. If the total unit time for each part of the assembly or subassembly and prices of those parts are known, it is possible to determine the

underage cost in preselected time intervals, based on the proposed method.

REFERENCES

Andrei, N. 2006. An acceleration of gradient descent algorithm with backtracking for unconstrained optimization. Numerical Algorithms, 42(1), pp. 63-73.

Hill, A. V. 2011. The Newsvendor Problem. Clamshell Beach Press.

Kontrec, N., Milovanović, G.V., Panić, S., & Milošević, H. 2015. A Reliability-Based Approach to Nonrepairable Spare Part Forecasting in Aircraft Maintenance System. Mathematical Problems in Engineering, 2015. Article ID731437, 7 pages, doi:10.1155/2015/731437.

Petrović, M. J., & Stanimirović, P.S. 2014. Accelerated double direction solving unconstrained optimization problems. Mathematical Problems in Engineering, . Article ID965104, 8 pages.

Petrović, M. J. 2015. An accelerated double step size model in unconstrained optimization. Applied Mathematics and Computation, 250, pp. 309-319.

Stanimirović, P. S., & Miladinović, M.B. 2010. Accelerated gradient descent methods with line search. Numerical Algorithms, 54(4), pp. 503-520.

Stanimirović, P. S., Milovanović, G.V., Petrović, M.J., & Kontrec, N. 2015. A Transformation of Accelerated Double Step Size Method for Unconstrained Optimization. Mathematical Problems in Engineering, 2015(8). Article ID2836798 pages. doi:10.1155/2015/283679.

Tian, Z., Wu, B., & Chen, M. 2013. Condition based maintenance optimization considering inproving prediction accuracy. Journal of the Operational Research Society, 65(9), pp. 1412-1422.

Wu, B., Tian, Z., & Chen, M. 2013. Condition-based maintenance optimization using neural network-based health condition prediction. Quality and Reliability Engineering International, 29(8), pp. 1151-1163.

* E-mail: natasa.kontrec@pr.ac.rs

UNIVERSITY THOUGHT doi:10.5937/univtho6-10968
Publication in Natural Sciences, Vol. 6, N^o 1, 2016, pp. 75-79. Original Scientific Paper

CONCEPT OF STATISTICAL CAUSALITY AND LOCAL MARTINGALES

Dragana Valjarević[1*], Ljiljana Petrović[2]

[1]Faculty of Mathematics and Sciences, University of Priština, Kosovska Mitrovica, Serbia.

[2]Department of Mathematics and Statistics, Faculty of Economics, University of Belgrade, Belgrade, Serbia.

ABSTRACT

In this paper we consider a statistical concept of causality in continuous time in filtered probability spaces which is based on Granger's definitions of causality. The given causality concept is closely connected to the preservation of the property being a local martingale if the filtration is getting larger. Namely, the local martingale remains unpredictable if the amount of information is increased. We proved that the preservation of this property is equivalent with the concept of causality.

Key words: Causality, filtration, local martingale, martingale.

1. INTRODUCTION

One of the goals of science is to find causal relations. This cannot always be done by experiments and researchers are restricted to observing the system they want to describe. This is the case in economics, demography and many other fields. Causality concepts expressed in terms of orthogonality in Hilbert spaces of square integrable random variables was studied by (Hosoya, 1977), (Florens & Mouchart, 1985). In the papers (Florens & Mouchart, 1982), (Mykland, 1986), (Gill & Petrović, 1987) and (Petrović, 1996) it is shown how conditional independence can serve as a basis for a general probabilistic theory of causality for both processes and single events.

Linear Granger--causality was introduced by (Granger, 1969). We shall study a nonlinear version of the concept. Like the linear one, it defines that the process $\mathbf{Y} = \{Y_t,\ t \in I\}, (I \subseteq \mathbf{R})$ does not cause the process $\mathbf{X} = \{X_t,\ t \in I\}$ if, for all t, the orthogonal projection of the L^2-space representing $X_s,\ s > t$ on the space representing X_s and $Y_s,\ s \leq t$ is contained in the space representing $X_s, s \leq t$. However, the spaces representing stochastic variables are those over the σ-field generated by these variables, while in the linear case they are the smallest closed linear spaces containing the variables. The concept was first suggested in (Granger & Newbold, 1977) and studied by (Chamberlain, 1982) and (Florens & Mouchart, 1982).

The study of Granger--causality has been mainly preoccupied with time series. We shall instead concentrate on continuous time processes. Many of systems to which it is natural to apply tests of causality, take place in continuous time. For example, this is generally the case within economy. In this case, it may be difficult to use a discrete time model. Also, the observed "causality" in a discrete time model may depend on the length of interval between each two successive samplings, as in the case with Granger--causality as shown, for example, by (McCrorie & Chambers, 2006).

This concept of causality is closely connected to the notion of extremality of measures and martingale problem (Petrović & Stanojević, 2010). Also, the given causality concept is related to the stable subspaces of H^p which contains right continuous modifications of martingales (Petrović & Valjarević, 2013) and with orthogonality of martingales (Valjarević & Petrović, 2012).

One of the aim of this paper is to give insight in known results which concern already mention concept of causality, but also to give some new. Results are mainly preoccupied with preservation of the local martingale property when the filtration is getting larger.

After Introduction, in the second part of the paper we give various concepts of causality relationship between flow of information (represented by filtrations). Also, we give a generalization of a causality relationship "G entirely causes H within F" which (in terms of σ-algebras) was first given in (Mykland, 1986) and which is based on Granger's

definition of causality from (Granger, 1969) and discuss the relationship to nonlinear Granger--causality.

In the third part we give some preliminaries on martingales where we consider the connection between the concept of causality and preservation of martingale property. The similar statement holds for local martingales, too.

2. PRELIMINARIES AND NOTATIONS

Let $(\Omega, \mathcal{F}, P)$ be an arbitrary probability space and let $\mathrm{F} = \{\mathcal{F}_t, t \in I(\subseteq \mathrm{R})\}$, be a family of sub $\sigma-$algebras of $\mathcal{F}$. Then $\mathcal{F}_t$ can be interpreted as the set of events observed up to time t. $(\mathcal{F}_\infty)$ is the smallest $\sigma-$algebra containing all the $\mathcal{F}_t$ (even if sup $I < +\infty$). So, we have $\mathcal{F}_\infty = \bigvee_{t\in I} \mathcal{F}_t$.

A filtration $\mathbf{F} = \{\mathcal{F}_t, t \in I\}$, is a nondecreasing family of $\sigma-$subalgebras of $\mathcal{F}$, that is:

$$\mathcal{F}_s \subseteq \mathcal{F}_t, s \leq t.$$

A probabilistic model for a time-dependent system is described by $(\Omega, \mathcal{F}, \mathcal{F}_t, P)$ where $(\Omega, \mathcal{F}, P)$ is a probability space and $\{\mathcal{F}_t, t \in I\}$ is a "framework" filtration, i.e. $\mathcal{F}_t$ is a set of all events in the model up to and including time t and $\mathcal{F}_t$ is a subset of $\mathcal{F}$. We suppose that the filtration $(\mathcal{F}_t)$ satisfies the "usual conditions", which means that $(\mathcal{F}_t)$ is right continuous and each $(\mathcal{F}_t)$ is complete.

Analogous notation will be used for filtrations $\mathrm{H} = \{\mathcal{H}_t\}$, $\mathrm{G} = \{\mathcal{G}_t\}$, and $\mathrm{J} = \{\mathcal{J}_t\}$.

Possibly the weakest form of causality can be introduced in the following way.

Definition 2.1 It is said that H is submitted to G or that H is a subfiltration of G (and written as $\mathrm{H} \subseteq \mathrm{G}$) if $\mathcal{H}_t \subseteq \mathcal{G}_t$ for each t.

It will be said that the filtrations H and G are equivalent (and written as $\mathrm{H} = \mathrm{G}$) if $\mathrm{H} \subseteq \mathrm{G}$ and $\mathrm{G} \subseteq \mathrm{H}$.

A family of $\sigma-$algebras induced by a stochastic process $\mathrm{X} = \{X_t, t \in I\}$, is given by $\mathrm{F}^{\mathrm{X}} = \{\mathcal{F}_t^X, t \in I\}$, where:

$$\mathcal{F}_t^X = \sigma\{X_u, u \in I, u \leq t\},$$

being the smallest $\sigma-$algebra with respect to which the random variables $X_u, u \leq t$ are measurable. The process X_t is $(\mathcal{F}_t)-$adapted if $\mathcal{F}_t^X \subseteq \mathcal{F}_t$ for each t.

A family of $\sigma-$algebras may be induced by several processes, e.g. $\mathrm{F}^{\mathrm{X,Y}} = \{\mathcal{F}_t^{X,Y}, t \in I\}$ where:

$$\mathcal{F}_t^{X,Y} = \mathcal{F}_t^X \vee \mathcal{F}_t^Y, t \in I.$$

On the probability space $(\Omega, \mathcal{F}, P)$ the process $\mathrm{Z} = \{Z_t, t \in I\}$, is a $(\mathcal{F}_t, P)-$ martingale if Z_t is $(\mathcal{F}_t)-$adapted and $Z_s = E(Z_t|\mathcal{F}_s)$ for all $t \geq s$.

Definition 2.2 (compare with (Rozanov, 1974)) Let $(\Omega, \mathcal{F}, P)$ be a probability space and $\mathcal{F}_1, \mathcal{F}_2$ and $\mathcal{G}$ arbitrary $\sigma-$ subalgebras from $\mathcal{F}$. It is said that $\mathcal{G}$ is splitting for $\mathcal{F}_1$ and $\mathcal{F}_2$ or that $\mathcal{F}_1$ and $\mathcal{F}_2$ are conditionally independent given $\mathcal{G}$ (and written as $\mathcal{F}_1 \perp \mathcal{F}_2 | \mathcal{G}$) if:

$$(\forall A_1)\,(A_1 \in \mathcal{F}_1)(\forall A_2)(A_2 \in \mathcal{F}_2)\, P(A_1A_2|\mathcal{G}) = P(A_1|\mathcal{G})P(A_2|\mathcal{G}).$$

The following results give an alternative way of defining splitting.

Lemma 2.1 (see (Gill & Petrović, 1987)) *$\mathcal{F}_1 \perp \mathcal{F}_2 | \mathcal{G}$ if and only if $\mathcal{F}_1 \perp \mathcal{F}_2 | \mathcal{G}$ if and only if $E(\mathcal{F}_i|\mathcal{F}_j \vee \mathcal{G}) \subseteq \mathcal{G}$ for $i, j = 1, 2,\ i \neq j$.*

Corollary 2.2 (Petrović and Stanojević, 2005) $\mathcal{F}_1 \perp \mathcal{F}_2 | \mathcal{G}$ if and only if $\mathcal{F'}_1 \perp \mathcal{F'}_2 | \mathcal{G}$ for all $\mathcal{F'}_i \subseteq \mathcal{F}_i \vee \mathcal{G},\ i = 1, 2.$

The intuitively plausible notion of causality formulated in terms of Hilbert spaces is given in (Petrović, 1989). We shall use its analogous in terms of filtrations.

Let J, G and H be arbitrary filtrations. We can say that " G is a cause of J within H " if:

$$\mathcal{J}_\infty \perp \mathcal{H}_t | \mathcal{G}_t \qquad (1)$$

because the essence of (1) is that all information about $(\mathcal{J}_\infty)$ that gives $(\mathcal{H}_t)$ comes via $(\mathcal{G}_t)$ for arbitrary t; equivalently, $(\mathcal{G}_t)$ contains all information from the $(\mathcal{H}_t)$ needed for predicting $(\mathcal{J}_\infty)$. According to Corollary 2.2, is equivalent to $\mathcal{J}_\infty \perp \mathcal{H}_t \vee \mathcal{G}_t | \mathcal{G}_t$ The last relation means that the condition $\mathrm{G} \subseteq \mathrm{H}$ does not represent essential restriction. Thus, it was natural to introduce the following definition of causality between filtrations.

Definition 2.3 (Petrović, 1989) It is said that G entirely causes (or just causes) J within H relative to P (and written as J|< G;H;P) if $\mathcal{J}_\infty \subseteq \mathcal{H}_\infty$, $\mathrm{G} \subseteq \mathrm{H}$ and if $(\mathcal{J}_\infty)$ is conditionally independent of $(\mathcal{H}_t)$ given $(\mathcal{G}_t)$ for each t, i.e.

$$\mathcal{J}_\infty \perp \mathcal{H}_t | \mathcal{G}_t$$

(i.e. $\mathcal{J}_u \perp \mathcal{H}_t | \mathcal{G}_t$ holds for each t and each u), or:

$$(\forall A \in \mathcal{J}_\infty) \quad P(A | \mathcal{H}_t) = P(A | \mathcal{G}_t).$$

If there is no doubt about P, we omit "relative to P ".

Intuitively, J|< G;H;P means that, for arbitrary t, information about $(\mathcal{J}_\infty)$ provided by $(\mathcal{H}_t)$ is not "bigger" than that provided by $(\mathcal{G}_t)$.

A definition, similiar to Definition 2.3 was first given in (Mykland, 1986). However, the definition from (Mykland, 1986) contains also the condition J ⊆ H (instead of $\mathcal{J}_\infty \subseteq \mathcal{H}_\infty$) which does not have intuitive justification. Since Definition 2.3 is more general then the definition given in (Mykland, 1986), all results related to causality in the sense of Definition 2.3 will be true and in the sense of the Hilbert space version of the definition from (Mykland, 1986), when we add the condition J ⊆ H to them.

If G and H are such that G|< G; G ⋁ H ; P (where G ⋁ H is a family determined by $(\mathcal{G}\vee\mathcal{H})_t = \mathcal{G}_t \vee \mathcal{H}_t$), we shall say that H does not cause G. It is clear that the interpretation of, Granger--causality is now that H does not cause G if G|< G; G ⋁ H ; P (see (Mykland, 1986)). Without difficulty, it can be shown that this term and the term " H does not anticipate G " (as introduced in (Rozanov, 1977)) are identical.

If G and H are such that G|< G; H; P we shall say that G is its own cause within H (compare with (Mykland, 1986)). It should be mentioned that the notion of subordination (as introduced in (Rozanov, 1974)) is equivalent to the notion of being one's own cause, as defined here.

These definitions can be applied to stochastic processes. It will be said that stochastic processes are in a certain relationship if and only if the corresponding induced filtrations are in this relationship. For example, $(\mathcal{F}_t)$-adapted stochastic process X_t is its own cause if $\mathrm{F}^X = (\mathcal{F}_t^X)$ is its own cause within $\mathrm{F} = (\mathcal{F}_t)$ i.e. if:

$$\mathrm{F}^X \mid< \mathrm{F}^X;\ \mathrm{F};\ P.$$

We shall give some properties of causality relationship from Definition 2.3 which will be needed later.

Lemma 2.3 (see (Petrović, 1989)) *From* J |< G; H; P *and* J ⊆ H *it follows that* J ⊆ G.

The following result shows that a process X_t which is its own cause is completely described by its behavior relative to F^X.

Lemma 2.4 (Petrović & Stanojević, 2010) X = $\{X_t,\ t \in I\}$, *is a Markov process relative to filtration* $\mathrm{F} = (\mathcal{F}_t, t \in I)$ *on a filtered probability space* $(\Omega, \mathcal{F}, \mathcal{F}_t, P)$ *if and only if* X_t *is a Markov process (relative to* F^X *and the process is its own cause within relative to P.*

Corollary 2.5 (Petrović & Stanojević, 2010) *Brownian motion* $\mathrm{W} = \{W_t,\ t \in I\}$ *on a filtered probability space* $(\Omega, \mathcal{F}, \mathcal{F}_t, P)$ *is its own cause within* $\mathrm{F} = (\mathcal{F}_t, t \in I)$ *relative to probability* P.

From the following result it follows that relationship "being one's own cause" is the transitive relationship.

Lemma 2.6 (compare with (Petrović, 1989)) *From* G |< G; H; P *and* H |< H; J; P *it follows that* G |< G; J; P.

The following result gives the invariance under convergence for causality relationship from Definition 2.3.

Proposition 2.7 (Petrović & Dimitrijević, 2011) *In probability space* $(\Omega, \mathcal{F}, P)$ *let* F *and* G *be a filtrations. Let* $\{X^{(n)}\}$ *is a sequence of stochastic processes satisfying.*

$$X_t^{(n)} \xrightarrow{P} X_t \quad when \quad n \to \infty$$

for every $t \in I \subseteq R$ *and*

$$\mathrm{F}^{X^{(n)}} \mid< \mathrm{G}; \mathrm{F};\ P, for\ every\ n$$

Then for the process X_t *holds*

$$\mathrm{F}^X \mid< \mathrm{G};\ \mathrm{F};\ P.$$

Remark. For some results from part 2, the proofs in given literature are in terms of Hilbert spaces. The proofs are analogous in the σ −algebra concept.

Proposition 2.8 (Mykland, 1986) *Let* $\mathrm{G} = (\mathcal{G}_t)$, $\mathrm{H} = (\mathcal{H}_t)$, $\mathrm{J} = (\mathcal{J}_t)$ *and* $\mathrm{F} = (\mathcal{F}_t)$ *be filtrations in a probability space Then the following statements are equivalent:*

(i) J |< G; H; P *and* J |< H; F; P;

(ii) J |< G; F; P *and* G ⊆ H ⊆ F.

Lemma 2.9 (Mykland, 1986) *In the measurable space* $(\Omega, \mathcal{F},)$ *let the filtrations* $\mathrm{H} = \{\mathcal{H}_t\}$, $\mathrm{G} = \{\mathcal{G}_t\}$, *and* $\mathrm{J} = \{\mathcal{J}_t\}$ *be given and let* P *and* Q *be probability measures on* $\mathcal{F}$ *satisfying* $\mathrm{Q} \ll P$ *with* $\frac{dQ}{dP}$ *as* $(\mathcal{H}_\infty)$ −*measurable. Then:*

$$\mathrm{J} \mid< \mathrm{G}; \mathrm{H};\ P \quad \Longrightarrow \quad \mathrm{J} \mid< \mathrm{G}; \mathrm{H};\ Q.$$

Given causality concept links Granger--causality with the concept of adapted distribution, which have been introduced by Kiesler and Hoover in \cite{KH}.

3. CAUSALITY AND MARTINGALE PROPERTY

This section is concerned with the analysis of the connection between the preservation of the martingale property and the concept of causality.

The martingale property remains valid if the filtration decreases, but in general this property is not preserved if the filtration increases. When the filtration is getting larger, the preservation of the martingale property is strongly connected to the concept of causality, because martingale is the process which remains unpredictable even if the information σ −algebra increase.

Let $(\Omega, \mathcal{F}, \mathcal{F}_t, P), t \in I = [0, +\infty)$ be a filtered probability space with $\mathrm{F} = (\mathcal{F}_t, t \in I)$ right continuous and complete.

Let H be a set of right continuous modifications of the $(\mathcal{H}_t)$-adapted processes of the form

$$H = \{M_t : M_t = P(A \mid \mathcal{H}_t), A \in \mathcal{H}_\infty\}. \qquad (2)$$

Then, the following result holds.

Theorem 3.1 Suppose that $\mathcal{H}_\infty \subseteq \mathcal{F}_\infty$ and $\mathrm{G} \subseteq \mathrm{F}$. Then $\mathrm{H} \mid\!< \mathrm{G}; \mathrm{F}; P$ if and only if every $(\mathcal{H}_t)$-adapted, $(\mathcal{G}_t)$-martingale is $(\mathcal{F}_t)$- martingale.

PROOF. Suppose that $\mathrm{H} \mid\!< \mathrm{G}; \mathrm{F}; P$. Then $\mathcal{H}_\infty \subseteq \mathcal{F}_\infty$, $\mathrm{G} \subseteq \mathrm{F}$ and

$$(\forall A \in \mathcal{H}_\infty) \quad P(A \mid \mathcal{G}_t) = P(A \mid \mathcal{F}_t).$$

Suppose that elements of H, of the form (2) are $\mathcal{G}_t$ −martingales so:

$$\begin{aligned} M_t &= E(M_\infty \mid \mathcal{G}_t) = E(P(A \mid \mathcal{H}_\infty)\mathcal{G}_t) \\ &= E(E(\chi_A \mid \mathcal{H}_\infty)\mathcal{G}_t) = \mathrm{E}(\chi_A \mid \mathcal{G}_t) \\ &= P(A \mid \mathcal{G}_t) = P(A \mid \mathcal{F}_t) = E(\chi_A \mid \mathcal{F}_t) \\ &= E(E(\chi_A \mid \mathcal{H}_\infty) \mid \mathcal{F}_t) \\ &= E(P(A \mid \mathcal{H}_\infty) \mid \mathcal{F}_t) = E(M_\infty \mid \mathcal{F}_t). \end{aligned}$$

where χ_A is a indicator function for $A \in \mathcal{H}_\infty$, so

$$M_t = E(M_\infty \mid \mathcal{F}_t)$$

which means that elements of H are $(\mathcal{F}_t)$ - martingales.

Conversely, suppose that every $(\mathcal{H}_t, P)$ −adapted $(\mathcal{G}_t, P)$ −martingale is $(\mathcal{F}_t, P)$ −martingale, i.e.

$$\begin{gathered} E(M_\infty \mid \mathcal{F}_t) = M_t = E(M_\infty \mid \mathcal{G}_t) \\ E(P(A \mid \mathcal{H}_\infty) \mid \mathcal{F}_t) = E(P(A \mid \mathcal{H}_\infty) \mid \mathcal{G}_t) \\ E(E(\chi_A \mid \mathcal{H}_\infty) \mid \mathcal{F}_t) = E(E(\chi_A \mid \mathcal{H}_\infty) \mid \mathcal{G}_t) \\ E(\chi_A \mid \mathcal{F}_t) = E(\chi_A \mid \mathcal{G}_t) \\ P(A \mid \mathcal{F}_t) = P(A \mid \mathcal{G}_t) \end{gathered}$$

for $A \in \mathcal{H}_\infty$ and also the definition of causality is satisfied, so $\mathrm{H} \mid\!< \mathrm{G}; \mathrm{F}; P$.

The similar result is shown in (Florens & Fougere, 1996) but expressed in terms of noncausality.

Corollary 3.2 *Let* $\mathrm{H} \subseteq \mathrm{F}$. *Then* $\mathrm{H} \mid\!< \mathrm{H}; \mathrm{F}; P$. *if and only if every element of* H *is* $(\mathcal{F}_t, P)$*- martingale.*

PROOF. It is the special case of the previous theorem (if $\mathrm{G} = \mathrm{H}$).

As the special case we can observe the process of Brownian motion (see Corollary 2.5) and Markovian process (see Lemma 2.4). By previous results we can conclude that the process which is its own cause is completely described by its behavior with respect to its natural filtration ($\mathrm{F}^W, \mathrm{F}^X$ respectively).

Also, the concept of causality can be connected and to the larger class of processes. Let us recall, the random process $\mathrm{N} = \{N_t, t \in I\}$ is called a local martingale with respect to the filtration $(\mathcal{F}_t)$ on the probability space $(\Omega, \mathcal{F}, P)$ if there exist an increasing sequence of stopping times $(T_n), n = 1,2, \ldots,$ such that $P(T_n \leq n) = 1, P(\lim T_n = \infty) = 1$ and for any $n = 1,2, \ldots,$ the sequences $\{N_{t \wedge T_n}\}$ are uniformly integrable martingales.

Let G be a set of right continuous modifications of the $(\mathcal{G}_t)$ −adapted processes of the form:

$$G = \{N_t : N_t = P(A \mid \mathcal{G}_t), A \in \mathcal{G}_\infty\} \qquad (3)$$

Then, we have the following result.

Theorem 3.3 $\mathrm{G} \subseteq \mathrm{F}$. Then $\mathrm{G} \mid\!< \mathrm{G}; \mathrm{F}; P$ if and only if every $(\mathcal{G}_t, P)$ -local martingale is $(\mathcal{F}_t, P)$-local martingale.

PROOF. Suppose that $\mathrm{G} \mid\!< \mathrm{G}; \mathrm{F}; P$ holds, i.e.

$$(\forall A \in \mathcal{G}_\infty) \quad P(A \mid \mathcal{G}_t) = P(A \mid \mathcal{F}_t).$$

Also, suppose that process N_t is of the form (3), and that N_t is a $(\mathcal{G}_t, P)$ -local martingale. Then there exists a sequence (T_n), of stopping times with respect to G for which $N_{t \wedge T_n}$ is a $(\mathcal{G}_t, P)$-martingale, for each n. According to Theorem 3 in (Bremaud & Yor, 1978) the sequence (T_n), of stopping times with respect to G is a sequence of stopping times with respect to F too. Due to Theorem 3.1, for each n every $(\mathcal{G}_t, P)$-martingale $N_{t \wedge T_n}$, is $(\mathcal{F}_t, P)$- martingale. Considering that (T_n) are stopping times with respect to F, the process N_t is $(\mathcal{F}_t, P)$- local martingale.

Conversely, suppose that every $(\mathcal{G}_t, P)$-local martingale is $(\mathcal{F}_t, P)$- local martingale. If the assumption is true for every local martingale, then it is true for martingales (because every martingale is local martingale), and according to Theorem 3.1 we have $\mathrm{G} \mid\!< \mathrm{G}; \mathrm{F}; P$.

ACKNOWLEDGMENT

The work is supported by Serbian Ministry of Science and Technology.

REFERENCES

Bremaud, P., & Yor, M. 1978. Changes of filtrations and of probability measures. Z. Wahrscheinlichkeitstheorie verw. Gebiete, 45(4), pp. 269-295, doi:10.1007/BF00537538.

Chamberlain, G. 1982. The General Equivalence of Granger and Sims Causality. Econometrica, 50(3), pp. 569-581, doi:10.2307/1912601.

Florens, J. P., & Fougere, D. 1996. Noncausality in Continuous Time. Econometrica, 64(5), p. 1195, doi:10.2307/2171962.

Florens, J. P., & Mouchart, M. 1982. A Note on Noncausality. Econometrica, 50(3), pp. 583-591, doi:10.2307/1912602.

Florens, J. P., & Mouchart, M. 1985. A Linear Theory for Noncausality. Econometrica, 53(1), pp. 157-175, doi:10.2307/1911729.

Granger, C. W. J. 1969. Investigating Causal Relations by Econometric Models and Cross-spectral Methods.Econometrica, 37(3), pp. 424-438, doi:10.2307/1912791.

Granger, C. W. J., & Newbold, P. 1977. Forecasting Economic Time Series.New York: Academic Press.

Gill, J. B., & Petrović, Lj. 1987. Causality and Stochastic Dynamic Systems. SIAM J. Appl. Math., 47, pp. 1361-1366.

Hoover, D., & Keisler, J. 1984. Adapted probability distributions. Trans. Amer. Math. Soc., 286, pp. 159-201.

Hosoya, Y. 1977. On the Granger Condition for Noncausality. Ecomometrica, 45, pp. 735-1736.

Mykland, P. A. 1986. Statistical Causality. Statistical Report, University of Bergen, 4, pp. 1-28.

Mccrorie, J. R., & Chambers, M. J. 2006. Granger causality and sampling of economic processes. Journal of Econometrics, 132, pp. 311-336.

Petrović, Lj. 1989. Causality and Stochastic Realization Problem. Publ. Inst. Math., Beograd, 45(59), pp. 203-212.

Petrović, Lj. 1996. Causality and Markovian Representations. Statistics and Probability Letters, 29, pp. 223-227.

Petrović, Lj., & Stanojević, D. 2005. Some Models of Causality and Weak Solutions of Stochastic Differential Equations with Driving Semimartingales. Facta Universitatis (Niš), Ser. Mathematics and Informatics, 5, pp. 103-112.

Petrović, Lj., & Stanojević, D. 2010. Statistical Causality, Extremal Measures and Weak Solutions of Stochastical Differential Equations With Driving Semimartingales, J. Math. Model. Algor, 9, pp. 113-128.

Petrović, Lj., & Dimitrijević, S. 2011. Invariance of Statistical Causality Under Convergence. Statistic and Probability Letters, 81, pp. 1445-1448.

Petrović, Lj., & Valjarević, D. 2013. Statistical Causality and Stable subspaces of Hp. Bulletin of Australian Mathematical Society, 88, pp. 17-25.

Rozanov, Y. A. 1974. Theory of Innovation Processes. In Monographs in Probability Theory and Mathematical Statistics.Moscow: Izdat, Nauka.

Rozanov, Y. A. 1977. Innovation Processes.New York: V. H. Winston and Sons..

Valjarević, D., & Petrović, Lj. 2012. Statistical Causality and Orthogonality of Local Martingales. Statistic and Probability Letters, 82, pp. 1326-1330.

* E-mail: dragana.valjarevic@pr.ac.rs

UNIVERSITY THOUGHT
Publication in Natural Sciences, Vol. 6, N^{o} 1, 2016, pp. 80-83.
doi:10.5937/univtho6-10948
Original Scientific Paper

MONITORING OF THE ABSORBED DOSE OF RATES RADIATION IN THE RURAL AREAS

Biljana Vučković[1*], Smilja Čanaćević[1]

[1]Faculty of Natural Sciences and Mathematics, University of Priština, Kosovska Mitrovica, Serbia.

ABSTRACT

Man is constantly exposed to radiation from the radionuclides from the environment. This study presents the results of measuring the absorbed dose rates of natural ionizing radiation in rural areas in the municipality of Štrpce, in southern part of Kosovo and Metohija. The measurements were conducted in 20 houses in two cycles: when rooms were not heated, and when they were warmed up in the same season. Ten observed houses were with basement rooms, and ten others were without basements. The absorbed dose rate of radiation was measured by Gaiger-Miller's counter DR-M3. Mean value of the measured absorbed dose rate was 1.93 μGy/h - in the first cycle and 1.47 μGy/h - in the second cycle. At the same time the values of the absorbed dose of radiation in the environmental were measured, and obtained values were 1.77 μGy/h and 1.33 μGy/h, respectively. Relations between absorbed dose in the premises and in the environment were 1.09 in first cycle, and 1.1 in the second cycle of measurements.

Key words: intensity of absorbed dose, GM counter, unheated and heated rooms, inside of houses, outside of houses.

1. INTRODUCTION

Unlike a number of other harmful effects of physical agents to which humans are exposed, ionizing radiation is one of the most dangerous. Radiation is carcinogenic and causes damage to genes (Dainiak, 1997), (Janković-Mandić et al., 2007), (Turner, 2007), (Župunski et al., 2008). The most significant sources of ionizing radiation in the environment are terrestrial radionuclides whose half-life is comparable with the age of the Earth (10^5 -10^{16} years) (Abdel-Rahman et al., 2010), (Draganić, 1996), (Vučina et al., 2005). Another important source of natural radiation is cosmic radiation. Primary galactic cosmic radiation is of the solar origin, and consists of charged particles of very high energy (Rajković, 2001). It rarely reaches the earth's surface, but it creates secondary cosmic radiation and radionuclides (Draganić, 1996), (Veriš et al., 2009). A total cosmic radiation on earth has a greater impact at the poles than at the equator, due to a stronger electromagnetic impact that turns radiation. Also with increasing altitude radiation increases due to diluted air, so that at 4000-12000 m altitude radiation is higher as about 25% (Crnogorac et al., 2012).

In addition to natural sources of ionizing radiation, in the second part of the 20th century anthropogenic (artificial) sources become a significant problem which presents 5% of total radiation on Earth (Crnogorac et al., 2012).

Investigation of external exposure in the environment is done by measuring the absorbed dose rate of radiation. In addition to the above mention reason the dose of radiation to which man is exposed depends on food and water that man enters into body (UNSCEAR, 2000). The received dose can be three to four times higher in the mountains than on the surface (Rajković, 2001), (UNSCEAR, 1993). The average worldwide value of the absorbed dose rate is 59 nGy/h, with a variation in the range from 18 nGy/h to 93 nGy/h (UNSCEAR, 2000). When the annual radiation exposure is estimated time spent inside should be also considered, since the building materials contain natural radionuclides. The mean value of the absorbed dose rate of radiation in an enclosed space at a global level is 84 nGy/h, with a variation in the range from 20 nGy/h to 200 nGy/h (UNSCEAR, 2000).

The aim of this study was to measure the absorbed dose rate of radiation in rural areas, inside and outside of houses, in the municipality of Štrpce. Since there are no measured values in this area, the results of this monitoring can be a basis for further research.

2. INVESTIGATING AREA

Measurement of the absorbed dose rate was conducted in 20 houses in the area of the municipality of Štrpce (42˚14'N, 21˚01'E), which has around 13.600 citizens. Štrpce is situated at an altitude of 974 m, fig. 1. The municipality is located on Sar Mountain, whose geological structure is characterized by igneous and metamorphic rocks, primarily diabase (Sehić, 2007).

3. MATERIALS AND METHODS

The absorbed dose rate of radiation in the municipality of Štrpce was measured by Geiger-Miller's counter DR-M3. Its interface is very simple and easy for use. During measurements the device was located at a height of 1 m from the floor (on the premises) or on the ground (in the open). GM counter operation is based on the ionization of the gas by passage of radiation. The ionization is considerably amplified by means of the avalanche effect to produce an easily measured detection – pulse. The pulses are counted at certain intervals of time and on basis of that information absorbed dose rate was calculated.

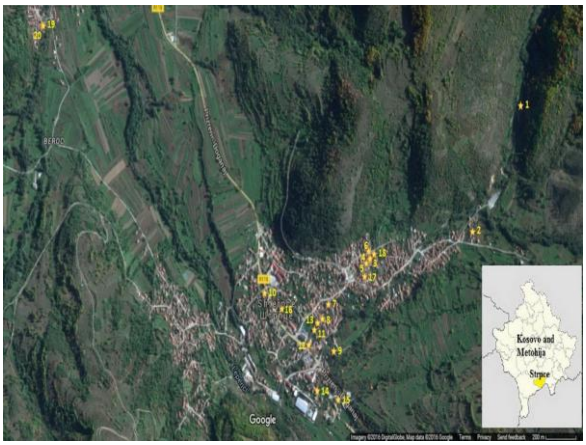

Fig. 1. Map of measuring places in Štrpce.

Table 1. The absorbed dose rates (D) measured inside and outside of homes.

	No	Intensity of absorbed doses in the air (μGy/h)			
		The first cycle of measurements (unheated rooms)		The second cycle of measurements (heated rooms)	
		Inside	Outside	Inside	Outside
Houses without basement	1.	1	1	0.8	0.7
	2.	0.7	0.7	0.5	0.7
	3.	2	2	0.8	0.8
	4.	2	1.5	1	1
	5.	0.7	0.8	1	1
	6.	2	2	0.7	0.7
	7.	1	1	2	1.5
	8.	2	2	0.7	0.6
	9.	1.5	1.5	0.5	0.7
	10.	1.5	1	0.8	0.6
Houses with basement	11.	1.5	1.5	6	5
	12.	2	2	5	4
	13.	1.5	1.5	2	2
	14.	2	2	0.6	0.5
	15.	2	2	0.7	0.7
	16.	2	2	0.7	0.6
	17.	1.5	1.5	3	3
	18.	10	8	1	1
	19.	0.8	0.7	0.8	0.9
	20.	1	0.7	0.8	0.7

Table 2. Descriptive statistic of measured values of absorbed dose rates.

		No	Min (μGy/h)	Max (μGy/h)	SD	Median (μGy/h)	Mean (μGy/h)	GM (μGy/h)	GSD
First cycle	inside	20	0.7	10	1.96	1.5	1.935	1.753	2.086
	outside	20	0.7	8	1.55	1.5	1.770	1.619	1.990
Second cycle	inside	20	0.5	6	1.52	0.8	1.470	1.276	2.219
	outside	20	0.5	5	1.24	0.7	1.335	1.207	2.081

SD-standard deviation, GM-geometric mean, GSD-geometric standard deviation.

4. RESULTS AND DISCUSSION

The study included 20 houses - 10 without basements and 10 with basements. Results are presented in Table 1. These houses were mostly built in the second part of 20th century with the common materials - bricks and concrete. All measurements were taken in the same season – autumn, in the ground floor rooms with concrete floors, as follows: when the rooms are not heated, and then when they are heated. At the same time the values of the absorbed dose rates were measured in the environment.

In the first cycle of measurements when the rooms were not heated, the values of the dose rates were same inside and outside of houses at 14 measuring places. In five measuring places values of doses were lower outside the house. Only at one measuring place measured dose from outside was higher than the dose from inside of the house. The same measured values of the dose suggest that additional sources of radionuclides in the house do not exist. Also in warmer days the room is ventilated more frequently, which causes the equalization of the concentration of radionuclides.

In the second cycle of measurements, when the rooms were heated, at ten locations higher doses were measured inside than outside, which could be the result of lower ventilation in cold period. At eight locations measured values of the dose rates were same in both cases - inside and outside of houses. The higher doses outside the house were measured only at three locations.

From results obtained in this study it could be seen that there are three extreme values. In the first cycle of measurement one of extreme values was at measuring place 18: 10 μGy/h - inside of house, and 8 μGy/h- outside of house. Reason of that could be sudden influx of radionuclides due to the increased air turbulence. But when the room was heated at this measuring place, both measured values were not extreme. In the second cycle of measurements slightly higher values of 6 and 5 μGy/h were measured in the houses at the measuring places 11 and 12, respectively. Also, at these measuring places the higher value of external dose (5 μGy/h and 4 μGy/h) was measured. This all leads to the conclusion that there is increased concentration of radionuclides due to the air flow, as well as increased penetration into the interior, through cracks in the walls or through the cavity around the window.

Table 2 presents the descriptive statistic of these measured values of the absorbed dose rates. The values were obtained using the KS test.

Mean values of the absorbed dose rate from outside of houses are 1.77 μGy/h (first cycle) and 1.33 μGy/h (second cycle). Relations between the mean values of the absorbed dose inside and outside of houses totaled to 1.09 in the first cycle, and 1.1 in the second cycle of measurement, which corresponds to the global average (interval from 0.6 to 2.3) (Crnogorac et al., 2012). From these mean values of the absorbed dose rates can be seen that this area is characterized by increased radioactivity of air. It is influenced by its environment, primarily the altitude, weather conditions and the morphology of the soil.

The fig. 2 and 3 present interdependence of the measured values of the dose rates inside of houses. If the images are compared it can be seen that a greater range of measured values was noted in houses without basements. This leads to the conclusion that the existence of the basement reduced the direct penetration of radionuclides from the soil to the interior of the building.

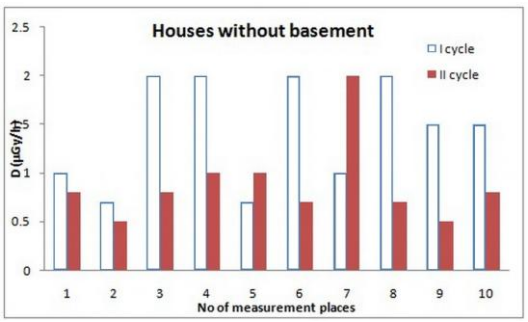

Fig. 2. The measured values of the absorbed dose rate (D) in houses without basements

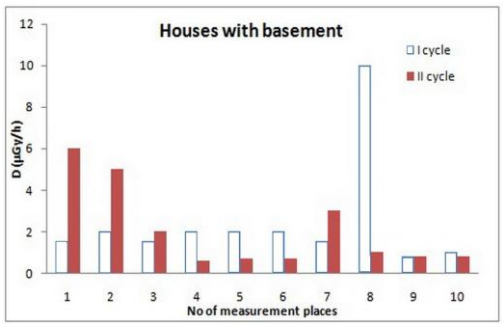

Fig. 3. The measured values of the absorbed dose rate (D) in houses with basements

Results of measurement subjected to t-test showed that two-tailed P values in three different cases equal: (1) 0.2699 - when rooms in all houses were without heating, (2) 0.0817 - when rooms in all houses were warmed, and (3) 0.7303 - when rooms in 10 houses

with basements were without heating. By conventional criteria, these differences are considered not to be statistically significant. Results of measurement subjected to t-test showed that two-tailed P value equals 0.0208 for 10 houses without basements, where rooms were without heating and when heated. By conventional criteria, this difference is considered to be statistically significant.

5. Conclusion

In this study, monitoring of the absorbed dose rates was conducted in the area of the municipality of Štrpce in 20 houses, (10 houses with basements and 10 without basements). GM counter DR-M3 was used to measure the value of the absorbed dose rates of radiation inside and outside, when the rooms were not heated (first cycle) and when they were heated (second cycle). From the graph of their interdependence can be concluded that the higher the dose rates were measured in houses without basements. This leads to the conclusion that the existence of the basement reduced the direct penetration of radionuclides from the soil into the interior of a house.

The results also show that the territory of the municipality of Štrpce is characterized by high absorbed dose rates inside (1.93 μGy/h and 1.47 μGy/h) and outside of houses (1.77 μGy/h and 1.33 μGy/h). The mean values of the absorbed dose inside and outside of homes totaled to 1.09 in first cycle, and 1.1 in the second cycle of measurement, which corresponds to the global average. This may be a result of higher altitudes, where Štrpce lies on one hand, and the geological structure of the soil on the other hand. Large fluctuations of air radioactivity can be caused by a number of other meteorological conditions (temperature, humidity, pressure, velocity air mixture).

Acknowledgements

The authors are grateful to the owners of houses in which these measurements e carried out.

References

Abdel-Rahman, W., & Podgorsak, E. B. 2010. Energy transfer and energy absorption in photon interactions with matter revisited: A step-by-step illustrated approach. Radiat. Phys. Chem., 79, pp. 552-566.

Crnogorac, Č., & Spahić, M. 2012. Basics of ecology.Banja Luka: ARTPRINT. on Serbian.

Dainiak, N. 1997. Mechanisms of radiation injury: Impact of molecular medicine. Stem cells, 15, pp. 1-5.

Draganić, I. 1996. Through the world of radiation and radioactivity.Beograd: Geoinstitut; Beograd: Zavod za izdavanje udžbenika. (on Serbian).

Janković-Mandić, L., & Dragović, S. 2007. Terrestrial radiation risk due to exposure to the population of cities Serbia. .In: 'Terrestrial radiation risk due to exposure to the population of cities Serbia', XXIV Symposium DZZSCG, Zlatibor. , pp. 63-67 on Serbian.

Rajković, M. B. 2001. Depleted uranium I: Uranium, radioactivity and legal regulations. Hem. Ind., 55(4), pp. 167-182. (on Serbian).

Sehić, D. 2007. Geological atlas of Serbia-for schools and home.Belgrade: Monde Neuf.. (on Serbian).

Turner, E. J. 2007. Atoms, Radiation, and Radiation Protection.Weinheim: WILEY-VCH Verlag GmbH & Co. KGaA..

-United Nations Scientific Committee on the Effects of Atomic Radiation, UNSCEAR. 1993. United Nations Sources and Effects of Ionizing Radiation. Report to the General Assembly, with Scientific Annexes.New York: United Nations.

-United Nations Scientific Committee on the Effects of Atomic Radiation, UNSCEAR. 2000. Sources and effects of ionizing radiation. Report to General Assembly, with Scientific Annexes.New York: United Nations.

Veriš, A., Ćetojević, D., Mijatović, D., & Tramošljika, Lj. 2009. The impact of radiation on the human body. . In: Ist International Conference ECOLOGICAL SAFETY IN POST_MODERN ENVIROMENT, 2009-06-26, Banja Luka, RS,BiH. (on Serbian).

Vučina, J., Orlić, M., & Vranješ, S. 2006. Radionuclides and ionising radiation. Acta Clinica, 5(1), pp. 9-22. (on Serbian).

Župunski, L., Trobok, M., Gordanić, V., Jokić-Spasić, V., & Sovilj, P. 2009. The impact of population exposure to natural radionuclides radium at increased risk of developing a tumor by entering the parent nuclide uranium via ingestion or by inhalation. . In: XXV Symposium DZZSCG,, Kopaonik., pp. 43-45 (on Serbian).

* E-mail: biljana.vuckovic@pr.ac.rs

UNIVERSITY THOUGHT doi:10.5937/univtho6-11246
Publication in Natural Sciences, Vol. 6, N^{o} 1, 2016, pp. 84-96. Review Paper

SOME PROPERTIES OF ONE-DIMENSIONAL POINT INTERACTIONS

Saša Kočinac[1*]

[1]Department of Physics, Faculty of Technology and Metallurgy, University of Belgrade, Belgrade, Serbia.

ABSTRACT

In this review paper we shall give a brief account of some properties of so called point interactions that describe a potentials spatially localized. A different families of one-dimensional point interactions are investigated and then relevant tunneling times are calculated. Than we demonstrate how a bound state in the continuum may be generated applying supersymmetric quantum mechanics. Finally, it is shown how the latter method may be used to tailor phase rigidity of one-dimensional point interactions.

Key words: one dimensional point interactions; tunneling times; phase rigidity.

1. INTRODUCTION

Point interactions represent strictly localized potentials which are zero everywhere except at the origin, where suitable boundary conditions have to be imposed. An elementary and simultaneously the first example of point interaction is δ potential introduced by Fermi some 80 years ago, and ever since they have found a variety of applications in areas such as quantum mechanics (Demkov & Ostrovskii, 1975), (Albeverio et al., 1988), solid state physics (Avron, 1994), (Exner, 1995), (Cheon et al., 2000a), (Kurasov et al., 1994), (Dzhezherya et al., 2010), (Bogolyubov et al., 2003), (Šeba, 1986) or in optics (Milanović & Ikonić, 1997). Point interactions may be viewed as self-adjoint extensions (SAE) of kinetic energy (KE) operator. Interesting properties of this interactions such as scattering coefficients, time reversibility etc. are subject of many papers oriented both mathematically and physically (Berezin & Faddeev, 1961), (Winful, 2006), (Carreau, 1990), (Albeverio et al.,1993), (Kurasov, 1996), (Soldatov,et al., 2006), (Cheon et al., 2000b), (Coutinho et al., 2008), (Christiansen et al., 2003).

In the first part of review, using a general approach for the calculation of tunneling times given in (Winful, 2006), we will show how an analytical expressions for the tunneling times can be derived in one-dimensional case. Then we turn our intention to some particular type of interactions and its various interpretations in literature to discuss the relevant times.

The second part deals with bound states in the continuum (BIC) generated by supersymmetry quantum mechanics (SUSY). SUSY is a method that allows one to start with any given potential and then generate a family of isospectral potentials, ie. potentials having the exact set of eigenenergies as the original one but different wave functions (Milanović, & Ikonić, 2002), (Pappademos, et al., 1993). This allows to manipulate certain properties while retaining the original set of potential's eigenenergies. In this way it is possible to introduce bound state in continuum (BIC) on the half line of real potential (Román, & Tarrach, 1996) or on the whole line with complex potentials (Kruchinin et al., 2010).

Third part concerns a phase rigidity of wave functions. By varying the relevant SUSY parameter λ, a shape of wave functions is also varied, thus affecting the phase rigidity of point interaction. We investigate both rigidity of continuous and bound part of the spectrum, as well as that of BIC. It turns out, however, that only phase rigidity of states from discrete part may be tailored via SUSY quantum mechanics and to this case we pay attention. For bound states in the continuum (BIC) phase rigidity is always zero, while for bound states from discrete part of spectrum phase rigidity may vary from zero to unity, depending on the strength of point interaction.

2. TUNNELING TIMES OF POINT INTERACTIONS

Let $V(x)$ be an arbitrary shaped complex potential. One-dimensional Schrödinger equation describing interaction is given by:

$$-\frac{d^2\psi}{dx^2}+V(x)\psi=E\psi. \quad (1)$$

In ((1), E is particle energy, and the units are chosen such that $\hbar=1$ and $2m=1$. The assumption is that both real and complex part of the potential extend only over the same infinitesimally small part of x-axes $-\varepsilon<x<+\varepsilon$. In limiting case of $\varepsilon\to 0$ potential $V(x)$ describes point interaction.. Outside the region of the interaction the general shape of the wave function that satisfies Eq.((1) is:

$$\begin{aligned}\psi_L&=e^{ikx}+Re^{-ikx};-\infty<x<-\varepsilon\\ \psi_R&=Te^{ikx};\qquad +\varepsilon<x<+\infty;\end{aligned} \quad (2)$$

where $T=|T|\exp(i\varphi_t)$ and $R=|R|\exp(i\varphi_r)$ represent the transmission and reflection coefficients respectively, and $E=k^2$. As we shall see later, depending on the specific situation, shape of wave function given by (2) is not necessarily the only choice. It should be pointed out that since the potential in ((1) is generally complex, so is the energy on the right hand side. However, the wavefuction given by (2) in that case would not be of purely oscillatory character due to complex κ and would not account for the propagation. The tunneling times being the quantities of interest, we restrict ourselves to real energies only. Upon differentiating ((1) with respect to energy and using its complex conjugate, the following is obtained:

$$\int_{-\varepsilon}^{+\varepsilon}\psi\psi^*dx=\left(\frac{\partial\psi}{\partial E}\frac{\partial\psi^*}{\partial x}-\psi^*\frac{\partial^2\psi}{\partial E\partial x}\right)\Bigg|_{-\varepsilon}^{+\varepsilon}+2i\int_{-\varepsilon}^{+\varepsilon}V_i\psi^*\frac{\partial\psi}{\partial E}dx. \quad (3)$$

In (3), V_i stands for the imaginary part of potential V. Upon substituting (2) in (3), and carrying out some basic algebraic manipulations, the relationship among relevant tunneling times is derived and goes as follows:

$$\tau_d=\tau_g-\tau_i+\tau_a. \quad (4)$$

For a detailed account on derivation of (4), Refs. (Zolotaryuk, 2010), (Kočinac et al., 2008) should be consulted. The left side term τ_d in (4) is known as dwell time and represents the total time the particle spends in the barrier of length 2ε, whether being transmitted or reflected:

$$\tau_d=\frac{1}{k}\int_{-\varepsilon}^{\varepsilon}|\psi(x)|^2dx. \quad (5)$$

The first term on the right side of (4) is known as the bidirectional group delay τ_g and consists of two parts:

$$\tau_g=|T|^2\tau_{gt}+|R|^2\tau_{gr}. \quad (6)$$

describing group delay times in transmission τ_{gt} and reflection τ_{gr} defined as:

$$\tau_{gt}=d\varphi_0/dE,\qquad \tau_{gr}=d\varphi_r/dE, \quad (7)$$

with $\varphi_0=\varphi_t+2\varepsilon k$. As $\varepsilon\to 0$ phases in transmission and reflection obviously become identical $\varphi_0=\varphi_t$ due to zero length of barrier. Generally, for a barrier of finite dimension, the group delay times in transmission and reflection are different, but in a rather important case of real and symmetric barrier, it is shown that $\tau_{gt}=\tau_{gr}$. The following term, self-interference time τ_i is defined as follows:

$$\tau_i=-\frac{1}{2E}\mathrm{Im}(R). \quad (8)$$

It may be viewed as a consequence of overlap of incident and reflected part of the wave function in front of the barrier, therefore interference. The last term τ_a in (4) is a consequence of a non-zero imaginary part of the potential and accounts for the absorption:

$$\tau_a=\frac{1}{k}\int_{-\varepsilon}^{\varepsilon}V_i\mathrm{Im}\left(\psi^*\frac{d\psi}{dE}\right)dx. \quad (9)$$

For a point (zero range) interaction, the dwell time (barrier time) disappears and we have $\tau_g=\tau_i+\tau_a$. Additionally, if the potential is real, only one relevant tunneling time remains since $\tau_a=0$ and Eq. (4) reduces to simple $\tau_g=\tau_i$.

Requirement for the self-adjointness of the operator A yields:

$$\int_{-\infty}^{+\infty} \varphi^* A\psi dx - \int_{-\infty}^{+\infty} (A\varphi)^* \psi dx = 0. \qquad (10)$$

If we are dealing with kinetic energy (KE) operator $p^2/2m = -d^2/dx^2$, Eq. (10) becomes:

$$\int_{-\infty}^{+\infty} (\varphi^{*\prime\prime}\psi - \varphi^*\psi^{\prime\prime})\, dx = \left[\varphi^*\psi' - \varphi'^*\psi\right]_{0-}^{0+} = 0. \qquad (11)$$

When Eq. (11) equals zero, operator A is self adjoint. The most obvious case for this to be fulfilled is the continuity of both wave functions $\varphi(x)$ and $\psi(x)$ and its derivatives at $x=0$, There is, however, a whole set of boundary conditions at $x=0$ that $\varphi(x)$ and $\psi(x)$ may satisfy to hold (11), although continuity of wave functions (and/or derivatives) is not fulfilled. Corresponding set of boundary conditions that satisfy (11) represent so called self-adjoint extensions (SAE) of KE operator. The general point-interactions are such SAEs whose wave functions at the origin ($x=0$) are subject to boundary conditions of the following form:

$$\begin{pmatrix} \psi_+ \\ \psi'_+ \end{pmatrix} = e^{i\Theta} \begin{pmatrix} a & b \\ c & d \end{pmatrix} \begin{pmatrix} \psi_- \\ \psi'_- \end{pmatrix} = U \begin{pmatrix} \psi_- \\ \psi'_- \end{pmatrix}, \qquad (12)$$

where $\psi' = d\psi/dx$ is the first derivative of the wave function with respect to x, $\psi'_\pm = \psi'(\pm 0)$ and $\psi_\pm = \psi(\pm 0)$. For the sake of simplicity, we will restrict ourselves to the real parameters case ($a, b, c, d, \Theta \in \Re$). Because the wave function is determined up to a random multiplicative constant of the form $e^{i\Theta}$, we may put $e^{i\Theta}=1$ without losing generality (Coutinho et al., 1999). Furthermore, from Eq. (11). it follows that $ac - bd = 1$ (Coutinho et al., 1999), (Christiansen et al., 2003). which finally leaves us with three independent parameters out of four (a, b, c, d) . Applying boundary conditions from (12) and using appropriate wave functions from (2) we can calculate coefficients T and R from (2) which are for obvious reasons defined as the transmission and reflection coefficients:

$$T(k) = \frac{2k}{(a+d)k + i(c - bk^2)}$$
$$R(k) = -\frac{k(a-d) + i(c+bk^2)}{(a+d)k + i(c-bk^2)} \qquad (13)$$

Shape of wave function given in (2) presumes that the particle is moving from left to right. i.e. in the positive direction of x-axes, so called left incidence. Closer examination reveals that the simple exchange of a with d (and vice versa) will account for the right case incidence. Note that the transmission coefficient is invariant to the direction of the incidence. For the real potential sum of the transmission and the reflection probabilities equals one (since the potential is real there is no absorption):

$$|T(k)|^2 + |R(k)|^2 = 1$$

which follows from the (13) having in mind that $ad - bc = 1$. Combinations of the three independent parameters describe all SAEs of the KE operator and account for the physically important cases of point interactions. Using Eq. (13) and following the definitions in (7), we derive the following general expressions for the group times in transmission and reflection:

$$\tau_{gt} = \frac{1}{2k} \frac{(a+d)(c+bk^2)}{(a+d)^2k^2 + (c-bk^2)^2}$$
$$\tau_{gr} = \tau_{gt} + \frac{1}{2k} \frac{(a-d)(bk^2-c)}{(a-d)^2k^2 + (c+bk^2)^2}. \qquad (14)$$

Furthermore, substituting (14) and (13) in (7) one gets that the total group time is given via:

$$\tau_g = \frac{1}{k} \frac{abk^2 + cd}{(a+d)^2k^2 + (c-bk^2)^2}. \qquad (15)$$

The group time for the right incidence is obtained by simply interchanging a and d in (15). Using expression (8) for interference time, it is easily confirmed that for $a, b, c, d \in \Re$ $\tau_g = \tau_i$ holds. Also note that if $a=d$, i.e. the potential is the symmetric one, than we have (Eq. (14)) $\tau_{gt} = \tau_{gr} = \tau_g$. In the next section we will deal with tunneling times of the specific point interactions, namely Dirac δ function and δ' function. Regarding the latter, various interpretations of the function are still present, so we take them into consederation.

2.1. δ function and tunneling times

The textbook example of one-dimensional point interaction is δ function. Let the potential be of the form $V(x) = c\cdot\delta(x)$, $c>0$ - infinite barrier. For such a barrier we have:

$$U=\begin{pmatrix}1 & 0\\ c & 1\end{pmatrix}. \qquad (16)$$

This can be easily verified by integrating Schrödinger equation from $-\varepsilon$ to $+\varepsilon$ and then letting $\varepsilon\to 0$, having in mind the definition of delta function itself and the definition of its integral. Due to the fact that $a=d=1$ which is consequence of delta function simmetry, there is no distinction between left and right incidence. Note that condition $ac-bd=1$ holds even for complex c. However, in the case of complex point interaction the relation connecting relevant times has an additional term responsible for the absorption as we already mentioned (see (4)). Putting $a=d=1$, $b=0$ in (13), we get

$$T(k)=\frac{2k}{2k+\imath c},\quad R(k)=\frac{-\imath c}{2k+\imath c}. \qquad (17)$$

Then, using relation for (6), we get the following expression for the group time:

$$\tau_g=\frac{c}{k}\frac{1}{4k^2+c^2}. \qquad (18)$$

Since potential under consideration is a real and symmetric one, we have $\varphi_0=\varphi_r+\pi/2$ and consequently $\tau_{gt}=d\varphi_0/dE=d\varphi_r/dE=\tau_{gr}$. Note that if $c<0$ in (18), then we have $\tau_g=\tau_i<0$ for all the values of particle incident energy. Also, in the case of strong δ interaction, we have $T(k)=0$, $R(k)=-1$. which is to be expected since in that case particle may only be reflected.

2.2. δ' function and tunneling times

Next real potential to consider is $V(x)=b\delta'(x)$ potential. As already told in introductory part, there is a great deal of controversy in literature regarding the meaning of the $\delta'(x)$ potential. Since no final consensus on this has not been reached, we will consider both of the known interpretations of $\delta'(x)$ potential.

In (Šeba, 1986) Šeba considered a δ function dipole potential. Roughly speaking, this interpretation of $\delta'(x)$ treats it as if resembles a first derivative of common delta potential.

$$V(x)=\lambda\lim_{\varepsilon\to 0}\frac{1}{2\varepsilon^{\nu}}[\delta(x+\varepsilon)-\delta(x-\varepsilon)]. \qquad (19)$$

In the limiting case $\varepsilon k\ll 1$, the transmission and reflection coefficients become (Coutinho et al., 1999):

$$T(k)=\frac{\imath k}{\lambda^2\varepsilon^{1-2\nu}+\imath k}\quad R(k)=\frac{\lambda^2\varepsilon^{1-2\nu}k}{\lambda^2\varepsilon^{1-2\nu}+\imath k}. \qquad (20)$$

From the definitions of the tunneling times we have:

$$\tau_g=\tau_i=-\frac{1}{2E}\mathrm{Im}(R)=-\frac{1}{2k}\frac{\lambda^2\varepsilon^{1-2\nu}}{k^2+(\lambda^2\varepsilon^{1-2\nu})^2}. \qquad (21)$$

Both the transmission (reflection) coefficient and tunneling times depend on parameter ν (convergence factor) as $\varepsilon\to 0$. However, when $\varepsilon\to 0$, either $\nu>1/2$ ($T\to 0$, $R\to 1$) or $\nu<1/2$ ($T\to 1$, $R\to 0$), two subspaces $x<0$ and $x<0$ are disjointed and there is no interaction; either we have total reflection or total transmission and tunneling times disappear $\tau_g=0$. In case that remains $\nu=1/2$, the dipole interaction case of (19) coincides with simple δ interaction with $\lambda^2=-c/2$ and τ_g is that of (18).

In their paper, (Christiansen et al.,2003) used two different limiting procedures in approximating $\delta'(x)$ function via :

$$\Delta_{\varepsilon,l}(x)=\begin{cases}\pm(\varepsilon l)^{-1} & \text{for } -(\varepsilon\pm l)/2<x<(\varepsilon\mp l)/2\\ 0 & \text{elewhere}\end{cases} \qquad (22)$$

which are in fact two rectangles of different 'polarity' having width ε and centered around $\pm l/2$ points. Two different limiting procedures were analyzed:

$$\delta'(x)=\lim_{\varepsilon\to 0}\lim_{l\to\varepsilon}\Delta_{\varepsilon,l}(x) \qquad (23)$$

and

$$\delta'(x)=\lim_{l\to 0}\lim_{\varepsilon\to 0}\Delta_{\varepsilon,l}(x). \qquad (24)$$

Note that the latter procedure (24) is in fact the Šeba's dipole interaction described by Eq. (19) with regularizing parameter set to one ($\nu=1$).

In (Christiansen et al., 2003) then showed that the first limiting procedure (243) leads to completely different transmission and reflection properties than that of Šeba dipole interaction. The transmission and reflection coefficients limiting values are $T\to 0$ and $R\to -1$. Two subspaces are disjointed except for some specific values of interaction strength λ_n subjected to the following condition:

$$\tan\sqrt{\lambda}_n=\tanh\sqrt{\lambda}_n, \qquad (25)$$

at which the $\delta'(x)$ potential becomes partially transparent. For this countable set of λ's, both the wave function and its first derivative become discontinuous. These jumps may be described by U matrix as follows:

$$U=\begin{pmatrix} \cosh\sqrt{\lambda}_n/\cos\sqrt{\lambda}_n & 0 \\ 0 & \cos\sqrt{\lambda}_n/\cosh\sqrt{\lambda}_n \end{pmatrix}. \quad (26)$$

The transmission coefficient is given by: (Christiansen et al., 2003) $T=2/(a+d)=\sec\sqrt{\lambda}_n \operatorname{sech}\sqrt{\lambda}_n$. As may be expected, due to the transparency of the potential, group time at λ_n is $\tau_g=0$. The same follows from Eq. (13) for $b=c=0$, i.e. in the sense of tunneling times, the interaction disappears.

Previous interpretation of δ' function leads to different values of transmission (reflection) coefficients and therefore tunneling times. Now we turn our attention to the $V(x)=b\delta'(x)$ interaction defined by the following boundary condition (Albeverio et al., 1988), (Exner, 1996), (Winful, 2006), (Gesztesy & Holden, 1987):

$$U=\begin{pmatrix} 1 & b \\ 0 & 1 \end{pmatrix}. \quad (27)$$

Here we have the continuity of wave functions first derivatives unlike in the case of δ interaction where the wave function itself is continuous. Since $a=d=1$, the group time is independent on the particle propagation direction. Thus defined δ' is invariant under the space reflection ($x\rightarrow -x$) in contrast to the $\delta'(x):=d\delta(x)/dx$ definition. The relevant scattering coefficients are:

$$T(k)=\frac{2\imath}{bk+2\imath}, \quad \mathrm{R(k)}=\frac{bk}{bk+2\imath}, \quad (28)$$

The group time is given by:

$$\tau_g=\frac{b}{k}\frac{1}{4+k^2b^2}. \quad (29)$$

Just like for δ potential, τ_g has negative values for all particle incident energies if $b<0$. In both cases there is a bound state of energy $-\kappa^2$ with $\kappa^2=c^2/4=4/b^2$ for δ and δ' potentials respectively.

3. Point interaction generated bound states in the continuum

3.1. Supersymmetric quantum mechanics

Suppose that $\psi_\varepsilon(x)$ is a particular solution of the one-dimensional Schrödinger equation describing a particle of energy $E=\varepsilon$ moving in a real potential $U_1(x)$

$$\hat{H}_1\psi_\varepsilon(x)=\left[-d^2/dx^2+U_1(x)\right]\psi_\varepsilon(x)=\varepsilon\psi_\varepsilon(x).$$

One more time, the units are such that $\hbar^2/2m=1$. Knowing the particular solution of (30), the general solution for the specific energy is given as:

$$\bar{\psi}_\varepsilon(x)=\psi_\varepsilon(x)+C\psi_\varepsilon\int_{x_0}^{x}\frac{dt}{\psi_\varepsilon^2(t)}, \quad (30)$$

where x_0 is real. Employing SUSY quantum mechanics (Cooper et sl., 1995) one can generate a whole family of isospectral potentials $U_2(x)$ having exactly the same energy spectrum as the initial potential $U_1(x)$. The corresponding SUSY potential is:

$$U_2(\lambda,x)=U_1(x)-\frac{d^2}{dx^2}\ln\left[\lambda+I(x)\right] \quad (31)$$

with $I(x)=\int_{x_0}^{x}\bar{\psi}_\varepsilon(t)^2dt$. SUSY wave function for the state of energy $E=\varepsilon$ is defined as

$$\psi_{2\varepsilon}(\lambda,x)=C_{2\varepsilon}\frac{\bar{\psi}_\varepsilon(x)}{\lambda+I(x)}, \quad (32)$$

The corresponding supersymmetric wave functions for all the states of energies $E_n\neq\varepsilon$ is somewhat lengthy to be written down so we"ll skip it. More details can be found in (Kočinac & Milanović, 2012b).

We state that constants λ and C in Eqs. (30) and (32) may be complex constants. In most general case $C_{2\varepsilon}$ cannot be determined analytically, though for some specific cases an analytical expressions are obtainable. For a more detailed discussion on this subject see Ref. (Pappademos et al., 1993).

We shall now apply SUSY to manipulate wave functions and potential of point interactions. Transfer matrix connecting wave functions' first derivatives and wave function at the origin may be rewritten in a more

convenient way (Carreau et al., 1990) (Román & Tarrach, 1996):

$$\begin{pmatrix} -\psi'(0^-) \\ \psi'(0^+) \end{pmatrix} = \begin{pmatrix} \varrho+\alpha & -\varrho e^{\imath\Theta} \\ -\varrho e^{-\imath\Theta} & \varrho+\beta \end{pmatrix} \begin{pmatrix} \psi(0^-) \\ \psi(0^+) \end{pmatrix}. \qquad (33)$$

Depending on the direction of particle propagation, we distinguish left and right incidence cases. For the particle propagating in the positive direction of *x*-axes the wave function is given by:

$$\psi_1(x) = \begin{cases} e^{ikx} + R_L e^{-ikx} & \text{for } x<0 \\ T_L e^{ikx} & \text{for } x>0; \end{cases}$$

while for the right incidence we have:

$$\psi_2(x) = \begin{cases} T_R e^{-ikx} & \text{for } x<0 \\ e^{-ikx} + R_R e^{ikx} & \text{for } x>0. \end{cases} \qquad (34)$$

and. $T_{L(R)}$ and $R_{L(R)}$ in (34) represent transmission and reflection coefficients for the left and right incidence respectively. Taking the values of the wave function and it's first derivative at the origin, we calculate the reflection and transmission coefficients for the left and right incidence to be:

$$T_L(k) = -\frac{2\imath k\varrho e^{-\imath\Theta}}{(\imath k-\varrho-\alpha)(\imath k-\varrho-\beta)-\varrho^2} = T_R(k)e^{-2\imath\Theta}$$
$$R_L(k) = \frac{(\imath k+\varrho+\alpha)(\imath k-\varrho-\beta)+\varrho^2}{(\imath k-\varrho-\alpha)(\imath k-\varrho-\beta)-\varrho^2}$$
$$R_R(k) = \frac{(\imath k-\varrho-\alpha)(\imath k+\varrho+\beta)+\varrho^2}{(\imath k-\varrho-\alpha)(\imath k-\varrho-\beta)-\varrho^2}. \qquad (35)$$

The transmission coefficient for the left and right incidence differ only for the phase factor $e^{-2\imath\Theta}$. Furthermore, when α=β and Θ=0 in (35), then we have $R_L=R_R$, $T_L=T_R$, i.e. the potential $U(x)$ is symmetrical and there is no distinction between left and right incidence regarding the transmission and reflection probabilities which are proportional to the square modulus of respective coefficients.

3.2. Total reflection case

The first case we consider is when the two subspaces $L^2(R^-)$ and $L^2(R^+)$ are effectively disjoint and there is no probability flowing from one half-line to the other. Formally, this situation corresponds to $\varrho\to 0$ in transfer matrix. The transmission coefficients disappear ($T_L\to 0$, $T_R\to 0$), so there are only reflected parts of wave functions regardless of the incidence.

Eq. (34) can be rearranged in a more suitable form, namely:

$$\psi_1(x) = \begin{cases} \sin(kx+\phi_0) & \text{for } x<0 \\ 0 & \text{for } x>0; \end{cases}$$
$$\psi_2(x) = \begin{cases} 0 & \text{for } x<0 \\ \sin(kx+\Theta_0) & \text{for } x>0; \end{cases} \qquad (36)$$

with $\tan\phi_0=-k/\alpha$ and $\tan\Theta_0=k/\beta$. Energy spectra corresponding to wave functions given by (36) is a continuous one, since any $k=\sqrt{E}>0$ is a satisfying solution.

However, it is possible to get a bound state in the continuum using supersymmetric quantum mechanics. This is done by deleting and then restoring a bound state with energy E=ε and corresponding wave function Ψ_ε. Newly generated potential has the identical energy spectrum to the original one but with modified wave functions.

We proceed as follows: for a continuous state characterized by energy $\varepsilon=k^2$ and corresponding wave function, we perform SUSY transformation according to (31) and (33). In this case it is possible to determine constants C and $C_{2\varepsilon}$ from (30) and (32) analytically.

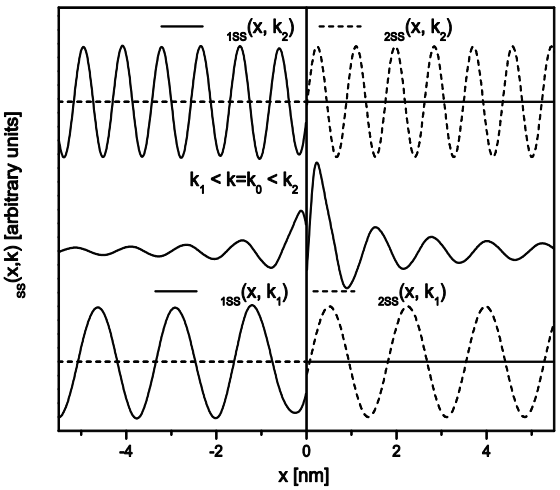

Fig. 1 Sypersymmetric wave functions at different energies for the case of total reflection ($T\to 0$). SUSY is applied for the energy ε_0= 1 eV and wave functions for energies ε_1= 0.5 eV and ε_2= 2.0 eV are also depicted. Parameter λ is *real* and is set to 1.5. Phase factors $\tan\phi=-k/\alpha$ and $\tan\Theta=k/\beta$ are calculated for α=0.2 and β=−0.1, in the units of *k*.

3.2. SUSY and general point interaction

In the previous section we have considered particle on the halfline with zero transmission ($T_{R(L)}$=0). For the more general case of finite transmission probability, rather then employing equations (34), we use the parameterized representation of the transmission and reflection coefficients (Kočinac et al., 2012b):

$$T_L=\cos\sigma e^{\imath\tau}=T_R \quad R_L=\imath\sin\sigma e^{\imath(\tau+\xi)}$$
$$R_R=\imath\sin\sigma e^{\imath(\tau-\xi)}. \tag{37}$$

Given a particle energy $E=k^2$, parameters σ, τ and ξ are determined for a specific point interaction defined by α, β and ϱ in transfer matrix representation (33). In that we have assumed that Θ of equals zero without losing generality in the approach.

We will simply state that unlike the case of total reflection considered in 3.2, corresponding wave functions may be presented in a form that allows an analytical derivation of SUSY wave function and potential:

$$\hat{\psi}_1(x,k)=\begin{cases}\cos\left[(kx-\xi/2)-\omega\right]; & x<0\\ \cos\left[(kx-\xi/2)+\omega\right]; & x>0\end{cases}$$

$$\hat{\psi}_2(x,k)=\begin{cases}\sin\left[(kx-\xi/2)+\omega\right]; & x<0\\ \sin\left[(kx-\xi/2)-\omega\right]; & x>0\end{cases} \tag{38}$$

where ω=(σ+τ)/2. So we are dealing with double degenerate states from continuum. Details can be found in (Kočinac et al., 2012b). Fig. 2 shows wave SUSY wave functions for a case of finite transmission.

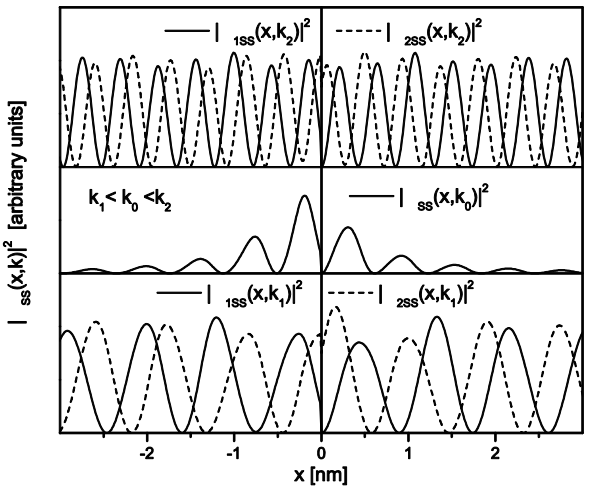

Fig. 2 Squared modulus of sypersymmetric wave functions at different energies for the case of non vanishing transmission coefficient T. SUSY is applied for the energie ε_0= 1 eV. Also are shown SUSY wave functions for double degenerate states at energies ε_1= 0.5 eV and ε_2= 2.0 eV. Other parameters are λ=1.0+ı3.0. Parameters ϱ, α and β are ρ=√3/3, α=0.3 and β=-0.5 in the units of *k*.

4. BIORTHOGONALITY

One more possible interpretation of transfer matrix is the one connecting wave function and its first derivative on the right and left hand side of the origin. Rearranging (33) we get (Carreau & Gutmann,1990), (Soldatov et al., 2006):

$$\begin{pmatrix}\psi'(0^+)\\ \psi(0^+)\end{pmatrix}=e^{-\imath\Theta}\begin{pmatrix}1+\beta/\varrho & \alpha+\beta+\alpha\beta/\varrho\\ 1/\varrho & 1+\alpha/\varrho\end{pmatrix}\begin{pmatrix}\psi'(0^-)\\ \psi(0^-)\end{pmatrix} \tag{39}$$

The convenience of (39) is clearly seen for limiting case ϱ→∞. All the coefficients in (39) are real with an additional restriction on ϱ which is nonnegative. It can also be seen that parity of the interaction (39) is not violated as long as α=β and Θ=0. There are several cases of particular interest, such as ϱ→0 corresponding to complete separation of left and right half line, and therefore no transmission between two subspaces. For ϱ→∞ and Θ=0 Eq. (39) reduces to the well known δ interaction and so on. What we are interested in is to explore the dependence of rigidity on the initial particle energy ε for the *bound* (ε<0) states (unlike free particle whose energy is positive). In this case the wave function is defined may be defined via:

$$\psi_\varepsilon(x)=\begin{cases}A_- e^{\kappa x} & \text{for } x<0\\ A_+ e^{-\kappa x} & \text{for } x>0;\end{cases} \tag{40}$$

where $\kappa=\sqrt{-\varepsilon}$. Upon replacing the relevant quantities in (39), the system of equations is obtained whose determinant must equal zero for the system not to have trivial solution:

$$\kappa_{1/2}=-\varrho-\frac{1}{2}(\alpha+\beta)\pm\frac{1}{2}\sqrt{4\varrho^2+(\alpha-\beta)^2}). \tag{41}$$

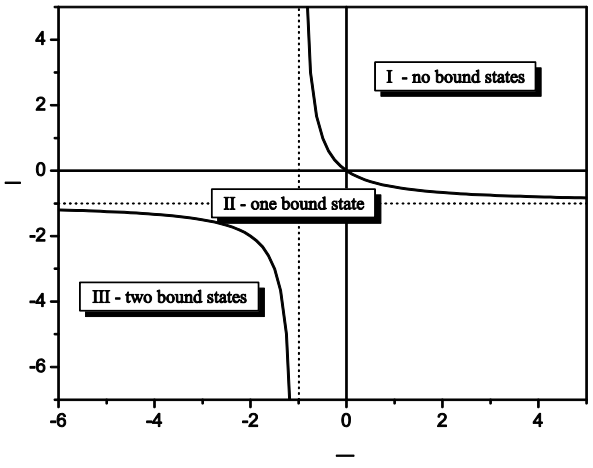

Fig. 3 Regions with two, one and no bound states are presented. Eq. (41) is rewritten in a dimensionless manner by simply dividing both sides) with ϱ so that $\underline{\alpha}=\alpha/\varrho$ and $\underline{\beta}=\beta/\varrho$. The curve presented is obtained from (41) and is defined via $\underline{\beta}=-\underline{\alpha}/(1+\underline{\alpha})$.

In order to have two bound states, $\kappa_{1/2}$ in (4) must be positive (Fig. 3). If we have only one bound state then the upper sign is relevant in (41). For $\varrho=0$ only one bound state exists with energy $\sqrt{-\varepsilon}=-\alpha$ and in order to have the same eigenvalues on the left and right half-line, we must have $\alpha=\beta<0$. SUSY wave function of discrete states for specific energy ε is calculated from (32):

$$\psi_{2\varepsilon}=\frac{A_{\pm}e^{\pm\kappa x}}{\lambda\pm\frac{1}{2\kappa A_{\pm}^{2}}\left(e^{\pm 2\kappa x}-1\right)} \qquad (42)$$

with the upper sign is used for negative part of $x-$ axes and lower for positive.

4.1. Biorthogonality of open systems

Systems that have non-Hermitian Hamiltonians are used to describe properties of a quantum systems that interact with environment, and are known as open quantum systems. Compared to so called closed systems that have real and orthogonal eigenvalues, this systems lack orthogonality of wave functions and interestingly enough energy eigenvalues are complex! Depending on the sign of eigenvalue imaginary part, this may lead to either decay or growth of wave function. This is overcome by the biorthogonality between wave functions.

We proceed as follows. Let us we have a complex potential:

$$U(x)=U_R(x)+\imath U_I(x).$$

The Schrödinger equations for two eigenvalues E_n and E_m read:

$$-\psi_n''+U\psi_n=E_n\psi_n \qquad (43)$$

$$-\psi_m''+U\psi_m=E_m\psi_m \qquad (44)$$

Upon multiplying (43) with Ψ_m and (44) with Ψ_n, and finally performing integration over the sum of those two, we get to:

$$-\psi_n'\psi_m+\psi_m'\psi_n\Big|_{-\infty}^{+\infty}=(E_n-E_m)\int_{-\infty}^{+\infty}\psi_n\psi_m dx. \qquad (45)$$

If Wronskian of the wave functions Ψ_m and Ψ_n

$$W(x)=-\psi_n'(x)\psi_m(x)+\psi_m'(x)\psi_n(x) \qquad (46)$$

satisfies $W(+\infty)-W(-\infty)=0$, then from (45) it follows:

$$\int_{-\infty}^{+\infty}\psi_n\psi_m dx=0,\ n\neq m, \qquad (47)$$

and the normalization condition is:

$$\int_{-\infty}^{+\infty}\psi_n^2 dx=1,\ n=m. \qquad (48)$$

Eqs. (4) and (4) are valid for all wave functions whether they belong to the discrete or continuous part of spectrum. Due to the complex nature of potential considered, we emphasize that we are dealing with non-Hermitian Hamiltonian. The normalizability condition from (4) now becomes:

$$\int_{-\infty}^{+\infty}(\psi_R^2(x)-\psi_I^2(x))dx=1 \qquad (49)$$

as long as the following is fulfilled:

$$\int_{-\infty}^{+\infty}\psi_R(x)\psi_I(x)dx=0, \qquad (50)$$

where ψ_R and ψ_I are real and imaginary part of the wave function ψ_n respectively. If condition (**Error! Reference source not found.**) is satisfied then for the *standard* norm (of the *n*-th eigenstate) we will have:

$$\int_{-\infty}^{+\infty}(\psi_R^2+\psi_I^2)dx=\int_{-\infty}^{+\infty}|\psi_n|^2dx>1. \qquad (51)$$

For a complex potential $U(x)=U_R+\imath U_I$ and single state of real eigenenergy ε, Eq. (**Error! Reference source not found.**), may be separated into two equations, i.e. rearranged in the matrix form:

$$\begin{bmatrix} H_0 & -U_I \\ U_I & H_0 \end{bmatrix}\begin{bmatrix} \psi_R \\ \psi_I \end{bmatrix}=\varepsilon\begin{bmatrix} \psi_R \\ \psi_I \end{bmatrix}. \qquad (52)$$

with $H_0=-d^2/dx^2+U_R$. Condition (49) needed for wave function's biorthogonality (4), (4) in general is not satisfied. However, we may "force" wave function to meet that condition. To that purpose, we construct a new wave function with ψ_R and ψ_I components that are related to the original ψ_R and ψ_I components in the following manner:

$$\begin{bmatrix} \psi_R \\ \psi_I \end{bmatrix}=\begin{bmatrix} e^{\imath\delta}\cos\phi & e^{\imath(\chi+\delta)}\sin\phi \\ e^{\imath\gamma}\sin\phi & -e^{\imath(\chi+\gamma)}\cos\phi \end{bmatrix}\begin{bmatrix} \psi_R \\ \psi_I \end{bmatrix}=U\begin{bmatrix} \psi_R \\ \psi_I \end{bmatrix}. \qquad (53)$$

It is easy to verify that $U\cdot U^{\dagger}=I$, I being the unitary matrix. Newly constructed wave function ψ also represents eigen wave function for the state of energy ε. Coefficients ϕ,χ,γ and δ in (5) are real numbers. From the definition of matrix U it is clear that $e^{\imath\gamma}$ and $e^{\imath\delta}$ will simply be the phase factors, therefore we may put γ=δ=0 without losing generality. Furthermore, in order for ψ_R and ψ_I to be real functions, we have χ=π (since χ=0 is not the solution of (52), so Eq. (5) reduces to:

$$\psi_R=\psi_R\cos\phi-\psi_I\sin\phi\,\psi_I=\psi_R\sin\phi+\psi_I\cos\phi. \qquad (54)$$

Equation (5) represents simple rotation of coordinate system through angle ϕ. Now we demand wave function $\psi=A(\psi_R+\imath\,\psi_I)$ to be biorthogonal, i.e.

$$\int_{-\infty}^{+\infty}\psi_R\psi_I dx=0 \qquad (55)$$

must hold. Constant A is normalization constant of $\psi(x)$ function. Replacing (5) in ((5), angle ϕ that allows for biorthogonality is determined:

$$\tan 2\phi=\frac{-2\int_{-\infty}^{+\infty}\psi_R\psi_I dx}{\int_{-\infty}^{+\infty}\psi_R^2dx-\int_{-\infty}^{+\infty}\psi_I^2dx}=\frac{q}{p} \qquad (56)$$

Biorthogonality condition now demands $\int_{-\infty}^{+\infty}\psi^2(x)dx=1$ and with help of simple trigonometric transformations $\cos 2\phi=p/\sqrt{p^2+q^2}$ and $\sin 2\phi=q/\sqrt{p^2+q^2}$, condition (**Error! Reference source not found.**) reduces to:

$$A^2\left[\frac{p^2}{\sqrt{p^2+q^2}}+\frac{q^2}{\sqrt{p^2+q^2}}\right]=1\Rightarrow A^2=\frac{1}{\sqrt{p^2+q^2}}, \qquad (57)$$

so finally a new wave function $\psi=A(\psi_R+\imath\,\psi_I)$ is obtained (see Eq. (26) in (Kočinac et al., 2013) finasl wzve function being normalized in the sense of (48).

5. PHASE RIGIDITY

Phase rigidity ϱ^2 is defined as:

$$\varrho=\frac{\int dr\Psi(r)^2}{\int dr\,|\Psi(r)|^2}. \qquad (58)$$

With the help of (57) rigidity becomes:

$$\varrho^2=\frac{\int_{-\infty}^{+\infty}\psi^2(x)dx}{\int_{-\infty}^{+\infty}|\psi(x)|^2dx}=\frac{1}{\int_{-\infty}^{+\infty}|\psi(x)|^2dx}=\frac{\sqrt{p^2+q^2}}{\int_{-\infty}^{+\infty}(\psi_R^2+\psi_I^2)dx}, \qquad (59)$$

or finally, upon substituting p and q from Eq. (5), we have

$$\varrho^2=\frac{\left[\int_{-\infty}^{+\infty}(\psi_R^2-\psi_I^2)dx\right]^2+\left[2\int_{-\infty}^{+\infty}\psi_R\psi_I dx\right]^2}{\left[\int_{-\infty}^{+\infty}(\psi_R^2+\psi_I^2)dx\right]^2}. \qquad (60)$$

From the definition of rigidity, with the aid of Cauchy-Schwartz inequality, it is clear that $\varrho^2\in(0,1]$, and

$$\varrho^2=\frac{(J_1-J_2)^2+(2J_3)^2}{(J_1+J_2)^2} \tag{61}$$

where

$$J_1=\int_{-\infty}^{\infty}\psi_R^2(x)dx,\ J_2=\int_{-\infty}^{\infty}\psi_I^2(x)dx \tag{62}$$

and

$$J_3=\int_{-\infty}^{\infty}\psi_R(x)\psi_I(x)dx. \tag{63}$$

We note one more time that in determining phase rigidity through (60) we do not need to have

$$\int_{-\infty}^{\infty}\psi_R(x)\psi_I(x)dx=0.$$

6. PHASE RIGIDITY OF SUSY MANIPULATED POINT INTERACTIONS

We will assume that constants C=0 in (30) so that $\psi_\varepsilon(x)=\psi_\varepsilon(x)$. For the state of energy $E_n=\varepsilon$ we perform SUSY transformation.

It is crucial to emphasize at this point that state of energy $E_n=\varepsilon$ may belong to either continuous or discrete part of the spectrum. If $\varepsilon>0$ we have double degenerate continuous states and if $\varepsilon<0$ we have bound state(s) depending on (41). As far as rigidity is concerned, constant $C_{2\varepsilon}$ in (32) is irrelevant, so we may put $C_{2\varepsilon}=1$. Hence, J_1, J_2 and J_3 from (62) and (63) are given as:

$$\begin{aligned}
J_1&=\int_{-\infty}^{\infty}\frac{\psi_\varepsilon^2(\lambda_R+I(x))^2dx}{\left[(\lambda_R+I(x))^2+\lambda_I^2\right]^2}\\
J_2&=\lambda_I^2\int_{-\infty}^{\infty}\frac{\psi_\varepsilon^2dx}{\left[(\lambda_R+I(x))^2+\lambda_I^2\right]^2}\\
J_3&=-\lambda_I\int_{-\infty}^{\infty}\frac{\psi_\varepsilon^2(\lambda_R+I(x))dx}{\left[(\lambda_R+I(x))^2+\lambda_I^2\right]^2}.
\end{aligned} \tag{64}$$

Integrals J_1, J_2 and J_3 are easily rearranged noting that $d(\lambda_R+I(x))=\psi_\varepsilon^2dx$. The solution of the integrals are respectively:

Solutions of the form given in Eq. (63) are valid for both SUSY generated bound states in continuum and SYSY manipulated bound states from discrete part of the spectrum. In the most general case, expression for rigidity that is calculated from (61) with help of (64).

Asymptotic behavior of integral $I(x)$ is different for bound states and those belonging to continuous part of spectrum. If we are dealing wit bound states then we'll have $I(-\infty)=0$ and $I(+\infty)=r$, where r is nonnegative.

Note that $\varrho^2\to1$ when $\lambda_I\to0$.

6.1. Continuum states

For the states from the continuum manipulated via SUSYQM (*but* $E_n\neq\varepsilon$) the reasoning goes as follows: Wronskian in (46) tends to zero as $x\to\pm\infty$ and the constant C_{2n} may be determined analytically in this case, i.e. $C_{2n}=1/(E_n-\varepsilon)$. Thus the SUSY wave function $\psi_{2n}(x)\approx\psi_{1n}(x)$ for large enough $|x|$, where the latter is the original *real* wave function. The contribution of imaginary part of the integral is negligible and we have $\varrho^2\to1$.

6.2. Bound states in continuum (BIC)

For the bound state in the continuum (which may exist only if ψ_ε belongs to the continuous part of the spectrum) the integral $I(x)$ will have a term proportional to x due to the oscillatory nature of the original wave function. Therefore, we will have $I(x)(x\to\pm\infty)\to\pm\infty$, thus first terms in integrals J_1 and J_2 as well as integral J_3 disappear, leaving $J_1=J_2$ and consequently $\varrho^2=0$. T

6.3. Discrete states

If ψ_ε is wave function of a bound state, then for all ψ_m that belong to double degenerate state from continuum we will have $\varrho^2=1$. If there is only one bound state the SUSY wave function is calculated according to (32). If, however, there are two discrete states, then we perform SUSY for only one state of energy $E=\varepsilon$ while SUSY wave function for the remaining discrete state is done using (6) in Ref. (Kočinac, 2013), i.e:

$$\psi_{2n}=\psi_{1n}-\psi_{\varepsilon}\frac{\int_{-\infty}^{x}\psi_{\varepsilon}\psi_{1n}dx}{(\lambda_R+I)+i\lambda_I}=(\psi_{2n})_R+i(\psi_{2n})_I.$$

Here we have chosen to calculate phase rigidity for a single discrete state corresponding to region II in Fig. 3. Although analytical solution to the problem is formally possible, no reasonable expression (from which to deduce rigidity dependence on relevant interaction parameters) is obtainable. So we turn to the numerical results and vary parameter ϱ (and particle energy ε therefore) to demonstrate how rigidity depends on particle energy. One such dependence is presented in Fig. 4 where for different values of complex SUSY parameter λ we have varied point interaction strength parameter ϱ from (41). Phase rigidity is calculated using (58) with ψ_R=Re{$\psi_{2\varepsilon}$} and ψ_I=Im{$\psi_{2\varepsilon}$} where $\psi_{2\varepsilon}$ is given by (42).

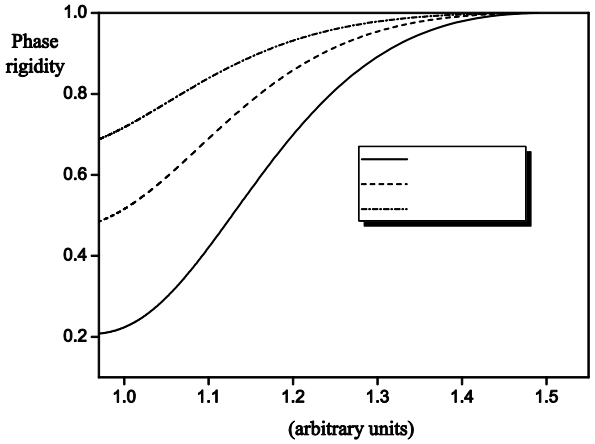

Fig. 4 Phase rigidity for SUSY manipulated bound state of general point interaction. SUSY parameter λ=(λ$_R$, λ$_I$) from the top to the bottom curve is set to (0.2, 0.2), (0.15, 0.15), (0.2, 0.2) vrespectively. Parameters of point interaction (see Eq. (4)) are set to α=−1.5 and β=−0.4. To different values of interaction parameter ϱ correspond different values of parameter κ=$\sqrt{-\varepsilon}$, where ε is the particle energy. For large values of κ phase rigidity tends to 1.

7. Conclusion

The aim of this review paper was to give a brief survey of some properties of one dimensional point interactions that describe spatially localized potentials.

First part deals with tunneling times. After the general relation connecting various times for the case of complex point interaction was derived, it was shown that for point interaction described by real parameters only one tunneling time is relevant. It is group time which measures the delay in the appearance of the wave packet at the front and at the end of the potential barrier. Then for some specific potential shapes tunneling times were calculated. So called point dipole interaction discussed by Šeba (Christiansen, et al., 2003) leads to either trivial case of τ_g=0 for ν≦1/2, i.e, the interaction disappears, or reduction to group time identical to that of simple δ potential apart for different interaction strength. by Christiansen et al. (Christiansen, et al., 2003) proposed different limiting procedure that leads to the partial transparency at specific interaction strengths for which τ_g=0. Various nterpretations of δ' function used in (Albeverio et al., 1988), (Exner, 1996), (Gesztesy & Holden, 1987), (Šeba, 1986). (continuous first derivative and jump in wavefunction itself) gives non-trivial $\tau_g\neq 0$ values of group time. For interactions defined through Eqs. (16) and (27), if the interaction strength coefficients *b* and *c* are negative, then the tunneling times also have negative values regardless of particle incident energy.

A bound state that may be embedded in the continuum by applying supersymmetric quantum mechanics. We used this technique to one dimensional point interactions by applying supersymmetric quantum mechanics. When dealing with the continuum on the half line, which is a case of total reflection, the SUSYQM parameterization constant λ is allowed to be real valued thus providing normalizability of the SUSY wave function. For the general case of continuum states along the entire line (double degenerate states), only complex λ allows for bound states in the continuum to be embedded. One possible application of the method presented here is in photonic crystals with complex dielectric constant where potentials described in the paper can be realized, thereby generating bound states in the continuum. Point interactions in two and three dimensionse to which SUSY is applied is possible extension of research presented.These problems are rather complex since one encounters divergence and renormalization in order to define proper point interactions.

Finally, a four-parameter family of one-dimensional point interactions and its biorthogonal eigenfunctions, which were generated through SUSY quantum mechanics, was constructed. We proceeded by investigation of the phase rigidity of this complex

wave functions. It was demonstrated analytically that for SUSY generated bound state in continuum phase rigidity is always zero no matter what the incident particle energy was. Other states from continuum have unity rigidity, while states from discrete part of spectrum may have intermediate values depending on the particle energy.

REFERENCES

Albeverio, S. 1988. Solvable models in quantum mechanics. New York: Springer-Verlag.

Albeverio, S., Gesztesy, F. & Holden, H. 1993. Comments on a recent note on the Schrodinger equation with a delta' -interaction. J. Phys. A: Math. Gen., 26 (15), pp. 3903-3904.

Albeverio, S., Dabrowski, L. & Kurasov, P. 1998. Symmetries of Schrödinger Operator with Point Interactions. Lett. Math. Phys., 45 (1), pp. 33-47, doi: 10.1023/A:1007493325970.

Avron, J. E., Exner, P. & Last, Y. 1994. Periodic Schrödinger operators with large gaps and Wannier–Stark ladders. Phys. Rev. Lett., 72 (6), pp. 896-899.

Berezin, F. A. & Faddeev, L. D. 1961. A remark on Schrödinger equation with a singular potential. Sov. Math. Dokl., 2, pp. 372-375.

Bogolyubov Jr., N. N. & Kruchinin, S. 2003. Modern approach to the calculation of the correlation function in superconductivity models. Mod. Phys. Lett. B, 17, pp. 709-724.

Carreau, M., Farhi, W. & Gutmann, S. 1990. Functional integral for a free particle in a box. Phys. Rev. D, 42, pp. 1194-1202.

Cheon, T., Exner, P. & Šeba, P. 2000a. Wave function shredding by sparse quantum barriers. Phys. Lett. A, 277, pp. 1-6. Doi: 10.1016/S0375-9601(00)00690-3.

Cheon, T., Shigehara, T. & Takayanagi, K. 2000b. Equivalence of local and separable realizations of discontinuity-inducing contact. J. Phys. Soc. Japan., 69, pp. 345-350.

Christiansen, P. L., Arnbak, H. C., Zolotaryuk, A. V., Ermakov, V. N. & Gaidei, Y. B. 2003. On the existence of resonances in the transmission probability for interactions arising from derivatives of Dirac's delta function. J. Phys. A: Math. Gen., 36, pp. 7589-7600.

Cooper, F., Khare, A. & Sukhatme, U. 1995. Supersymmetry and quantum mechanics. Phys. Rep. 251 (5-6), pp. 267-385.

Coutinho, F. A. B., Nogami,Y. & Perez, J. F. 1999. Time-reversal aspect of the point interactions in one-dimensional quantum mechanics. J. Phys. A: Math. Gen., 32 (12), pp. L133-L136.

Coutinho, F. A. B., Toyama, F. M. & Nogami, Y. 2008. One-dimensional point interaction with three complex parameter. J. Phys. A: Math. Gen., 41 (23), p. 253306.

Demkov, Y. N. & Ostrovskii, V. N. 1975. Zero-Range Potentials and their Applications in Atomic Physics. Leningrad: Leningrad University Press.

Dzhezherya, Y., Novak, I. Y. & Kruchinin, S. 2010. Orientational phase transitions of lattice of magnetic dots embedded in a London type superconductors. Supercond. Sci.Technol., 23 (10), pp. 105011.

Exner, P. 1995. Lattice Kronig-Penney Models. Phys. Rev. Lett., 74 (18), pp. 3503-3506.

Exner, P. 1996. Contact interactions on graph superlattices. J. Phys. A: Math. Gen., 29 (1), pp. 87-102.

Gadella, M., Negro, J. & Nieto, L. M. 2009. Bound states and scattering coefficients of the $a\delta(x)+b\delta'(x)$ potential. Phys. Lett. A, 373 (15), pp. 1310-1313.

Gesztesy, F. & Holden, H. 1987. A new class of solvable models in quantum mechanics describing point interactions on the line. J. Phys. A: Math. Gen., 20 (15), pp. 5157- 5177.

Kočinac, S. Lj. S., Milanović, V., Ikonić ,Z. & Indjin, D. 2007. Influence of nonparabolicity on tunneling times in semiconductor structures. Phys. Lett. A, 366 (1-2), pp. 130-133.

Kočinac, S. Lj. S. & Milanović, V. (2008). Tunneling times in complex potentials. Phys. Lett. A, 372 (3), pp. 191-196.

Kočinac, S. Lj. S. & Milanović, V. 2012a. Generalized point interaction and tunneling times. Mod. Phys. Lett. B, 26 (15), p. 1250092. doi: 10.1142/S021798491250092.

Kočinac, S. Lj. S. & Milanović, V. 2012b. Bound states in continuum generated by point interaction and supersymmetric quantum mechanics. Mod. Phys. Lett. B, 26 (27), 1250177. doi: 10.1142/S0217984912501771.

Kočinac, S. Lj. S. & Milanović, V. 2013. Phase Rigidity Of Point Interactions. Mod. Phys. Lett. B, 27 (1), 1350001. doi: 10.1142/S0217984913500012

Kruchinin, S., Nagao, H. & Aono, S. 2010. Modern aspect of superconductivity: theory of superconductivity. World Scientific. ISBN-9814261602.

Kurasov, P. B., Scrinzi, A. & Elander, N. 1994. δ' potential arising in exterior complex scaling. Phys. Rev. A, 49 (6), pp. 5095-5097.

Kurasov, P. 1996. Distribution theory for discontinuous test functions and differential operators with generalized coefficients. J. Math. Anal. Appl., 201 (1), pp. 297-323.

Marcuse, D. 1974. Theory of Dielectric Optical Waveguides. New York: Academic Press.

Milanović, V. & Ikonić, Z. 1997. Optimization of nonlinear optical rectification in semiconductor quantum wells using the inverse spectral theory. Solid State Commun., 104 (8), pp. 445-450.

Milanović, V. & Ikonić, Z. 2002. Supersymmetric generated complex potential with complete real spectrum. Phys. Lett. A, 293 (1-2), pp. 29-35.

Pappademos, J., Sukhatme, U. & Pagamenta, A. 1993. Bound states in the continuum from supersymmetric quantum mechanics. Phys. Rev. A, 48 (5), pp. 3525-3531.

Román, J. M. & Tarrach, R. 1996. The regulated four-parameter one-dimensional point interaction. J. Phys. A: Math. Gen., 29 (18), pp. 6073-6085.

Soldatov,V., Bogolyubov Jr, N. N. & Kruchinin, S. P. 2006. Method of intermediate problems in the theory of Gaussian quantum dots placed in a magnetic field. Condensed Matter Physics, 9 (1), pp. 151-159.

Šeba, P. 1986. Some remarks on the δ′-interaction in one dimension. Rep.Math. Phys., 24 (1), pp. 111-120.

Winful, H. G. 2006. Tunneling time, the Hartman effect, and superluminality: A proposed resolution of an old paradox. Phys. Rep., 436 (1-2), pp. 1-69.

Zolotaryuk, V. 2010. Boundary conditions for the states with resonant tunnelling across the δ -potential. Phys. Lett. A, 374 (15-16), pp. 1636-1641.doi:10.1016/j.physleta.2010.02.005.

* E-mail: skocinac@gmail.com

CIP - Каталогизација у публикацији
Народна библиотека Србије, Београд

5

The UNIVERSITY thought. Publication in natural sciences / editor in chief Nebojša Živić. - Vol. 3, no. 1 (1996)- . - Kosovska Mitrovica : University of Priština, 1996- (Kosovska Mitrovica : Art studio KM). - 29 cm

Polugodišnje. - Prekid u izlaženju od 1999-2015. god. - Je наставак: Универзитетска мисао. Природне науке =
ISSN 0354-3951
ISSN 1450-7226 = The University thought. Publication in natural sciences
COBISS.SR-ID 138095623

Available Online

This journal is available online. Please visit http://www.utnsjournal.pr.ac.rs to search and download published articles.